Title
Structural Behavior of a Curved 2-Span Reinforced Concrete Box Girder Bridge Model, Vol. 2 -- Reduction Analysis and Interpretation of Results

Authors
Scordelis, Alex
Bouwkamp, Jack
Larsen, Per

Publication Date
1974-09-01

REPORT NO.
UC SESM 74-6

STRUCTURES AND MATERIALS RESEARCH
DEPARTMENT OF CIVIL ENGINEERING

STRUCTURAL BEHAVIOR OF A CURVED TWO SPAN REINFORCED CONCRETE BOX GIRDER BRIDGE MODEL

VOL. II – REDUCTION, ANALYSIS AND INTERPRETATION OF RESULTS

by

A. C. SCORDELIS
J. G. BOUWKAMP
P. K. LARSEN

In cooperation with the State of California, Business and Transportation Agency, Department of Transportation and the U. S. Department of Transportation, Federal Highway Administration.

SEPTEMBER 1974

COLLEGE OF ENGINEERING
OFFICE OF RESEARCH SERVICES
UNIVERSITY OF CALIFORNIA
BERKELEY CALIFORNIA

TECHNICAL REPORT STANDARD TITLE PAGE

1. Report No.	2. Government Accession No.	3. Recipient's Catalog No.
4. Title and Subtitle STRUCTURAL BEHAVIOR OF A CURVED TWO SPAN REINFORCED CONCRETE BOX GIRDER BRIDGE MODEL, VOL. II - REDUCTION, ANALYSIS AND INTERPRETATION OF RESULTS		5. Report Date September 1974 6. Performing Organization Code
7. Author(s) A. C. Scordelis, J. G. Bouwkamp, P. K. Larsen		8. Performing Organization Report No. UC SESM 74-6
9. Performing Organization Name and Address Department of Civil Engineering University of California Berkeley, California 94720		10. Work Unit No. 11. Contract or Grant No. HPR - 1 (12) D04110
12. Sponsoring Agency Name and Address California Department of Transportation Sacramento, California 95807		13. Type of Report and Period Covered Final Report 14. Sponsoring Agency Code RTA 13945 - 14647

15. Supplementary Notes

Prepared in cooperation with the State of California, Business and Transportation Agency, Department of Transportation and the U.S. Department of Transportation, Federal Highway Administration.

16. Abstract

This is the second of a three volume sequence as follows: Vol. I - Design, Construction, Instrumentation and Loading; Vol. II - Reduction, Analysis and Interpretation of Results; and Vol. III - Detailed Tables of Experimental and Analytical Results. In the present volume a detailed presentation of the reduction, analysis and interpretation of the experimental and theoretical results obtained in testing a large scale, horizontally curved, two span, four cell, reinforced concrete box girder bridge model is given. The various computer programs used in obtaining theoretical results are described and compared. The methods and computer programs used for reduction of experimental data are also presented. Results, in terms of reactions, deflections, strains and moments, for the response of the bridge to dead load, working stress loads and at overload stress levels are given and comparisons between experimental and theoretical values are made. A review of the behavior under sustained dead load during the load history of the model is given with respect to strains, deflections and cracking. The loading to failure, and observations of structural behavior during this final phase are considered in detail. Throughout, a comparison is made between the behavior of the curved bridge, studied in this investigation, and of a similar straight bridge, studied previously.

17. Key Words	18. Distribution Statement
Curved box girder bridge; continuous box girder; dead load; live load; overloads; ultimate strength; reinforced concrete model; large scale model; experimental study; theoretical study; computer programs.	Unlimited

19. Security Classif. (of this report)	20. Security Classif. (of this page)	21. No. of Pages	22. Price
Unclassified	Unclassified	337	

Form DOT F 1700.7 (8-69)

DISCLAIMER

Structures and Materials Research
Department of Civil Engineering
Division of Structural Engineering
and
Structural Mechanics

UC-SESM Report No. 74-6

STRUCTURAL BEHAVIOR OF A CURVED TWO SPAN REINFORCED CONCRETE BOX GIRDER BRIDGE MODEL

VOL. II - REDUCTION, ANALYSIS AND INTERPRETATION OF RESULTS

by

A. C. Scordelis

J. G. Bouwkamp

Professors of Civil Engineering

and

P. K. Larsen

Assistant Research Engineer

In cooperation with

State of California
Business and Transportation Agency
Department of Transportation
Under Research Technical Agreement
No. 13945-14647
and
U. S. Department of Transportation
Federal Highway Administration

College of Engineering
Office of Research Services
University of California
Berkeley, California

September 1974

ABSTRACT

This is the second of a three volume sequence as follows: Vol. I - Design, Construction, Instrumentation and Loading; Vol. II - Reduction, Analysis and Interpretation of Results; and Vol. III - Detailed Tables of Experimental and Analytical Results. In the present volume a detailed presentation of the reduction, analysis and interpretation of the experimental and theoretical results obtained in testing a large scale, horizontally curved, two span, four cell, reinforced concrete box girder bridge model is given. The various computer programs used in obtaining theoretical results are described and compared. The methods and computer programs used for reduction of experimental data are also presented. Results, in terms of reactions, deflections, strains and moments, for the response of the bridge to dead load, working stress loads and at overload stress levels are given and comparisons between experimental and theoretical values are made. A review of the behavior under sustained dead load during the load history of the model is given with respect to strains, deflections and cracking. The loading to failure, and observations of structural behavior during this final phase are considered in detail. Throughout, a comparison is made between the behavior of the curved bridge, studied in this investigation, and of a similar straight bridge, studied previously.

KEYWORDS

Curved box girder bridge; continuous box girder; cellular structure; dead load; live load; overloads; failure load; ultimate strength; reinforced concrete model; large scale model; experimental study; theoretical study; structural analysis; direct stiffness method; harmonic analysis; finite element method; computer programs.

TABLE OF CONTENTS

LIST OF TABLES

LIST OF FIGURES

Figure		Page

1. INTRODUCTION

1.1 General Remarks

The present volume is the second of a three volume sequence on the "Structural Behavior of a Curved Two Span Reinforced Concrete Box Girder Bridge Model". The material included in each volume is as follows:

Vol. I - Design, Construction, Instrumentation and Loading

Vol. II - Reduction, Analysis and Interpretation of Results

Vol. III - Detailed Tables of Experimental and Analytical Results

These volumes deal with the complete experimental and analytical study of a horizontally curved, continuous, two span, four cell, reinforced concrete box girder bridge model, Fig. 1.1. The model was 72 ft. long along its longitudinal centerline, 12 ft. wide and 1 ft. 8 9/16 in. in depth, with a radius of curvature of 100 ft. It was built and tested in the Structural Engineering Materials Laboratory (S.E.M.L.) of the University of California, Berkeley. Objectives of the program, concrete dimensions, location and amounts of reinforcing steel, instrumentation, construction, loading and the experimental program for the model have been described in detail in Vol. I. For easy reference in the present volume, Figs. 1.2 and 1.3 depict the general dimensions of the model and the designation of transverse sections and longitudinal girder lines which are of pertinent interest.

1.2 Scope of Volume II

The present volume comprises the analysis of experimental data from the box girder bridge model. While the main emphasis is placed on the part dealing with load distribution properties of the box girder bridge at working stresses, the dead load and overload cases and the

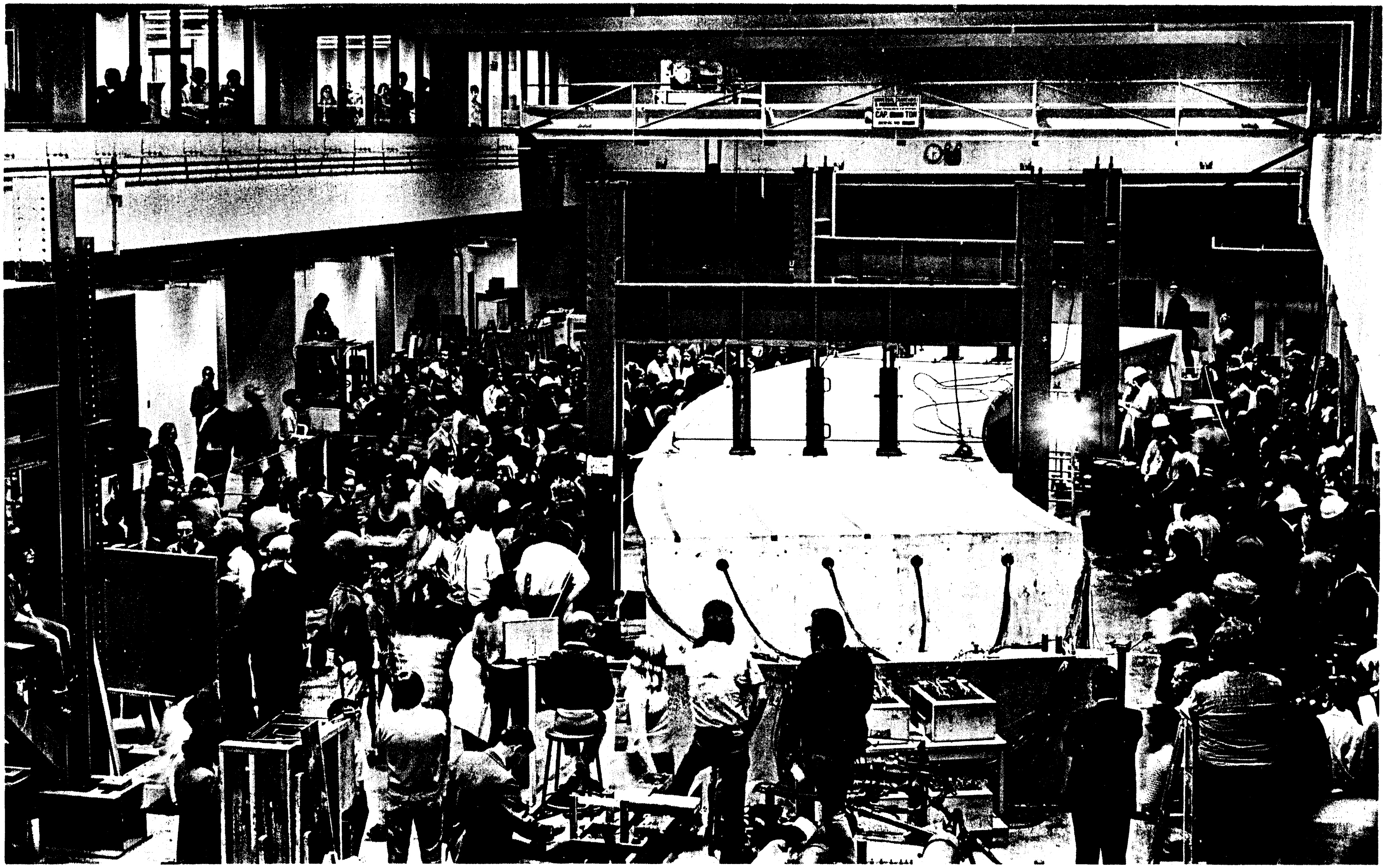

FIG. 1.1 FINAL LOAD TEST ON CURVED BOX GIRDER BRIDGE MODEL

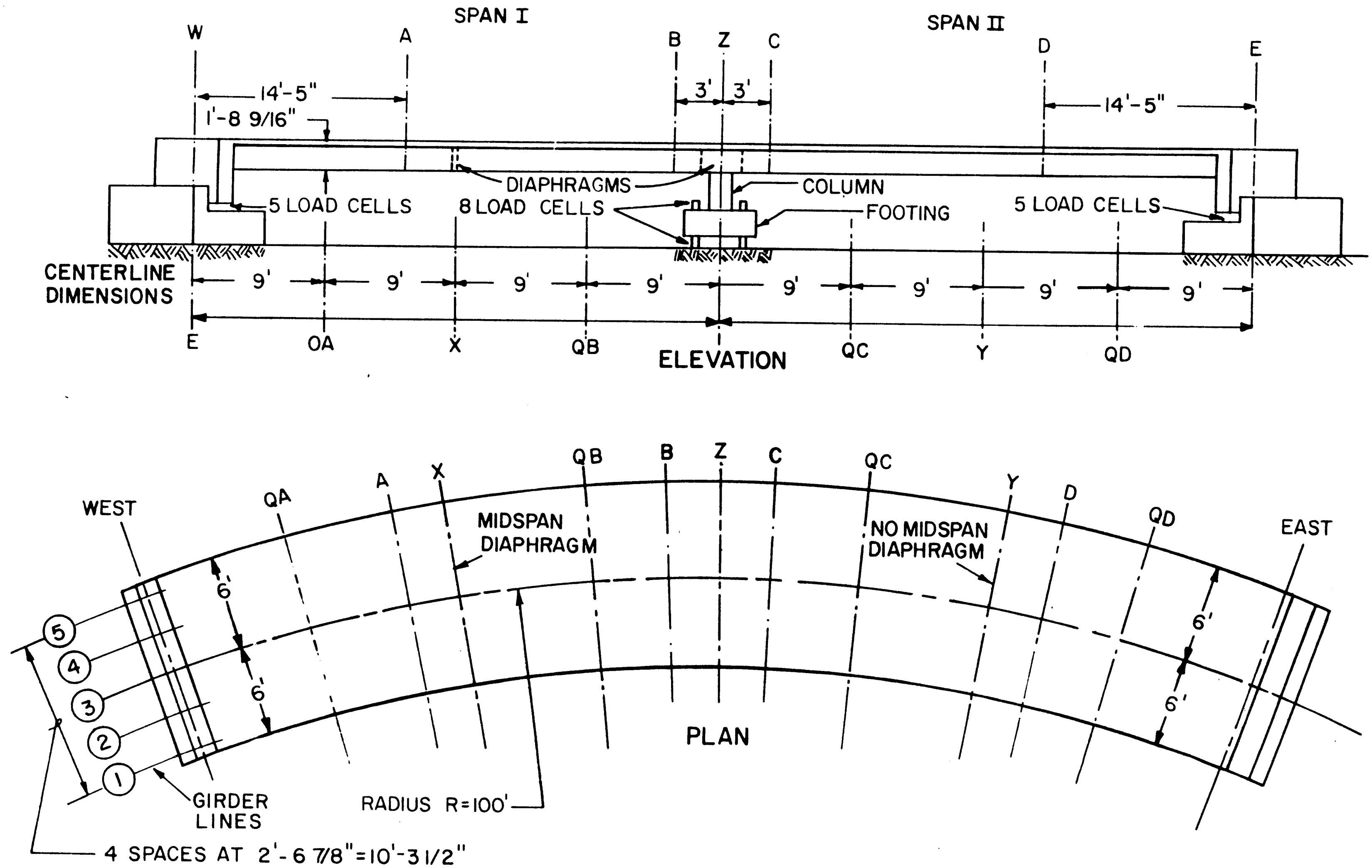

FIG. 1.2 DIMENSIONS OF BOX GIRDER BRIDGE MODEL WITH LOCATIONS OF TRANSVERSE SECTIONS AND LONGITUDINAL GIRDER LINES

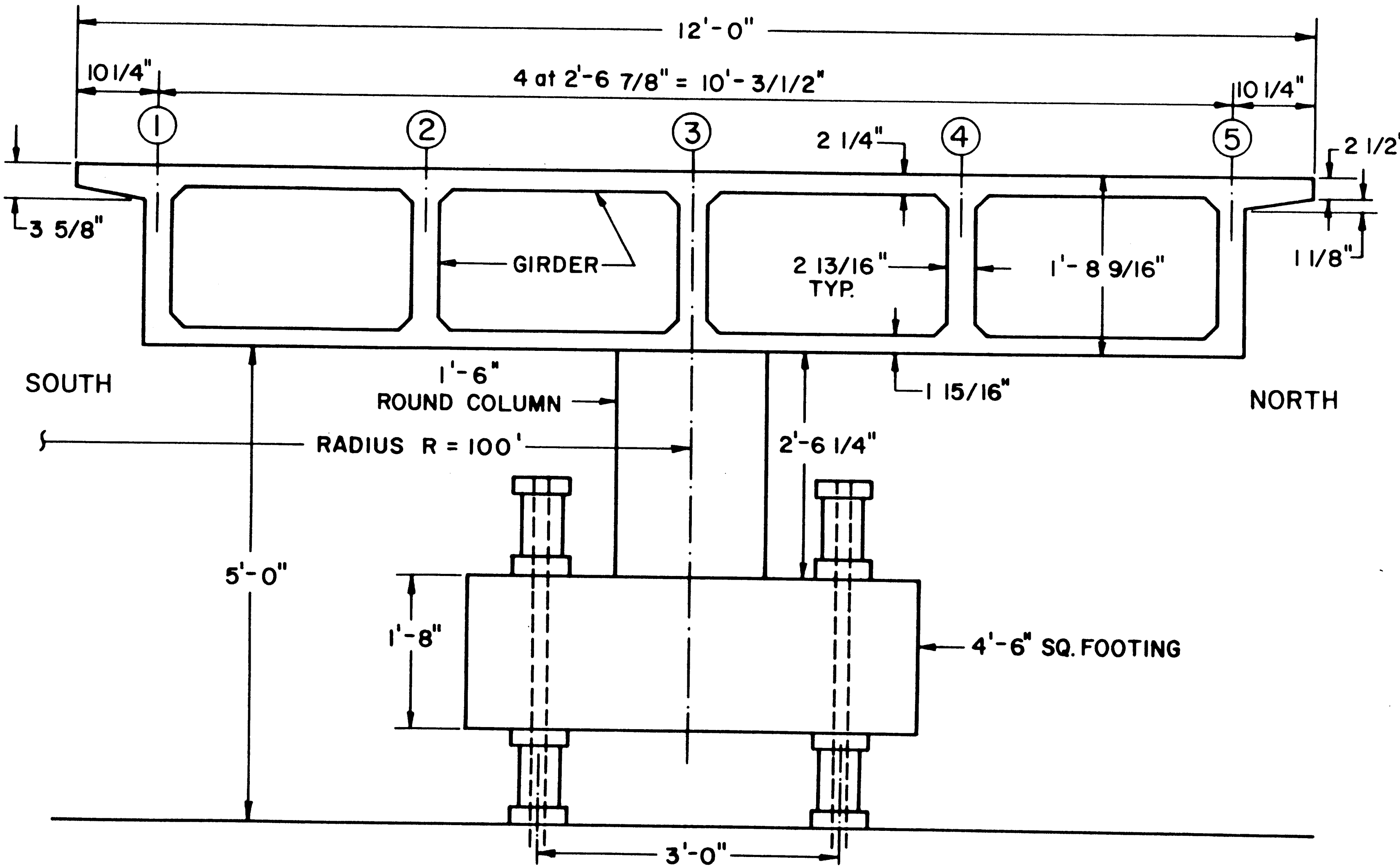

FIG. 1.3 TYPICAL SECTION OF BOX GIRDER BRIDGE MODEL

whole history of the bridge are also treated in detail. Experimental data reduction is described, and data is presented for almost all loading cases of interest. Theoretical values obtained from the SAP, CURDI and CELL computer programs are also given.

Each presentation of theoretical and experimental results is accompanied by interpretation and discussion with special reference to correlations and corroborations between the sets of results, checks for superposition and symmetry, evaluation of the effect of the midspan diaphragm, and comparisons with results from a previous study of a similar straight bridge [9, 10, 11]. Where possible, implications of the results with regard to design are considered.

Of particular interest from a load distribution standpoint at the working stress level is how accurate the proposed theoretical methods predict the results found in the experimental study with respect to the following two important items for a load anywhere on the bridge.

1. The total moment at the midspan Sections A and D and at the support Sections B and C.

2. The transverse distribution of these total moments at a section across the width of the bridge.

General detailed tables comparing theoretical and experimental results for reactions, deflections, strains, longitudinal stresses and moments are given in Volume III for all load cases considered. Selected typical cases are taken from these tables and discussed in detail in the present volume. Results for dead load and for live loads producing a working stress of 30 ksi in the steel reinforcement are considered at length. Response of the bridge at and after overload stresses of 40, 50 and 60 ksi in the reinforcement is also examined. The linearity of the structural response during the overloading as well as afterwards is studied.

Attention is paid to the interpretation and applicability of theoretical results given by different analytical models. The relative merits of the folded plate (CURDI program) and finite element (CELL program) approaches are discussed, and comparisons are also made with results obtained by idealizing the box girder bridge model as a three dimensional frame composed of one dimensional members (SAP program).

In addition, the whole scheme of cataloguing, classifying and editing experimental data in several specially prepared computer programs giving normalized results for comparison with theoretical values is also treated. These comparisons are made mainly for reactions, deflections, strains and moments. In most cases, pertinent theoretical and experimental data are presented in the text.

A study is also made of the history of strains at different locations in the box girder bridge model. The deterioration of the structure after the completion of each succeeding load phase and as indicated by cracking patterns for each load phase is presented.

The loading to failure and observations of structural behavior during this final phase are considered in detail.

Lastly, a critical evaluation of the entire experimental study, incorporating conclusions reached and recommendations for implementation is presented.

2. THEORETICAL ANALYSES

2.1 General Remarks

Three different analytical methods were used in various phases of the theoretical studies for the model. All three assume the bridge model to be an elastic, homogeneous, isotropic and uncracked concrete structure. The computer programs associated with these three analytical solutions are entitled: (1) SAP; (2) CURDI; and (3) CELL. A brief description of these programs is given below.

SAP program (1972) [34]

The purpose of this program is to perform linear elastic analyses of three dimensional structural systems. These systems may be composed of combinations of a number of structural element types. For the bridge model studies, SAP was only used to analyze the bridge structure as an idealized three dimensional frame made up of one dimensional beam and column members.

CURDI Program (1973) [35]

This program is capable of analyzing prismatic folded plate structures, which are circular in plan and made up of orthotropic plate elements. The structure must be simply supported by rigid radial diaphragms at its two ends and may have up to twelve interior diaphragms or supports between the two ends. Diaphragms may be defined by flexible beams and supports may be defined by two dimensional planar rigid frame bents. Options permit evaluation of the internal forces in the frame bents as well as in the plate elements of the bridge. Each plate element is idealized by a number of circumferential finite strips. The finite strip method is used to determine the strip stiffness. The displacement patterns are assumed to vary as harmonics in the circumferential direction. In the transverse direction, a linear variation of the in plane displacements and a cubic variation of the normal displacements are chosen. A direct stiffness harmonic analysis is used to analyze the assembled folded plate system. Compatibility at the interior diaphragms or supports is accomplished by the force method of analysis. Loads and redundant forces may be approximated by up to 100 non-zero terms of the appropriate Fourier series.

CELL Program (1970) [7]

> This finite element program analyzes cellular structures of constant depth with arbitrary plan geometry. The structure must be made up of top and bottom decks and vertical webs and diaphragms. Two different finite element types incorporating both membrane and plate bending effects are used to capture the main behavior of the deck and web components. Each of these elements has five degrees of freedom at its corner nodes. Orthotropic plate properties and arbitrary loadings and boundary conditions can be treated. Automatic element and coordinate generation options minimize the required input data.

CURDI, which is an extension of an earlier program CURSTR [6], and CELL are two of a number of computer programs, which have been developed especially for box girder bridges at the University of California. A summary of the various analytical solutions and computer programs developed may be found in Reference [19]. Details of each of these programs including input-output formats and Fortran source listings, are given in the research reports [1 to 13].

2.2 SAP Analysis

For the SAP analyses the bridge was assumed to be a simple three dimensional frame made up of straight one dimensional beam and column members. The 72 ft. long, horizontally curved bridge is idealized by dividing it into 24 straight segments lying in a horizontal plane. The section properties of each of these one dimensional members is obtained by considering the entire four cell bridge cross-section, Fig. 1.3, as an uncracked beam section. In calculating the section properties the fillets were ignored and the cantilever edges were taken as having a constant average thickness of 0.255 ft. The center of bottom slab to center of top slab cross-sectional depth was 1.539 ft. The centroid of the cross-section was found to be 0.852 ft. above the mid-depth of the bottom slab or 0.687 ft. below the mid-depth of the top slab. The section and material properties used for the bridge one dimensional members were taken as follows:

Axial Area	=	A_x = 5.62 ft.^{2}
Shear Area	=	A_y shear deformations neglected as small
Shear Area	=	A_z shear deformations neglected as small
Torsion Constant	=	J_x = 7.67 ft.^{4}
Moment of Inertia	=	I_y = 2.64 ft.^{4} (horizontal axis)
Moment of Inertia	=	I_z = 66.83 ft.^{4} (vertical axis)
Modulus of Elasticity	=	E = 400,000 ksf
Poisson's Ratio	=	ν = 0.15

The above E was taken as an approximate average of the actual measured E values for the top and bottom slab concrete in the model.

The center bent column was idealized by two members. The first was a rigid and one dimensional member extending from the centroid of the bridge cross-section to the mid-depth of the bottom slab and was therefore 0.852 ft. long. The second was a member, with a 1.5 ft. diameter cross-section, extending from the mid-depth of the bottom slab to the top of the footing and was taken to be 2.600 ft. long. This member's properties were taken as follows:

Axial Area	=	A_x = 1.767 ft.^{2}
Shear Area	=	$A_y = A_z$ = 1.767 ft.^{2}
Torsion Constant	=	J_x = 0.498 ft.^{4}
Moment of Inertia	=	$I_y = I_z$ = 0.249 ft.^{4}
Modulus of Elasticity	=	E = 498,000 ksf
Poisson's Ratio	=	ν = 0.15

All load cases were analyzed using two different boundary conditions. In the first, designated SAPX, the two end supports were assumed to be restrained only against vertical displacement and rotation about the longitudinal axis of the bridge, while the center support under the column was assumed completely fixed against all three translations and three rotations. The second analysis, designated SAPXR, had identical boundary conditions to SAPX, except for the addition of a horizontal radial restraint against displacement at each of the two end supports. The results for vertical deflections, and for bending moments about the horizontal axis of the bridge were essentially the same from the two analyses for all load conditions. The end and center reactions were also very similar with the important exception that for the SAPX solution no force reactions in a horizontal plane were developed, while for SAPXR they were. The latter developed a couple due to the vertical lever arm between the horizontal reactions at the end supports and the bottom of the center column support, which came into play primarily for the highly eccentric loads on the bridge deck. For SAPX, internal bending moments only about the horizontal axis of the bridge and torques were developed, while for SAPXR, internal bending moments about both the horizontal and vertical axes of the bridge cross-section and torques were developed.

While the differences in the results were not large for the bridge model, which had a relatively short column, they could be considerably larger for bridge decks on long columns. This emphasizes that the boundary conditions assumed in an analysis should reflect the true conditions existing in an actual three dimensional structure, such as a complex bridge system. In the test program on the bridge model, as explained in Section 3.4 of Volume I, the end supports were designed to permit horizontal displacements in both radial and tangential directions, thus simulating the assumptions used in the SAPX analysis.

It is obvious that the SAP analyses can only be used to give an indication of the longitudinal distribution of total reactions, moments and torques, but they give no information on the transverse distribution of these quantities or the internal membrane forces and plate bending moments in each element which are obtained from the more complex CURDI and CELL programs.

Results obtained from the SAPX analysis for all load cases of interest are presented in Figs. 2.1 to 2.17. These values of reactions, deflections, moments and torques form a useful convenient reference. It will be of particular interest to study whether this relatively simple three dimensional frame analysis can be used to accurately predict the total reaction and moments found from the more complete folded plate analyses by CURDI and CELL as well as those found from the experimental results.

A careful study of Figs. 2.1 to 2.17 gives considerable information regarding the structural behavior of the bridge as the applied point loads are moved successively from inner girder 1, to center girder 3 and finally to outer girder 5.

First considering the reactions, Figs. 2.2, 2.6, 2.10, the vertical reaction at the center footing gets progressively larger and conversely the vertical reactions at the end support get smaller as the loads move from girder 1 to 3 to 5. The moment due to the eccentric loading is taken partly by the couple formed by these vertical reactions

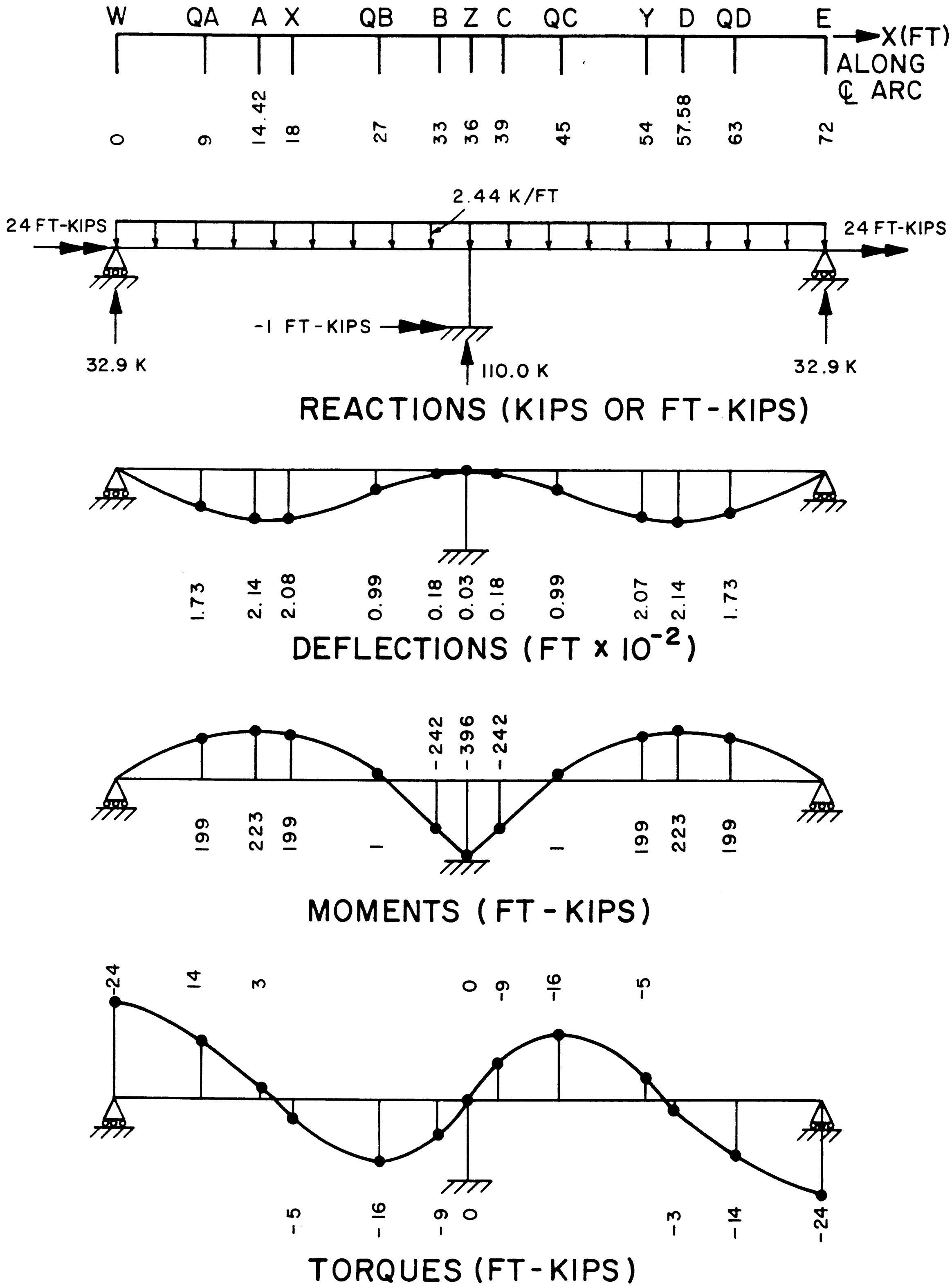

FIG. 2.1 SAPX RESULTS FOR DEAD LOAD

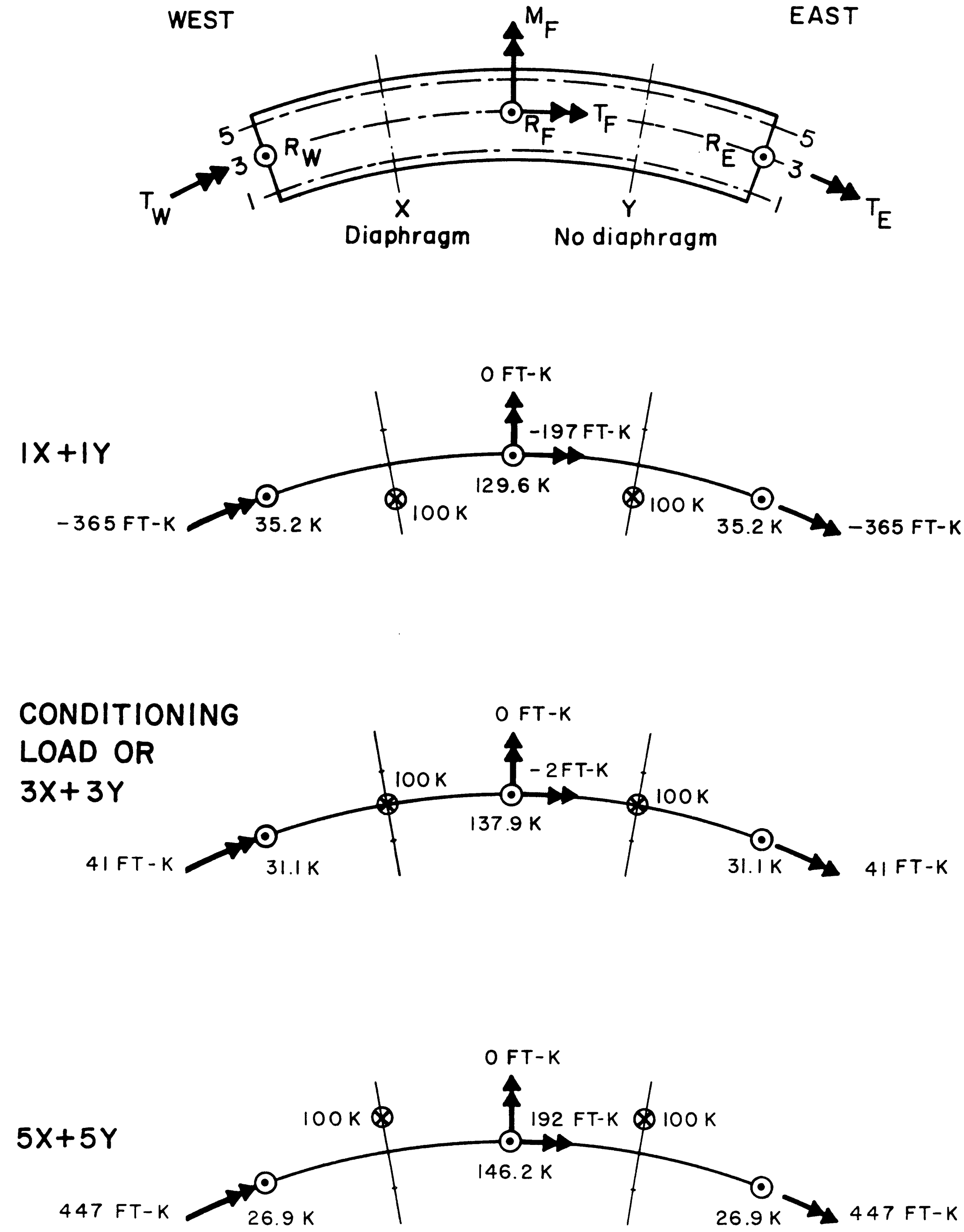

FIG. 2.2 SAPX REACTIONS (KIPS OR FT-KIPS) FOR 100 KIP MIDSPAN LOADS AT 1X+1Y, CONDITIONING LOAD OR 3X + 3Y, 5X + 5Y

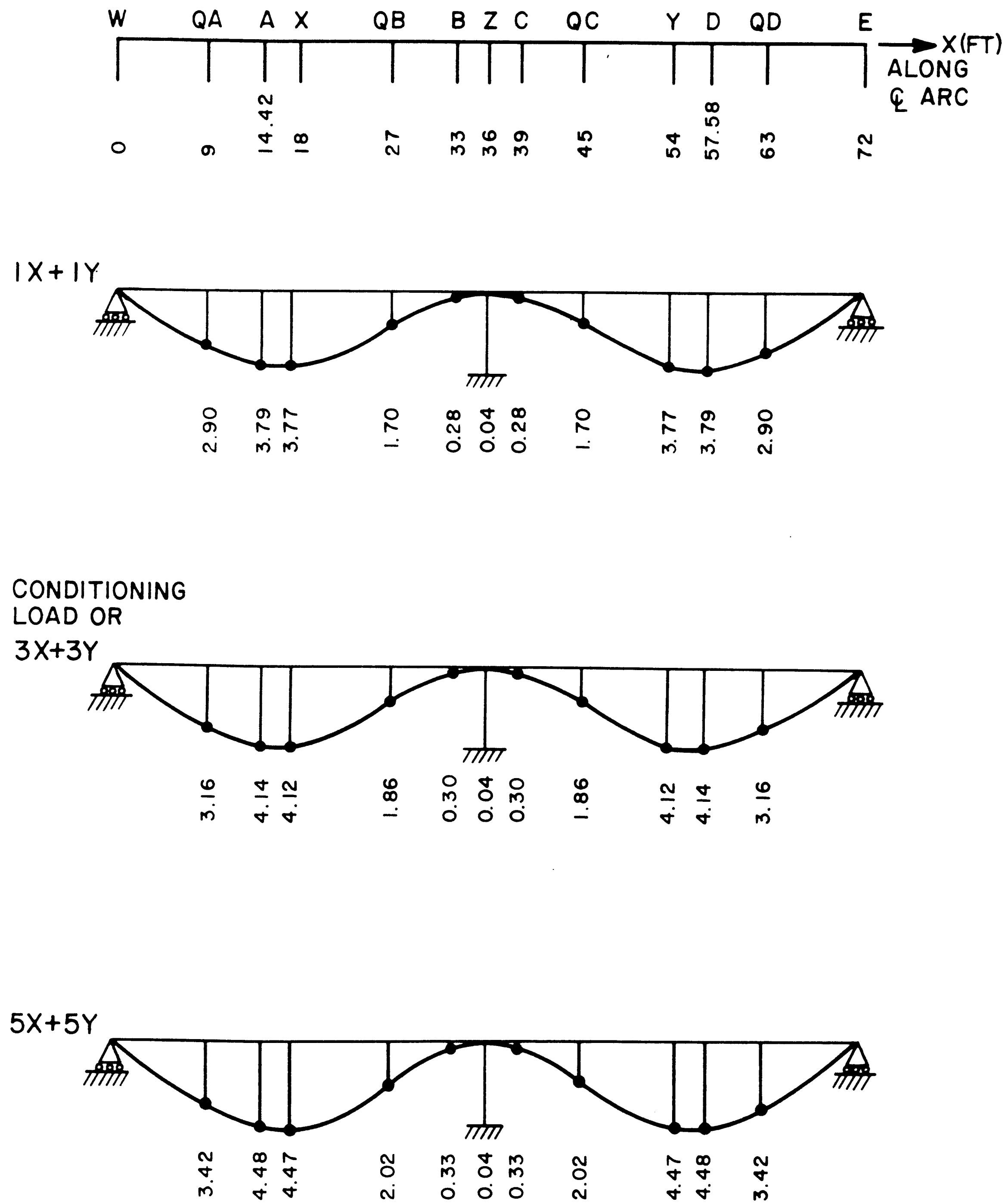

FIG. 2.3 SAPX LONGITUDINAL DISTRIBUTION OF DEFLECTIONS (FT X 10^{-2}) AT CENTER GIRDER 3 FOR 100 KIP MIDSPAN LOADS AT 1X+1Y, CONDITIONING LOAD OR 3X+3Y, 5X+5Y

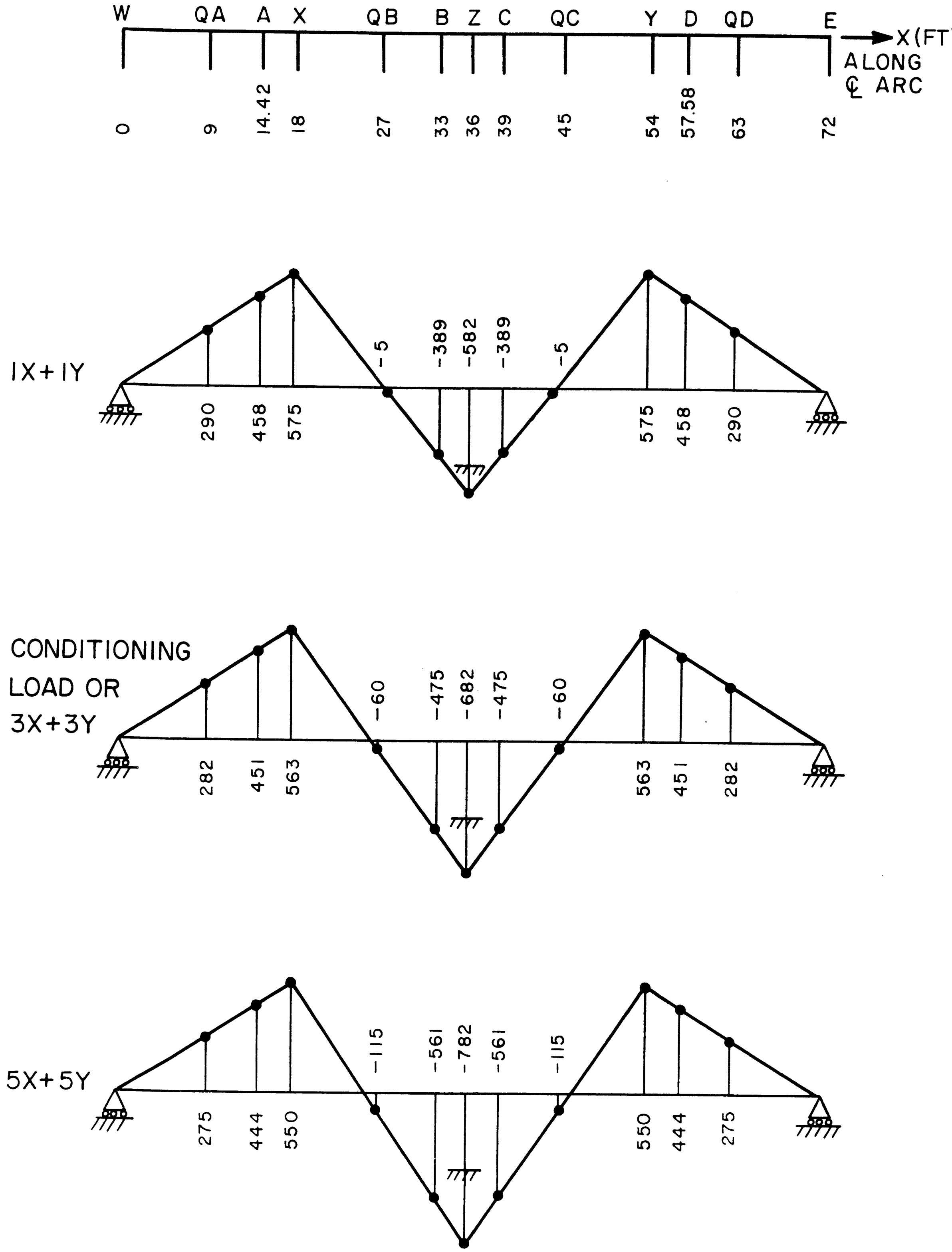

FIG. 2.4 SAPX LONGITUDINAL DISTRIBUTION OF MOMENTS (FT–KIPS) FOR 100 KIP MIDSPAN LOADS AT 1X + 1Y, CONDITIONING LOAD OR 3X + 3Y, 5X + 5Y

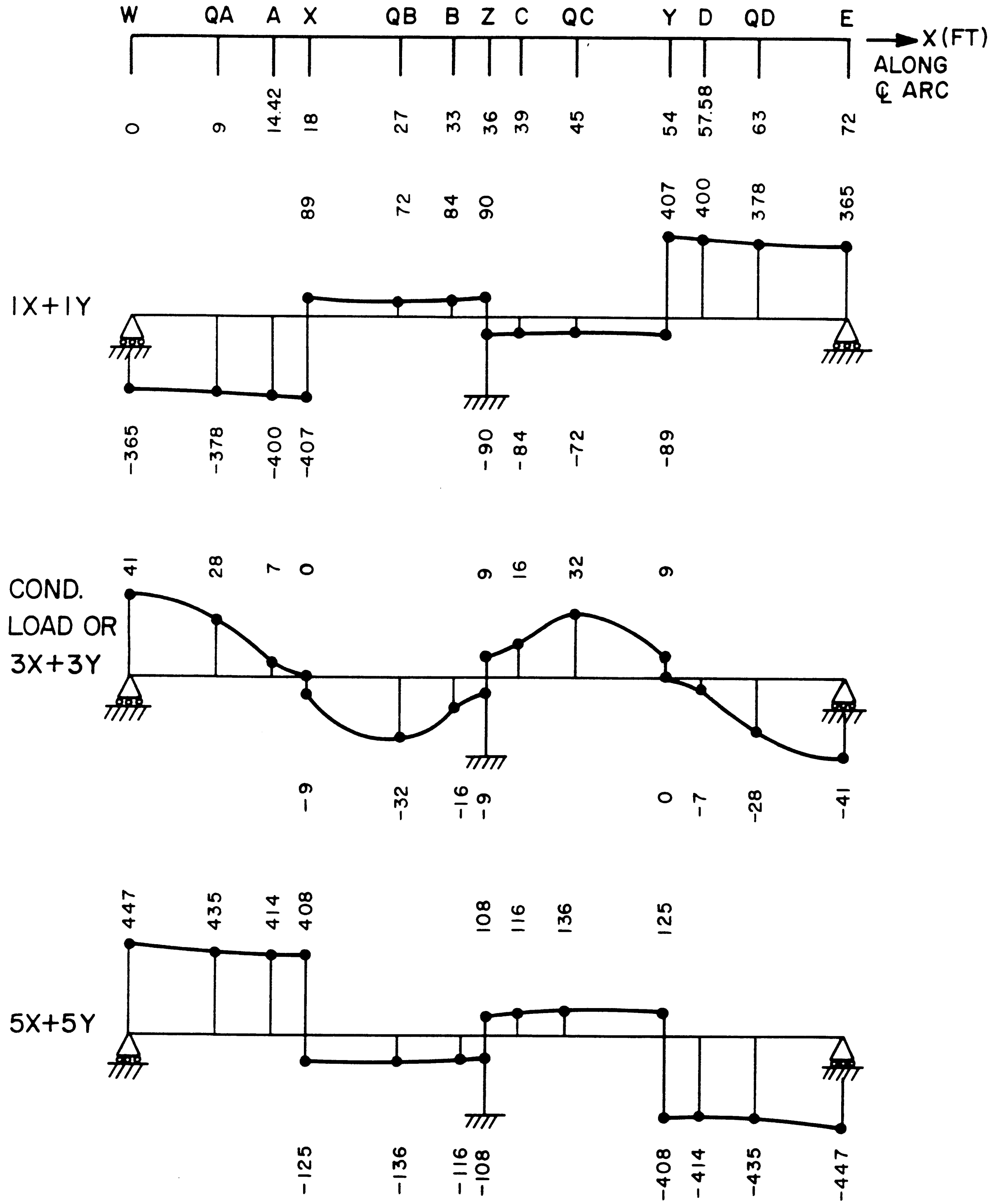

FIG. 2.5 SAPX LONGITUDINAL DISTRIBUTION OF TORQUES (FT-KIPS) FOR 100 KIP MIDSPAN LOADS AT 1X+1Y, CONDITIONING LOAD OR 3X+3Y, 5X+5Y

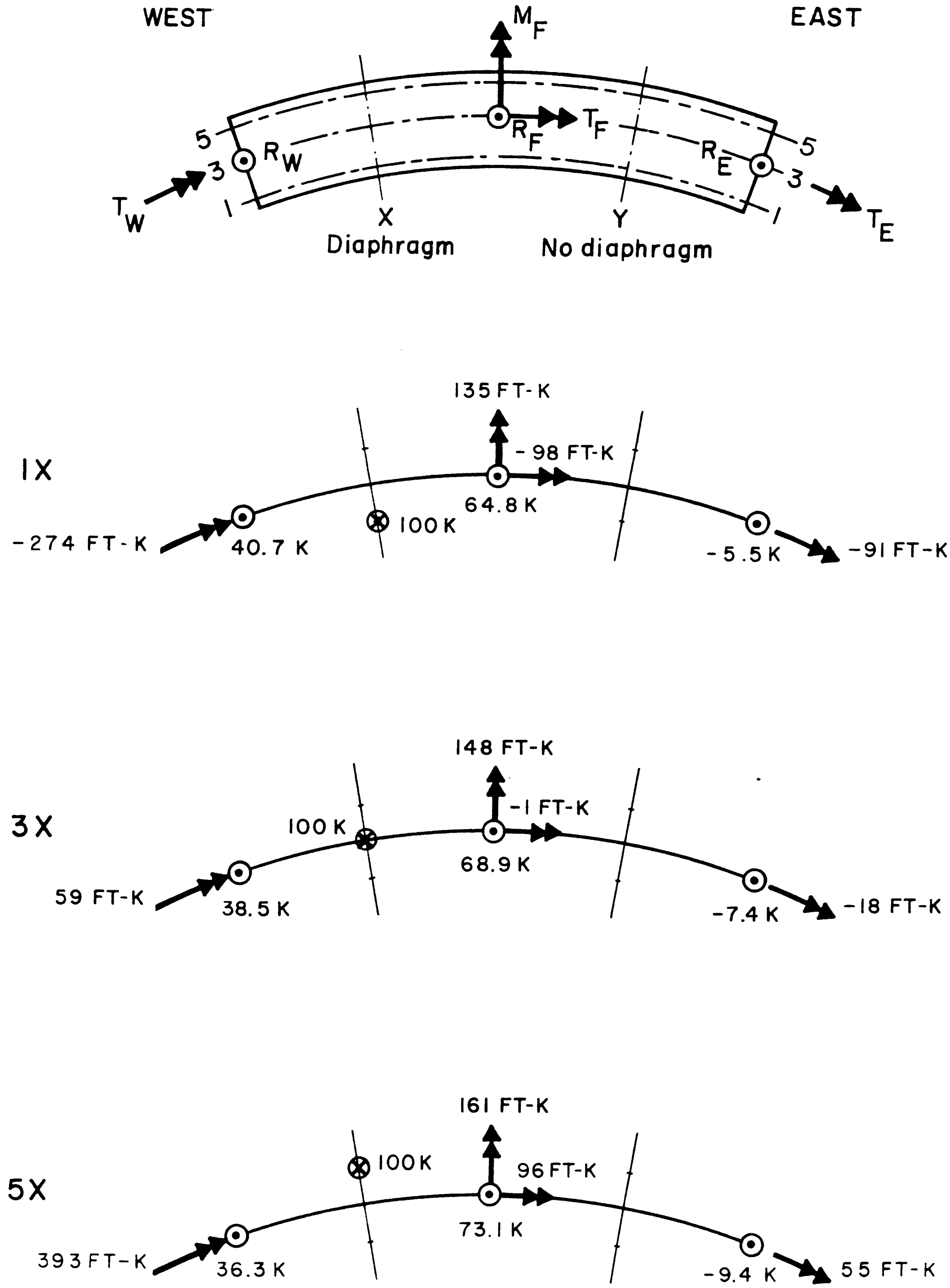

FIG. 2.6 SAPX REACTIONS (KIPS OR FT-KIPS) FOR 100 KIP MIDSPAN LOADS AT 1X, 3X, 5X

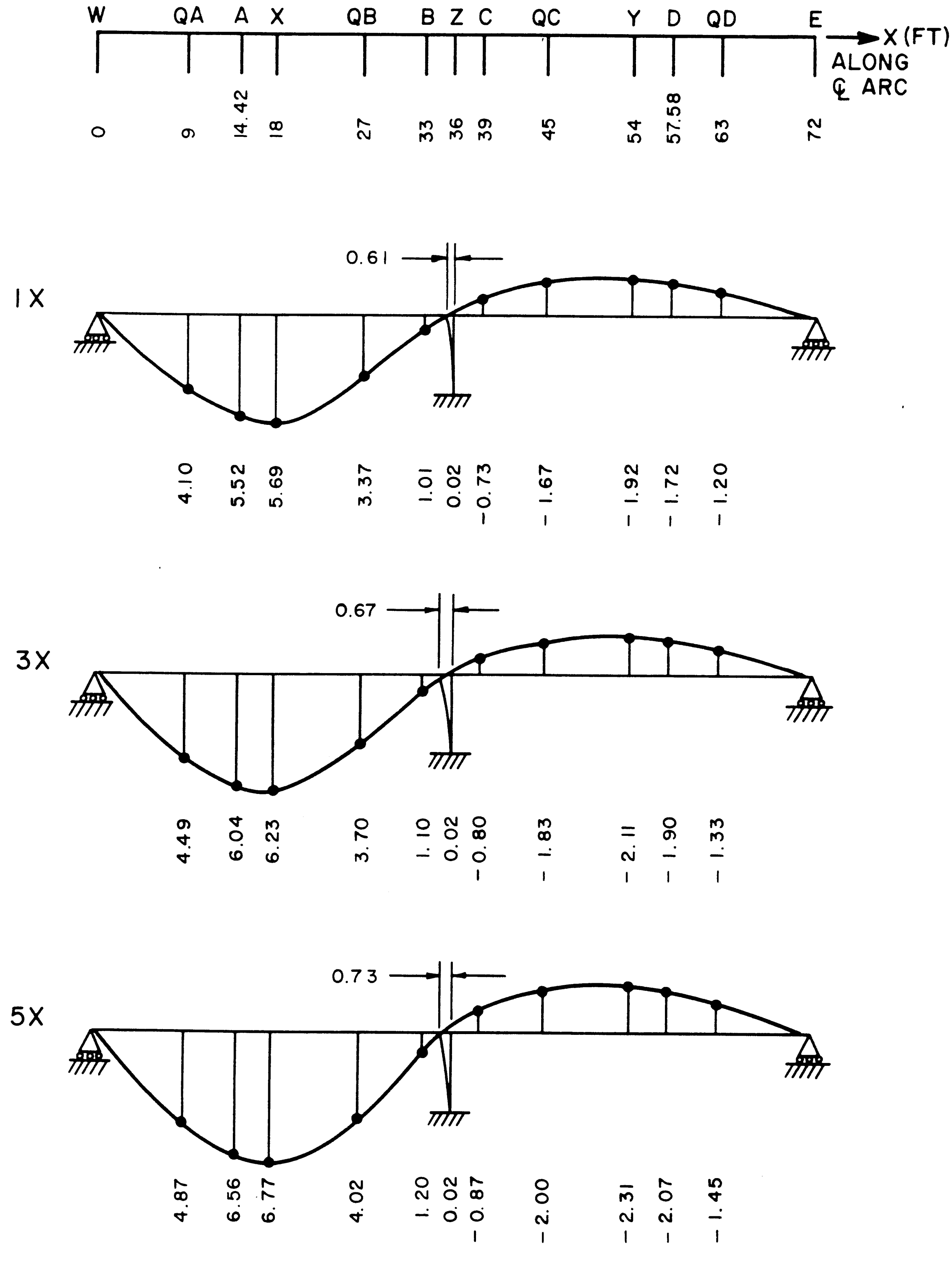

FIG. 2.7 SAPX LONGITUDINAL DISTRIBUTION OF DEFLECTIONS (FT X 10^{-2})
AT CENTER GIRDER 3 FOR 100 KIP MIDSPAN LOADS AT 1X, 3X, 5X

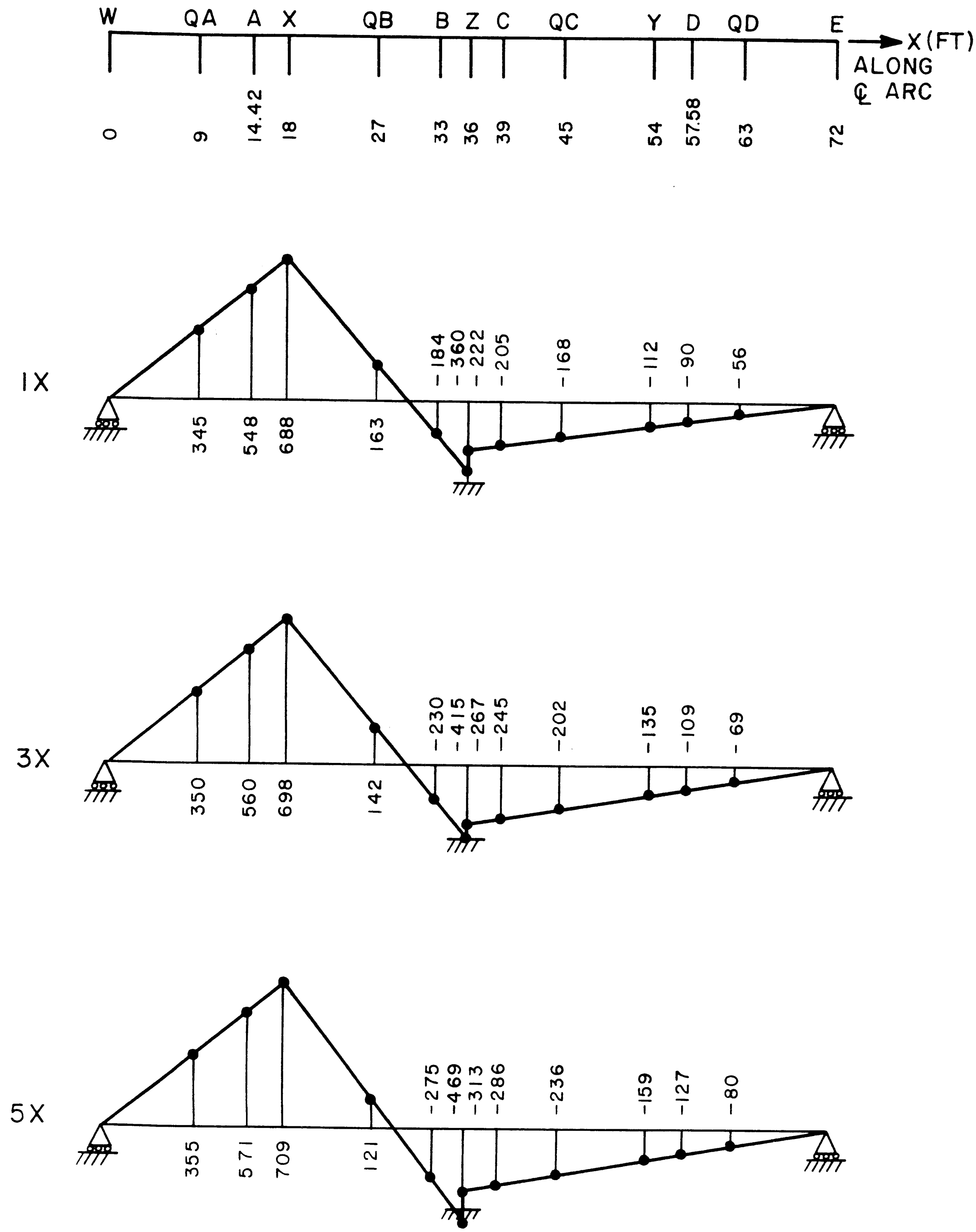

FIG. 2.8 SAPX LONGITUDINAL DISTRIBUTION OF MOMENTS (FT-KIPS) FOR 100 KIP MIDSPAN LOADS AT 1X, 3X, 5X

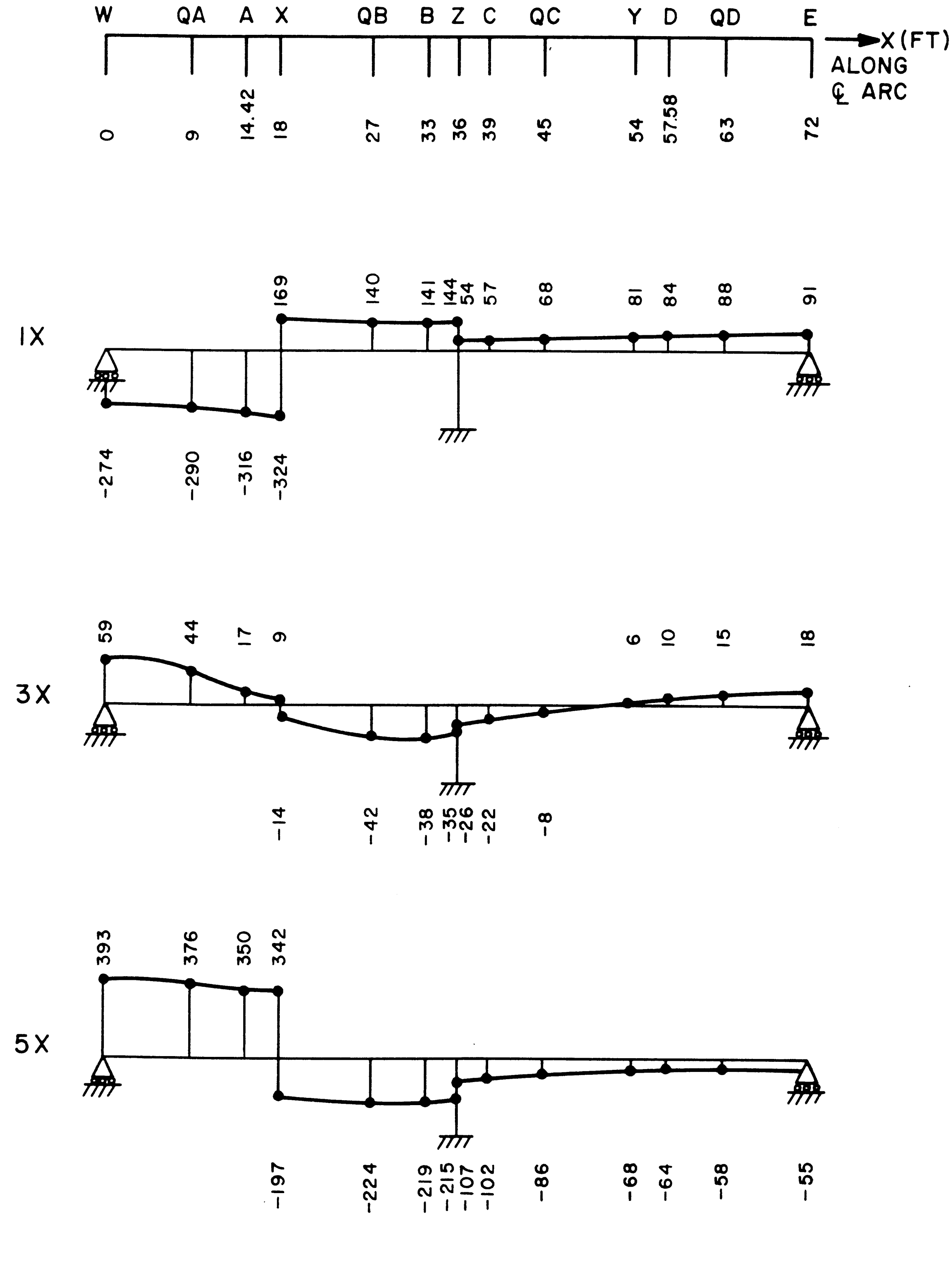

FIG. 2.9 SAPX LONGITUDINAL DISTRIBUTION OF TORQUES (FT-KIPS) FOR 100 KIP MIDSPAN LOADS AT 1X, 3X, 5X

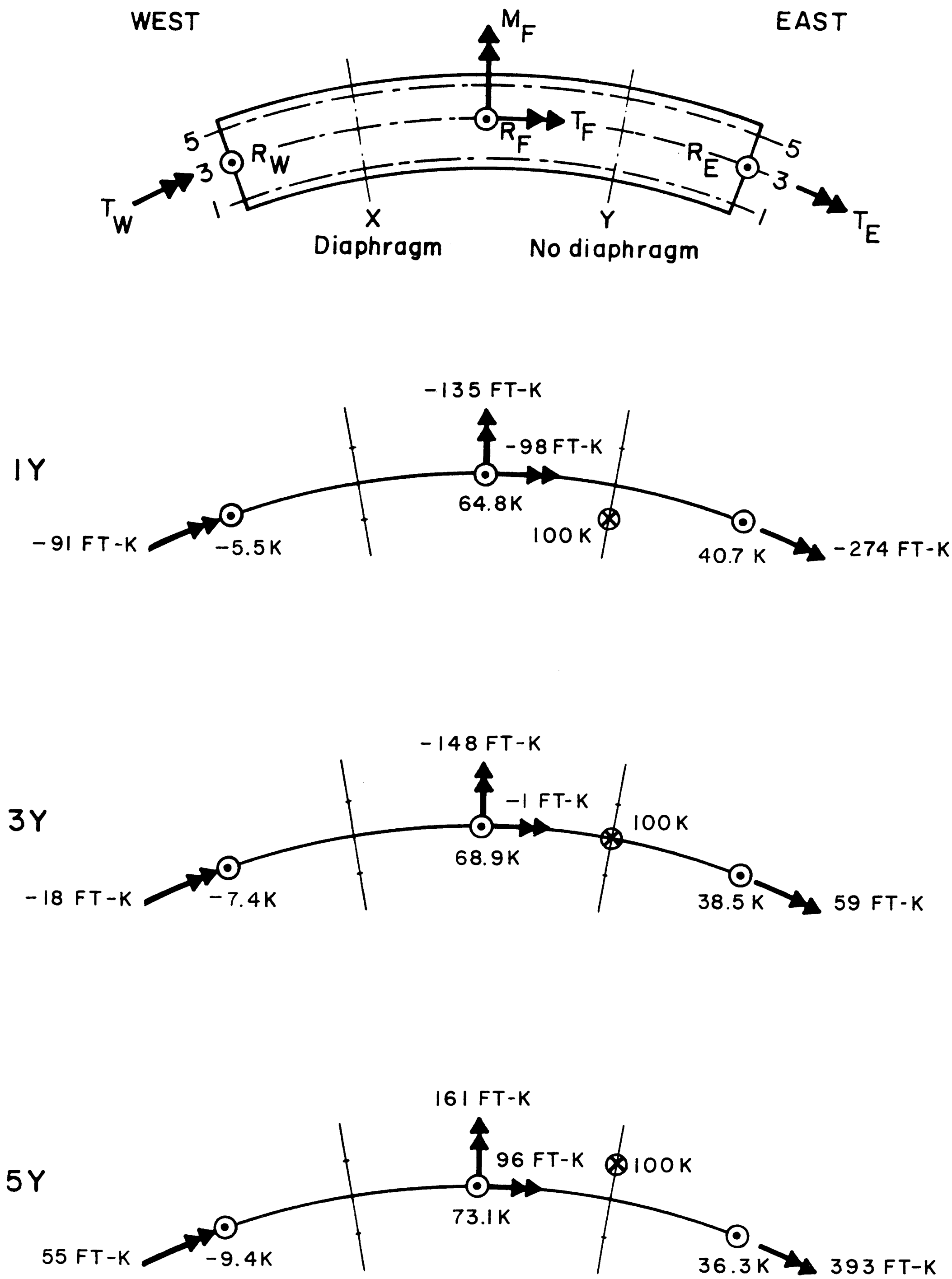

FIG. 2.10 SAPX REACTIONS (KIPS OR FT-KIPS) FOR 100 KIP MIDSPAN LOADS AT 1Y, 3Y, 5Y

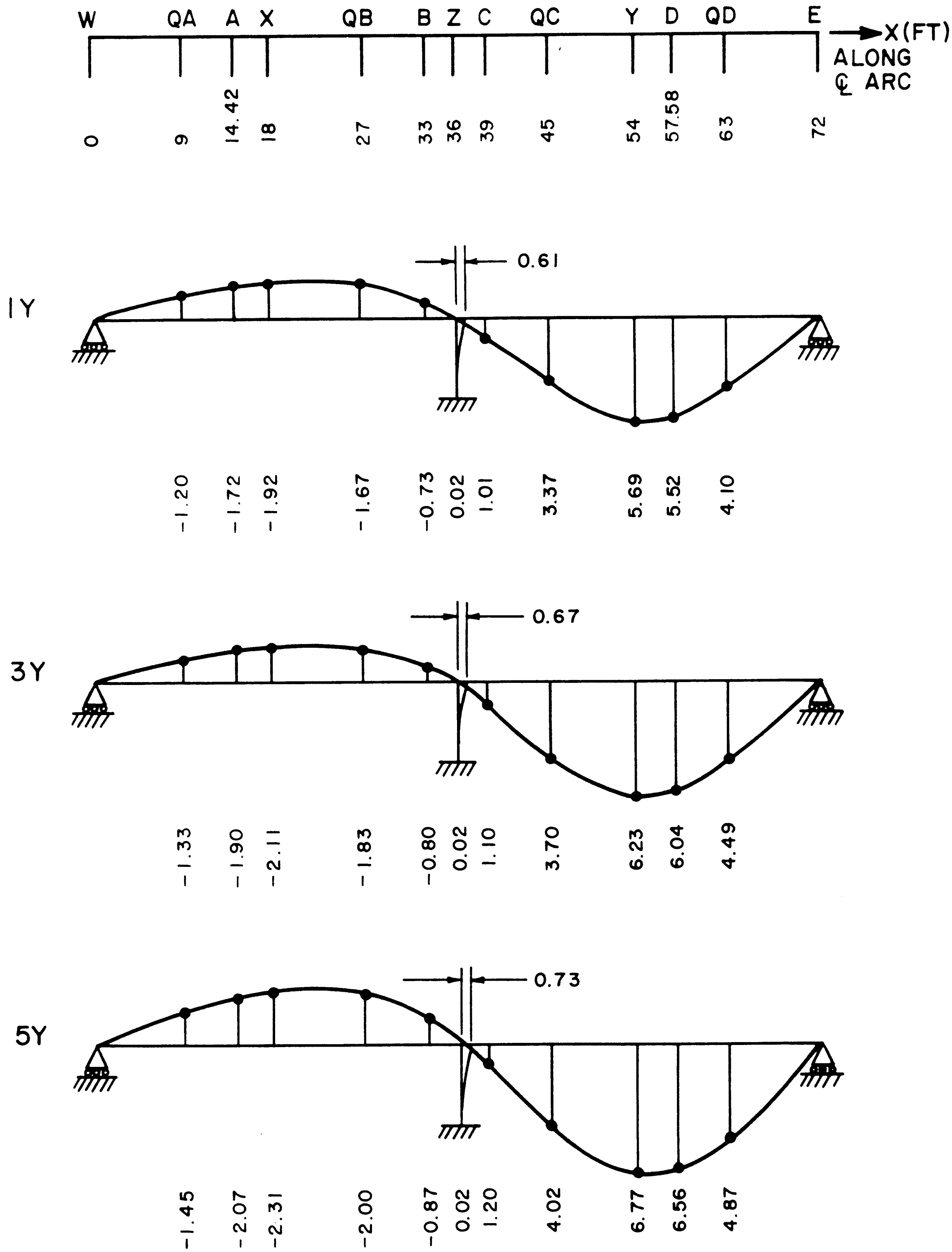

FIG. 2.11 SAPX LONGITUDINAL DISTRIBUTION OF DEFLECTIONS (FT X 10^{-2}) AT CENTER GIRDER 3 FOR 100 KIP MIDSPAN LOADS AT 1Y, 3Y, 5Y

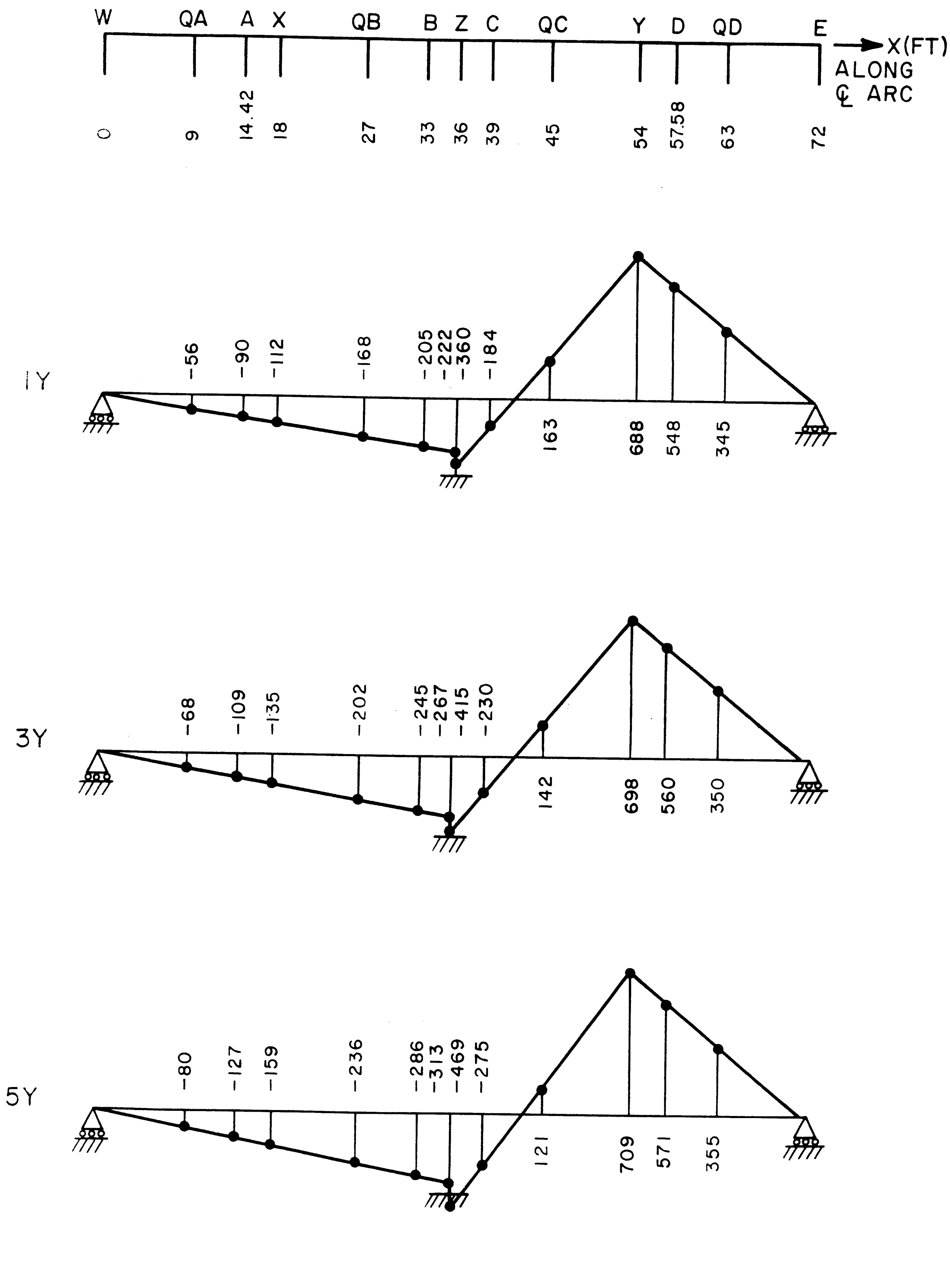

FIG. 2.12 SAPX LONGITUDINAL DISTRIBUTION OF MOMENTS (FT-KIPS) FOR 100 KIP MIDSPAN LOADS AT 1Y, 3Y, 5Y

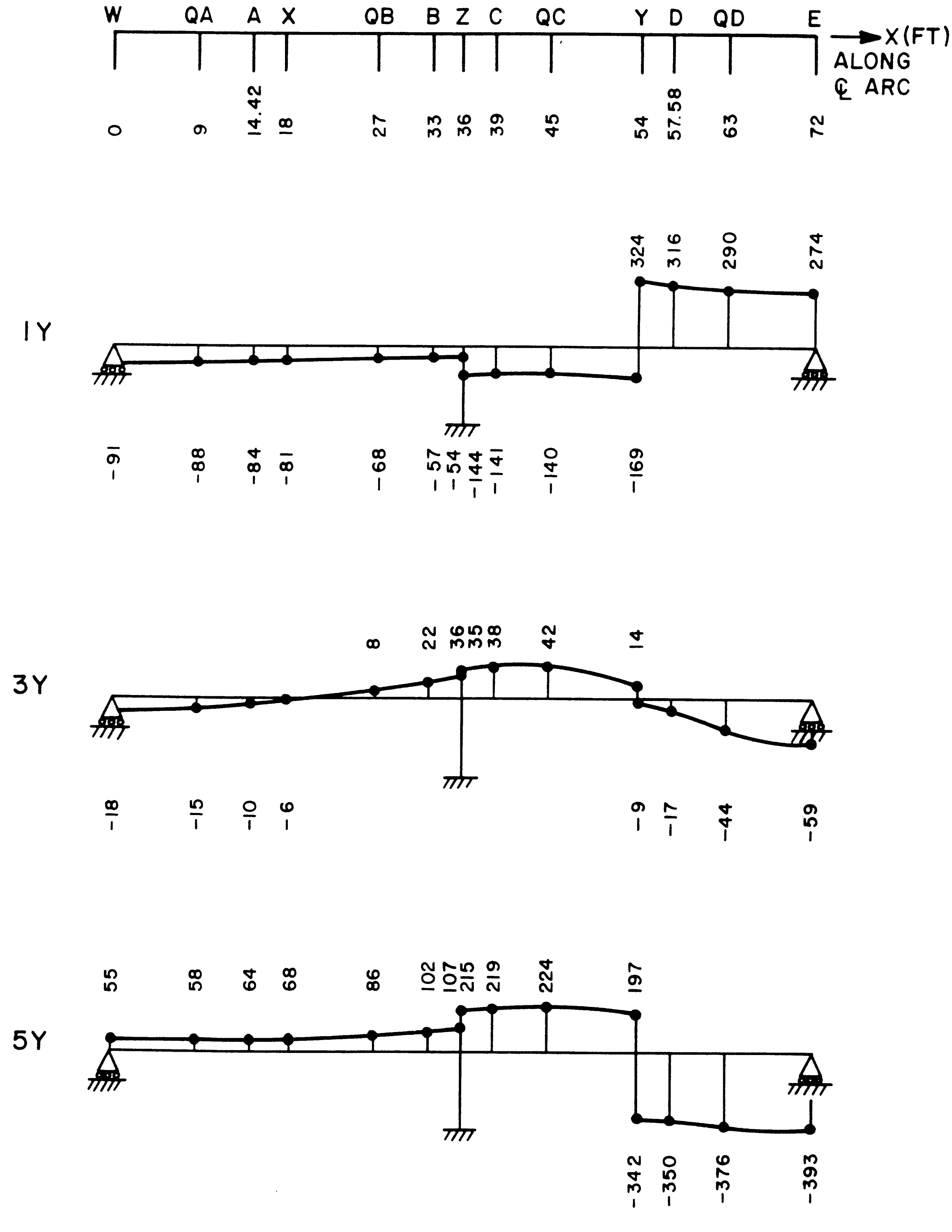

FIG. 2.13 SAPX LONGITUDINAL DISTRIBUTION OF TORQUES (FT-KIPS) FOR 100 KIP MIDSPAN LOADS AT 1Y, 3Y, 5Y

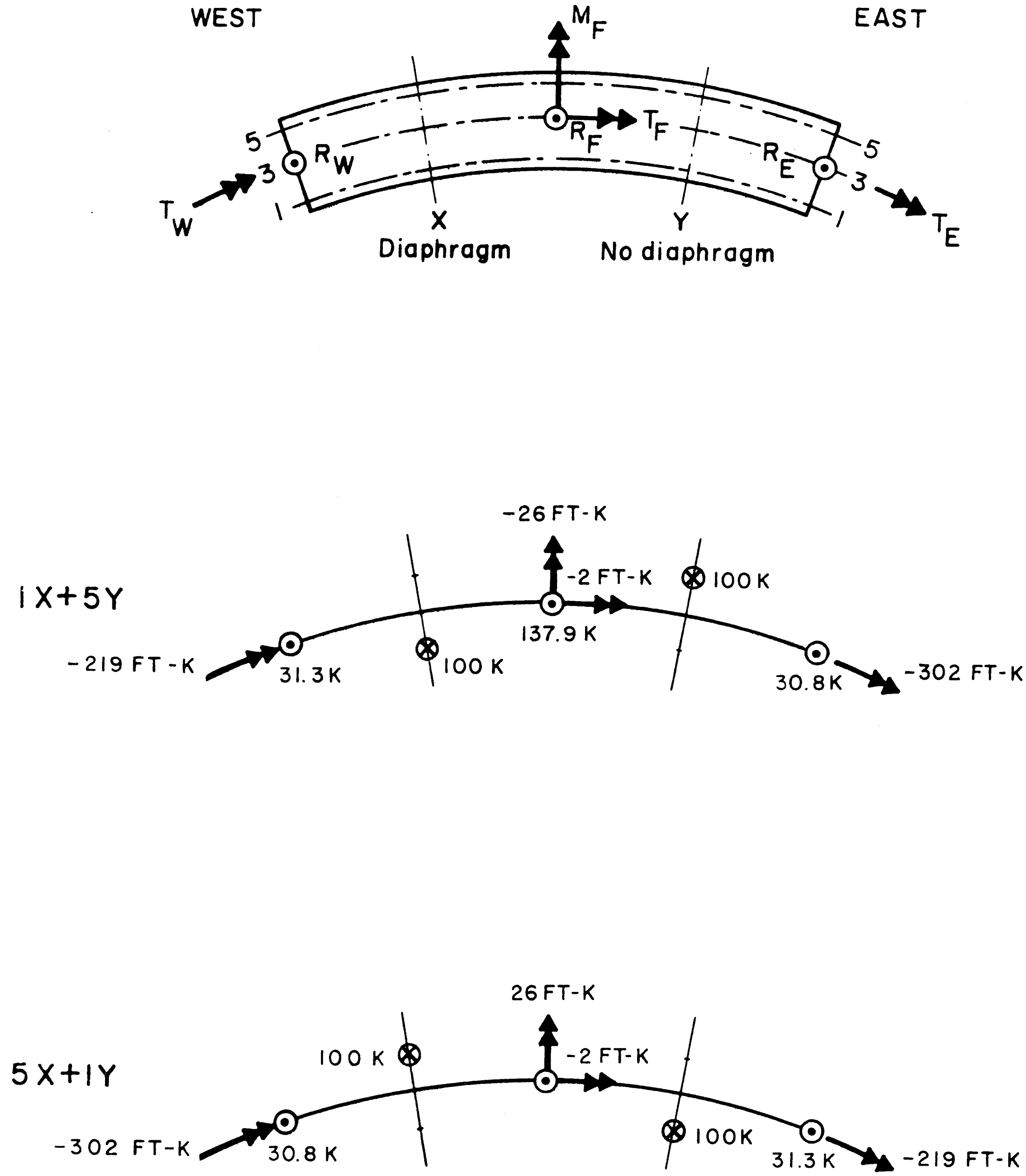

FIG. 2.14 SAPX REACTIONS (KIPS OR FT-KIPS) FOR 100 KIP MIDSPAN LOADS AT 1X+5Y, 5X + 1Y

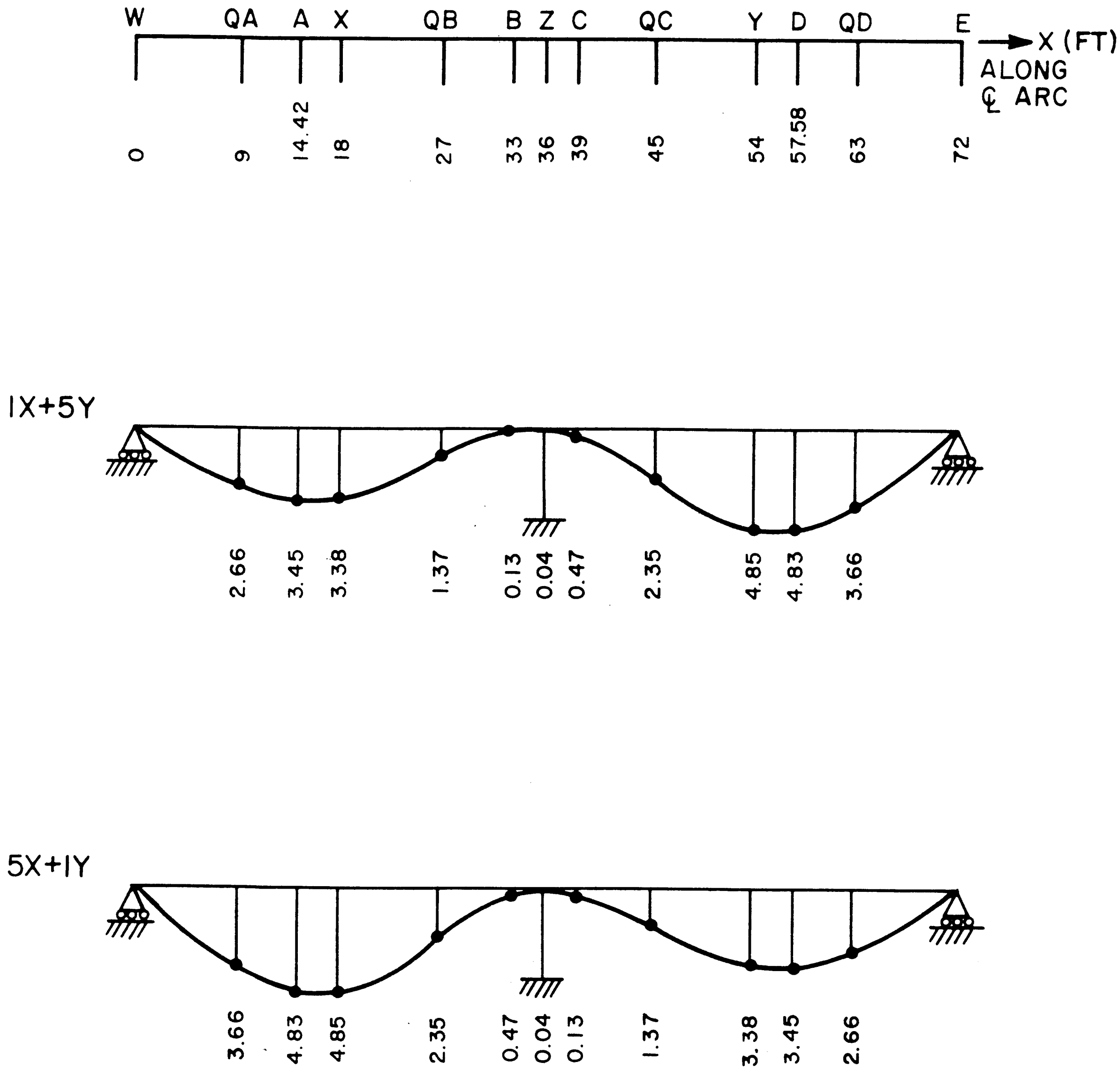

FIG. 2.15 SAPX LONGITUDINAL DISTRIBUTION OF DEFLECTIONS ($FT \times 10^{-2}$) AT CENTER GIRDER 3 FOR 100 KIP MIDSPAN LOADS AT 1 X + 5 Y, 5 X + 1 Y

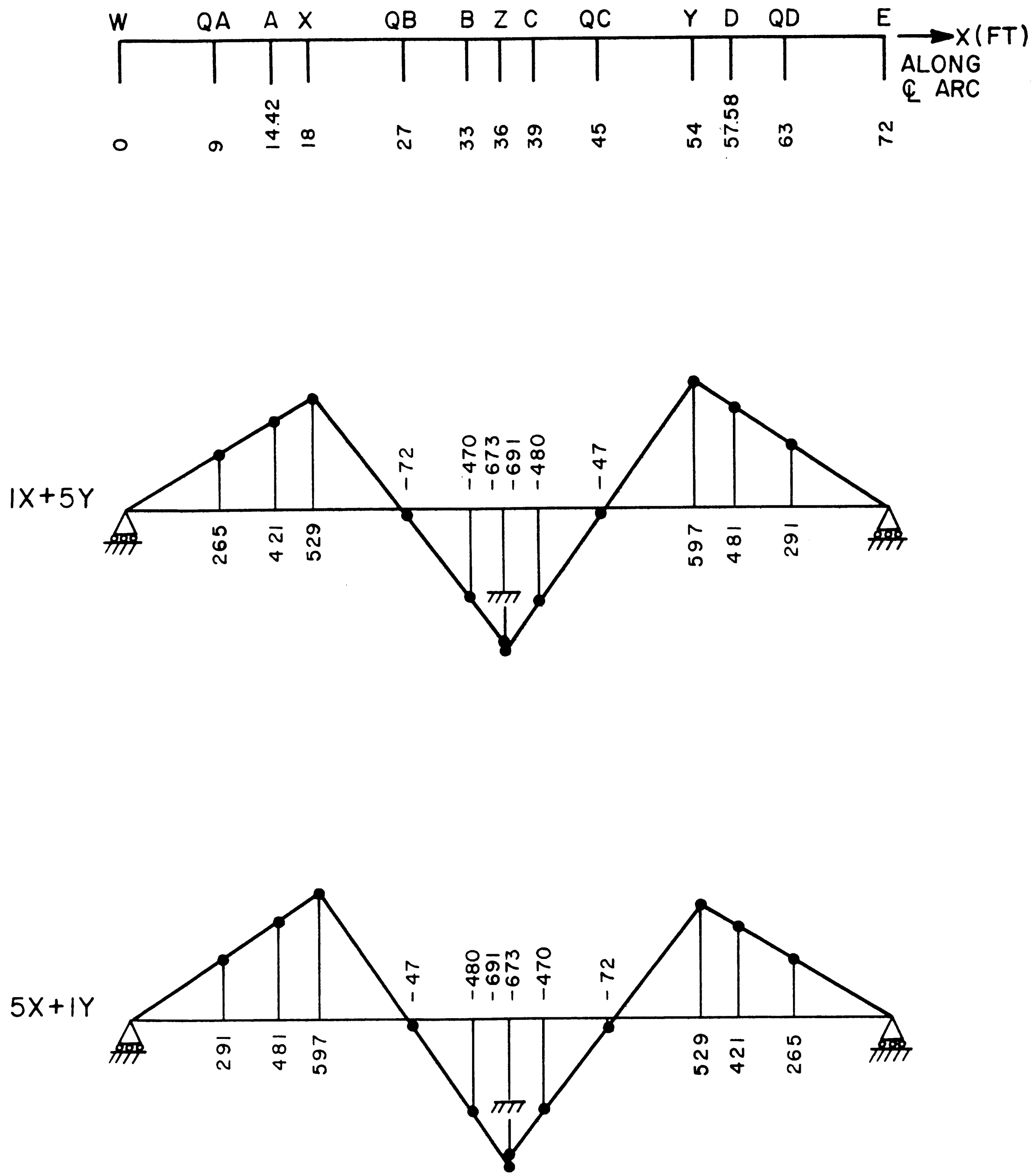

FIG. 2.16 SAPX LONGITUDINAL DISTRIBUTION OF MOMENTS (FT-KIPS) FOR 100 KIP MIDSPAN LOADS AT 1X + 5Y, 5X + 1Y

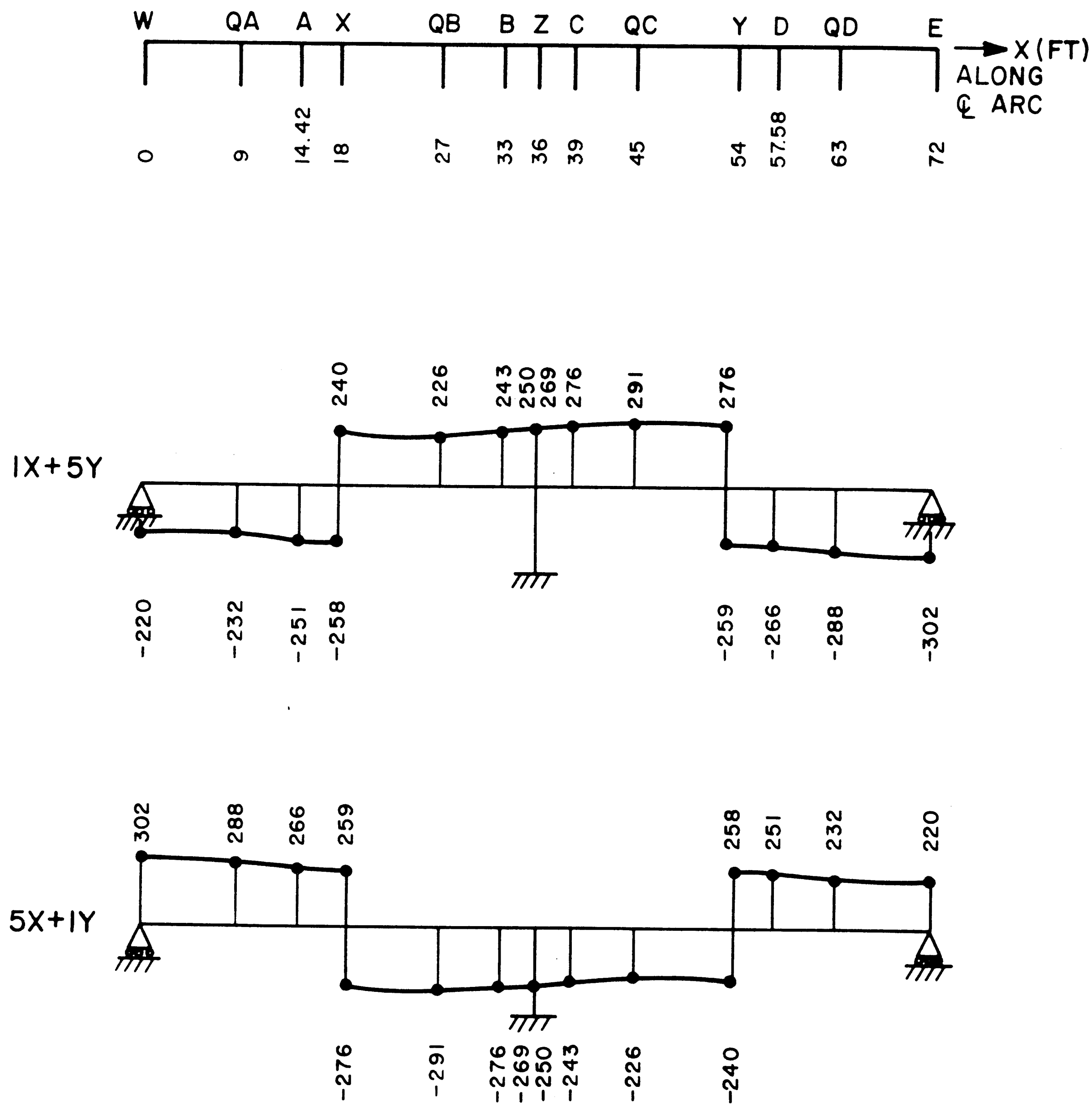

FIG. 2.17 SAPX LONGITUDINAL DISTRIBUTION OF TORQUES (FT-KIPS) FOR 100 KIP MIDSPAN LOADS AT 1X + 5Y, 5X + 1Y

and partly by the reaction torques. The latter, of course, reverse directions as the loads move from girder 1 to 3 to 5.

For deflections, Figs. 2.3, 2.7, 2.11, as would be expected, the values become larger as the loads move from girder 1 to 3 to 5.

The bending moments shown in Figs. 2.4, 2.8, 2.12 reveal the interesting fact that the changes in the positive moments in the loaded spans are very small compared to the changes in the negative moments over the support as the loads move from girder 1 to 3 to 5.

For torques, Figs. 2.5, 2.9, 2.13, as would be expected, the values are quite small for loads on girder 3 and much larger for loads on girders 1 and 5. Also it can be seen that much larger torques occur in the regions between the end supports and the midspan sections than in the rest of the bridge.

2.3 CURDI Analysis

For the CURDI analyses, 100 harmonics were used to approximate the applied loading in each case. This program treats the center single column bent as a transverse planar rigid frame, and therefore it cannot account for the longitudinal bending moment developed at the base of the column under unsymmetrical loading in the two spans. For symmetrical loadings it yields very accurate results. This has been verified in a study [16] recently made in which theoretical results obtained with CURSTR [6], of which CURDI is an extension, were compared with experimental results from tests on a number of curved, four cell, small scale elastic aluminum models.

In CURDI, the diaphragms at the end supports are assumed to be infinitely rigid in their own plane and perfectly flexible normal to their own plane. For this reason, the end boundary conditions are similar to those of SAPXR in which end supports are restrained against vertical and radial displacements and rotation about the longitudinal axis of the bridge. Because of this, all solutions obtained by CURDI have been entitled CURDXR in the tables. The center bent support for the cellular bridge was assumed to be 1.90 ft. thick, which was the diaphragm thickness. The column of the center bent support was assumed to have the same properties used in the SAP analyses (Section 2.2) and it was fixed at the base.

The bridge cross-section was assumed to be prismatic and the following average values of moduli of elasticity, taken from the experimental data, were used in the analysis of the uncracked concrete section.

Top slab	-	417,600 ksf
Bottom slab	-	381,600 ksf
Webs	-	381,600 ksf
Column	-	498,000 ksf

Poisson's ratio was taken as 0.15

A comparison of theoretical results obtained by CURDI (entitled CURDXR) with those from other methods is presented in Section 2.5. Because of its proven accuracy in comparisions with results from the aluminum model studies [16] mentioned earlier, the results from CURDI can be used to check the accuracy of the CELL results.

2.4 CELL Analysis

For the finite element analyses using the CELL program, the bridge was subdivided transversely by selecting nodal points at the top and bottom of each web and at the edges of the cantilever. This resulted in 17 finite elements transversely, which included two of zero thickness for the bottom slab elements directly below the top flange cantilever elements at the edges. Longitudinally the bridge was divided into 30 segments. Including diaphragms, a total of 534 finite elements connecting a total of 434 nodal points were used for the analytical model. Since each nodal point had 5 degrees of displacement freedom, each load case involved the solution of 5(434) = 2170 simultaneous equations.

The moduli of elasticity used were identical to those used for CURDXR (Section 2.4). Since CELL does not have an automatic provision for introducing the center column stiffness, it was modified especially for the bridge model, by adding this stiffness to the solution.

Because CELL permits the use of arbitrary boundary conditions at any of the nodal points as well as variations in element properties throughout the structure, three separate analyses were made: (1) CELLXR; (2) CELLX; and (3) CELL.

In CELLXR the assumptions used in the CURDXR solution were duplicated, with the exception that the center column was capable of carrying longitudinal as well as transverse moments at its base. For symmetrical loadings in the two spans, the results of CELLXR could be compared with CURDXR to establish the accuracy of the CELL program. CURDXR and CELLXR both had all nodal points at the end supports restrained radially as well vertically.

The CELLX solution conditions were identical to those of CELLXR, with the exception that now at the end supports the only restraints were at the nodal points at the bottom of each girder web.

These were restrained against vertical displacement only and thus simulated the actual support condition used in the bridge model.

The CELL solution conditions were identical to those of CELLX, with the exception that the flares in the girder webs at the end and center supports existing in the actual bridge model were accounted for by increasing the thickness of the finite elements in these zones in a stepped fashion. Since this solution simulated the bridge model in the closest manner possible, theoretical results from CELL were used in all detailed tables of comparison between experiment and theory presented in Volumes II and III.

A comparison of theoretical results obtained from CELLXR, CELLX and CELL with those from other methods is presented in Section 2.5.

2.5 Comparison of Theoretical Results for Curved Bridge Model

For comparison purposes the following load cases (described in detail in Chapter 5 of Volume I) were analyzed using the conditions previously described for SAPX, SAPXR, CURDXR, CELLXR, CELLX and CELL: (1) dead load of only the cellular portion of bridge, equivalent to 2.44 kips/ft.; (2) conditioning load; (3) point loads 1X + 1Y; (4) 3X + 3Y; (5) 5X + 5Y; (6) 1X; (7) 3X; (8) 5X; (9) 1Y; (10) 3Y; (11) 5Y; and (12) 1X + 5Y. Except for the dead load, the analyses in all cases were made for a normalized 100 kip load in the loaded spans. Longitudinal distributions of reactions, deflections, total moments at a section; and transverse distributions of deflections, total moments and longitudinal membrane forces N_x at a section were tabulated and compared.

The purpose of these theoretical studies was to answer several basic questions.

1. Can the simple three dimensional analysis using SAP be used to predict the longitudinal distribution of reactions, deflections and total moments found by the more complete folded plate analyses of CURDI and CELL?

2. Comparing results from CELLXR with CURDXR, whose accuracy has previously been established [16], does the CELL program give an accurate solution for the longitudinal and transverse distribution of reactions, deflections and internal forces and moments. The bridge properties and boundary conditions assumed in CELLXR and CURDXR were identical.

3. Comparing results for solutions with radial restraints at the end supports SAPXR, CURDXR, CELLXR with solutions without this restraint SAPX, CELLX, CELL, does this additional restraint have any significant effect on the results?

4. Comparing the CELLX and CELL solutions, in which the analytical models are identical in all respects, except that the latter includes the girder web flares existing in the actual bridge model, while the former does not, are there any significant differences in the results?

To answer these questions, selected typical results from the total compilation of tables are presented in Tables 2.1 to 2.13 for the following load cases: (1) dead load; (2) conditioning load; (3) 1X + 1Y; (4) 3X + 3Y; (5) 5X + 5Y; (6) 1X; (7) 3X; and (8) 5X. For the load cases 1X; 3X; and 5X; involving loads in one span only, results from

CURDXR are not given, because it cannot account for the longitudinal bending moment developed at the base of the column under unsymmetrical loadings in the two spans.

The tables for reactions and deflections, Tables 2.1 to 2.8, are self explanatory. The SAP program gives total reactions and deflections only along the bridge center line. The CELL program gives end reactions at each of the five girder supports which can be converted statically to give the total end reactions. The CURDI program outputs only reactions under the center footing, however, for the symmetrical loading in the two spans analyzed, the end support reactions can thence be found by statics. Both the CELL and the CURDI programs give the transverse distribution of deflections at any section, Tables 2.7 and 2.8, but SAP does not.

The total internal moment at a section, Tables 2.9 to 2.11, and its distribution to each girder, Table 2.12, are found in the CURDI and CELL programs by automatic subroutines which perform the operations described below.

The actual box girder bridge cross-section is first divided into a number of similar interior I girders plus two exterior girders. Each interior girder consists of a web and a top and bottom flange equal in width to the web spacing while each exterior girder consists of an exterior web with a top flange extending from the midpoint between girder webs to the edge of the cantilever overhang and the bottom flange being equal in width to half of the web spacing. Thus the bridge model, shown in Fig. 1.3, has three interior girders 2, 3 and 4 and two exterior girders 1 and 5.

The girder moment at any section taken by an individual girder

TABLE 2.1 - REACTIONS (KIPS OR FT-KIPS) FOR DEAD LOAD OR FOR CONDITIONING LOAD OF 100 KIPS IN EACH SPAN

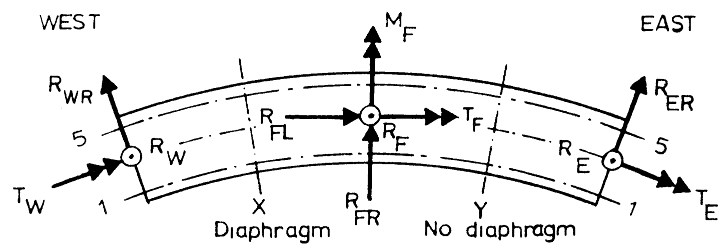

LOAD CASE	SOLUTION	REACTIONS (KIPS AND FT-KIPS)										
		WEST END			CENTER COLUMN					EAST END		
		R_W	R_{WR}	T_W	R_F	R_{FR}	R_{FL}	M_F	T_F	R_E	R_{ER}	T_E
DEAD LOAD	SAPX	32.9	0.0	24	110.0	0.0	0.0	0	-1	32.9	0.0	24
	SAPXR	32.9	0.1	24	110.0	-0.2	0.0	0	-1	32.9	0.1	24
	CURDXR	31.8	-0.3	38	112.0	0.5	0.0	0	-3	33.4	-0.3	38
	CELLXR	32.9	0.3	31	110.0	0.5	0.0	-2	-3	33.0	0.3	31
	CELLX	32.8	0.0	32	110.0	0.0	0.0	-2	-4	32.9	0.0	31
	CELL	32.7	0.0	32	113.5	0.0	0.0	-2	-4	32.8	0.0	30
COND. LOAD	SAPX	31.1	0.0	41	137.9	0.0	0.0	0	-2	31.1	0.0	41
	SAPXR	31.1	0.1	41	137.9	-0.3	0.0	0	-2	31.1	0.1	41
	CURDXR	29.6	0.0	30	140.8	0.0	0.0	0	0	29.6	0.0	30
	CELLXR	31.1	0.0	41	137.8	0.0	0.0	0	0	31.1	0.0	41
	CELLX	31.1	0.0	40	137.8	0.0	0.0	0	0	31.1	0.0	40
	CELL	30.8	0.0	39	138.4	0.0	0.0	0	-1	30.8	0.0	39

TABLE 2.2 - REACTIONS (KIPS OR FT-KIPS) FOR 100 KIP LOADS AT 1X + 1Y, 3X + 3Y, 5X + 5Y

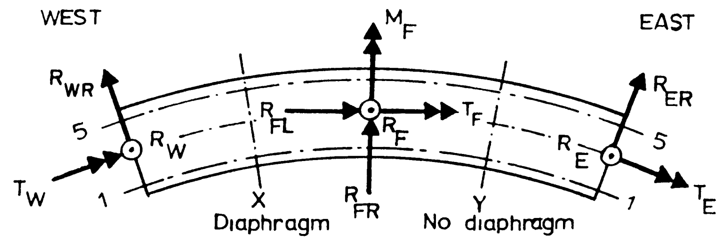

LOAD CASE	SOLUTION	REACTIONS (KIPS AND FT-KIPS)										
		WEST END			CENTER COLUMN					EAST END		
		R_W	R_{WR}	T_W	R_F	R_{FR}	R_{FL}	M_F	T_F	R_E	R_{ER}	T_E
1X + 1Y	SAPX	35.2	0.0	-365	129.6	0.0	0.0	0	-197	35.2	0.0	-365
	SAPXR	35.0	12.5	-350	130.1	-23.4	0.0	0	-147	35.0	12.5	-350
	CURDXR	33.7	10.6	-368	132.6	-21.3	0.0	0	-148	33.7	10.6	-368
	CELLXR	35.4	10.4	-372	129.3	-19.4	0.0	0	-122	35.4	10.4	-372
	CELLX	35.6	0.0	-382	128.8	0.0	0.0	0	-166	35.6	0.0	-382
	CELL	35.3	0.0	-382	129.3	0.0	0.0	0	-168	35.3	0.0	-382
3X + 3Y	SAPX	31.1	0.0	41	137.9	0.0	0.0	0	-2	31.1	0.0	41
	SAPXR	31.1	0.1	41	137.9	-0.3	0.0	0	-2	31.1	0.1	41
	CURDXR	29.7	0.0	30	140.7	0.0	0.0	0	0	29.7	0.0	30
	CELLXR	31.2	0.0	41	137.6	0.0	0.0	-2	0	31.2	0.0	41
	CELLX	31.1	0.0	41	137.6	0.0	0.0	0	-3	31.1	0.0	41
	CELL	30.9	0.0	39	138.3	0.0	0.0	-3	-1	30.8	0.0	39
5X + 5Y	SAPX	26.9	0.0	447	146.2	0.0	0.0	0	192	26.9	0.0	447
	SAPXR	27.2	-12.2	433	145.7	22.9	0.0	0	144	27.2	-12.2	433
	CURDXR	25.3	-10.7	427	149.4	21.4	0.0	0	147	25.3	-10.7	427
	CELLXR	26.6	-10.6	451	146.7	19.6	0.0	3	121	26.7	-10.5	451
	CELLX	26.5	0.0	461	147.2	0.0	0.0	3	166	26.5	0.0	461
	CELL	26.0	0.0	458	147.9	0.0	0.0	3	166	26.1	0.0	458

TABLE 2.3 - REACTIONS (KIPS OR FT-KIPS) FOR 100 KIP LOADS AT 1X, 3X, 5X

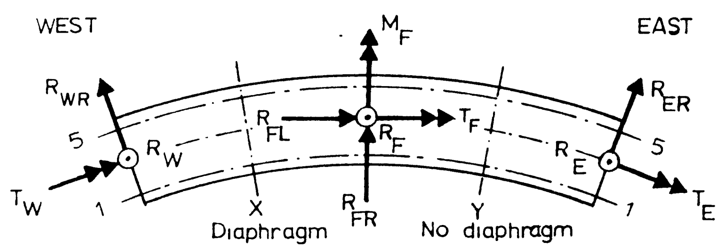

LOAD CASE	SOLUTION	REACTIONS (KIPS AND FT-KIPS)										
		WEST END			CENTER COLUMN					EAST END		
		R_W	R_{WR}	T_W	R_F	R_{FR}	R_{FL}	M_F	T_F	R_E	R_{ER}	T_E
1X	SAPX	40.7	0.0	-274	64.8	0.0	0.0	135	-98	-5.5	0.0	-91
	SAPXR	40.5	6.2	-267	65.0	-11.7	0.0	135	-74	-5.6	6.3	-83
	CELLXR	41.2	5.0	-279	64.5	-9.6	-1.6	106	-60	-5.7	5.3	-93
	CELLX	41.4	0.0	-283	64.3	0.0	0.0	109	-82	-5.6	0.0	-98
	CELL	41.2	0.0	-283	64.5	0.0	0.0	110	-83	-5.7	0.0	-99
3X	SAPX	38.5	0.0	59	68.9	0.0	0.0	148	-1	-7.4	0.0	-18
	SAPXR	38.5	0.0	59	68.9	-0.1	0.0	148	-1	-7.4	0.1	-18
	CELLXR	38.9	0.1	58	68.8	0.0	-1.5	118	0	-7.7	0.1	-17
	CELLX	38.9	0.0	58	68.8	0.0	0.0	121	0	-7.7	0.0	-17
	CELL	38.8	0.0	57	69.0	0.0	0.0	122	0	-7.9	0.0	-17
5X	SAPX	36.3	0.0	393	73.1	0.0	0.0	161	96	-9.4	0.0	55
	SAPXR	36.4	-6.1	385	72.8	11.4	0.0	161	72	-9.2	-6.1	47
	CELLXR	36.4	-5.3	394	73.5	9.7	-1.4	129	60	-9.9	-5.1	58
	CELLX	36.4	0.0	397	73.7	0.0	0.0	131	82	-10.0	0.0	63
	CELL	36.2	0.0	395	74.1	0.0	0.0	133	82	-10.2	0.0	63

TABLE 2.4 - LONGITUDINAL DISTRIBUTION OF DEFLECTIONS (FT X 10^{-2}) AT CENTER GIRDER 3 FOR DEAD LOAD OR FOR CONDITIONING LOAD OF 100 KIPS IN EACH SPAN

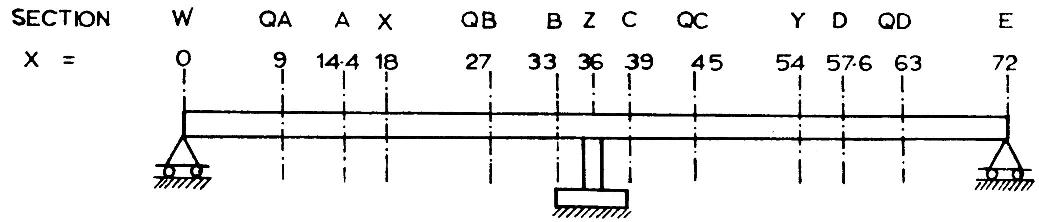

LOAD CASE	SOLUTION	DEFLECTIONS (FT X 10^{-2})										
		QA	A	X	QB	B	Z	C	QC	Y	D	QD
DEAD LOAD	SAPX	1.73	2.14	2.08	0.99	0.18	0.03	0.18	0.99	2.07	2.14	1.73
	SAPXR	1.73	2.14	2.07	0.99	0.18	0.03	0.18	0.99	2.07	2.14	1.73
	CURDXR	1.85	2.28	2.23	1.11	0.23	0.03	0.23	1.11	2.23	2.28	1.85
	CELLXR	1.90	2.36	2.30	1.16	0.25	0.04	0.23	1.08	2.18	2.23	1.80
	CELLX	1.90	2.36	2.30	1.16	0.25	0.05	0.25	1.08	2.18	2.23	1.80
	CELL	1.87	2.32	2.26	1.11	0.34	0.04	0.20	1.03	2.12	2.19	1.77
COND LOAD	SAPX	3.16	4.14	4.12	1.86	0.30	0.04	0.30	1.86	4.12	4.14	3.16
	SAPXR	3.16	4.14	4.12	1.86	0.30	0.04	0.30	1.86	4.12	4.14	3.16
	CURDXR	3.30	4.37	4.41	2.03	0.36	0.04	0.36	2.03	4.41	4.36	3.30
	CELLXR	3.27	4.32	4.36	2.00	0.37	0.04	0.37	2.00	4.34	4.31	3.27
	CELLX	3.27	4.32	4.36	2.01	0.37	0.05	0.37	2.00	4.35	4.31	3.27
	CELL	3.21	4.23	4.26	1.92	0.33	0.04	0.33	1.92	4.24	4.23	3.21

TABLE 2.5 - LONGITUDINAL DISTRIBUTION OF DEFLECTIONS (FT X 10^{-2}) AT CENTER GIRDER 3 FOR 100 KIP LOADS AT 1X+1Y, 3X+3Y, 5X+5Y

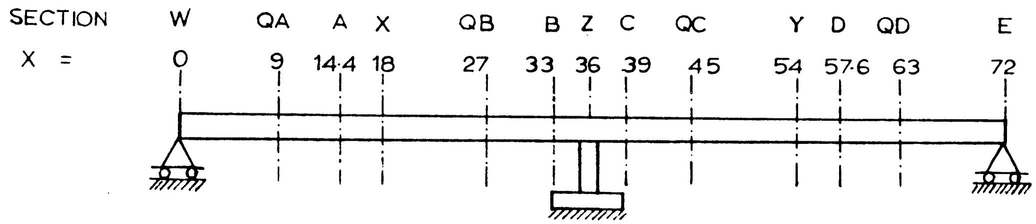

LOAD CASE	SOLUTION	DEFLECTIONS (FT X 10^{-2})										
		QA	A	X	QB	B	Z	C	QC	Y	D	QB
1X+1Y	SAPX	2.90	3.79	3.77	1.70	0.28	0.04	0.28	1.70	3.77	3.79	2.90
	SAPXR	2.90	3.79	3.77	1.70	0.28	0.04	0.28	1.70	3.77	3.79	2.90
	CURDXR	2.93	3.84	3.85	1.77	0.31	0.04	0.30	1.72	3.62	3.69	2.89
	CELLXR	2.91	3.82	3.83	1.75	0.32	0.04	0.31	1.70	3.58	3.64	2.85
	CELLX	2.91	3.82	3.83	1.75	0.32	0.05	0.31	1.70	3.57	3.64	2.85
	CELL	2.85	3.74	3.75	1.68	0.29	0.04	0.29	1.63	3.49	3.57	2.80
3X+3Y	SAPX	3.16	4.14	4.12	1.86	0.30	0.04	0.30	1.86	4.12	4.14	3.16
	SAPXR	3.16	4.14	4.12	1.86	0.30	0.04	0.30	1.86	4.12	4.14	3.16
	CURDXR	3.41	4.60	4.72	2.13	0.37	0.04	0.43	2.36	5.21	5.12	3.64
	CELLXR	3.35	4.47	4.53	2.08	0.38	0.04	0.43	2.33	5.38	5.07	3.60
	CELLX	3.35	4.47	4.47	2.08	0.37	0.05	0.43	2.33	5.45	5.07	3.60
	CELL	3.28	4.38	4.44	1.99	0.34	0.04	0.39	2.23	5.28	4.98	3.54
5X+5Y	SAPX	3.42	4.48	4.47	2.02	0.33	0.04	0.33	2.02	4.47	4.48	3.42
	SAPXR	3.42	4.49	4.47	2.02	0.33	0.04	0.33	2.02	4.47	4.49	3.42
	CURDXR	3.55	4.66	4.68	2.18	0.40	0.04	0.34	1.98	4.20	4.28	3.35
	CELLXR	3.53	4.65	4.67	2.16	0.40	0.04	0.35	1.96	4.16	4.24	3.32
	CELLX	3.54	4.65	4.67	2.16	0.40	0.05	0.35	1.96	4.16	4.25	3.35
	CELL	3.46	4.56	4.56	2.06	0.37	0.04	0.32	1.87	4.05	4.14	3.26

TABLE 2.6 - LONGITUDINAL DISTRIBUTION OF DEFLECTIONS (FT X 10^{-2}) AT CENTER GIRDER 3 FOR 100 KIP LOADS AT 1X, 3X, 5X

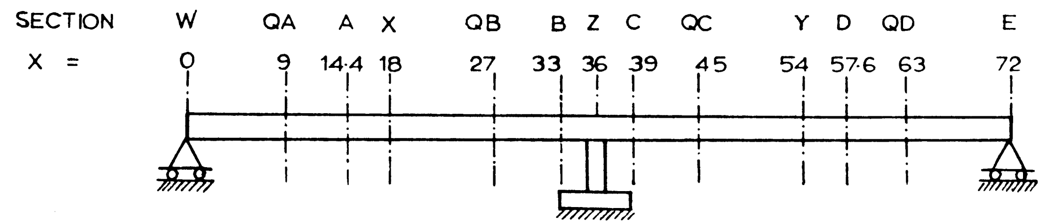

LOAD CASE	SOLUTION	DEFLECTIONS (FT X 10^{-2})										
		QA	A	X	QB	B	Z	C	QC	Y	D	QD
1X	SAPX	4.10	5.52	5.69	3.37	1.01	0.02	-0.73	-1.67	-1.92	-1.72	-1.20
	SAPXR	4.10	5.52	5.69	3.37	1.01	0.02	-0.73	-1.67	-1.92	-1.72	-1.20
	CELLXR	4.16	5.61	5.82	3.44	1.01	0.02	-0.68	-1.67	-1.96	-1.76	-1.23
	CELLX	4.16	5.61	5.83	3.45	1.01	0.02	-0.68	-1.67	-1.96	-1.77	-1.24
	CELL	4.13	5.56	5.77	3.39	0.99	0.02	-0.69	-1.69	-1.99	-1.79	-1.26
3X	SAPX	4.49	6.04	6.23	3.70	1.10	0.02	-0.80	-1.83	-2.11	-1.90	-1.33
	SAPXR	4.48	6.04	6.23	3.69	1.10	0.02	-0.80	-1.83	-2.11	-1.90	-1.33
	CELLXR	4.69	6.39	6.67	3.90	1.13	0.02	-0.75	-1.82	-2.13	-1.92	-1.34
	CELLX	4.69	6.39	6.69	3.90	1.13	0.02	-0.75	-1.82	-2.14	-1.92	-1.35
	CELL	4.65	6.33	6.61	3.84	1.10	0.02	-0.75	-1.84	-2.17	-1.95	-1.37
5X	SAPX	4.87	6.56	6.77	4.02	1.20	0.02	-0.87	-2.00	-2.31	-2.07	-1.45
	SAPXR	4.87	6.56	6.77	4.02	1.20	0.02	-0.87	-2.00	-2.31	-2.07	-1.45
	CELLXR	5.00	6.74	7.00	4.14	1.21	0.02	-0.82	-2.00	-2.35	-2.12	-1.48
	CELLX	5.00	6.75	7.00	4.14	1.20	0.02	-0.82	-2.01	-2.36	-2.12	-1.46
	CELL	4.96	6.68	6.93	4.07	1.18	0.02	-0.83	-2.03	-2.40	-2.16	-1.51

TABLE 2.7 - TRANSVERSE DISTRIBUTION OF DEFLECTIONS (FT x 10^{-2}) AT MIDSPAN SECTIONS X AND Y FOR 100 KIP LOADS AT 1X + 1Y, 3X + 3Y, 5X + 5Y

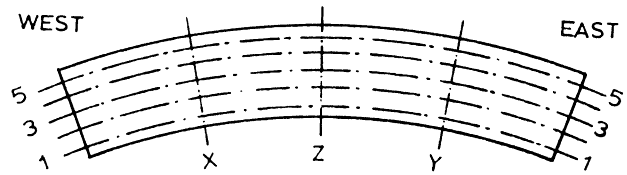

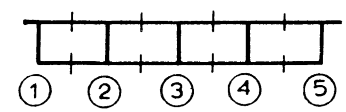

LOAD CASE	SOLUTION	SECTION X					SECTION Y				
		GIRDERS					GIRDERS				
		1	2	3	4	5	1	2	3	4	5
1X + 1Y	CURDXR	6.70	5.11	3.85	2.83	1.98	7.95	5.29	3.62	2.53	1.79
	CELLXR	6.56	5.10	3.83	2.77	1.84	7.89	5.27	3.58	2.44	1.65
	CELLX	6.65	5.15	3.83	2.72	1.74	7.99	5.32	3.57	2.38	1.55
	CELL	6.58	5.07	3.75	2.63	1.65	7.90	5.24	3.49	2.30	1.46
3X + 3Y	CURDXR	3.87	4.21	4.72	4.59	4.63	3.61	4.19	5.52	4.51	4.25
	CELLXR	3.86	4.18	4.53	4.57	4.64	3.55	4.12	5.38	4.45	4.19
	CELLX	3.86	4.18	4.53	4.57	4.64	3.54	4.12	5.38	4.45	4.19
	CELL	3.78	4.09	4.44	4.47	4.53	3.46	4.03	5.28	4.34	4.08
5X + 5Y	CURDXR	2.05	3.27	4.68	6.37	8.40	1.72	2.76	4.20	6.27	9.39
	CELLXR	1.90	3.21	4.67	6.36	8.27	1.59	2.67	4.16	6.26	9.33
	CELLX	1.80	3.16	4.67	6.42	8.37	1.49	2.62	4.16	6.32	9.44
	CELL	1.71	3.06	4.56	6.29	8.23	1.40	2.52	4.05	6.19	9.30

TABLE 2.8 - TRANSVERSE DISTRIBUTION OF DEFLECTIONS (FT x 10^{-2}) AT MIDSPAN SECTIONS X AND Y FOR 100 KIP LOADS AT 1X, 3X, 5X

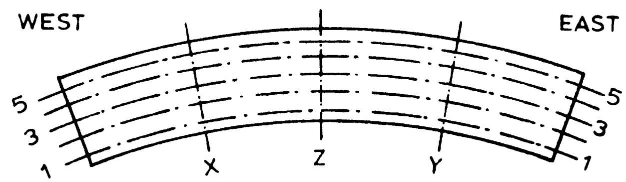

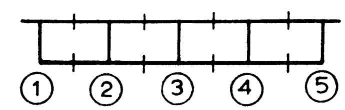

LOAD CASE	SOLUTION	SECTION X GIRDERS 1	2	3	4	5	SECTION Y GIRDERS 1	2	3	4	5
1X	CELLXR	7.85	6.74	5.82	5.12	4.56	-1.30	-1.64	-1.96	-2.30	-2.66
	CELLX	7.91	6.77	5.82	5.09	4.51	-1.26	-1.62	-1.96	-2.33	-2.71
	CELL	7.85	6.71	5.77	5.04	4.46	-1.28	-1.64	-1.99	-2.36	-2.74
3X	CELLXR	5.82	6.22	6.67	6.81	6.99	-1.99	-2.06	-2.13	-2.22	-2.33
	CELLX	5.82	6.23	6.67	6.82	7.00	-1.99	-2.07	-2.14	-2.23	-2.33
	CELL	5.77	6.17	6.61	6.74	6.93	-2.02	-2.10	-2.17	-2.26	-2.37
5X	CELLXR	4.56	5.70	7.00	8.54	10.31	-2.72	-2.53	-2.35	-2.20	-2.05
	CELLX	4.51	5.68	7.00	8.58	10.38	-2.77	-2.56	-2.36	-2.18	-2.00
	CELL	4.46	5.61	6.93	8.49	10.28	-2.80	-2.60	-2.40	-2.22	-2.05

TABLE 2.9 - LONGITUDINAL DISTRIBUTION OF TOTAL INTERNAL MOMENTS (FT-KIPS) AT A SECTION DUE TO DEAD LOAD OR FOR CONDITIONING LOAD OF 100 KIPS IN EACH SPAN

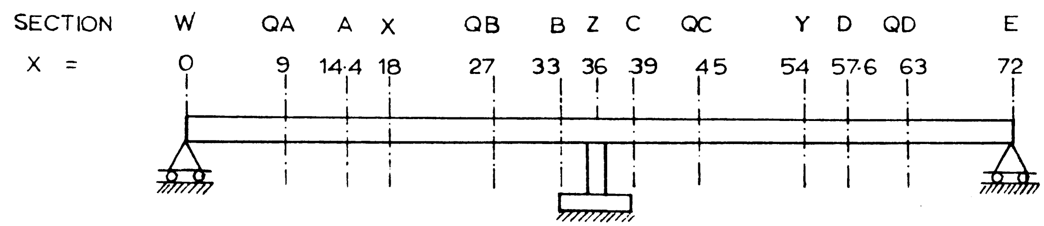

LOAD CASE	SOLUTION	INTERNAL MOMENTS (FT-KIPS)										
		QA	A	X	QB	B	Z	C	QC	Y	D	QD
DEAD LOAD	SAPX	199	223	199	1	-242	-396	-242	1	199	223	199
	SAPXR	199	223	199	1	-242	-396	-242	1	199	223	199
	CURDXR	198	222	197	-2	-244	-372	-244	-2	197	222	198
	CELLXR	201	232	210	-3	-232	-368	-232	-9	197	221	194
	CELLX	201	232	210	-3	-232	-368	-232	-9	197	221	194
	CELL	200	230	210	-8	-238	-378	-239	-13	194	221	193
COND. LOAD	SAPX	282	451	563	-60	-475	-682	-475	-60	563	451	282
	SAPXR	282	451	563	-60	-475	-682	-475	-60	563	451	282
	CURDXR	283	452	557	-58	-474	-647	-474	-58	557	452	283
	CELLXR	285	457	570	-59	-479	-688	-479	-59	570	457	285
	CELLX	285	457	570	-59	-479	-688	-479	-59	570	457	285
	CELL	282	452	564	-68	-489	-700	-489	-68	564	452	282

TABLE 2.10 - LONGITUDINAL DISTRIBUTION OF TOTAL INTERNAL MOMENTS (FT-KIPS) AT A SECTION DUE TO 100 KIP LOADS AT 1X+1Y, 3X+3Y, 5X+5Y

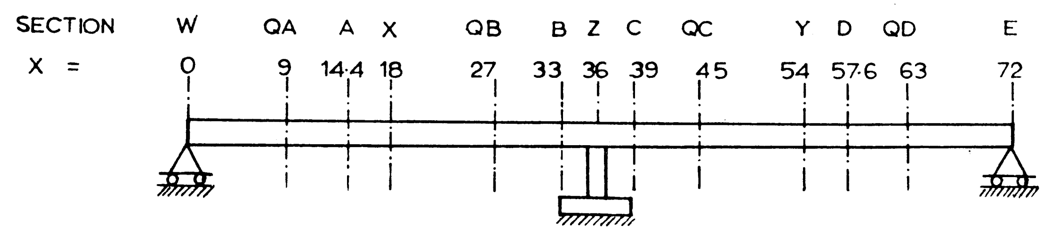

LOAD CASE	SOLUTION	INTERNAL MOMENTS (FT-KIPS)										
		QA	A	X	QB	B	Z	C	QC	Y	D	QD
1X+1Y	SAPX	290	458	575	-5	-389	-582	-389	-5	575	458	290
	SAPXR	288	456	573	-8	-393	-586	-393	-8	573	456	288
	CURDXR	284	452	557	-12	-396	-557	-396	-12	557	452	284
	CELLXR	287	460	574	-8	-396	-590	-395	-8	573	459	286
	CELLX	288	461	575	-5	-392	-586	-394	-6	575	461	288
	CELL	286	458	572	-12	-401	-596	-402	-13	570	457	285
3X+3Y	SAPX	282	451	563	-60	-475	-682	-475	-60	563	451	282
	SAPXR	282	451	563	-60	-475	-682	-475	-60	563	451	282
	CURDXR	284	453	558	-56	-471	-644	-471	-56	558	453	284
	CELLXR	285	457	570	-56	-474	-683	-475	-57	570	457	285
	CELLX	285	457	570	-56	-474	-683	-475	-57	570	457	285
	CELL	283	453	565	-64	-484	-694	-486	-66	564	452	282
5X+5Y	SAPX	275	444	550	-115	-561	-782	-561	-115	550	444	275
	SAPXR	276	446	553	-112	-557	-778	-557	-112	553	446	276
	CURDXR	281	449	553	-110	-557	-744	-557	-110	553	449	281
	CELLXR	282	452	564	-116	-569	-794	-566	-114	564	452	282
	CELLX	281	450	562	-119	-573	-798	-569	-117	562	450	281
	CELL	277	444	554	-130	-586	-812	-584	-128	555	445	278

TABLE 2.11 - LONGITUDINAL DISTRIBUTION OF TOTAL INTERNAL MOMENTS (FT-KIPS) AT A SECTION DUE TO 100 KIP LOADS AT 1X, 3X, 5X

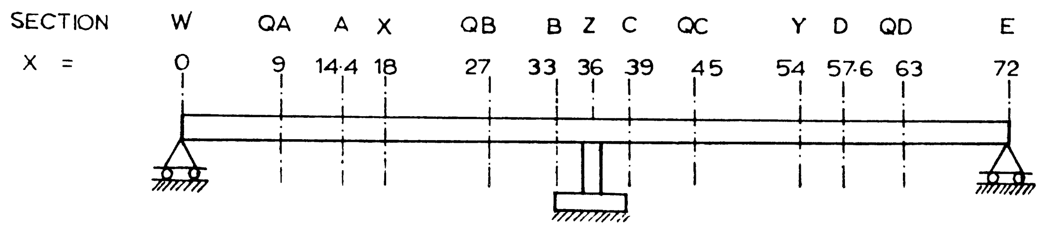

LOAD CASE	SOLUTION	INTERNAL MOMENTS (FT-KIPS)											
		QA	A	X	QB	B	Z		C	QC	Y	D	QD
1X	SAPX	345	548	688	163	-184	-360	-222	-205	-168	-112	-90	-56
	SAPXR	345	547	687	162	-186	-362	-224	-206	-170	-113	-91	-56
	CELLXR	348	558	697	175	-173	-347	-240	-220	-180	-120	-96	-60
	CELLX	349	559	698	177	-170	-344	-240	-220	-180	-120	-96	-60
	CELL	348	557	695	172	-177	-351	-242	-222	-182	-121	-97	-61
3X	SAPX	350	560	698	142	-230	-415	-267	-245	-202	-135	-109	-68
	SAPXR	350	560	698	142	-230	-415	-267	-245	-202	-135	-109	-68
	CELLXR	356	571	713	156	-215	-401	-285	-261	-213	-142	-114	-71
	CELLX	357	572	714	157	-214	-400	-285	-261	-213	-142	-114	-71
	CELL	355	569	710	152	-220	-406	-290	-265	-217	-145	-116	-72
5X	SAPX	355	571	709	121	-275	-469	-313	-286	-236	-159	-127	-80
	SAPXR	355	572	710	122	-273	-467	-310	-284	-234	-158	-126	-79
	CELLXR	366	586	731	133	-266	-465	-337	-309	-253	-169	-135	-84
	CELLX	365	585	730	132	-267	-466	-340	-311	-255	-170	-136	-85
	CELL	363	582	726	126	-274	-474	-347	-318	-260	-174	-139	-87

TABLE 2.12 - TRANSVERSE DISTRIBUTION OF TOTAL MOMENT AT SECTION A TO EACH GIRDER (FT-KIPS AND PERCENT) FOR 100 KIP LOADS AT 1X + 1Y, 3X + 3Y, 5X + 5Y

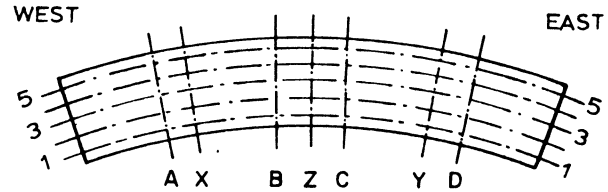

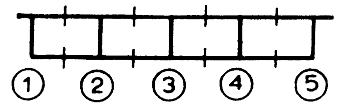

LOAD CASE	SOLUTION	INTERNAL MOMENTS (FT-KIPS)						PERCENTAGE OF TOTAL INTERNAL MOMENTS					
		GIRDERS					TOTAL	GIRDERS					TOTAL
		1	2	3	4	5		1	2	3	4	5	
1X + 1Y	CURDXR	97	117	97	83	58	452	21.3	26.0	21.5	18.4	12.8	100.0
	CELLXR	98	119	98	85	60	460	21.4	25.8	21.3	18.5	13.0	100.0
	CELLX	101	119	98	85	59	462	21.8	25.8	21.3	18.5	12.7	100.0
	CELL	100	118	97	84	58	458	21.8	25.8	21.3	18.4	12.6	100.0
3X + 3Y	CURDXR	73	104	105	102	69	453	16.1	23.0	23.2	22.5	15.1	100.0
	CELLXR	74	105	106	103	70	457	16.2	22.9	23.1	22.5	15.3	100.0
	CELLX	74	105	106	103	70	457	16.2	22.9	23.1	22.5	15.4	100.0
	CELL	73	104	105	102	69	453	16.2	22.9	23.1	22.5	15.3	100.0
5X + 5Y	CURDXR	62	86	98	114	89	449	13.8	19.1	21.8	25.4	19.8	100.0
	CELLXR	63	86	98	114	91	452	14.0	19.1	21.6	25.3	20.1	100.0
	CELLX	61	86	97	114	92	450	13.5	19.1	21.6	25.3	20.5	100.0
	CELL	60	84	96	113	91	444	13.4	19.0	21.6	25.4	20.5	100.0

TABLE 2.13 - TRANSVERSE DISTRIBUTION OF LONGITUDINAL MEMBRANE FORCES N_X (KIPS/FT) AT SECTION A FOR 100 KIP LOADS AT 3X + 3Y, 5X + 5Y

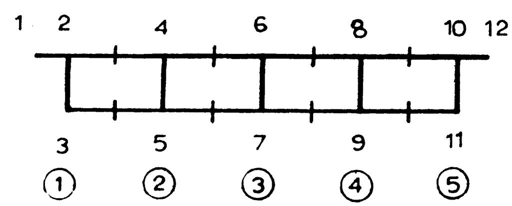

LOAD CASE	LOCATION	SOLUTION	TOP NODES							BOTTOM NODES				
			1	2	4	6	8	10	12	3	5	7	9	11
3X + 3Y	PLATE	CURDXR	-27.4	-24.5	-22.5	-22.9	-22.2	-23.3	-24.8	23.1	23.7	23.7	23.3	21.3
		CELLXR	-27.5	-24.5	-22.3	-23.2	-22.0	-23.4	-25.0	23.0	23.6	23.8	23.2	21.4
		CELLX	-27.5	-24.5	-22.3	-23.2	-22.0	-23.4	-25.0	23.0	23.6	23.8	23.2	21.4
		CELL	-27.2	-24.2	-20.1	-23.0	-21.8	-23.1	-24.7	22.8	23.3	23.5	23.0	21.2
	WEB	CURDXR		-24.3	-26.1	-26.4	-25.7	-23.1		33.8	34.6	34.4	34.0	31.3
		CELLXR		-24.2	-25.8	-26.7	-25.5	-23.1		33.7	34.4	34.6	33.9	31.4
		CELLX		-24.2	-25.8	-26.7	-25.5	-23.1		33.7	34.4	34.6	33.9	31.5
		CELL		-23.9	-25.6	-26.4	-25.3	-22.9		33.4	34.0	34.2	33.6	31.1
5X + 5Y	PLATE	CURDXR	-28.8	-23.2	-19.6	-21.0	-23.1	-27.6	-32.9	16.6	18.1	21.9	27.1	31.3
		CELLXR	-28.6	-22.9	-19.5	-21.0	-23.0	-27.4	-34.4	16.7	18.1	21.8	26.8	31.2
		CELLX	-24.7	-20.0	-18.2	-20.9	-24.0	-29.8	-37.6	18.4	18.9	21.8	25.9	29.5
		CELL	-24.3	-19.7	-18.0	-20.7	-23.8	-29.5	-37.3	18.1	18.6	21.5	25.6	29.3
	WEB	CURDXR		-23.0	-23.1	-25.0	-27.4	-27.6		24.6	26.9	32.7	40.2	46.2
		CELLXR		-22.7	-22.9	-25.0	-27.3	-27.3		24.8	26.9	32.5	39.7	46.1
		CELLX		-19.9	-21.6	-24.9	-28.5	-29.6		27.2	28.0	32.4	38.4	43.7
		CELL		-19.6	-21.2	-24.6	-28.2	-29.3		26.8	27.6	32.0	38.0	43.3

can be found by integrating the longitudinal membrane stresses, over the proper slab and web areas to obtain forces and then multiplying these forces by their respective lever arms to the neutral axis of the gross uncracked section. The girder moments, at a particular section, can then be summed to determine the total moment on an entire cross-section. Each girder moment can then be divided by the total moment at a section to determine the percentage distribution to each girder.

Statics checks, not shown in the tables, were performed on the internal forces found by the CURDI and CELL programs in which the total longitudinal compressive and tensile forces on the section, which should be equal when no horizontal reactions exist, were compared. In addition the total internal moment found as described above was compared with the external moment at the same section as found from the external loads and reactions. In all cases these statics checks were quite good, with maximum differences being of the order of 2 or 3%.

Turning now to the four questions raised at the beginning of this section, a study of the tables reveals the following answers.

1. SAP can be used to accurately predict the longitudinal distribution of total reactions, moments and deflections along the bridge longitudinal centerline (girder 3) found by the CURDI and CELL programs. Differences in general are quite small, with the largest differences occurring for the deflections at 3X and 3Y, under loadings 3X + 3Y and 3X, Tables 2.5 and 2.6. SAP gives smaller values of deflections, because it cannot account for the concentration of deflection directly under the load as shown in the transverse distributions for the CURDI and CELL solutions in Tables 2.7 and 2.8.

2. Results for all quantities obtained in CELLXR are very similar to those found in CURDXR, therefore it can be concluded that the CELL program will give accurate solutions for all load cases to be studied for comparisons with experimental results. It might be noted, that the largest difference, with the CURDXR value being about 8% smaller, occurs for the internal moment at Section Z over the center bent support, Tables 2.9, 2.10. This is due to the fact that in the harmonic analysis used in CURDXR the support is assumed to extend longitudinally over 1.90 ft. (the thickness of the bent girder), while in the finite element analysis used in CELLXR the support is concentrated along the transverse bridge centerline.

3. Results for solutions with radial restraints at the end supports SAPXR, CURDXR, CELLXR are very similar to those without this restraint SAPX, CELLX, CELL with the exception that reactions are developed in a horizontal plane at the end supports and center footing in the former, but not the latter cases, Tables 2.1, 2.2, 2.3. These horizontal reactions appear to have a minor effect on changing the deflections and total internal moments about a horizontal axis of the bridge cross-section, Tables 2.4 to 2.11. However, since they do produce a moment about a vertical axis of the cross-section, they do alter the transverse distribution of N_x forces at a section somewhat for the eccentric loadings 1X + 1Y and 5X + 5Y, Table 2.13. While the differences are

not great for the bridge model, for bridge systems with longer columns they might be more significant. This stresses the importance of using the true boundary conditions in any three dimensional analysis of a bridge system.

4. Finally comparing all of the results from CELL with CELLX, the differences are very minor indicating that inclusion of girder web flares, by thickening the web elements as done in CELL is not important.

On the basis of the above study it was concluded that the theoretical results from the CELL solutions would be used in Vols. II and III for making detailed comparisons with experimental results from the bridge model testing program.

2.6 Comparison of Theoretical Results for Straight and Curved Bridge Models

Comparisons of the longitudinal distribution of total reactions and internal moments and of the transverse distribution of deflections, moments, and longitudinal membrane forces are presented in Tables 2.14 to 2.18. Results for the straight bridge, which was identical to the curved bridge except for horizontal curvature, are from a previous study [9, 10, 11] and were obtained using a finite element computer program entitled FINPLA2 [12]. Results for the curved bridge are from the CELL analysis. Boundary conditions were in general similar in the two solutions. The end supports were restrained vertically at the bottom nodes in both solutions, however, in the FINPLA2 solution they were also restrained transversely while in the CELL solution they were not.

TABLE 2.14 - COMPARISON OF THEORETICAL REACTIONS (KIPS OR FT-KIPS) FOR STRAIGHT AND CURVED BRIDGE MODELS

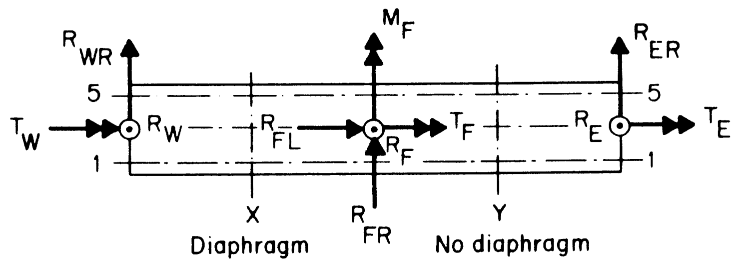

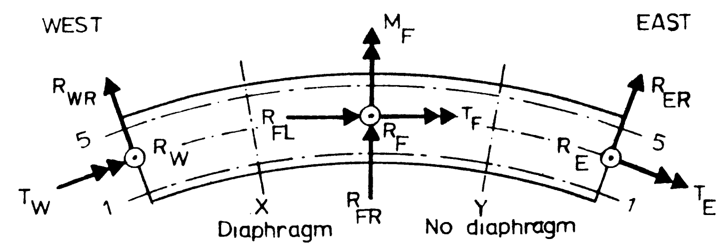

LOAD CASE	BRIDGE MODEL	REACTIONS (KIPS AND FT-KIPS)										
		R_W	R_{WR}	T_W	R_F	R_{FR}	R_{FL}	M_F	T_F	R_E	R_{ER}	T_E
DEAD LOAD	STRAIGHT	33.0	0.0	0	109.8	0.0	0.0	0	0	33.0	0.0	0
	CURVED	32.7	0.0	34	113.5	0.0	0.0	-2	-4	32.8	0.0	32
COND. LOAD	STRAIGHT	31.1	0.0	0	137.8	0.0	0.0	0	0	31.1	0.0	0
	CURVED	30.8	0.0	39	138.4	0.0	0.0	0	-1	30.8	0.0	39
1X+1Y	STRAIGHT	31.0	-12.9	-432	138.0	25.8	0.0	0	-84	31.0	-12.9	-431
	CURVED	35.3	0.0	-382	129.3	0.0	0.0	0	-168	35.3	0.0	-382
3X+3Y	STRAIGHT	31.2	0.0	0	137.7	0.0	0.0	0	0	31.2	0.0	0
	CURVED	30.9	0.0	39	138.3	0.0	0.0	-3	1	30.8	0.0	39
5X+5Y	STRAIGHT	31.0	12.9	432	138.0	-25.8	0.0	0	84	31.0	12.9	431
	CURVED	26.0	0.0	458	147.9	0.0	0.0	3	166	26.1	0.0	458
1X	STRAIGHT	39.2	-6.4	-335	69.0	12.9	0.0	96	-42	-8.2	-6.5	-95
	CURVED	41.2	0.0	-283	64.5	0.0	0.0	110	-83	-5.7	0.0	-99
3X	STRAIGHT	39.3	0.0	0	68.8	0.0	0.0	96	0	-8.1	0.0	0
	CURVED	38.8	0.0	57	69.1	0.0	0.0	122	0	-7.9	0.0	-17
5X	STRAIGHT	39.2	6.4	335	69.0	-12.9	0.0	96	42	-8.2	6.5	95
	CURVED	36.2	0.0	395	74.1	0.0	0.0	133	82	-10.2	0.0	63

TABLE 2.15 - COMPARISON OF THEORETICAL TOTAL INTERNAL MOMENTS (FT-KIPS) AT A SECTION FOR STRAIGHT AND CURVED BRIDGE MODELS

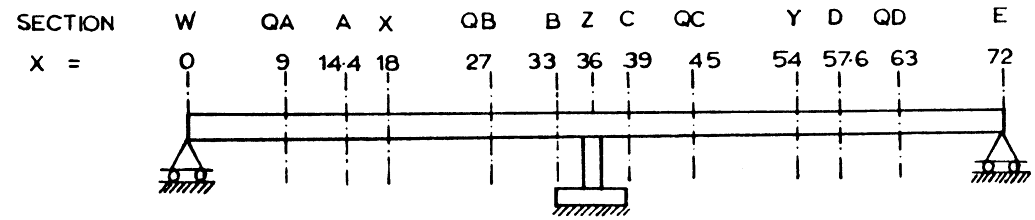

LOAD CASE	BRIDGE MODEL	INTERNAL MOMENTS (FT-KIPS)											
		QA	A	X	QB	B	Z		C	QC	Y	D	QD
DEAD LOAD	STRAIGHT	197	222	199	2	-238	-395		-238	2	199	222	197
	CURVED	200	230	210	-8	-238	-378		-239	-13	194	221	193
COND. LOAD	STRAIGHT	279	447	558	-58	-469	-674		-468	-58	557	446	278
	CURVED	282	452	564	-68	-489	-700		-489	-68	564	452	282
1X + 1Y	STRAIGHT	280	448	559	-61	-474	-678		-470	-61	553	443	276
	CURVED	286	458	572	-12	-401	-596		-402	-13	570	457	285
3X + 3Y	STRAIGHT	278	446	557	-56	-464	-670		-466	-56	559	448	280
	CURVED	283	453	565	-64	-484	-694		-486	-66	564	452	282
5X + 5Y	STRAIGHT	280	448	559	-61	-474	-678		-470	-61	553	443	276
	CURVED	277	444	554	-130	-586	-812		-584	-128	555	445	278
1X	STRAIGHT	353	565	705	151	-219	-403	-295	-270	-221	-147	-118	-74
	CURVED	348	557	695	172	-177	-351	-242	-222	-182	-121	-97	-61
3X	STRAIGHT	350	561	700	153	-212	-394	-290	-265	-217	-145	-116	-72
	CURVED	355	569	710	152	-220	-406	-290	-265	-217	-145	-116	-72
5X	STRAIGHT	353	565	705	151	-219	-403	-295	-270	-221	-147	-118	-74
	CURVED	363	582	726	126	-274	-474	-347	-318	-260	-174	-139	-87

TABLE 2.16 - COMPARISON OF TRANSVERSE DISTRIBUTION OF DEFLECTIONS (FT x 10^{-2}) AT MIDSPAN SECTIONS X AND Y FOR STRAIGHT AND CURVED BRIDGE MODELS

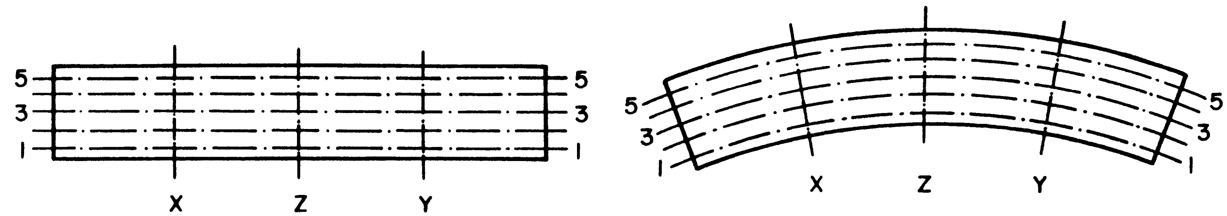

LOAD CASE	BRIDGE MODEL	SECTION X GIRDERS					SECTION Y GIRDERS				
		1	2	3	4	5	1	2	3	4	5
1X + 1Y	STRAIGHT	7.54	5.79	4.26	3.94	1.77	8.80	5.82	3.84	2.48	1.49
	CURVED	6.58	5.07	3.75	2.63	1.65	7.90	5.24	3.49	2.30	1.46
3X + 3Y	STRAIGHT	4.24	4.37	4.54	4.37	4.24	3.85	4.27	5.39	4.27	3.85
	CURVED	3.78	4.09	4.44	4.47	4.53	3.46	4.03	5.28	4.34	4.08
5X + 5Y	STRAIGHT	1.77	2.94	4.26	5.80	7.54	1.49	2.47	3.84	5.82	8.80
	CURVED	1.71	3.06	4.56	6.29	8.23	1.40	2.52	4.05	6.19	9.30
1X	STRAIGHT	9.11	7.66	6.43	5.42	4.58	-1.57	-1.88	-2.19	-2.50	-2.80
	CURVED	7.85	6.71	5.77	5.04	4.46	-1.28	-1.64	-1.99	-2.36	-2.74
3X	STRAIGHT	6.44	6.55	6.70	6.55	6.44	-2.18	-2.16	-2.16	-2.16	-2.18
	CURVED	5.77	6.17	6.61	6.74	6.93	-2.02	-2.10	-2.17	-2.26	-2.37
5X	STRAIGHT	4.58	5.43	6.44	7.66	9.12	-2.80	-2.50	-2.19	-1.88	-1.58
	CURVED	4.46	5.61	6.93	8.49	10.28	-2.80	-2.60	-2.40	-2.22	-2.05

TABLE 2.17 - COMPARISON OF TRANSVERSE DISTRIBUTION OF TOTAL MOMENT AT SECTION A TO EACH GIRDER (FT-KIPS AND PER CENT) FOR STRAIGHT AND CURVED BRIDGE MODELS

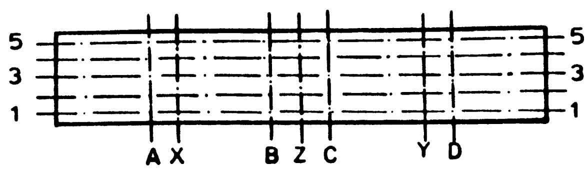

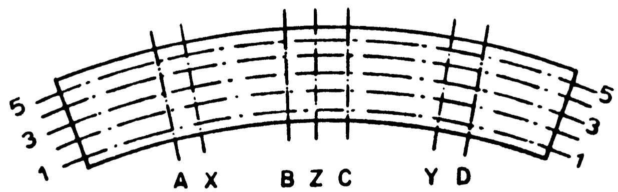

LOAD CASE	BRIDGE MODEL	INTERNAL MOMENTS (FT -KIPS)						PERCENTAGE OF TOTAL INTERNAL MOMENTS					
		GIRDERS					TOTAL	GIRDERS					TOTAL
		1	2	3	4	5		1	2	3	4	5	
1X+1Y	STRAIGHT	89	116	99	86	59	448	19.8	25.9	22.1	19.2	13.1	100.0
	CURVED	100	118	97	84	58	458	21.8	25.8	21.3	18.4	12.6	100.0
3X+3Y	STRAIGHT	68	103	105	103	68	446	15.2	23.0	23.5	23.0	15.2	100.0
	CURVED	73	104	105	102	69	453	16.2	22.9	23.1	22.5	15.3	100.0
5X+5Y	STRAIGHT	59	86	99	116	89	448	13.1	19.2	22.1	25.9	19.8	100.0
	CURVED	60	84	96	113	91	444	13.4	19.0	21.6	25.4	20.5	100.0

TABLE 2.18 - COMPARISON OF TRANSVERSE DISTRIBUTION OF LONGITUDINAL MEMBRANE FORCES N_x (KIPS/FT) AT SECTION A FOR STRAIGHT AND CURVED BRIDGE MODELS

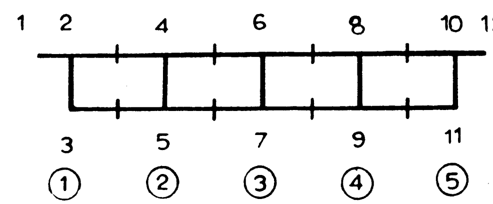

LOAD CASE	LOCATION	BRIDGE MODEL	TOP NODES							BOTTOM NODES				
			1	2	4	6	8	10	12	3	5	7	9	11
1X+1Y	PLATE	STRAIGHT	-28.1	-26.2	-24.1	-22.1	-20.7	-21.6	-23.2	32.3	27.0	21.6	17.6	15.6
		CURVED	-41.6	-32.3	-24.7	-20.8	-18.0	-19.4	-22.5	32.5	26.7	21.8	18.6	17.2
	WEB	STRAIGHT		-25.6	-24.5	-22.5	-20.9	-20.9		47.5	39.9	32.1	26.1	32.2
		CURVED		-32.0	-29.1	-24.6	-21.2	-19.3		48.0	39.5	32.2	27.6	25.4
3X+3Y	PLATE	STRAIGHT	-21.6	-22.1	-23.0	-23.8	-23.0	-22.1	-21.6	21.7	22.8	23.1	22.8	21.7
		CURVED	-27.2	-24.2	-20.1	-23.0	-21.8	-23.1	-24.7	22.8	23.3	23.5	23.0	21.2
	WEB	STRAIGHT		-21.4	-22.9	-23.6	-22.9	-21.4		31.8	32.2	33.5	33.2	31.8
		CURVED		-23.9	-25.6	-26.4	-25.3	-22.9		33.4	34.0	34.2	33.6	31.1
5X+5Y	PLATE	STRAIGHT	-23.2	-21.6	-20.7	-22.1	-24.1	-26.2	-28.1	15.6	17.6	21.6	27.0	32.3
		CURVED	-24.3	-19.7	-18.0	-20.7	-23.8	-25.9	-37.3	18.1	18.6	21.5	25.6	29.3
	WEB	STRAIGHT		-20.9	-20.9	-22.5	-24.5	-25.6		23.2	26.1	32.1	39.9	47.5
		CURVED		-19.6	-21.2	-24.6	-28.2	-29.3		26.8	27.6	32.0	38.0	43.3

From Table 2.14 it can be seen that for the straight bridge the total vertical reactions at the two end supports and the center support remain essentially unchanged as the loads move from girder 1 to 3 to 5, the applied torque created by the eccentric loads being taken by torsional reactions T_W, T_F, and T_E. Comparing the results for the curved bridge to these, it can be seen that vertical reactions do change as the loads move from girder 1 to 3 to 5 and that the applied torque is taken partially by torsional reactions and partially by the couples formed by the changing vertical reactions. The results for loads on center girder 3 are generally quite similar for the straight and curved bridges.

The results in Table 2.15 reveal that the total internal moments at a section for the straight bridge are practically independent of transverse load position. The same is essentially true for the curved bridge positive moment values in the loaded spans between the end support and midspan, and they are very similar to the straight bridge values. However, in the negative moment regions over the center support and in the unloaded span, the curved bridge results vary somewhat as the loads are moved from girder 1 to 3 to 5. For loads on girder 3 the straight and curved bridge values are quite close along the entire span. The values of internal moments for the straight bridge in Table 2.15 have been adjusted from those given in References [10, 11] to account for interpolations required by the mesh size used in the finite element analysis.

The transverse distribution of deflections at midspan section X and Y are given in Tables 2.16. Values taken from the straight bridge results have been multiplied by a factor of 491/400 = 1.23 to reflect the fact that the average values of E used in the straight and curved bridge analyses were 491,000 and 400,000 ksf respectively. As can be seen for loads on girder 3, the deflections at 3X and 3Y are almost identical for the two bridges, however, at the outer girder (longer and more flexible) points 5X and 5Y, the deflections are larger and at the inner girder (shorter and stiffer) points 1X and 1Y, the deflections are smaller for the curved bridge compared to the straight bridge. For the straight bridge the values are identical at girders 5 and 1 for loads on girder 3 because of symmetry. Similar reasoning can be used to explain the differences for loads on other girders. The differences between the deflections of the straight and curved bridges are small and from a design standpoint would certainly not be considered important.

A summary of a typical transverse distribution of internal moments to each girder and of the longitudinal membrane forces at Section A is presented in Tables 2.17 and 2.18. Once again while some differences exist between the straight and curved bridge values, they would not be considered significant from a design standpoint. The greatest difference occurs in the N_x forces in top slab adjacent to loaded girders 1 or 5.

2.7 Computer Times for Curved Bridge Model Analyses

Of particular interest in comparing solutions by various computer programs are the computer times and costs involved in obtaining the solutions. Table 2.19 summarizes a comparison of typical runs made on the CDC 6400 computer at the University of California Computer Center for analyses of the curved bridge model using SAP, CURDI and CELL.

The half band width, Column (2), is equal to the number of degrees of freedom per node times the sum of the maximum difference in nodal point numbers of any element plus one. Proper numbering of the nodes will keep the band width to a minimum and thus reduce the computer time accordingly. The number of equations, Column (4), equals the total number of nodes times the degrees of freedom per node. SAP and CELL solve the number of equations shown once, while CURDI solves its number 100 times, once for each harmonic. For multiple load cases, Column (5), SAP and CELL reduce the stiffness matrix for the first load case, and this can then be also used for subsequent load cases. Thus additional load cases can be treated more economically than the first one. Because of the harmonic analysis used in CURDI, this is not possible and thus each load case must be treated as a new problem.

Columns (6) to (11) give the computer times in seconds. CP stands for central computer processing time and PP stands for peripheral unit processing time. For programs such as CURDI and CELL, which require large core storage, PP time is charged at a rate of 0.9 to 1.6 times CP time. For comparative purposes only, Column (12) indicates actual costs charged by the University of California Computer Center for running the total number of load cases shown in Column (5). Actual costs on other computer systems would of course depend on the system and the rate schedule.

A study of Table 2.19 makes it evident that the cost for a SAP analysis is very small compared to analyses by CURDI or CELL. The latter two programs of course involve a complete analysis of the folded plate system. Comparing CURDI and CELL, for a single load case, Columns (6) and (7), CURDI is faster, but for additional load cases, Columns (8) and (9), the reverse is true. CURDI will give more accurate results with a

TABLE 2.19 CDC 6400 CP AND PP COMPUTER TIMES (SECONDS) FOR CURVED BRIDGE MODEL ANALYSIS

PROGRAM	BAND WIDTH	NUMBER OF HARMONICS	NUMBER OF EQUATIONS	NUMBER OF LOAD CASES	FIRST LOAD CASE		NEXT LOAD CASE		TOTAL		COST ($)
					CP	PP	CP	PP	CP	PP	
(1)	(2)	(3)	(4)	(5)	(6)	(7)	(8)	(9)	(10)	(11)	(12)
SAP	18	-	186	10	8	6	1	6	17	60	4
CURDI	12	100	48	5	205	126	205	126	1025	630	90
CELL	90	-	2170	12	406	160	56	160	1022	1920	165

coarser mesh than CELL, in cases for which it is applicable. However, CELL has much greater generality in terms of the material and geometry properties as well as boundary conditions of the structures which it can analyze.

In comparing computer times and cost, it must be recognized that additional time and costs involved in preparing the input data and interpreting the results from the output generally involve costs which are many times that of the computer cost itself.

2.8 Comments on Comparison of Theoretical Deflections and Strains with Experimental Values

Analytical methods used for comparison with experimental results, e.g. the folded plate theory with the associated CURDI computer program, the finite element approach with the associated CELL program, or the three dimensional frame analysis used in the SAP program, are based on the linear elastic behavior of an uncracked, homogeneous, isotropic structure. The theoretical values given by these analyses for the deflection of a box girder bridge at a certain point or the strain at a cross-section are not immediately applicable to those experimentally obtained from the cracked reinforced concrete box girder bridge model. It is clear that the assumption of a completely uncracked section as made in the theories would result in underestimation of the actual deflection of the box girder bridge model. Again, the strain values predicted by the theories in the part of the box girder cross-section subject to tension can not directly be compared with the experimental case where, due to concrete cracking, most of the stress was concentrated in the steel reinforcement.

Theoretical deflections based on an uncracked section should form a lower bound on the actual deflection in the model. An upper bound should be formed by assuming a fully cracked transformed section throughout, since it neglects participation of the concrete between cracks. Various empirical formulae have been proposed for interpolating between these two bounds, in calculating the deflection of straight reinforced concrete beams. For complex systems such as bridge decks, which involve transverse as well as longitudinal distributions of deflections, it will be important to ascertain whether a relatively uniform ratio of experimental to theoretical deflections (based on uncracked section using CELL) exists under various loadings and if so, what this ratio is for various stress levels. If these can be established then the deflections from analyses based on an uncracked section can be utilized to predict deflections in an actual reinforced concrete bridge structure under a given loading.

Direct comparisons between the longitudinal strains predicted by the CURDI and CELL programs, with their analytical models of homogeneous linear elastic material without cracking, and the actual experimental strains measured in the concrete and steel of the cracked box girder bridge model are difficult to make. If it is assumed that the force distribution over the width of the box girder model given by the CELL programs is representative of the actual force distribution, then bearing in mind that each girder of the box girder bridge model essentially behaves like an I-beam with the T-C couple acting in the flanges, approximate expressions for the strains in the girders can be derived.

Thus, for comparison with experimental values, compressive strains were obtained from the theoretical results given by the CELL program by dividing the values for the longitudinal compressive force N_x per unit length at each gaged location by the respective plate thickness and the concrete elastic modulus E_c. Theoretical steel strains were obtained by considering a fully cracked section and dividing the total longitudinal tensile force N_x per girder by the product of the steel area of the girder and the steel elastic modulus E_s.

As the contribution of the transverse membrane force N_y to the strains was found to be negligible it was ignored in the calculations.

Hereafter, comparisons for strains are based on theoretical strain values derived as above from the CELL analysis.

2.9 Summary

A comprehensive discussion of the various theoretical analyses made on the curved bridge model has been presented. Results obtained using various computer programs as well as for the straight and curved bridge models have been compared. The following important conclusions may be stated.

1. An analysis such as provided by the SAP program, in which the bridge system is assumed to be a simple three dimensional frame made up of one dimensional elements, can be used to accurately predict the longitudinal distribution of theoretical total reactions, moments and centerline deflections.

2. The finite element program CELL provides a solution of the bridge system as a three dimensional folded plate system, which can be used to accurately predict the longitudinal and transverse distribution of theoretical reactions, moments, deflections and internal membrane and plate bending forces.

Henceforth, the CELL solution will be used for all theoretical values to be compared with experimental results.

3. Comparing the theoretical results for the similar straight and curved bridge models, while differences exist, they are not large or significant from a design standpoint. It should be noted that the horizontal curvature of the bridge model studied was selected as being the sharpest generally encountered in present California highway design. It is important to point out that the similarity of behavior exhibited by the straight and curved concrete box girder bridge models will not be valid for a flexible cross-section such as might exist for a composite box girder bridge consisting of a thick concrete top slab combined with a thin walled steel box girder. A limited number of analytical studies on this latter bridge type without intermediate diaphragms have shown that significant differences can exist between the response of straight and curved bridge models. The addition of intermediate diaphragms tends to decrease these differences in behavior.

3. REDUCTION OF EXPERIMENTAL DATA

3.1 General Remarks

In order to process the large volume of data obtained from the experimental program, so as to evaluate the reactions, forces, moments, etc., four computer programs were developed. The programs, which will be considered in detail below, were designated as DATAMAN, MANIP, REDUCE and TABLEP. Experimental data as obtained from the S.E.S.M. Low Speed Scanner for each loading step on the box girder bridge model were handled by these four computer programs in succession, or separately as instructed, and all calculations necessary for theoretical comparisons, equilibrium checks and important quantities were made and printed in desired formats.

3.2 DATAMAN Program

DATAMAN, representing Data management, was an extremely versatile program able to handle all kinds of data as well as to help in the editing of "raw" data. In the form used to reduce data pertaining to the box girder bridge model, DATAMAN performed the following functions for each loading step. The data output from the Low Speed Scanner was on punched paper tape. This was fed through a teletype into the CDC 6400 computer and written onto magnetic tape. The DATAMAN program was then used to extract the data files from the magnetic tape, and output the data in the form of punched cards and printed output. At the same time the magnetic tape was scanned for parity errors, which were listed in the printed output.

3.3 MANIP Program

MANIP, representing Manipulate, was used to obtain the net readings for the load step by taking the difference of the readings for the load step considered from the pre-load condition readings. All strain readings coming from over-range (i.e. unbalanced) or faulty gages were screened by the MANIP program, and replaced by a zero reading. All these substitutions were separately catalogued in a list of "diagnostics" for each load case. The net readings were then punched out on two sets of punched cards. The first set was the data input for the data reduction program REDUCE, and the second set was used for graphic plotting of the raw data.

Using the plots of the raw data, readings which were obviously grossly inconsistent were deleted and replaced in the punched card deck by interpolated values. When possible, symmetry considerations were also used to replace these readings. The number of replaced readings for any load case never exceeded 7 to 8 channels out of a total of 192 channels. Of these, 5 channels were inactive due to damage to the gages during the construction of the model.

The edited card decks were then used as input for the main data reduction program REDUCE.

3.4 REDUCE Program

The REDUCE program consisted of a main program, and the three subprograms ADJSTRN, MOMENT and REACTION.

The main program arranged the data under the categories of standard resistor, applied jack loads, weldable gage readings, concrete strain meter readings, potentiometer deflection readings and load cell reactions. To facilitate comparisons, the net readings were normalized to a load of 100 kips in the span loaded. All strains were rounded off to the nearest micro in/in, all loads and reactions to the nearest hundredth of a kip and all deflections to the nearest ten-thousandths of an inch.

An example of the output from the main program REDUCE is shown in Fig. 3.1.

3.5 ADJSTRN Subprogram

At each instrumented section of the box girder bridge model, Fig. 3.2, the strains in the top slab and bottom slab were treated separately. The top slab was divided into six regions, four regions corresponding to the four cell bays of the box girder model and two regions corresponding to the cantilever overhangs on either side. The bottom slab was divided into four regions corresponding to the four cell bays of the box girder model.

Each cell bay of the top or bottom slab whether in tension or in compression was instrumented at 5 points (i.e. at the girder lines, midbays and quarter bays), the girder locations being common to contiguous bays. The cantilever overhangs were instrumented at 2 points (i.e. exterior girder and edge of overhang). The arrangement of gages can be seen in Fig. 3.2.

The operation of the ADJSTRN program at an instrumented section was as follows:

1. Averages of observed, i.e. measured strain values, were taken at necessary instrumented locations.
2. The gages were checked for tension or compression readings and the strain values compared with ceiling values of strain, the yield strain of 2070 μ in./in. for steel and the crushing strain of 1000 μ in./in. for concrete. Any weldable gage reading in

BOX GIRDER CURVED BRIDGE MODEL

REDUCTION OF EXPERIMENTAL DATA

II.2.17. 30 KSI. (5-X)+(5-Y) TO 19.34 KIPS. NORMALIZED TO 100 KIPS.
MULTIPLICATOR USED TO NORMALIZE LOAD..... 5.27777

SERIAL	NAME	CH.NO.	TYPE	READING
STANDARD RESISTORS				
1	STDR1	63	0	11.61
2	STDR2	127	0	9.50
3	STDR3	191	0	14.78
4	STDR4	251	0	7.39
APPLIED LOADS IN KIPS				
5	R000J1	201	3	-100.00
6	R000J2	202	3	-103.53
LOAD CELL REACTIONS IN KIPS				
7	R100E1	203	3	23.42
8	R200E1	209	3	13.09
9	R300E1	210	3	-5.90
10	R400E1	211	3	-13.19
11	R500E1	217	3	-44.48
12	R000S1	218	3	-66.14
13	R000S2	219	3	-15.42
14	R000S3	225	3	-5.49
15	R000S4	226	3	-56.48
16	R000S5	227	3	3.86
17	R000S6	233	3	.74
18	R000S7	234	3	.16
19	R000S8	235	3	3.07
20	R100W1	241	3	20.60
21	R200W1	242	3	18.67
22	R300W1	243	3	1.51
23	R400W1	249	3	-19.51
24	R500W1	250	3	-49.92
STEEL MICRODOT STRAINS IN MICRO-INCH PER INCH				
25	W100A	0	1	620.
26	W125A	1	1	509.
27	W150A	2	1	568.
28	W175A	3	1	338.
29	W200A	4	1	648.
30	W225A	5	1	493.
31	W250A	6	1	505.
32	W275A	7	1	691.
33	W300A	8	1	765.
34	W325A	9	1	766.
35	W350A	10	1	661.
36	W375A	11	1	919.
37	W400A	12	1	828.
38	W425A	13	1	825.
39	W450A	14	1	639.
40	W475A	15	1	958.
41	W500A	16	1	1201.
42	W000B	17	1	556.
43	W100B	18	1	573.
44	W125B	19	1	625.
45	W150B	20	1	501.
46	W175B	21	1	660.
47	W200B	22	1	725.
48	W225B	23	1	679.
49	W250B	24	1	658.
50	W275B	25	1	864.
51	W300B	26	1	797.
52	W325B	27	1	975.
53	W350B	28	1	725.
54	W375B	29	1	854.
55	W400B	30	1	852.
56	W425B	31	1	975.
57	W450B	32	1	835.
58	W475B	33	1	1001.
59	W500B	34	1	825.
60	W600B	35	1	868.
61	W000C	36	1	501.
62	W100C	37	1	473.
63	W125C	38	1	442.
64	W150C	39	1	458.
65	W175C	40	1	587.
66	W200C	41	1	717.
67	W225C	42	1	586.
68	W250C	43	1	591.
69	W275C	44	1	673.
70	W300C	45	1	861.
71	W325C	46	1	730.
72	W350C	47	1	641.
73	W375C	48	1	842.
74	W400C	49	1	989.
75	W425C	50	1	883.
76	W450C	51	1	773.
77	W475C	52	1	785.
78	W500C	53	1	897.
79	W600C	54	1	934.
80	W100D	55	1	422.
81	W125D	56	1	453.
82	W150D	57	1	567.
83	W175D	58	1	480.
84	W200D	59	1	650.
85	W225D	60	1	588.
86	W250D	61	1	624.
87	W275D	62	1	588.
88	W300D	64	1	730.
89	W325D	65	1	769.
90	W350D	66	1	894.
91	W375D	67	1	890.
92	W400D	72	1	1267.
93	W425D	73	1	965.
94	W450D	74	1	1105.
95	W475D	75	1	1262.
96	W500D	80	1	511.

Fig. 3.1 TYPICAL OUTPUT FROM REDUCE PROGRAM

CONCRETE TELEDYNE STRAINS IN MICRO-INCH PER INCH

97	K000A	128	2	-209.
98	K100A	129	2	-325.
99	K125A	130	2	-176.
100	K150A	131	2	-208.
101	K175A	132	2	-289.
102	K200A	133	2	-260.
103	K225A	134	2	-291.
104	K250A	135	2	-248.
105	K275A	136	2	-240.
106	K300A	137	2	-280.
107	K325A	138	2	-329.
108	K350A	139	2	-265.
109	K375A	140	2	-308.
110	K400A	141	2	-369.
111	K425A	142	2	-313.
112	K450A	143	2	-277.
113	K475A	144	2	-371.
114	K500A	145	2	-386.
115	K600A	146	2	-228.
116	K100B	147	2	-465.
117	K125B	148	2	-463.
118	K150B	149	2	-461.
119	K175B	150	2	-415.
120	K200B	151	2	-466.
121	K225B	152	2	-383.
122	K250B	153	2	-451.
123	K275B	154	2	-436.
124	K300B	155	2	-451.
125	K325B	156	2	-466.
126	K350B	157	2	-450.
127	K375B	158	2	-435.
128	K400B	159	2	-432.
129	K425B	160	2	-461.
130	K450B	161	2	-470.
131	K475B	162	2	-443.
132	K500B	163	2	-415.
133	K100C	164	2	-440.
134	K125C	165	2	-367.
135	K150C	166	2	-390.
136	K175C	167	2	-352.
137	K200C	168	2	-404.
138	K225C	169	2	-521.
139	K250C	170	2	-391.
140	K275C	171	2	-438.
141	K300C	172	2	-422.
142	K325C	173	2	-448.
143	K350C	174	2	-563.
144	K375C	175	2	-546.
145	K400C	176	2	-431.
146	K425C	177	2	-491.
147	K450C	178	2	-439.
148	K475C	179	2	-460.
149	K500C	180	2	-481.
150	K000D	181	2	-95.
151	K100D	182	2	-178.
152	K125D	183	2	-320.
153	K150D	184	2	-369.
154	K175D	185	2	-295.
155	K200D	186	2	-270.
156	K225D	187	2	-262.
157	K250D	188	2	-258.
158	K275D	189	2	-343.
159	K300D	190	2	-313.
160	K325D	192	2	-477.
161	K350D	200	2	-421.
162	K375D	2C8	2	-463.
163	K400D	216	2	-427.
164	K425D	224	2	-237.
165	K450D	232	2	-630.
166	K475D	240	2	-681.
167	K500D	248	2	-460.
168	K600D	193	2	-181.

POTENTIOMETER DEFLECTIONS IN INCHES

169	P100X	68	4	.3045
170	P200X	69	4	.5241
171	P300X	70	4	.7785
172	P400X	71	4	1.0228
173	P500X	76	4	1.2899
174	P100B	77	4	-.0491
175	P200B	78	4	.1388
176	P300B	79	4	.3383
177	P400B	84	4	.5816
178	P500B	85	4	.7500
179	P100Z	86	4	-.2465
180	P200Z	87	4	-.1135
181	P400Z	92	4	.1816
182	P500Z	93	4	.3832
183	P100C	94	4	-.0222
184	P200C	95	4	.1499
185	P300C	100	4	.3431
186	P400C	101	4	.6228
187	P500C	102	4	.8972
188	P100Y	103	4	.3061
189	P200Y	1C8	4	.4702
190	P300Y	109	4	.7384
191	P400Y	110	4	1.0809
192	P500Y	111	4	1.6847

FIG. 3.1 (CONT.) TYPICAL OUTPUT FROM REDUCE PROGRAM

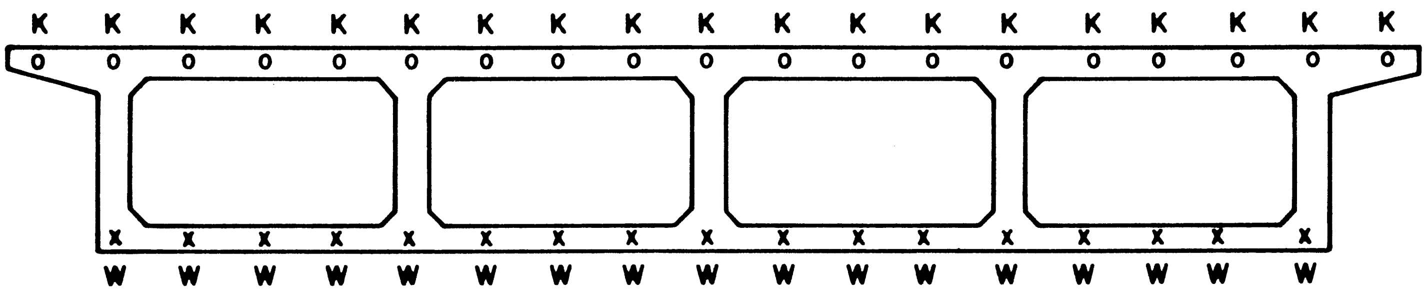

(a) SECTION A AND D

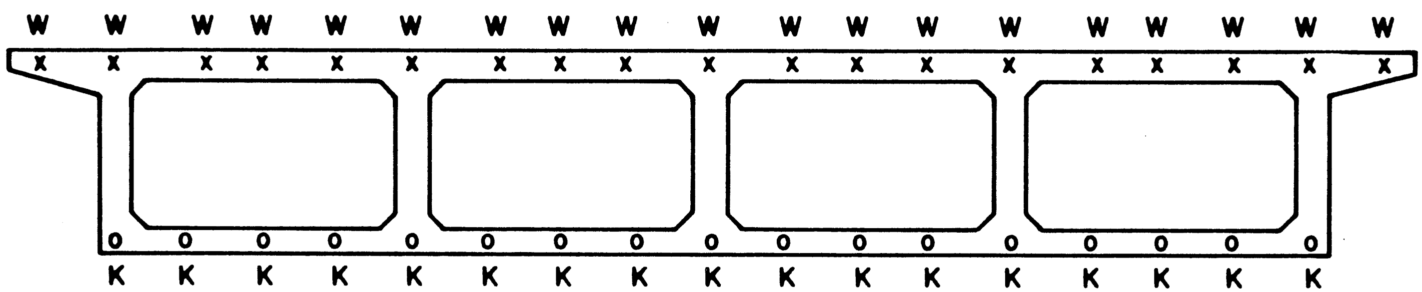

(b) SECTION B AND C

K-CONCRETE STRAIN METER
W-STEEL REINFORCEMENT
WELDABLE GAGE

FIG. 3.2 LOCATIONS OF INTERNAL CONCRETE STRAIN METERS AND STEEL REINFORCEMENT WELDABLE GAGES excess of the yield strain or any concrete strain meter in excess of the crushing strain was discarded. [In practice, because of the editing procedure, it was not necessary to use this option.]

3. The 5 point adjustment called for the passing of a least-squares parabola to fit the five points. At each gaged location the adjusted value was compared with the measured (observed) value. If the absolute value of the difference of these two values exceeded 20% of the maximum measured value in this particular bay, the largest violating strain value was discarded and a least squares parabola was passed to fit the remaining four points. The ordinates of the second parabola were then printed out at several locations to facilitate integration of strains, stresses, etc. If two values did not satisfy the requirement, the two violating strain values were discarded and a simple parabola was passed through the remaining three points. If all values lay between the prescribed limits, the first least squares parabola was taken as the curve for strain distribution in the bay and ordinates of this parabola were printed out at several locations to facilitate integration of strains, stresses, etc.

4. The strain values at the cantilever edges of the top slab were compared with those at the girders nearest them. If a cantilever edge strain value did not lie between 0.5 and 1.5 times the strain value for the adjacent girder, it was replaced by the strain value at the girder; otherwise, it was retained as the actual value. A straight line was passed through the two points.

A typical output from the ADJSTRN Subprogram is given in Fig. 3.3.

3.6 MOMENT Subprogram

At each instrumented section the MOMENT program first calculated the following from the adjusted strains for each girder separately: (1) the compressive forces in the slab concrete and steel; the girder web concrete and steel; and (2) the tensile forces in the slab and girder web steel. All these quantities were classified and then girder moments were calculated in terms of kip-ft and as percentages of the total moment at the section about four axes: the compression flange mid-depth; the line of main tensile reinforcement; the neutral axis of the box girder uncracked cross-section and the individual neutral axis of each girder as determined from the adjusted strain values. A typical output from the MOMENT Subprogram is given in Fig. 3.4.

3.7 REACTION Subprogram

The REACTION program printed the experimental reactions at the east and west abutments and center column footing of the box girder bridge model and compared the results with the applied loads and with reactions calculated using a 3-dimensional frame analysis (SAP Program) for each loading case. External moments of all experimental loads and reactions were calculated, first, about the N-S centerline and then about E-W centerline of the bridge, to provide additional external static checks on the experimental reaction values. Moments at the instrumented sections and the midspans were also computed from the experimental reactions and compared with analytical values from the SAP program. A typical output from the REACTION Subprogram is given in Fig. 3.5.

```
TI.2.17.  30 KSI.  (5-X)+(5-Y) TO 19.34 KIPS. NORMALIZED TO 100 KIPS.
STRAIN ADJUSTMENTS (ALL STRAINS IN MICRO-IN/IN)

SECTION A

OBSERVED STRAINS   -209. -325. -176. -208. -289. -260. -291. -248. -240. -280. -329. -265. -308. -369. -313. -277. -371. -386. -228.

                                                                     -298. -285. -292. -317. -360.
FIRST ADJUSTED           -297. -233. -210. -229. -290.                                         -364. -314. -304. -332. -400.
                                                 -274. -261. -256. -259. -269.

                                                                                               -364. -314. -304. -332. -400.
ADJUSTED STRAINS   -209. -325.                   -274. -261. -256. -259. -269.                                         -386. -228.
                         -297. -233. -210. -229. -290.                   -298. -285. -292. -317. -360.

                                                                                               1.01  1.00   .91  1.11   .96
RATIOS (OBS./ADJ.)  1.00  1.00                    .95  1.11   .97   .93  1.04                                          1.00  1.00
                          1.10   .76   .99  1.26  .90                     .94  1.15   .91   .97  1.02

       ****************************************************************************************************
             *                   *                    *                    *                    *
             *                   *                    *                    *                    *
             *                   *                    *                    *                    *
             *                   *                    *                    *                    *
             *                   *                    *                    *                    *
             ***************************************************************************************

OBSERVED STRAINS          620.  509.  568.  338.  648.  493.  505.  691.  765.  766.  661.  919.  828.  825.  639.  958. 1201.

                                                                         757.  747.  762.  803.  870.
FIRST ADJUSTED            639.  509.  458.  486.  593.                                           857.  731.  748.  907. 1208.
                                                  624.  532.  530.  618.  797.

                                                                                                 857.  731.  748.  907. 1208.
ADJUSTED STRAINS                                  624.  532.  530.  618.  797.
                          605.  549.  535.  573.  653.                    757.  747.  762.  803.  870.

                                                                                                  .97  1.13   .85  1.06   .99
RATIOS (OBS./ADJ.)                                1.04   .93   .95  1.12   .96
                          1.02   .93  1.06   .59   .99                    1.01  1.03   .87  1.14   .95
```

FIG. 3.3 TYPICAL OUTPUT FOR AN INSTRUMENTED SECTION FROM ADJSTRN SUBPROGRAM

BOX GIRDER BRIDGE MODEL - CALCULATION OF GIRDER FORCES AND MOMENTS

II.2.17. 30 KSI. (5-X)+(5-Y) TO 19.34 KIPS. NORMALIZED TO 100 KIPS.

SECTION A
MODULUS OF ELASTICITY FOR CONCRETE....(KSI).. .270E-02

	GIRDER 1	GIRDER 2	GIRDER 3	GIRDER 4	GIRDER 5	ALL GIRDERS
LOCATION OF GIRDER EXPERIMENTAL NEUTRAL AXIS (INCHES)						
DISTANCE OF N.A. FROM LINE OF COMP. METERS	6.27	5.65	4.94	5.46	4.53	
DISTANCE OF N.A. FROM LINE OF TENSILE STEEL	12.20	12.82	13.53	13.01	13.94	
DETAILED SUMMARY OF INTERNAL FORCES (KIPS)						
COMPRESSIVE FORCES						
CONCRETE IN FLANGE	-38.86	-46.76	-51.46	-60.08	-50.97	
STEEL IN FLANGE	-5.97	-7.21	-7.85	-9.23	-7.80	
TOTAL IN FLANGE	-44.83	-53.96	-59.31	-69.31	-58.77	
CONCRETE IN WEB	-10.91	-5.00	-4.24	-6.15	-10.93	
STEEL IN WEB	-.52	-.33	-.12	-.35	0.	
TOTAL IN WEB	-11.43	-5.33	-4.35	-6.50	-10.93	
TOTAL COMPRESSIVE FORCE	-56.25	-59.29	-63.66	-75.82	-69.70	-324.72
TENSILE FORCES						
STEEL IN FLANGE	23.29	42.59	50.40	58.79	40.17	
STEEL IN WEB	3.32	3.73	4.82	5.13	7.76	
TOTAL TENSION FORCE	26.61	46.32	55.21	63.92	47.94	239.99
NET AXIAL FORCE	-29.65	-12.97	-8.45	-11.90	-21.76	-84.73
RATIO OF COMP. FORCE TO TENSILE FORCE	2.11	1.28	1.15	1.19	1.45	1.35
DETAILED SUMMARY OF INTERNAL MOMENTS (KIP-FT)						
ABOUT COMPRESSION FLANGE MID-DEPTH						
STEEL IN TENSION FLANGE	35.84	65.55	77.56	90.48	61.83	
STEEL IN TENSION WEB	3.48	3.87	4.96	5.31	7.93	
CONCRETE IN COMPRESSION WEB	-1.97	-1.00	-.78	-1.20	-1.67	
STEEL IN COMPRESSION WEB	-.20	-.13	-.04	-.14	0.	
TOTAL MOMENT ABOUT COMPRESSION FLANGE	37.14	68.29	81.70	94.45	68.09	349.66
PERCENT OF TOTAL MOMENT TAKEN BY GIRDERS	(10.62)	(19.53)	(23.36)	(27.01)	(19.47)	(100.00)
ABOUT TENSION FLANGE STEEL						
CONCRETE IN COMPRESSION FLANGE	59.81	71.96	79.20	92.46	78.44	
STEEL IN COMPRESSION FLANGE	9.19	11.09	12.08	14.21	12.00	
CONCRETE IN COMPRESSION WEB	14.81	6.70	5.75	8.27	15.15	
STEEL IN COMPRESSION WEB	.60	.38	.13	.41	-0.	
STEEL IN TENSION WEB	-1.64	-1.87	-2.45	-2.58	-4.02	
TOTAL MOMENT ABOUT TENSION FLANGE	82.77	88.26	94.70	112.76	101.58	480.06
PERCENT OF TOTAL MOMENT TAKEN BY GIRDERS	(17.24)	(18.38)	(19.73)	(23.49)	(21.16)	(100.00)
ABOUT ENTIRE GROSS SECTION NEUTRAL AXIS (DISTANCE FROM TOP DECK FACE = 9.37 IN.)						
STEEL IN TENSION FLANGE	19.85	36.31	42.96	50.12	34.25	

FIG. 3.4 TYPICAL OUTPUT FOR AN INSTRUMENTED SECTION FROM MOMENT SUBPROGRAM

STEEL IN TENSION WEB	1.19	1.31	1.65	1.79	2.60	
CONCRETE IN COMPRESSION FLANGE	26.70	32.12	35.35	41.28	35.02	
STEEL IN COMPRESSION FLANGE	4.10	4.95	5.39	6.34	5.36	
CONCRETE IN COMPRESSION WEB	5.52	2.43	2.13	3.02	5.83	
STEEL IN COMPRESSION WEB	.16	.10	.03	.11	-0.	
TOTAL MOMENT ABOUT GROSS SECTION N.A.	57.52	77.22	87.53	102.65	83.06	407.97
PERCENT OF TOTAL MOMENT TAKEN BY GIRDERS	(14.10)	(18.93)	(21.45)	(25.16)	(20.36)	(100.00)
ABOUT GIRDER EXPERIMENTAL NEUTRAL AXIS						
STEEL IN TENSION FLANGE	23.68	45.49	56.83	63.76	46.66	
STEEL IN TENSION WEB	1.74	2.11	2.98	2.98	5.00	
CONCRETE IN COMPRESSION FLANGE	20.30	22.03	21.18	27.32	19.25	
STEEL IN COMPRESSION FLANGE	3.12	3.39	3.23	4.20	2.94	
CONCRETE IN COMPRESSION WEB	3.72	1.35	.97	1.59	2.45	
STEEL IN COMPRESSION WEB	.07	.03	.00	.02	-0.	
TOTAL MOMENT ABOUT EXPERIMENTAL N.A.	52.63	74.41	85.18	99.87	76.31	388.39
PERCENT OF TOTAL MOMENT TAKEN BY GIRDERS	(13.55)	(19.16)	(21.93)	(25.71)	(19.65)	(100.00)

BOX GIRDER BRIDGE MODEL - SUMMARY OF GIRDER FORCES AND MOMENTS

	GIRDER 1	GIRDER 2	GIRDER 3	GIRDER 4	GIRDER 5	ALL GIRDERS
LOCATION OF GIRDER EXPERIMENTAL NEUTRAL AXIS (INCHES)						
(1) DISTANCE OF N.A. FROM LINE OF COMP. METERS	6.27	5.65	4.94	5.46	4.53	
(2) DISTANCE OF N.A. FROM LINE OF TENSILE STEEL	12.20	12.82	13.53	13.01	13.94	
TOTAL INTERNAL FORCES (KIPS)						
(3) COMPRESSIVE FORCES	-56.25	-59.29	-63.66	-75.82	-69.70	-324.72
(4) TENSILE FORCE	26.61	46.32	55.21	63.92	47.94	239.99
(5) NET AXIAL FORCE	-29.65	-12.97	-8.45	-11.90	-21.76	-84.73
(6) RATIO OF COMP. FORCE TO TENSILE FORCE	2.11	1.28	1.15	1.19	1.45	1.35
TOTAL INTERNAL MOMENTS (KIP-FT)						
(7) ABOUT COMPRESSION FLANGE MID-DEPTH	37.14	68.29	81.70	94.45	68.09	349.66
(8) ABOUT TENSION FLANGE STEEL	82.77	88.26	94.70	112.76	101.58	480.06
(9) ABOUT ENTIRE GROSS-SECTION N.A.	57.52	77.22	87.53	102.65	83.06	407.97
(10) ABOUT GIRDER EXPERIMENTAL N.A.	52.63	74.41	85.18	99.87	76.31	388.39
MOMENT PERCENTAGES TAKEN BY EACH GIRDER						
(11) ABOUT COMPRESSION FLANGE MID-DEPTH	10.62	19.53	23.36	27.01	19.47	(100.00)
(12) ABOUT TENSION FLANGE STEEL	17.24	18.38	19.73	23.49	21.16	(100.00)
(13) ABOUT ENTIRE GROSS-SECTION N.A.	14.10	18.93	21.45	25.16	20.36	(100.00)
(14) ABOUT GIRDER EXPERIMENTAL N.A.	13.55	19.16	21.93	25.71	19.65	(100.00)

TOTAL SECTION MOMENTS
(15) CALCULATED FROM EXPERIMENTAL LOADS AND REACTIONS = 477.23
(16) RATIO (7) TO (15) = .73
(17) RATIO (8) TO (15) = 1.01
(18) RATIO (9) TO (15) = .85
(19) RATIO (10) TO (15) = .81

FIG. 3.4 (CONT.) TYPICAL OUTPUT FOR AN INSTRUMENTED SECTION FROM MOMENT SUBPROGRAM

******************************* SUMMARY OF MODIFIED FORCES AND MOMENTS IN SECTIONS A AND B *******************************

TENSILE AND COMPRESSIVE MODIFICATION FACTORS IN SECTION A 1.25600 .92100

TOTAL INTERNAL FORCES (KIPS)						
(3) COMPRESSIVE FORCES	-51.81	-54.61	-58.63	-69.83	-64.19	-299.07
(4) TENSILE FORCE	33.42	58.17	69.34	80.28	60.21	301.43
(5) NET AXIAL FORCE	-18.39	3.57	10.71	10.45	-3.98	2.36
(6) RATIO OF COMP. FORCE TO TENSILE FORCE	1.55	.94	.85	.87	1.07	.99
TOTAL INTERNAL MOMENTS (KIP-FT)						
(7) ABOUT COMPRESSION FLANGE MID-DEPTH	47.38	86.15	102.88	119.08	86.08	441.56
(8) ABOUT TENSION FLANGE STEEL	75.68	80.66	86.40	102.99	92.21	437.93
(9) ABOUT ENTIRE GROSS-SECTION N.A.	60.02	83.72	95.56	111.93	88.84	440.07
(10) ABOUT GIRDER EXPERIMENTAL N.A.	56.99	84.47	98.49	114.33	87.59	441.87
MOMENT PERCENTAGES TAKEN BY EACH GIRDER						
(11) ABOUT COMPRESSION FLANGE MID-DEPTH	10.73	19.51	23.30	26.97	19.49	(100.00)
(12) ABOUT TENSION FLANGE STEEL	17.28	18.42	19.73	23.52	21.06	(100.00)
(13) ABOUT ENTIRE GROSS-SECTION N.A.	13.64	19.02	21.71	25.43	20.19	(100.00)
(14) ABOUT GIRDER EXPERIMENTAL N.A.	12.90	19.12	22.29	25.88	19.82	(100.00)

TOTAL SECTION MOMENTS
(15) CALCULATED FROM EXPERIMENTAL LOADS AND REACTIONS = 477.23
(16) RATIO (7) TO (15) = .93
(17) RATIO (8) TO (15) = .92
(18) RATIO (9) TO (15) = .92
(19) RATIO (10) TO (15) = .93

FIG. 3.4 (CONT.) TYPICAL OUTPUT FOR AN INSTRUMENTED SECTION FROM MOMENT SUBPROGRAM

******************************* SUMMARY OF MODIFIED FORCES AND MOMENTS IN SECTIONS A AND B *******************************

TENSILE AND COMPRESSIVE MODIFICATION FACTORS IN SECTION A 1.25600 .92100

TOTAL INTERNAL FORCES (KIPS)						
(3) COMPRESSIVE FORCES	-51.81	-54.61	-58.63	-69.83	-64.19	-299.07
(4) TENSILE FORCE	33.42	58.17	69.34	80.28	60.21	301.43
(5) NET AXIAL FORCE	-18.39	3.57	10.71	10.45	-3.98	2.36
(6) RATIO OF COMP. FORCE TO TENSILE FORCE	1.55	.94	.85	.87	1.07	.99
TOTAL INTERNAL MOMENTS (KIP-FT)						
(7) ABOUT COMPRESSION FLANGE MID-DEPTH	47.38	86.15	102.88	119.08	86.08	441.56
(8) ABOUT TENSION FLANGE STEEL	75.68	80.66	86.40	102.99	92.21	437.93
(9) ABOUT ENTIRE GROSS-SECTION N.A.	60.02	83.72	95.56	111.93	88.84	440.07
(10) ABOUT GIRDER EXPERIMENTAL N.A.	56.99	84.47	98.49	114.33	87.59	441.87
MOMENT PERCENTAGES TAKEN BY EACH GIRDER						
(11) ABOUT COMPRESSION FLANGE MID-DEPTH	10.73	19.51	23.30	26.97	19.49	(100.00)
(12) ABOUT TENSION FLANGE STEEL	17.28	18.42	19.73	23.52	21.06	(100.00)
(13) ABOUT ENTIRE GROSS-SECTION N.A.	13.64	19.02	21.71	25.43	20.19	(100.00)
(14) ABOUT GIRDER EXPERIMENTAL N.A.	12.90	19.12	22.29	25.88	19.82	(100.00)

TOTAL SECTION MOMENTS
(15) CALCULATED FROM EXPERIMENTAL LOADS AND REACTIONS = 477.23
(16) RATIO (7) TO (15) = .93
(17) RATIO (8) TO (15) = .92
(18) RATIO (9) TO (15) = .92
(19) RATIO (10) TO (15) = .93

FIG. 3A (CONT.) TYPICAL OUTPUT FOR AN INSTRUMENTED SECTION FROM MOMENT SUBPROGRAM

TOTAL STATICAL MOMENTS (KIP FT) CALCULATED FROM APPLIED LOADS AND REACTIONS

			MEASURED	THEORETICAL	RATIO M/T
AT SECTION A,	X = 14.42 FT	MOMENT =	477.23	449.94	1.061
AT MIDSPAN I,	X = 18.00 FT	MOMENT =	595.28	561.14	1.061
AT SECTION B,	X = 33.00 FT	MOMENT =	-493.78	-555.59	.889
AT CENTER (FROM WEST FORCES),	X = 36.00 FT	MOMENT =	-710.81	-778.04	.914
AT CENTER (FROM EAST FORCES),	X = 36.00 FT	MOMENT =	-848.51	-783.51	1.083
AT SECTION C,	X = 39.00 FT	MOMENT =	-614.78	-554.97	1.108
AT MIDSPAN II,	X = 54.00 FT	MOMENT =	559.04	592.09	.944
AT SECTION D,	X = 57.58 FT	MOMENT =	448.17	474.37	.945

FIG. 3.5 (CONT.) TYPICAL OUTPUT FROM REACTION SUBPROGRAM

3.8 TABLEP Program

The main data reduction program REDUCE and its three subprograms gave, in addition to the printed output, a deck of punched cards. This deck consisted of measured and adjusted strains, moments, deflections and reactions for selected cross-sections and girders for each load case.

These punched decks together with similar decks obtained from the theoretical finite element analysis results from CELL, were used as input for the TABLEP program. TABLEP, representing Table Printer, printed summary tables of experimental and theoretical results for each load case. The tables are presented in detail in Volume III for all load cases. Typical outputs of these tables are shown in Figs. 3.6 to 3.9.

3.9 Modification of Experimental Data

After the scheme of experimental data reduction described in the previous sections was implemented for several loading cases, it was observed that the longitudinal compressive and tensile forces at a section as obtained from the MOMENT program did not balance as statics would require. The compressive forces were consistently larger than the tensile forces, and the discrepancy between the two was largest at sections A and D. The reason for this phenomenon is as follows.

The adjusted strain values in steel and concrete were converted to stresses and forces through the use of their moduli of elasticity obtained from tests on control specimens. In the case of the concrete considerable uncertainty was expected in the determination of the modulus. Six by twelve inch cylindrical control specimens were here used to simulate the 2 or 2 1/4 in. thick, heavily reinforced compression flanges. The significant difference in the geometry of the control cylinders and the flanges

SUMMARY OF REACTIONS (KIPS OR FT-KIPS)

SEE FIGURE FOR POSITIVE DIRECTIONS
MF = MOMENT AT FOOTING ABOUT Z-AXIS
TF = MOMENT AT FOOTING ABOUT 3-AXIS

RESULTS FOR 24 KSI, 30 KSI, 40 KSI
CONDITIONING LOAD STRESS LEVELS
SIMPLY SUPPORTED, NO RESTRAINTS

REACTION OR LOAD	CONDITIONING LOAD STRESS LEVEL 24 KSI THEORY	24 KSI EXPERM	30 KSI THEORY	30 KSI EXPERM	40 KSI THEORY	40 KSI EXPERM
1E	3.30	1.27	3.30	.76	3.30	2.14
2E	5.70	8.68	5.70	7.81	5.70	7.24
3E	4.90	6.23	4.90	7.50	4.90	5.93
4E	6.45	2.22	6.45	2.92	6.45	2.86
5E	10.44	11.79	10.44	10.09	10.44	10.91
1F	34.46	35.30	34.46	33.72	34.46	35.05
2F	34.77	31.56	34.77	32.35	34.77	33.60
3F	34.75	34.53	34.75	35.99	34.75	33.80
4F	34.45	38.04	34.45	36.64	34.45	33.96
1W	3.07	4.40	3.07	4.03	3.07	5.63
2W	5.78	2.19	5.78	4.10	5.78	1.79
3W	5.16	7.86	5.16	5.21	5.16	5.23
4W	6.60	6.20	6.60	8.17	6.60	7.04
5W	10.18	10.55	10.18	10.03	10.18	10.28
RE	30.79	30.19	30.79	29.08	30.79	29.08
RF	138.43	139.43	138.43	138.70	138.43	136.41
RW	30.79	31.20	30.79	31.54	30.79	29.97
SUMR	200.01	200.82	200.01	199.32	200.01	195.46
PX	-100.00	-100.00	-100.00	-100.00	-100.00	-100.00
PY	-100.00	-97.76	-100.00	-96.28	-100.00	-99.97
SUMP	-200.00	-197.76	-200.00	-196.28	-200.00	-199.97
SUMR/SUMP	1.00	1.02	1.00	1.02	1.00	.98
TW	38.70	41.96	38.70	41.35	38.70	37.44
MF	-.04	8.57	-.04	9.84	-.04	-1.34
TF	-.91	10.88	-.91	3.04	-.91	2.42
TE	38.67	37.51	38.67	35.43	38.67	33.86
ACTUAL PX		-7.74		-11.47		-17.57
ACTUAL PY		-7.57		-11.05		-17.57

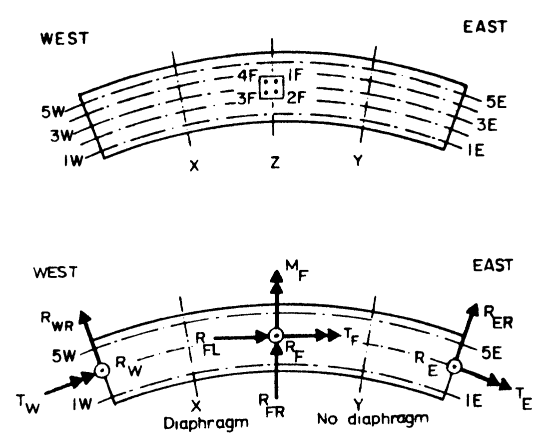

FIG. 3.6 TYPICAL SUMMARY OF REACTIONS FROM TABLEP PROGRAM

SUMMARY OF DEFLECTIONS (INCHES)

DEFLECTIONS POSITIVE DOWNWARDS

RESULTS FOR 24 KSI, 30 KSI, 40 KSI
CONDITIONING LOAD STRESS LEVELS
SIMPLY SUPPORTED, NO RESTRAINTS

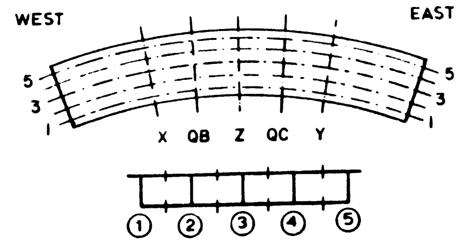

CONDITIONING LOAD STRESS LEVEL

DEFLECTION AT POINT		24 KSI THEORY	24 KSI EXPERM	24 KSI E/T	30 KSI THEORY	30 KSI EXPERM	30 KSI E/T	40 KSI THEORY	40 KSI EXPERM	40 KSI E/T
	1X	.476	.623	1.31	.476	.694	1.46	.476	.736	1.55
	2X	.491	.654	1.33	.491	.729	1.48	.491	.778	1.59
	3X	.511	.691	1.35	.511	.766	1.50	.511	.820	1.61
	4X	.537	.718	1.34	.537	.795	1.48	.537	.862	1.60
	5X	.569	.746	1.31	.569	.825	1.45	.569	.912	1.60
	1QB	.226	.298	1.31	.226	.336	1.49	.226	.345	1.53
	2QB	.226	.309	1.37	.226	.337	1.49	.226	.353	1.56
	3QB	.230	.312	1.36	.230	.347	1.51	.230	.360	1.56
	4QB	.246	.329	1.34	.246	.367	1.49	.246	.389	1.58
	5QB	.267	.343	1.29	.267	.372	1.39	.267	.409	1.53
	1Z	.030	.048	1.58	.030	.061	2.00	.030	.066	2.17
	2Z	.016	.025	1.60	.016	.026	1.69	.016	.036	2.26
	4Z	.014	.023	1.66	.014	.026	1.81	.014	.024	1.71
	5Z	.027	.044	1.65	.027	.047	1.76	.027	.054	2.02
	1QC	.230	.291	1.26	.230	.321	1.39	.230	.376	1.63
	2QC	.228	.290	1.28	.228	.318	1.40	.228	.370	1.62
	3QC	.230	.284	1.24	.230	.315	1.37	.230	.366	1.59
	4QC	.245	.312	1.27	.245	.339	1.38	.245	.396	1.61
	5QC	.267	.331	1.24	.267	.350	1.31	.267	.424	1.59
	1Y	.486	.630	1.30	.486	.685	1.41	.486	.809	1.67
	2Y	.493	.621	1.26	.493	.680	1.38	.493	.797	1.62
	3Y	.509	.643	1.26	.509	.702	1.38	.509	.814	1.60
	4Y	.534	.678	1.27	.534	.734	1.37	.534	.862	1.61
	5Y	.567	.713	1.26	.567	.777	1.37	.567	.924	1.63
LOAD	PX	-100.0	-100.0		-100.0	-100.0		-100.0	-100.0	
LOAD	PY	-100.0	-97.8		-100.0	-96.3		-100.0	-100.0	
ACTUAL	PX		-7.7			-11.5			-17.6	
ACTUAL	PY		-7.6			-11.1			-17.6	

FIG. 3.7 TYPICAL SUMMARY OF DEFLECTIONS FROM TABLEP PROGRAM

SUMMARY OF STRAINS (MICRO IN/IN)

RESULTS FOR 24 KSI, 30 KSI, 40 KSI
CONDITIONING LOAD STRESS LEVELS
SIMPLY SUPPORTED, NO RESTRAINTS

SECTION C

TENSION = +
COMPRESSION = -

K = CONCRETE STRAIN METERS
W = WELDABLE STRAIN GAGES

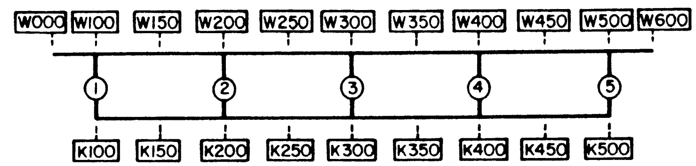

CONDITIONING LOAD STRESS LEVEL

GAGE TYPE	GAGE LOC.	24 KSI THEORY	24 KSI MEASR	24 KSI ADJUST	30 KSI THEORY	30 KSI MEASR	30 KSI ADJUST	40 KSI THEORY	40 KSI MEASR	40 KSI ADJUST
W	W000	680	544	544	680	641	641	680	688	688
W	W100	629	552	553	629	598	598	629	655	658
W	W150		497	512		524	535		550	577
W	W200	533	607	614	533	586	599	533	735	741
W	W250		552	546		576	587		593	615
W	W300	526	732	717	526	781	764	526	804	803
W	W350		498	536		516	575		543	604
W	W400	532	607	633	532	577	611	532	699	722
W	W450		497	523		527	560		558	585
W	W500	609	540	532	609	584	572	609	649	640
W	W600	621	544	544	621	577	577	621	627	627
K	K100	-287	-372	-372	-287	-380	-379	-287	-393	-385
K	K150		-339	-332		-343	-335		-341	-343
K	K200	-248	-369	-375	-248	-366	-373	-248	-360	-376
K	K250		-376	-399		-369	-399		-358	-399
K	K300	-216	-383	-378	-216	-384	-379	-216	-377	-369
K	K350		-424	-408		-425	-412		-411	-405
K	K400	-248	-335	-334	-248	-340	-342	-248	-334	-342
K	K450		-381	-377		-386	-385		-381	-391
K	K500	-273	-332	-329	-273	-343	-339	-273	-364	-357
LOAD	PX (KIPS)	-100.0	-100.0		-100.0	-100.0		-100.0	-100.0	
LOAD	PY (KIPS)	-100.0	-97.8		-100.0	-96.3		-100.0	-100.0	
ACTUAL	PX (KIPS)		-7.7			-11.5			-17.6	
ACTUAL	PY (KIPS)		-7.6			-11.1			-17.6	

FIG. 3.8 TYPICAL SUMMARY OF STRAINS AT SECTIONS FROM TABLEP PROGRAM

SUMMARY OF STRAINS (MICRO IN/IN)

RESULTS FOR 24 KSI, 30 KSI, 40 KSI
CONDITIONING LOAD STRESS LEVELS
SIMPLY SUPPORTED, NO RESTRAINTS

SECTION D

TENSION = +
COMPRESSION = -

K = CONCRETE STRAIN METERS
W = WELDABLE STRAIN GAGES

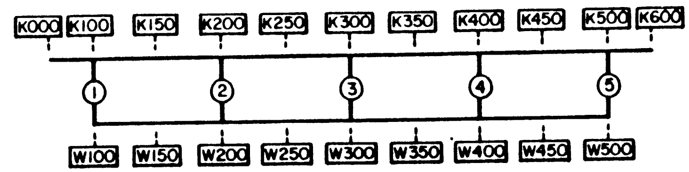

		CONDITIONING LOAD STRESS LEVEL								
		24 KSI			30 KSI			40 KSI		
GAGE TYPE	GAGE LOC.	THEORY	MEASR	ADJUST	THEORY	MEASR	ADJUST	THEORY	MEASR	ADJUST
K	K000	-241	-148	-148	-241	-144	-144	-241	-171	-171
K	K100	-204	-236	-237	-204	-236	-239	-204	-243	-247
K	K150		-367	-346		-360	-342		-322	-321
K	K200	-177	-290	-289	-177	-290	-288	-177	-288	-289
K	K250		-265	-290		-264	-294		-293	-322
K	K300	-183	-271	-283	-183	-274	-286	-183	-280	-292
K	K350		-320	-345		-331	-355		-337	-362
K	K400	-173	-274	-259	-173	-283	-269	-173	-282	-269
K	K450		-372	-347		-385	-356		-346	-332
K	K500	-190	-296	-300	-190	-301	-302	-190	-284	-285
K	K600	-216	-137	-296	-216	-136	-301	-216	-153	-153
W	W100	889	540	571	889	579	609	889	672	693
W	W150		648	646		698	700		755	758
W	W200	771	778	757	771	791	776	771	804	797
W	W250		696	655		708	669		738	700
W	W300	806	607	611	806	717	711	806	828	816
W	W350		640	626		673	646		725	688
W	W400	746	808	783	746	822	800	746	877	855
W	W450		655	643		686	680		742	744
W	W500	808	688	718	808	696	729	808	668	707
LOAD	PX (KIPS)	-100.0	-100.0		-100.0	-100.0		-100.0	-100.0	
LOAD	PY (KIPS)	-100.0	-97.8		-100.0	-96.3		-100.0	-100.0	
ACTUAL	PX (KIPS)		-7.7			-11.5			-17.6	
ACTUAL	PY (KIPS)		-7.6			-11.1			-17.6	

FIG. 3.8 (CONT.) TYPICAL SUMMARY OF STRAINS AT SECTIONS FROM TABLEP PROGRAM

DISTRIBUTION OF MOMENTS TO EACH GIRDER
(KIP-FT AND PERCENTAGE)

MOMENTS ABOUT ENTIRE GROSS SECTION N.A.

RESULTS FOR 24 KSI, 30 KSI, 40 KSI
CONDITIONING LOAD STRESS LEVELS
SIMPLY SUPPORTED, NO RESTRAINTS

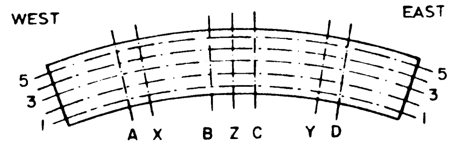

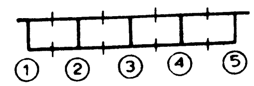

CONDITIONING LOAD STRESS LEVEL

SECTION	GIRDER	24 KSI THEORY K-FT	24 KSI THEORY PCT	24 KSI EXPERIMENTAL K-FT	24 KSI EXPERIMENTAL PCT	30 KSI THEORY K-FT	30 KSI THEORY PCT	30 KSI EXPERIMENTAL K-FT	30 KSI EXPERIMENTAL PCT	40 KSI THEORY K-FT	40 KSI THEORY PCT	40 KSI EXPERIMENTAL K-FT	40 KSI EXPERIMENTAL PCT
A	1	76.9	17.0	70.1	16.2	76.9	17.0	70.7	16.2	76.9	17.0	69.6	16.8
A	2	102.4	22.7	95.2	22.1	102.4	22.7	96.6	22.1	102.4	22.7	89.7	21.6
A	3	100.2	22.2	95.4	22.1	100.2	22.2	96.3	22.1	100.2	22.2	92.3	22.2
A	4	100.2	22.2	99.8	23.1	100.2	22.2	101.4	23.2	100.2	22.2	96.4	23.2
A	5	72.2	16.0	70.9	16.4	72.2	16.0	71.4	16.4	72.2	16.0	67.1	16.2
A	SUM	451.8		431.5		451.8		436.3		451.8		415.1	
B	1	-80.4	16.5	-69.7	15.4	-80.4	16.5	-68.1	15.4	-80.4	16.5	-75.0	15.2
B	2	-110.1	22.5	-105.7	23.4	-110.1	22.5	-102.7	23.2	-110.1	22.5	-112.6	22.9
B	3	-110.7	22.6	-112.2	24.8	-110.7	22.6	-109.5	24.8	-110.7	22.6	-122.8	25.0
B	4	-109.8	22.5	-100.9	22.3	-109.8	22.5	-99.8	22.6	-109.8	22.5	-110.6	22.5
B	5	-77.8	15.9	-63.2	14.0	-77.8	15.9	-62.1	14.0	-77.8	15.9	-70.7	14.4
B	SUM	-488.7		-451.7		-488.7		-442.1		-488.7		-491.7	
C	1	-80.8	16.5	-66.2	14.6	-80.8	16.5	-69.3	14.9	-80.8	16.5	-77.7	15.0
C	2	-110.3	22.6	-102.9	22.8	-110.3	22.6	-104.2	22.4	-110.3	22.6	-118.4	22.8
C	3	-110.6	22.6	-113.8	25.2	-110.6	22.6	-117.7	25.3	-110.6	22.6	-127.6	24.6
C	4	-109.5	22.4	-102.8	22.8	-109.5	22.4	-105.5	22.6	-109.5	22.4	-117.8	22.7
C	5	-77.5	15.9	-66.0	14.6	-77.5	15.9	-69.0	14.8	-77.5	15.9	-78.0	15.0
C	SUM	-488.7		-451.7		-488.7		-465.7		-488.7		-519.4	
D	1	77.7	17.2	59.2	14.1	77.7	17.2	57.2	14.1	77.7	17.2	59.1	14.6
D	2	103.0	22.8	100.2	23.9	103.0	22.8	95.0	23.5	103.0	22.8	94.4	23.4
D	3	100.0	22.1	90.2	21.5	100.0	22.1	89.1	22.0	100.0	22.1	93.1	23.0
D	4	99.5	22.0	100.1	23.8	99.5	22.0	96.1	23.7	99.5	22.0	96.3	23.8
D	5	71.7	15.9	70.2	16.7	71.7	15.9	67.3	16.6	71.7	15.9	61.3	15.2
D	SUM	451.8		419.8		451.8		404.8		451.8		404.2	
LOAD	PX (KIPS)	-100.0		-100.0		-100.0		-100.0		-100.0		-100.0	
LOAD	PY (KIPS)	-100.0		-97.8		-100.0		-96.3		-100.0		-100.0	
ACTUAL	PX (KIPS)			-7.7				-11.5				-17.6	
ACTUAL	PY (KIPS)			-7.6				-11.1				-17.6	

FIG. 3.9 TYPICAL SUMMARY OF MOMENTS FROM TABLEP PROGRAM

of the model implied that the curing and drying would be different, and hence also the moduli. Generally it was found that the control cylinders gave values of the modulus of elasticity that were 5 - 10% too high, except in section D where the difference was of the order of 20%.

The tensile forces were computed assuming the concrete to be cracked on the tension side, and all tensile forces taken by the reinforcement. The crack was assumed to pass through the gaged section, and the strain readings assumed to be those of the cracked section. However, even though a crack initiator was placed at the instrumented sections, it was clear that these assumptions were not satisfied in the bridge model. In many cases the strains measured were not the strains at the crack, but rather at a point somewhere between two cracks. Since the concrete was uncracked at this point, part of the tensile force was carried by the concrete, resulting in a reduction in the steel strains. The part of the tensile force carried by the concrete was larger the larger the spacing between the cracks, which accounted for the fact that the largest discrepancy between tensile and compressive forces were observed in sections A and D. A study of the crack pattern in the model confirmed that the crack spacing in the bottom flange at sections A and D was significantly larger than in the top flange at section B and C.

It was therefore decided to modify the tensile and compressive forces at all sections, rather than to attempt to modify the strains. The purpose of this modification was to ensure as much as possible, that equilibrium was satisfied at all instrumented sections. Using the measured reactions and applied loads and their respective lever arms, the gross moments for the entire cross section were computed at sections

A, B, C and D. Taking the internal moment arm equal to the distance between the top and bottom flanges, a "theoretical" equilibrating force was computed by dividing the gross moment by this lever arm. A set of modification factors were then obtained by dividing the "theoretical" force by the experimental tensile and compressive forces as computed by the MOMENT program. This procedure was repeated for each conditioning load and the results plotted in Fig. 3.10 as a function of conditioning load stress level. It can be seen that the variation in the modification factors with stress level is quite smooth.

In essence, the curves of Fig. 3.10 represent the modification factors required to convert the moduli of elasticity of the concrete, and steel as obtained from control specimens, to effective stiffnesses. When these effective stiffnesses are used to convert measured strains to forces, longitudinal force equilibrium will be satisfied at the specified sections under the given conditioning loads shown in Fig. 3.10.

For the 24, 30, 40, 50 and 60 ksi conditioning loads, the modification factors plotted in Fig. 3.10 were used to obtain experimental internal forces and moments at the sections indicated, thus satisfying equilibrium for these load cases.

For all other load cases, with the exception of dead load which is treated separately in Chapter 4, the modification factors obtained from the 30 ksi conditioning load were used. These other load cases (totalling to 134 cases) which have been described in Table 5.1 of Vol. I, included the point load combinations, designed to produce 24 to 30 ksi total stresses in the reinforcement, which were applied after each conditioning load, as well as truck load combinations and the moving fork lift loads applied after the 30 ksi conditioning load. All experimental

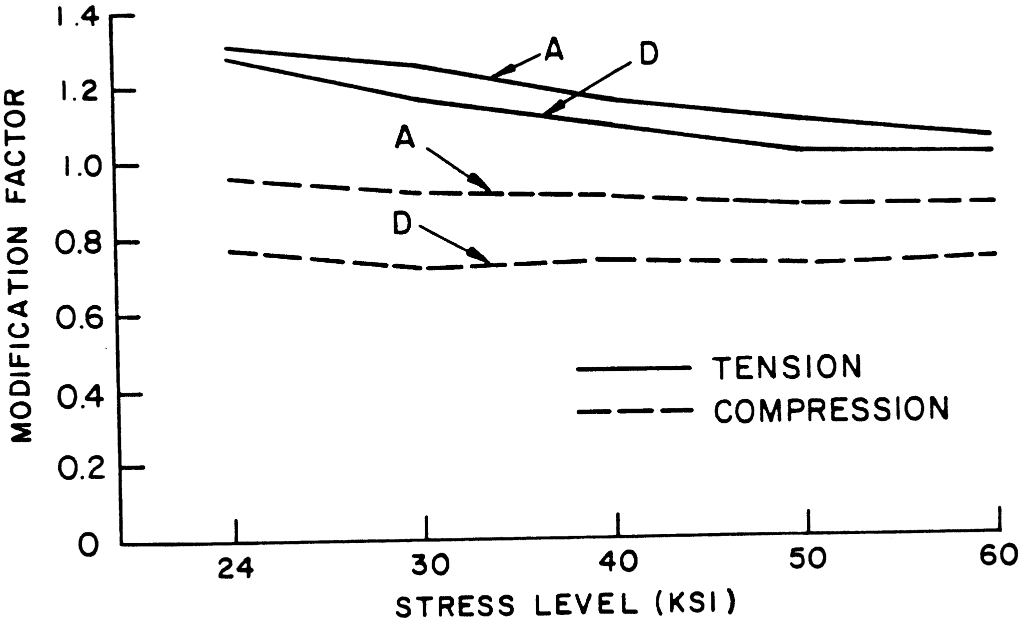

MODIFICATION FACTORS FOR SECTION A & D

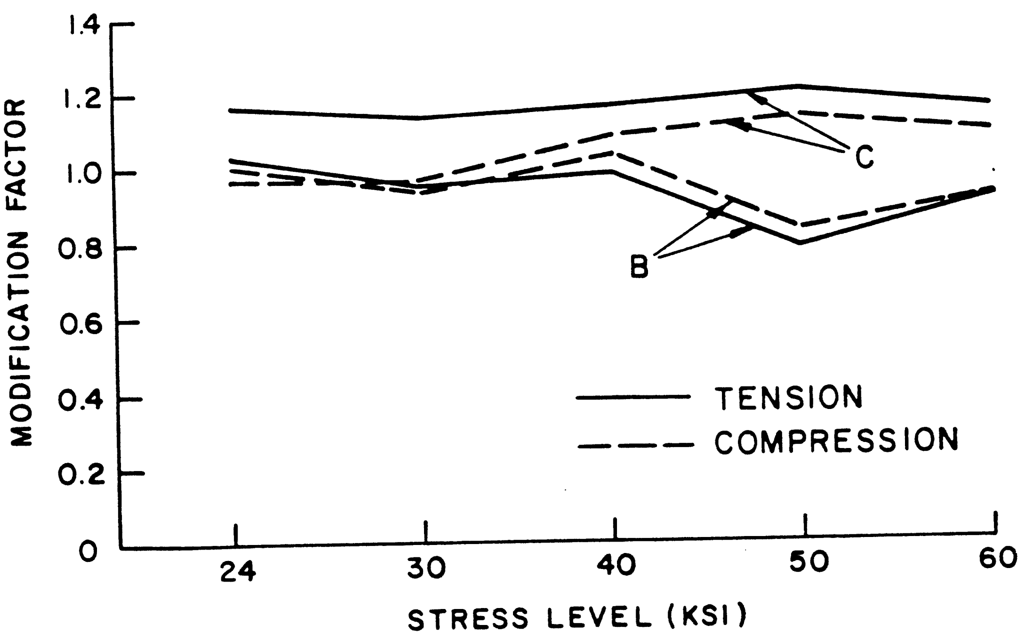

MODIFICATION FACTORS FOR SECTION B & C

FIG. 3.10 MODIFICATION FACTORS FOR EXPERIMENTAL INTERNAL FORCES AND MOMENTS AT A SECTION results for internal forces and moments at a section presented in Vols. II and III for these load cases have therefore been modified by these factors, which are taken from Fig. 3.10 and tabulated below in Table 3.1. The experimental strains, reactions and deflections, however, remain unchanged.

TABLE 3.1 MODIFICATION FACTORS FOR INTERNAL FORCES FROM 30 KSI CONDITIONING LOAD

Force	Section A	Section B	Section C	Section D
Tension	1.256	0.953	1.134	1.172
Compression	0.921	0.939	0.957	0.722

Since this common set of factors was used for a large number of different loading cases, perfect equilibrium could not be expected for all these cases. The effect of this modification procedure is shown in Table 3.2 for three typical point load cases after the 30 ksi conditioning load. A significant improvement in the results was obtained both for the ratio of compressive to tensile forces, and for the various moment ratios. The improvement was most significant at sections A and D. Even though the spread of the moment ratios at section D was still larger than desired, the procedure was judged satisfactory for general use in the data reduction.

Table 3.3 shows the same ratios for three point load combinations after the 60 ksi conditioning load. The first column within each section represents the unmodified ratios, the second the ratios using the modification factors of the 60 ksi conditioning load, and the third those obtained using 30 ksi conditioning load. As seen the latter results always gives the closest agreement between tensile and compressive forces, and also the smallest variation in the moment ratios, and hence justified

TABLE 3.2 COMPARISON OF ORIGINAL AND MODIFIED FORCE AND MOMENT RATIOS FOR POINT LOADS AFTER 30 KSI CONDITIONING LOAD

LOAD CASE		SECTION A		SECTION B		SECTION C		SECTION D	
		ORIGINAL	MODIFIED	ORIGINAL	MODIFIED	ORIGINAL	MODIFIED	ORIGINAL	MODIFIED
(5X)	(15) MOMENT	579.1		-263.9		-300.6		-133.1	
	RATIO F_c/F_t	1.38	1.01	0.93	0.92	1.36	1.15	2.16	1.33
	RATIO (7)/(15)	0.80	1.01	1.16	1.11	0.71	0.81	0.81	0.96
	RATIO (8)/(15)	1.12	1.02	1.08	1.01	0.98	0.94	1.81	1.30
	RATIO (9)/(15)	0.94	1.01	1.12	1.06	0.86	0.88	1.26	1.11
	RATIO (10/(15)	0.89	1.01	1.14	1.08	0.82	0.87	1.13	1.07
(5X + 5Y)	(15) MOMENT	477.2		-493.8		-614.8		448.2	
	RATIO F_c/F_t	1.35	0.99	1.02	1.00	1.19	1.00	2.01	1.24
	RATIO (7)/(15)	0.73	0.93	1.15	1.10	0.78	0.89	0.79	0.94
	RATIO (8)/(15)	1.01	0.92	1.18	1.10	0.94	0.89	1.64	1.17
	RATIO (9)/(15)	0.85	0.92	1.17	1.10	0.87	0.89	1.17	1.04
	RATIO (10)/(15)	0.81	0.93	1.17	1.11	0.84	0.89	1.10	1.04
(1X + 5Y)	(15) MOMENT	431.5		-443.3		-484.1		482.8	
	RATIO F_c/F_t	1.48	1.09	1.05	1.04	1.19	1.01	1.97	1.21
	RATIO (7)/(15)	0.69	0.87	1.03	0.99	0.81	0.92	0.72	0.85
	RATIO (8)/(15)	1.05	0.96	1.09	1.02	0.97	0.93	1.46	1.04
	RATIO (9)/(15)	0.85	0.91	1.07	1.01	0.90	0.92	1.05	0.94
	RATIO (10)/(15)	0.80	0.90	1.05	1.00	0.86	0.92	1.00	0.95

F_c = COMPRESSIVE FORCE: F_t = TENSILE FORCE

(7) = INTERNAL MOMENT ABOUT COMPRESSION FLANGE MID-DEPTH
(8) = INTERNAL MOMENT ABOUT TENSION FLANGE STEEL
(9) = INTERNAL MOMENT ABOUT ENTIRE GROSS-SECTION N.A.
(10) = INTERNAL MOMENT ABOUT EXPERIMENTAL N.A.
(15) = TOTAL EXTERNAL MOMENT FROM EXPERIMENTAL LOADS AND REACTIONS (KIP-FT)

TABLE 3.3 COMPARISON OF ORIGINAL AND MODIFIED FORCE AND MOMENT RATIOS FOR POINT LOADS AFTER 60 KSI CONDITIONING LOAD

LOAD CASE		SECTION A			SECTION B			SECTION C			SECTION D		
		ORIG.	MOD 60	MOD 30	ORIG.	MOD 60	MOD 30	ORIG.	MOD 60	MOD 30	ORIG.	MOD 60	MOD 30
(5Y)	(15) MOMENT	139.4			314.8			320.7			554.0		
	RATIO F_c/F_t	1.69	1.40	1.21	1.55	1.57	1.53	1.22	1.15	1.03	2.06	1.49	1.27
	RATIO (7)/(15)	0.75	0.80	0.98	0.78	0.71	0.75	0.88	1.01	1.00	0.80	0.81	0.95
	RATIO (8)/(15)	1.31	1.14	1.20	1.24	1.14	1.17	1.08	1.17	1.03	1.70	1.24	1.22
	RATIO (9)/(15)	1.00	0.95	1.08	1.04	0.95	0.98	0.99	1.10	1.02	1.20	1.00	1.07
	RATIO (10)/(15)	0.98	0.95	1.09	1.00	0.91	0.94	0.97	1.08	1.03	1.14	0.99	1.08
(5X)	(15) MOMENT	581.8			257.7			318.4			141.0		
	RATIO F_c/F_t	1.48	1.23	1.07	0.88	0.89	0.87	1.59	1.50	1.34	2.76	2.00	1.70
	RATIO (7)/(15)	0.94	0.99	1.22	1.43	1.30	1.36	0.75	0.86	0.86	0.90	0.92	1.08
	RATIO (8)/(15)	1.42	1.24	1.30	1.25	1.15	1.18	1.22	1.32	1.16	2.61	1.90	1.87
	RATIO (9)/(15)	1.16	1.00	1.25	1.33	1.22	1.26	1.01	1.12	1.03	1.66	1.36	1.43
	RATIO (10)/(15)	1.13	1.00	1.27	1.39	1.26	1.31	0.96	1.06	0.99	1.53	1.28	1.37
(5X + 5Y)	(15) MOMENT	478.6			336.8			389.1			443.6		
	RATIO F_c/F_t	1.98	1.64	1.42	1.19	1.21	1.17	1.23	1.16	1.04	1.81	1.31	1.11
	RATIO (7)/(15)	0.82	0.87	1.07	1.31	1.19	1.25	0.84	0.96	0.96	0.91	0.93	1.08
	RATIO (8)/(15)	1.18	1.02	1.08	1.48	1.36	1.39	0.97	1.05	0.92	2.07	1.51	1.49
	RATIO (9)/(15)	0.98	0.94	1.07	1.40	1.28	1.33	0.91	1.01	0.94	1.43	1.19	1.26
	RATIO (10)/(15)	0.97	0.95	1.11	1.39	1.27	1.32	0.89	1.00	0.95	1.38	1.19	1.28

F_c = COMPRESSIVE FORCE: F_t = TENSILE FORCE

(7) = INTERNAL MOMENT ABOUT COMPRESSION FLANGE MID-DEPTH
(8) = INTERNAL MOMENT ABOUT TENSION FLANGE STEEL
(9) = INTERNAL MOMENT ABOUT ENTIRE GROSS-SECTION N.A.
(10) = INTERNAL MOMENT ABOUT EXPERIMENTAL N.A.
(15) = TOTAL EXTERNAL MOMENT FROM EXPERIMENTAL LOADS AND REACTIONS (KIP-FT)

the use of the 30 ksi conditioning load modification factors for the point load cases after the 40, 50 and 60 ksi conditioning loads as well as those after the 24 and 30 ksi conditioning loads.

A more complete study of modification factors is made in Section 2.1 of Vol. III, where the conditioning load cases and nine point load cases 1X, 1Y, 1X+1Y, 3X, 3Y, 3X+3Y, 5X, 5Y and 5X+5Y are studied. For stress levels at or after the 24, 30, 40, 50 and 60 ksi levels, unmodified tension and compression forces at Sections A, B, C and D are tabulated to verify the consistency of the experimental data. These results are given in Tables 2.1, 2.2, 2.3 of Vol. III, and then modification factors for each individual case are computed and tabulated in Tables 2.4, 2.5, 2.6 of Vol. III. A study of these detailed tables indicates that the adopted procedure of using the modification factors from the 30 ksi conditioning load case described earlier is probably the best approach to use in reducing the data.

4. RESULTS FOR DEAD LOAD

4.1 General Remarks

During and after the construction of the bridge model, reactions and selected strain gages were measured manually using a strain indicator box and a switching unit. This procedure was used to monitor variations in strains and reactions in the bridge due to creep and differential shrinkage until the gages were hooked up to the Data Acquisition System. This hook up for the load cells and strain gages took place one week before the removal of the shoring, while the linear potentiometers for the deflection measurements were installed immediately after the removal of the shoring.

Results for the dead load case of the box girder bridge model can be divided into results for reactions, deflections, longitudinal forces, strains and moments. Each is discussed below.

4.2 Reactions

The density of the plain concrete used in the bridge model was determined from 45 - 6 x 12 in. control cylinders at different ages. An average value of 139 pcf was found with a range from 136 to 142 pcf. Based on the additional weight of the reinforcing steel in the bridge, an average value for the density of the reinforced concrete was taken as 150 pcf. This value was used in calculating the dead load weight of the model given in Table 4.1.

TABLE 4.1 - TOTAL DEAD WEIGHT OF BOX GIRDER MODEL.

	Volume (cu. ft.)	Weight (kips)
Cellular portion of bridge	404.1	60.7
Two end diaphragms	79.0	11.8
Center bent diaphragm	24.9	3.7
Bent footing	34.0	5.1
Bent column	4.8	0.7
Mid span diaphragm	3.1	0.5
Total dead weight of concrete		82.5
Weight of steel billets and sand		116.3
Weight of drop soffitt forms		2.0
Total Dead Load		200.8

Before removal of the shoring, all load cells were read and the reactions obtained are listed in column (3) in Table 4.2. The uneven distribution of reactions in the load cells under the center footing was caused by the sequence of prestressing of the footing tie-down rods to the test floor before the bridge proper was cast. Similarly, the uneven distribution between individual load cells under the end diaphragms is caused by differential shrinkage and creep, which tended to lift the diaphragms up from the reaction assemblages. The total reaction taken by all load cells at this time was 64.8 kips. Part of this reaction was caused by the weight of the end diaphragms, center bent, column and footing, which was estimated to be about 21.4 kips. The remaining part of the reaction, 43.4 kips, was that part of the cellular portion of the bridge that was not carried by the shoring. Due to settlement of the shoring and creep and differential shrinkage in the concrete, this part of the dead load was gradually transferred from the shoring to the bridge proper and thence into its supports as time

TABLE 4.2 - SUMMARY OF DEAD LOAD REACTIONS (KIPS)

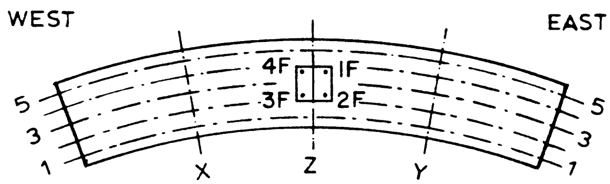

REACTION OR LOAD	THEORY	EXPERIMENTAL				
	TOTAL AFTER REMOVAL	BEFORE REMOVAL	DUE TO REMOVAL	TOTAL AFTER REMOVAL	DIAPHRAGMS AND FOOTING	NET REACTIONS
(1)	(2)	(3)	(4)	(5)	(6)	(7)
1E	4.27	0.14	1.95	2.09	0.58	1.51
2E	8.21	6.77	7.26	14.03	1.70	12.33
3E	7.46	1.91	3.22	5.13	1.39	3.74
4E	9.09	2.20	4.38	6.58	1.70	4.88
5E	9.61	1.88	6.90	8.78	0.58	8.20
ΣE	38.64	12.90	23.71	36.61	5.95	30.66
1F	30.56	-3.43	24.40	20.97	2.38	18.59
2F	30.03	24.12	20.32	44.44	2.38	42.08
3F	30.06	-0.04	19.89	19.85	2.38	17.47
4F	31.60	18.40	24.14	42.54	2.38	40.16
ΣF	122.24	39.05	88.75	127.80	9.52	118.50
1W	4.21	2.48	3.33	5.81	0.58	5.23
2W	8.29	2.40	2.99	5.39	1.70	3.69
3W	7.59	4.98	8.70	13.68	1.39	12.29
4W	9.15	1.05	1.13	2.18	1.70	0.48
5W	9.67	1.91	9.00	10.91	0.58	10.33
ΣW	38.95	12.82	25.15	37.97	5.95	32.02
ΣR	199.83	64.77	137.61	202.38	21.42	180.95
ΣP	-200.80			-200.80		-179.38
$\Sigma R/\Sigma P$	0.99			1.01		1.01

passed after casting. This transfer of load creates a problem for the interpretation of the dead load experimental results since the distribution of the load taken by the shoring along the bridge centerline is unknown. Without an estimate of this distribution it is impossible to compute the external moment acting on any section of the bridge. In order to get one such estimate, the shoring was considered as an elastic foundation for the bridge, and the elastic constants of the shoring were determined such that the reactions at the end abutments and center footing equalled those measured before the removal of the shoring. The result of this analysis will be discussed further in section 4.3.

The increase in reactions due to the removal of the shoring is given in column (4), and the total reactions after the removal in column (5) in Table 4.2. The sum of the total experimental reactions is 202.4 kips, which compares quite well with the computed dead weight of 200.8 kips given in Table 4.1.

The theoretical results in column (2) are obtained from CELL using an average concrete density to include the weight of the sand and steel billets, which was used to preserve dead load similitude between the model and prototype.

A comparison between the theoretical results, column (2), and the experimental results in column (5) indicate that a larger portion of the total dead weight reaction was taken by the center footing than the theory predicted. This again is caused by the load transfer from the shoring to the bridge before the removal of the shoring and shrinkage effects. Prior to the removal it was observed that due to the differential shrinkage the two end diaphragms partially lifted up from the end abutments. This indicates that the dead weight taken by the shoring was unevenly distributed.

The same effects make a comparison of the theoretical and experimental transverse distribution of dead load reactions at each end abutment unrealistic. Due to the bridge horizontal curvature, the lift-up was most significant at girder 1, as seen from column (4) in Table 4.2. When loaded the curvature also causes each load cell to undergo a different longitudinal displacement. Since the friction between the two teflon plates in each reaction assemblage was too large to accomodate this longitudinal displacement by relative sliding, the load cells tilted about the pivots causing differential vertical displacements of the load cells at the end diaphragms. Because the stiffness of the end diaphragm was large, these differential displacements at the load cells produced a redistribution of the total reaction forces. This also explains why the transverse distribution of experimental reactions at the east and west end abutments were not identical.

The theoretical solution from CELL assumes that the end diaphragms are each supported on five rigid supports, where the load cell reaction assemblies existed. In the actual structure any slight difference in the compressibility of the five reaction assemblies could give a situation where a very deep rigid end diaphragm rests on essentially five supports with slightly different spring constants. This could cause the difference between the experimental and theoretical transverse distributions of the five reactions at each end of the bridge. However, the experimental and theoretical total reactions at each end were in good agreement and these totals were distributed by the rigid end diaphragms into the bridge in a similar way, thus not affecting the overall response of the bridge differently. The above comments point out the sensitivity of the distribution of end reactions to the manner in which reactions supports are placed in prototype structures as well as in models.

4.3 Dead Load Distribution in Shoring

Due to differential shrinkage between top and bottom flanges, internal stresses are set up in the bridge that transfer part of the dead weight from the shoring to the bridge itself and thence into the supports prior to the removal of the shoring. The total weight carried by the bridge in this manner is known from the measured reactions in the load cells but not its distribution.

In order to estimate this distribution, the bridge was analyzed with the assumption that the shoring acted as an elastic foundation. A three dimensional frame analysis was made using SAP, where the shoring was modelled by discrete springs. The elastic constants of the springs were chosen such that the reactions at the end abutments and the center bent were approximately equal to those measured prior to the removal of the shoring, column (3) in Table 4.2.

The model for the analysis is shown in Fig. 4.1a, the resulting moments in the bridge in Fig. 4.1b, and the load distribution between bridge and shoring in Fig. 4.1c. Even though approximately 23% of the total dead weight is carried by the bridge itself prior to the removal of the shoring, the load distribution is such that only relatively small moments are produced at sections A and B. These moments are only 4% and 7% respectively of the moments obtained by a similar analysis for dead load taken entirely by the bridge without the shoring. The effect of the distribution of dead weight between shoring and bridge is therefore most important for the theoretical reactions computed in section 4.2, while its influence on theoretical deflections, moments and strains is

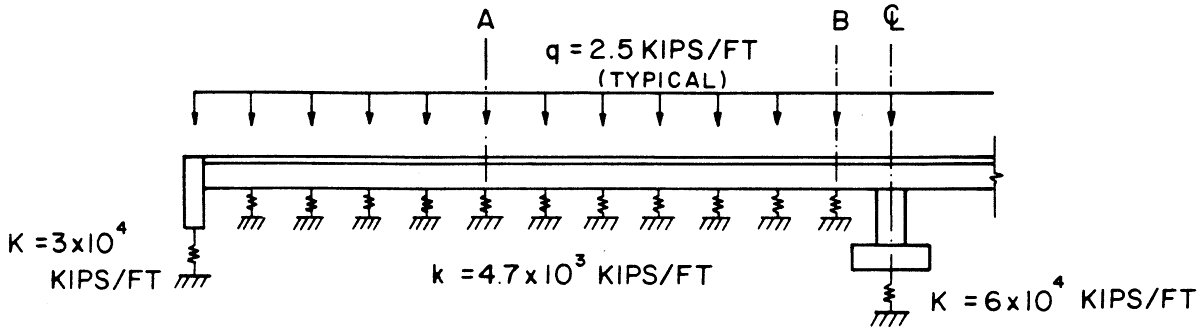

(a) MODEL FOR THE ANALYSIS

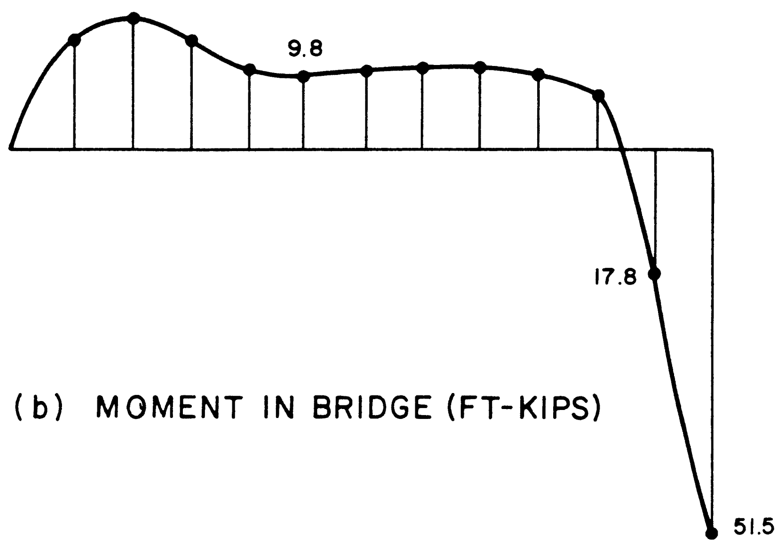

(b) MOMENT IN BRIDGE (FT-KIPS)

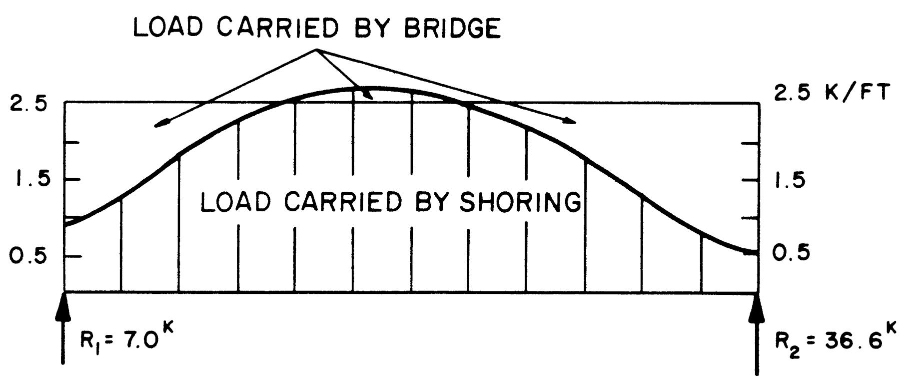

(c) DISTRIBUTION OF DEAD WEIGHT BETWEEN SHORING AND BRIDGE

FIG. 4.1 DEAD LOAD DISTRIBUTION AND MOMENTS FOR BRIDGE ON ELASTIC FOUNDATION

relatively small.

It should be noted that this analysis is only an attempt to model the effect of the differential shrinkage in the bridge. However, even though the real behavior of the bridge-shoring system may be somewhat different, this model is capable of explaining the close agreement between experimental and theoretical moments found in section 4.6 even though some differences in reactions occur.

4.4 Deflections

Experimental and theoretical deflections based on CELL are given in Table 4.3 for the sections X, QB, Z, QC and Y. For the dead load case experimental deflections could only be measured at girders 1 and 5, since the potentiometers could not be installed until the shoring was removed. The experimental deflections were therefore measured using scales attached to the cantilever slabs and a high precision level instrument. The scales were graduated to 0.01 in., and readings were taken before and after removal of the shoring. The resulting deflections are considered accurate to $\pm$ 0.02 in..

The theoretical deflections in column (3) are due to the total dead load. According to the discussion in the previous section it was determined that these deflections should represent the effect of the removal of the shoring quite accurately for which the experimental deflections in column (4) were measured.

The ratio of experimental to theoretical deflections are given in column (5) where it can be seen that experimental deflections are approximately 1.5 to 1.6 greater than those predicted by theory based on an uncracked section.

TABLE 4.3 SUMMARY OF DEAD LOAD DEFLECTIONS (INCHES)

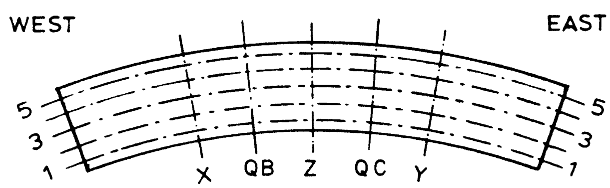

	SECTION	THEORY	EXPERI-MENTAL	$\frac{E}{T}$
(1)	(2)	(3)	(4)	(5)
GIRDER 1	X	0.26	0.40	1.54
	QB	0.14	0.20	1.43
	Z	0.02	0.06	
	QC	0.14	0.20	1.43
	Y	0.25	0.40	1.60
GIRDER 5	X	0.32	0.48	1.50
	QB	0.17	0.24	1.41
	Z	0.04	0.04	
	QC	0.16	0.24	1.50
	Y	0.30	0.48	1.60

When comparing the results it should be noted that theory predicts slightly larger deflections at section X than section Y, while the experimental results are identical at the two sections. However, the difference in the theoretical deflections is only 0.01 or 0.02 in., while the accuracy of measurement of the experimental deflections at the two sections is ± 0.02 in.

It is of interest to note that the maximum measured dead load deflection of 0.48 in. is 1/900 of the 36 ft. span and because of similitude this same ratio could be expected in a prototype structure.

4.5 Strains and Longitudinal Forces at a Section

The summary of dead load strains in micro-inches per inch at Sections A, B, C and D is given in Tables 4.4 and 4.5. Tensile and compressive forces at these instrumented sections are presented in Table 4.6.

The theoretical results are based on the CELL analysis for a uniform load along the entire span length. Theoretical strains are based on the resulting longitudinal membrane forces converted to strains using the procedure outlined in Section 2.8. As explained there, the compressive strains in the concrete (K gages) are the theoretical values at the points shown, but the tensile strains in the steel (W gages) are averages over the width of each individual girder flange. Theoretical longitudinal forces are obtained automatically from CELL by separately integrating the tensile and compressive longitudinal forces in the flanges and webs of the uncracked sections.

The experimental results were obtained directly from the data processing program described in Chapter 3. It should be recognized that the experimental strains and forces in Tables 4.4, 4.5 and 4.6 represent the net measured results in going from an unknown internal stress state and external loading (Fig. 4.1) just prior to the removal of the shoring to that existing just after the removal of the shoring. The precise loading producing these measured experimental strains and forces cannot be determined, however, it should be similar to the shaded portion shown in Fig. 4.1c. As discussed in section 4.3, this loading should produce longitudinal moments, strains and forces at the instrumented sections which are of similar magnitudes to those produced by the uniform dead load assumed in the theoretical solution. However, the reactions from the two loadings would be quite different.

Both the measured and adjusted experimental strains, obtained from the data reduction program are shown in Tables 4.4 and 4.5. As can be seen, the experimental strains are higher than those predicted by theory. The closest agreement between experimental and theoretical strains is found for the steel strains, and sections A and D show better agreement than B and C. The experimental concrete strains are in general much larger than the theoretical results at all four sections. This is probably due to the cracking in the model and the unknown internal stress field and true concrete stiffness prior to the removal of the shoring and formwork.

Table 4.6 shows theoretical and experimental values of the longitudinal membrane forces at the four instrumented sections. Both "measured" and modified experimental results are given. Theoretical tensile and compressive forces on a section are practically equal as required by statics. The agreement between theoretical and measured experimental values of tensile forces on the sections is quite good.

TABLE 4.4 - SUMMARY OF LONGITUDINAL STRAINS (MICRO-INCH/INCH
AT SECTIONS A AND D FOR DEAD LOAD CASE

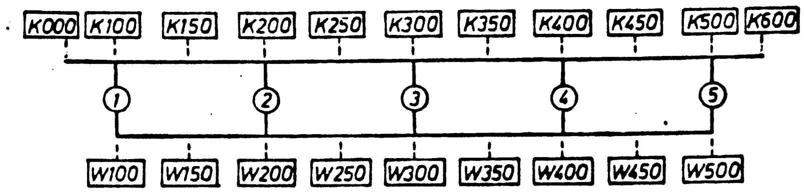

GAGE TYPE	GAGE LOCATION	LONGITUDINAL STRAINS					
		SECTION A			SECTION D		
		THEORY	EXPERIMENTAL		THEORY	EXPERIMENTAL	
			MEAS.	ADJUST.		MEAS.	ADJUST.
CONCRETE STRAIN METERS	K 000	-134	-237	-488	-114	-119	-119
	K 100	-115	-488	-467	- 98	-211	-219
	K 150		-173	-182		-410	-400
	K 200	-101	-324	-348	- 86	-317	-307
	K 250		-156	-149		-311	-305
	K 300	-105	-279	-276	- 89	-242	-264
	K 350		-202	-204		-398	-415
	K 400	-100	-298	-311	- 84	-506	-468
	K 450		-201	-248		-429	-463
	K 500	-111	-272	-270	- 93	-320	-344
	K 600	-122	-192	-192	-103	-112	-320
WELDABLE GAGES	W 100	443	524	521	426	446	458
	W 150		388	327		483	455
	W 200	388	613	595	372	552	535
	W 250		424	371		559	501
	W 300	414	601	602	393	370	376
	W 350		450	449		488	465
	W 400	382	588	586	362	622	599
	W 450		419	369		441	412
	W 500	414	693	681	393	593	603

TABLE 4.5 - SUMMARY OF LONGITUDINAL STRAINS (MICRO-INCH/INCH)
AT SECTIONS B AND C FOR DEAD LOAD CASE

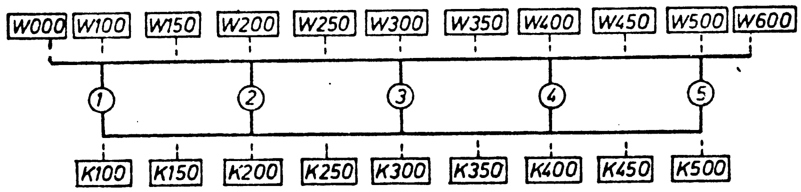

GAGE TYPE	GAGE LOCATION	LONGITUDINAL STRAINS					
		SECTION B			SECTION C		
		THEORY	EXPERIMENTAL		THEORY	EXPERIMENTAL	
			MEAS.	ADJUST.		MEAS.	ADJUST.
CONCRETE STRAIN METERS	K 100	-140	-257	-259	-142	-254	-253
	K 150		-270	-261		-243	-233
	K 200	-128	-260	-256	-129	-235	-241
	K 250		-264	-256		-308	-368
	K 300	-115	-268	-269	-114	-271	-271
	K 350		-264	-267		-279	-287
	K 400	-129	-228	-228	-130	-213	-218
	K 450		-235	-232		-243	-241
	K 500	-137	-206	-206	-137	-209	-206
WELDABLE GAGES	W 000	324	359	359	330	389	389
	W 100	311	364	371	316	357	359
	W 150		301	319		315	337
	W 200	275	408	401	276	525	524
	W 250		350	362		335	337
	W 300	280	398	412	378	485	489
	W 350		334	379		314	353
	W 400	278	343	337	379	460	464
	W 450		343	344		315	329
	W 500	306	306	309	308	326	330
	W 600	302	345	345	304	348	348

TABLE 4.6 - INTERNAL LONGITUDINAL FORCES (KIPS) AT INSTRUMENTED SECTIONS FOR DEAD LOAD CASE

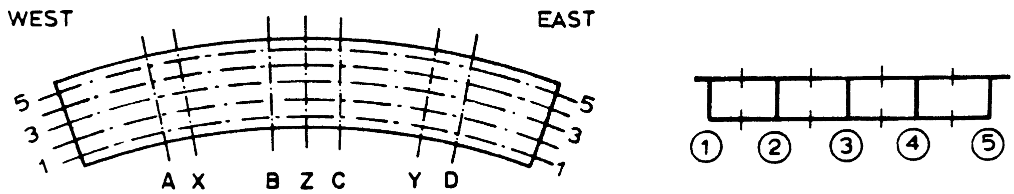

SECTION	GIRDER	THEORY		EXPERIMENTAL			
				MEASURED		MODIFIED	
		TENSILE	COMPRES.	TENSILE	COMPRES.	TENSILE	COMPRES.
A	1	23.6	-31.7	18.8	-86.4	18.8	-44.8
	2	37.6	-33.2	36.8	-56.4	36.8	-29.2
	3	37.0	-32.7	38.8	-49.3	38.8	-25.6
	4	36.9	-32.7	38.7	-61.7	38.7	-32.0
	5.	22.1	-30.1	25.3	-51.5	25.3	-26.7
	Σ	157.1	-160.4	158.5	-305.3	158.5	-158.2
B	1	30.8	-24.0	29.9	-32.0	29.9	-26.3
	2	35.5	-39.2	39.3	-51.8	39.3	-42.6
	3	37.0	-40.1	44.0	-56.7	44.0	-46.7
	4	35.7	-39.4	37.8	-48.4	37.8	-39.9
	5	30.1	-23.4	28.4	-26.6	28.4	-21.9
	Σ	169.2	-166.2	179.3	-215.5	179.3	-177.4
C	1	31.3	-24.4	28.0	-30.0	28.0	-23.8
	2	35.7	-39.5	41.8	-53.6	41.8	-42.5
	3	36.8	-40.0	40.3	-64.4	40.3	-51.0
	4	35.8	-39.6	39.7	-47.8	39.7	-37.9
	5	30.3	-23.5	26.6	-27.0	26.6	-21.4
	Σ	169.9	-167.0	176.4	-222.9	176.4	-176.5
D	1	22.6	-30.4	21.2	-61.2	21.2	-21.6
	2	36.0	-31.8	40.6	-89.2	40.6	-31.4
	3	35.3	-31.2	31.9	-83.4	31.9	-29.3
	4	34.9	-31.0	40.5	-124.4	40.5	-43.8
	5	21.0	-28.6	23.7	-91.0	23.7	-32.0
	Σ	149.9	-152.9	157.9	-449.3	157.9	-158.1

However, the measured experimental compression forces are much higher than the theoretical values, and consequently also higher than the measured experimental values of tensile forces. This is due partly to the difficulty of determining the proper modulus of elasticity of the concrete to use in converting strains to stresses as explained in section 3.9, and also to the lack of information about the internal stress distribution existing prior to the removal of the shoring.

The modified tensile and compressive forces in Table 4.6 are obtained using the following procedure. Since the precise dead load distribution producing the experimental values is unknown, as shown in Fig. 4.1c, the gross moments at the instrumented sections cannot be computed from the measured reactions and applied loads. The modification factors were therefore determined for the dead load case in the following way. The total measured tensile forces at each Section A, B, C and D given in Table 4.6, which compare favorably with the theoretical values, were assumed to be correct and all measured experimental compressive forces were converted to modified experimental compressive forces by multiplying them by modification factors equal to the ratio of the total experimental tensile to compressive force at each section. The resulting modification factors are given in Table 4.7.

TABLE 4.7 FORCE MODIFICATION FACTORS FOR DEAD LOAD CASE

FORCE	Section A	Section B	Section C	Section D
TENSION	1.000	1.000	1.000	1.000
COMPRESSION	0.518	0.823	0.792	0.352

4.6 Moments

Fig. 4.2 gives total internal moments at various sections. Theoretical results are based on the CELL analysis for a uniform dead load along the entire span. Experimental values are measured values at instrumented sections, due to the load produced by the removal of the shoring Fig. 4.1c, modified by the factors shown in Table 4.7. As would be expected, because agreement between the theoretical and measured total tensile forces was good (Table 4.6), the agreement for total moments is also good.

Table 4.8 gives a detailed breakdown of the transverse distribution of the internal moments to each girder. Theoretical results are from CELL, while the experimental results are given about four different axes for comparison. The different experimental values obtained for the four axes are due to the fact that the longitudinal compressive and tensile forces acting on each girder are not equal. Even though the total forces across a section are modified to give longitudinal equilibrium, this procedure does not result in equilibrium for each individual girder. Fig. 4.3 compares theoretical and experimental percentage distribution to each girder for the moment about the entire gross cross-section neutral axis. It can be seen that the percentage distribution is generally within 1 - 2% of each other. The only exceptions are at girder 1 in Section D, where the differential shrinkage caused girder 1 to lift up from its support at both the end abutments. This lift-up caused more of the dead weight to be carried by girder No. 2, as can also be seen from Fig. 4.4. It should be noted that if the gross moments were distributed to each girder according to the ratios of their moment of inertia to that of the total section, the following percentages are

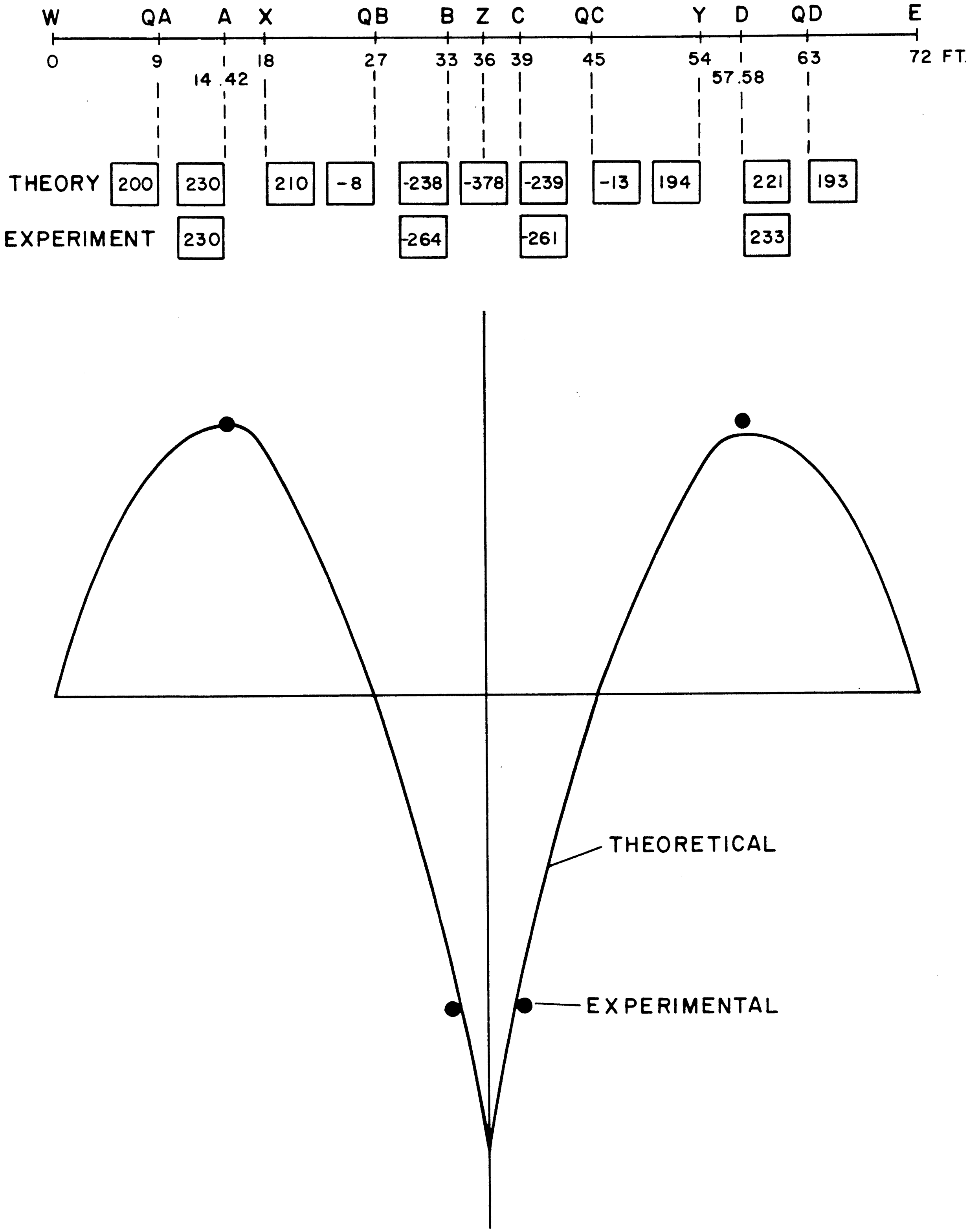

FIG. 4.2 TOTAL INTERNAL MOMENTS (FT – KIPS) AT A SECTION DUE TO DEAD LOAD

TABLE 4.8 - DISTRIBUTION OF MOMENTS (KIP- FT AND %) TO EACH GIRDER FOR DEAD LOAD CASE

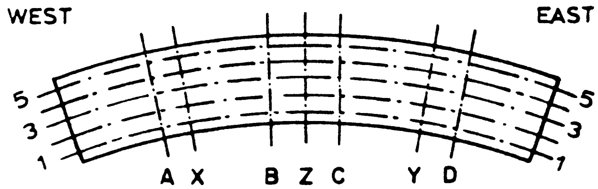

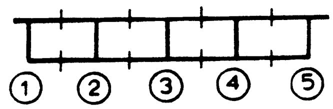

SECTION	GIRDER	THEORETICAL RESULTS (CELL)		EXPERIMENTAL MOMENTS BASED ON							
				COMPRESSION FLANGE MID-DEPTH		TENSION FLANGE STEEL		ENTIRE GROSS CROSS-SECTION NEUTRAL AXIS		GIRDER EXPERIMENTAL NEUTRAL AXIS	
		K-FT	%	K-FT	%	K-FT	%	K-FT	%	K-FT	%
A	1	38.7	16.9	25.3	11.0	65.3	28.4	43.2	18.8	44.2	18.8
	2	51.8	22.6	54.1	23.5	42.4	18.5	48.9	21.3	49.8	21.2
	3	51.1	22.3	57.5	25.0	37.0	16.1	48.3	21.0	51.0	21.7
	4	50.8	22.2	57.2	24.9	46.8	20.4	52.6	22.9	53.6	22.8
	5	36.6	16.0	36.2	15.7	38.2	16.6	37.1	16.1	36.7	15.6
	Σ	229.0		230.2		229.7		230.1		235.4	
B	1	-37.8	15.9	-43.8	16.5	-38.3	14.6	-40.8	15.5	-41.6	15.7
	2	-53.8	22.6	-58.2	21.9	-63.3	24.1	-61.0	23.1	-60.2	22.8
	3	-55.5	23.3	-65.3	24.6	-69.5	26.5	-67.6	25.6	-67.0	25.4
	4	-54.1	22.7	-56.1	21.2	-59.4	22.6	-57.9	22.0	-57.4	21.8
	5	-36.8	15.5	-42.0	15.8	-31.9	12.2	-36.4	13.8	-38.0	14.4
	Σ	-238.0		-265.4		-262.4		-263.8		-264.1	
C	1	-38.4	16.0	-50.0	15.7	-34.5	13.2	-37.4	14.3	-38.3	14.7
	2	-54.1	22.7	-62.0	23.8	-63.1	24.2	-62.6	24.0	-62.4	23.9
	3	-55.4	23.2	-59.6	22.8	-76.1	29.1	-68.8	26.3	-65.5	25.1
	4	-54.3	22.7	-59.1	22.7	-56.2	21.5	-57.5	22.0	-56.2	22.3
	5	-37.1	15.5	-39.2	15.0	-31.2	12.0	-34.8	13.3	-36.1	13.9
	Σ	-239.3		-260.8		-261.1		-261.1		-260.4	
D	1	37.2	17.0	30.8	13.0	34.3	13.5	31.1	13.4	31.0	13.3
	2	49.6	22.7	60.4	26.0	46.3	19.9	54.1	23.3	55.3	23.8
	3	48.6	22.3	47.6	20.5	43.6	18.7	45.8	19.7	46.0	19.8
	4	48.2	22.1	59.8	25.7	64.8	27.8	62.0	26.7	62.0	26.6
	5	34.7	15.9	33.8	14.6	46.7	20.1	39.6	17.0	38.5	16.6
	Σ	217.3		232.4		232.8		232.6		232.7	

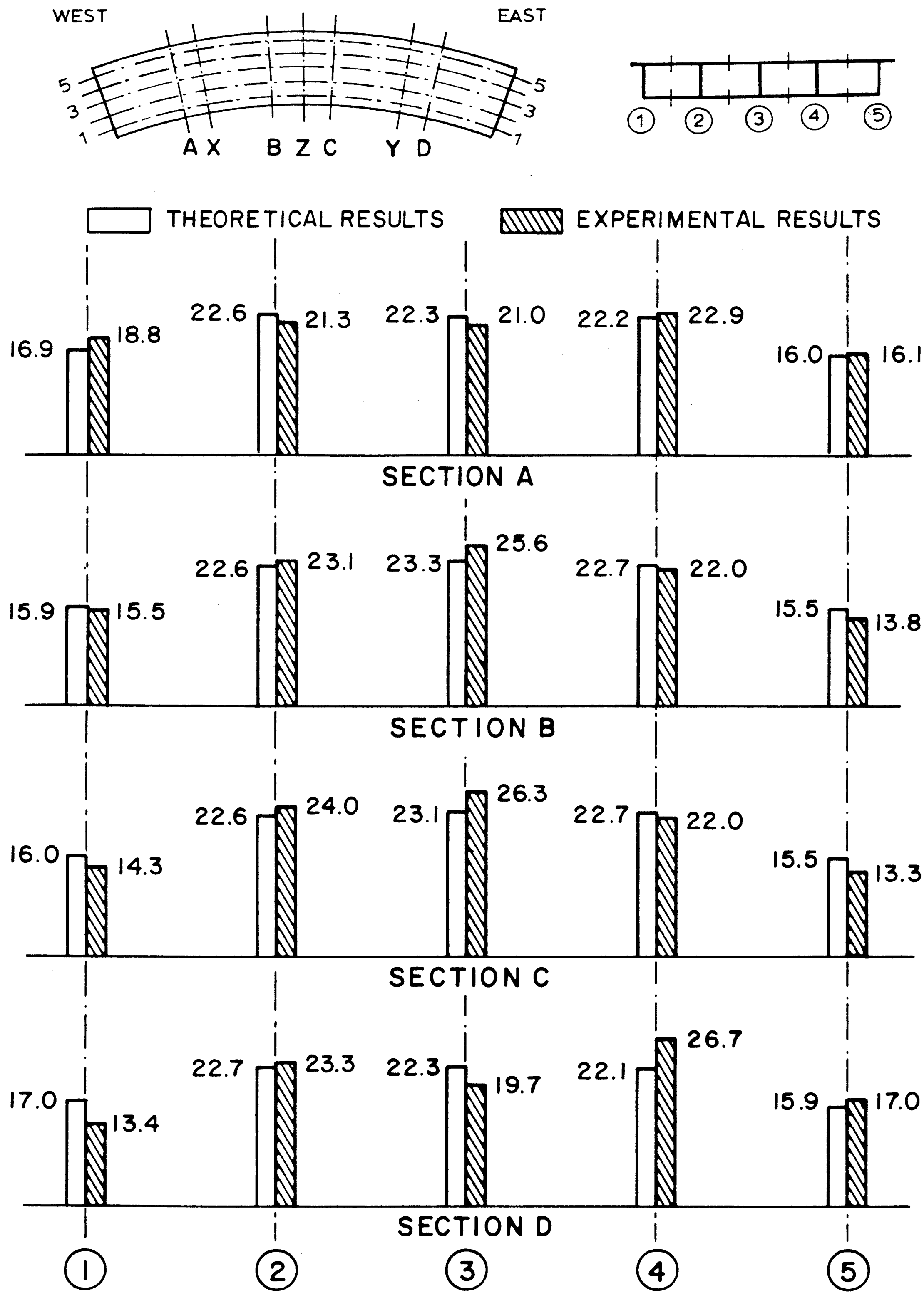

FIG. 4.3 PERCENTAGES OF TOTAL MOMENT AT A SECTION CARRIED BY EACH GIRDER FOR DEAD LOAD CASE

obtained: 16,5, 22.4, 22.4, 22.4, 16.5. The values in Fig. 4.3 closely approximate these percentages which represent a uniform stress distribution across the width of the entire section.

4.7. Comparison of Experimental Results for Straight and Curved Bridge Models

Experimental results for reactions, deflections, strains, and distribution of moments, due to dead load on the straight [10,11] and curved bridge models reveal generally similar behavior.

The straight and curved bridges had total measured dead weights of 199.1 and 202.4 kips respectively. The distribution of these total weights as vertical reactions between the east, center and west supports was 19.3%, 61.4% and 19.4% for the straight bridge and 18.0%, 63.3% and 18.7% for the curved bridge. The slightly higher center footing reaction for the curved bridge is primarily due to the eccentricity of the dead load with respect to a line joining the middle of the east and west end supports, which eccentricity does not exist for the straight bridge.

Vertical deflections at midspan Sections X and Y were 0.38 and 0.44 in. respectively for the straight bridge and were uniform across the width of the bridge. As shown in Table 4.3 deflections of outer girder 5 were slightly greater than those of girder 1 for the curved bridge due to the larger span length of girder 5. At both Sections X and Y, deflections at girders 1 and 5 (Table 4.3) were 0.40 and 0.48 in. averaging 0.44 in., which is close to the straight bridge values. However, these values have not been adjusted for E_c, which averaged 15% higher for the straight compared to the curved bridge during the dead load phase.

A comparison of experimental strains at positive moment Section D and negative moment Section C, both in the undiaphragmed span, is given in Fig. 4.4. The tensile strains in the steel at both sections show fairly good agreement. The compressive strains in the concrete at Section C follow a very similar pattern with the curved bridge values being slightly greater throughout, probably due to the lower modulus of elasticity in the concrete of the curved vs straight bridge. At Section D, near midspan, the concrete strains in the curved bridge are much higher partly due to the different moduli of elasticity, but also due to the difference in internal stress distributions at midspan caused by shrinkage prior to the removal of the shoring for the two bridges.

Total dead load moments at a section and transverse distribution of these moments are quite similar in the straight and curved bridge models. A comparison of transverse distributions of moments about the gross section neutral axis is given in Fig. 4.5. Agreement is quite good at all sections, with the largest differences occuring at girder 3, 4, 5 of Section D, due to the concentration of compressive strains measured at these points for the curved bridge shown in Fig. 4.4.

4.8 Summary

Experimental measurements of response due to dead load are more difficult to evaluate than those due to live load, because they are dependent on the sequence and manner of construction, placing of instrumentation, design and installation of reaction supports and removal of shoring. Nevertheless after comparing theoretical and experimental results the following conclusions can be made with

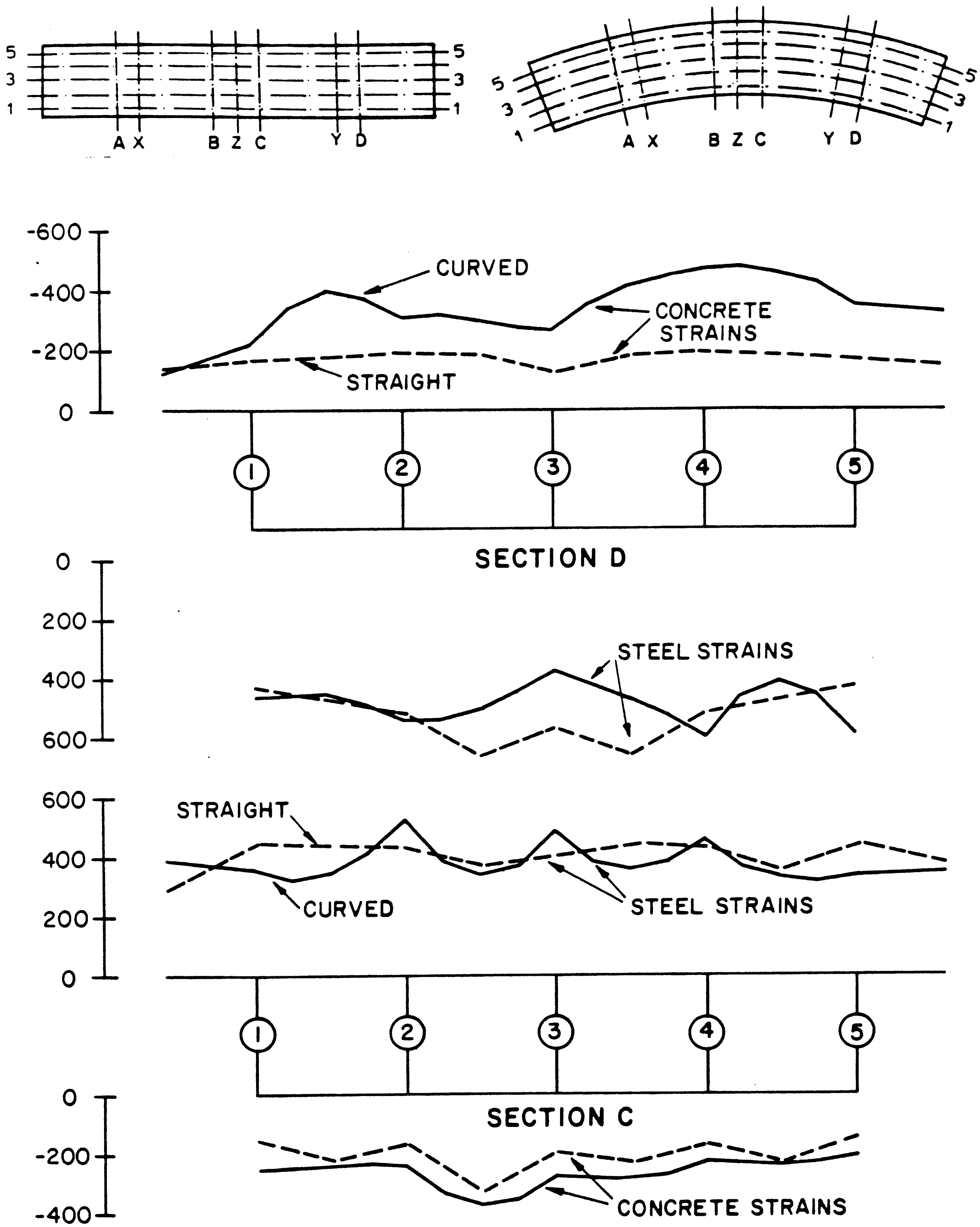

FIG. 4.4 EXPERIMENTAL LONGITUDINAL STRAINS (MICRO-INCH/INCH) IN TOP AND BOTTOM SLABS AT SECTIONS C AND D FOR DEAD LOAD CASE - STRAIGHT VS CURVED BRIDGE MODELS

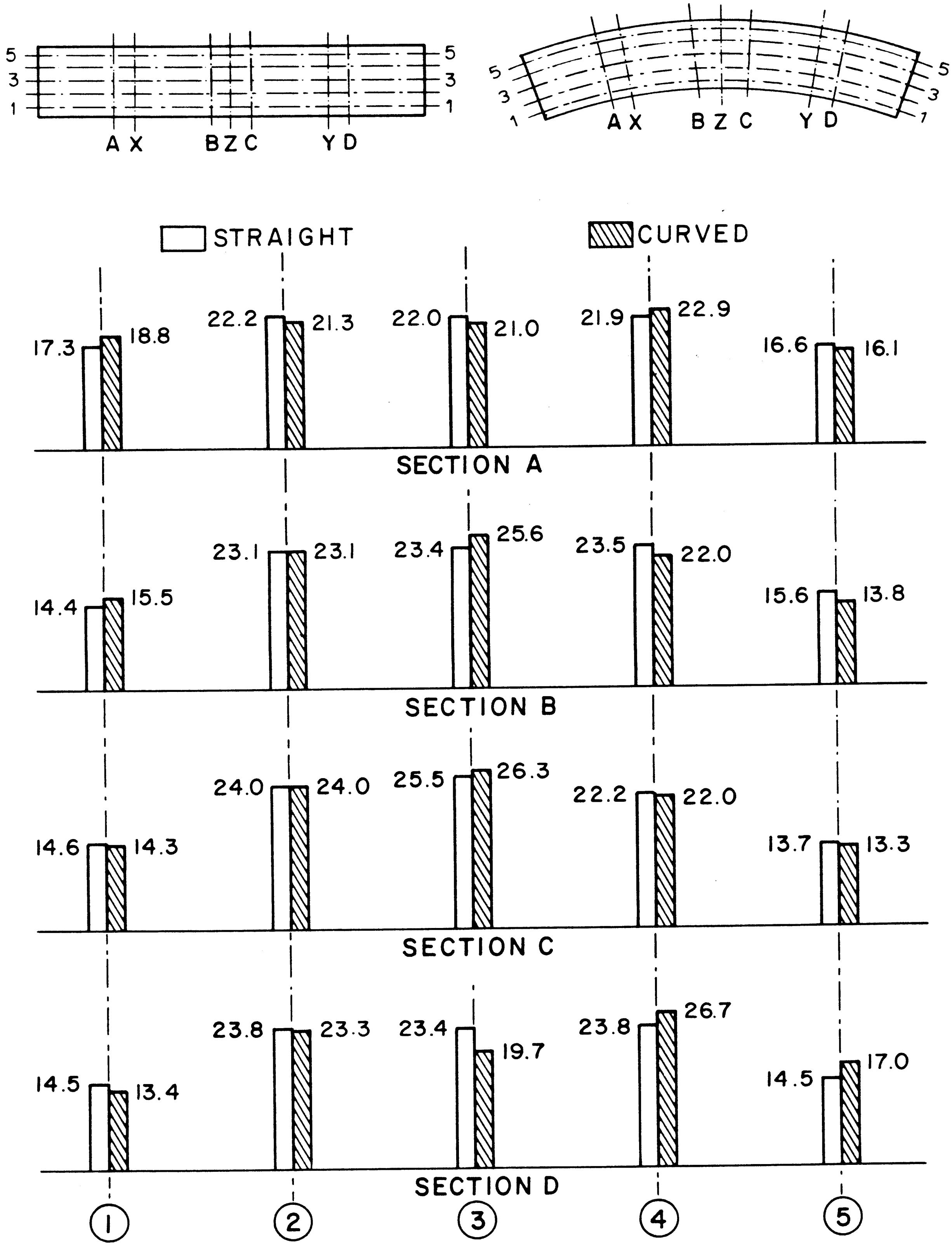

FIG. 4.5 EXPERIMENTAL PERCENTAGES OF TOTAL MOMENT AT A SECTION CARRIED BY EACH GIRDER FOR DEAD LOAD CASE – STRAIGHT VS CURVED BRIDGE MODELS

respect to the dead load case.

1. Distribution of the total reactions between the east, center and west supports is accurately predicted by theory.

2. The transverse distribution of the total reactions at each end to the five reaction supports is highly dependent on the manner of design and installation of these supports and cannot be accurately predicted by theory, which assumes that the rigid end diaphragm rests on five unyielding supports. Relative displacements due to support movements and differences in the spring constants of the support assemblies can totally change the transverse distribution of the reactions. However, the resultants of the five reactions remain essentially unchanged.

3. The deflections of outer girder 5 were 20% larger than those of inner girder 1, and throughout, the experimental deflections were 50 to 60% higher than the theoretical deflections based on an uncracked section.

4. Experimental and theoretical values of tensile strains in the steel were in good agreement.

5. The experimental values of compressive strains in the concrete and thus the internal longitudinal forces and moments at a section in several cases were not in good agreement with theory or statics. This was probably due to the assumed modulus of elasticity for the concrete and to the fact that it was impossible to measure the actual external and internal forces

and stresses existing in the model prior to the removal of the forms.

6. When the experimental longitudinal compressive forces were modified to equal the measured tensile forces, as required by statics, the resulting internal experimental moments on a section were very close to those predicted by theory.

7. The agreement between theory and experiment for the percentage of the total moment at any section taken by each girder was very good, within 1-2%.

8. The response of the straight bridge and curved bridge models to dead load was quite similar.

5. RESULTS FOR WORKING STRESS LOADS

5.1 General Remarks

As described in Volume I the loading program was divided into several phases in which initial conditioning loads were applied to create total maximum tensile stresses in the reinforcement of 24, 30, 40, 50 and 60 ksi. Each of these initial conditioning loads was then followed by a detailed sequence of point loads on the bridge.

One of the prime objectives of the test program was to determine the bridge response at working stress levels. The loading phase involving the initial application of conditioning loads to produce a maximum tensile stress of 30 ksi was chosen to be representative of response at working stress from the point of view of assessing actual box girder bridge behavior for design purposes. An advantage of using the 30 ksi stress level instead of the 24 ksi stress level was that 50% higher values of live load stresses could be registered for a total increase in the bridge model tensile stresses of only 6 ksi. All subsequent point loads in this phase, however, were chosen to produce maximum stresses, where applied, of the order of the working stresses, i.e. 24 to 30 ksi total maximum tensile stress in the reinforcement.

The 30 ksi working load phase contained the most complete and detailed loading schedule of any phase (See Table 5.1 in Vol. I). In this chapter a presentation and evaluation of results will be made for this phase for the following loadings and conditions.

(1) Point loads on girder webs at midspan.

(2) Effect of support restraints.

(3) Trucks and construction vehicle loads.

(4) Moving fork lift load.

5.2 Point Loads on Girder Webs at Midspans

Detailed tabulations of theoretical and experimental results related to reactions, deflections, strains and moments for each of the 19 point load combinations used are given in Vol. III. All theoretical and experimental values have been normalized for purposes of comparison to loads of 100 kips per span. Theoretical values for these point load cases have been obtained from computer analyses using CELL.

Because of the voluminous amount of data, only nine point load cases will be treated in detail in the text of the present volume. These cases are: point loads at locations 1X, 3X or 5X; point loads at locations 1Y, 3Y or 5Y; point loads at locations 1X +1Y, 3X + 3Y or 5X + 5Y. These cases have been chosen as typical of the 19 point load combinations, and comprise cases of loadings on the inner, center and outer girders of the bridge at the diaphragmed and undiaphragmed midspans. Loadings 1X, 3X and 5X produce maximum positive moments in diaphragmed Span I. Loadings 1Y, 3Y and 5Y produce maximum positive moments in undiaphragmed Span II. Loadings 1X + 1Y, 3X + 3Y and 5X + 5Y produce maximum negative moments at the center bent. Furthermore, these nine loading cases lend themselves to comparisons of superposition which can be used as a check on the reliability of the experimental data.

In addition to the detailed study of reactions, deflections, strains and moments of the above nine loading cases, a complete summary and discussion of theoretical and experimental moments for all 19 point load cases is given in Section 5.4.

5.2.1 Reactions

Table 5.1 gives a comparison of theoretical and experimental total reactions due to point loads normalized to 100 kips. The theoretical horizontal reactions R_{WR}, R_{FL}, R_{FR} and R_{ER} are zero in all cases and thus are not tabulated. Similarly the experimental values of these horizontal reactions are taken as zero for this normal restraint case at the reaction supports. As described in Sec. 3.4.1.2 of Vol. I, the normal restraint case assumed that simple supports were achieved at the two ends of the bridge and complete fixity was achieved at the base of the center bent footing by the reaction assemblies provided in this phase of the test program. It was not possible to determine whether any experimental horizontal reactions were actually developed due to friction or other causes in the end reaction assemblies, however, if any existed they should have been very small.

Theoretical values of the applied loads and reactions shown in Table 5.1, precisely satisfy overall equilibrium defined by the sum of vertical forces ($\Sigma V = 0$); the sum of moments about the NS centerline ($\Sigma M_{NS} = 0$); and the sum of moments about the EW centerline ($\Sigma M_{EW} = 0$). Static checks on experimental values were performed by summing the positive and negative contributions in each of the above equilibrium equations. The maximum percentage differences found between these contributions for ΣV, ΣM_{NS} and ΣM_{EW}, respectively, were 2.6, 3.6 and 7.1%, with most load cases yielding even much lower differences than these.

Table 5.1 shows that for the vertical reactions, the agreement between experimental and theoretical values is generally quite good with differences ranging from 0 to 2.7, 0.6 to 4.1, and 0.3 to 2.6 kips

TABLE 5.1 COMPARISON OF THEORETICAL AND EXPERIMENTAL REACTIONS (KIPS AND FT-KIPS) AT WORKING STRESS LEVEL

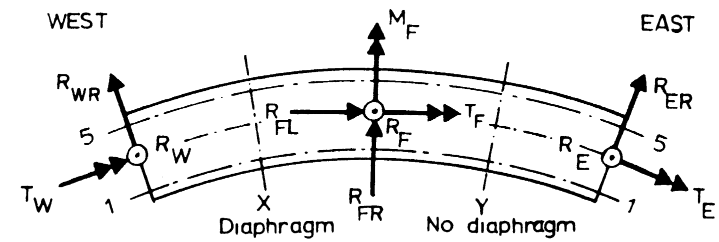

LOAD CASE	SOLUTION	REACTIONS (KIPS AND FT-KIPS)								LOAD (KIPS)		
		WEST END		CENTER FOOTING			EAST END		TOTAL	SEC X	SEC Y	TOTAL
		R_W	T_W	R_F	M_F	T_F	R_E	T_E	R	P_X	P_Y	P
1X	THEORY	41.2	-283	64.5	110	-83	-5.7	-99	100.0	100.0	0.0	100.0
	EXPER.	41.2	-280	68.1	24	-78	-7.1	-96	102.2	100.0	-0.1	99.9
1Y	THEORY	-5.9	-99	64.8	-111	-84	41.1	-283	100.0	0.0	100.0	100.0
	EXPER.	-7.2	-110	68.9	-15	-84	39.5	-256	101.2	0.3	100.0	100.3
1X + 1Y	THEORY	35.3	-382	129.3	0	-168	35.3	-382	200.0	100.0	100.0	200.0
	EXPER.	35.5	-381	132.5	-54	-149	33.2	-346	201.3	100.0	99.1	199.1
3X	THEORY	38.8	57	69.1	122	0	-7.9	-17	100.0	100.0	0.0	100.0
	EXPER.	40.0	67	69.7	103	9	-7.2	-20	102.5	100.0	0.0	100.0
3Y	THEORY	-7.9	-17	69.2	-125	0	38.7	57	100.0	0	100.0	100.0
	EXPER.	-8.0	-27	71.3	-146	-3	36.1	54	99.4	-0.1	100.0	99.9
3X + 3Y	THEORY	30.9	39	138.3	-3	1	30.8	39	200.0	100.0	100.0	200.0
	EXPER.	31.3	37	141.1	72	7	30.1	35	202.4	100.0	99.7	199.7
5X	THEORY	36.2	395	74.1	133	82	-10.2	63	100.0	100.0	0.0	100.0
	EXPER.	36.4	400	76.0	145	74	-9.7	45	102.6	100.0	0.0	100.0
5Y	THEORY	-10.1	63	73.8	-130	83	36.3	396	100.0	0.0	100.0	100.0
	EXPER.	-9.2	59	72.2	-130	98	36.6	366	99.6	0.1	100.0	100.1
5X + 5Y	THEORY	26.0	458	147.9	3	166	26.1	458	200.0	100.0	100.0	200.0
	EXPER.	28.7	461	151.4	-31	162	27.1	417	207.1	100.0	103.5	203.5

for R_W, R_F and R_E, respectively. Similar good agreement can also be noted for the external torsional reactions T_W, T_F and T_E. Finally for the external moment reaction under the center footing M_F, satisfactory agreement between experiment and theory is found for all point loadings except 1X, 1Y, 1X + 1Y and 3X + 3Y. The larger differences for these cases can be partially attributed to the sensitivity of M_F to slight differences in loadings or end reactions in the experimental program when compared to theory.

Superposition can also be checked in Table 5.1 by comparing the sum of the results for point loads at Section X and Y applied separately with those for the point loads applied simultaneously at Sections X and Y. It can be seen that theoretical values satisfy superposition exactly, while for experimental values superposition is quite good for all values except M_F.

Table 5.1 presents only the total end vertical (R_W and R_E) and torsional (T_W and T_E) reactions. These were obtained by summing the statical contributions to these quantities from each of the experimental or theoretical vertical reactions under the five girder supports at each end of the bridge. These individual girder reactions as well as the total reactions are given in detail in the tables of Vol. III. The transverse distribution of the total reactions at each end to the five individual girder reaction supports is highly dependent on the type and installation of the support assemblies and cannot be accurately predicted by theory. Because the deep rigid end diaphragm rests on five supports, any slight change at an invidudual support point can change drastically the magnitude of the reaction at each point. However, it is very important to note, as shown in Table 5.1, that this does not affect the total R and T reactions at the end supports. Consequently, these total reactions are distributed by the rigid end diaphragms into the bridge in a similar way and thus the overall response of the bridge is not affected by small changes or displacements at individual girder reaction support points.

5.2.2 Deflections

Vertical deflections for the nine point load cases are presented in Figs. 5.1 to 5.5. In each case, theoretical curves are given based on 1.0 and 1.5 times the theoretical values obtained from the CELL program, which assumes an uncracked gross concrete section. These curves may be compared with individually plotted experimental points.

Figs. 5.1, 5.2 and 5.3 show the longitudinal variation of the deflection under the loaded girder in each case. Figs. 5.4 and 5.5 depict the transverse distribution at the loaded sections in each case. A study of Figs. 5.1 to 5.5 indicates that theory predicts the general distribution of deflections quite well if the theoretical values based on an uncracked section are multiplied by a factor of about 1.5 to account for cracking at this stress level. It also appears that superposition is valid for both theoretical and experimental values. It can also be seen that deflections are slightly larger and more concentrated under the point loads in the undiaphragmed midspan Section Y than in the diaphragmed midspan Section X.

5.2.3 Strains

Comparisons of the transverse distributions of theoretical and experimental strains in the top and bottom slabs at the instrumented section under loading cases 1X + 1Y, 3X + 3Y and 5X + 5Y are given

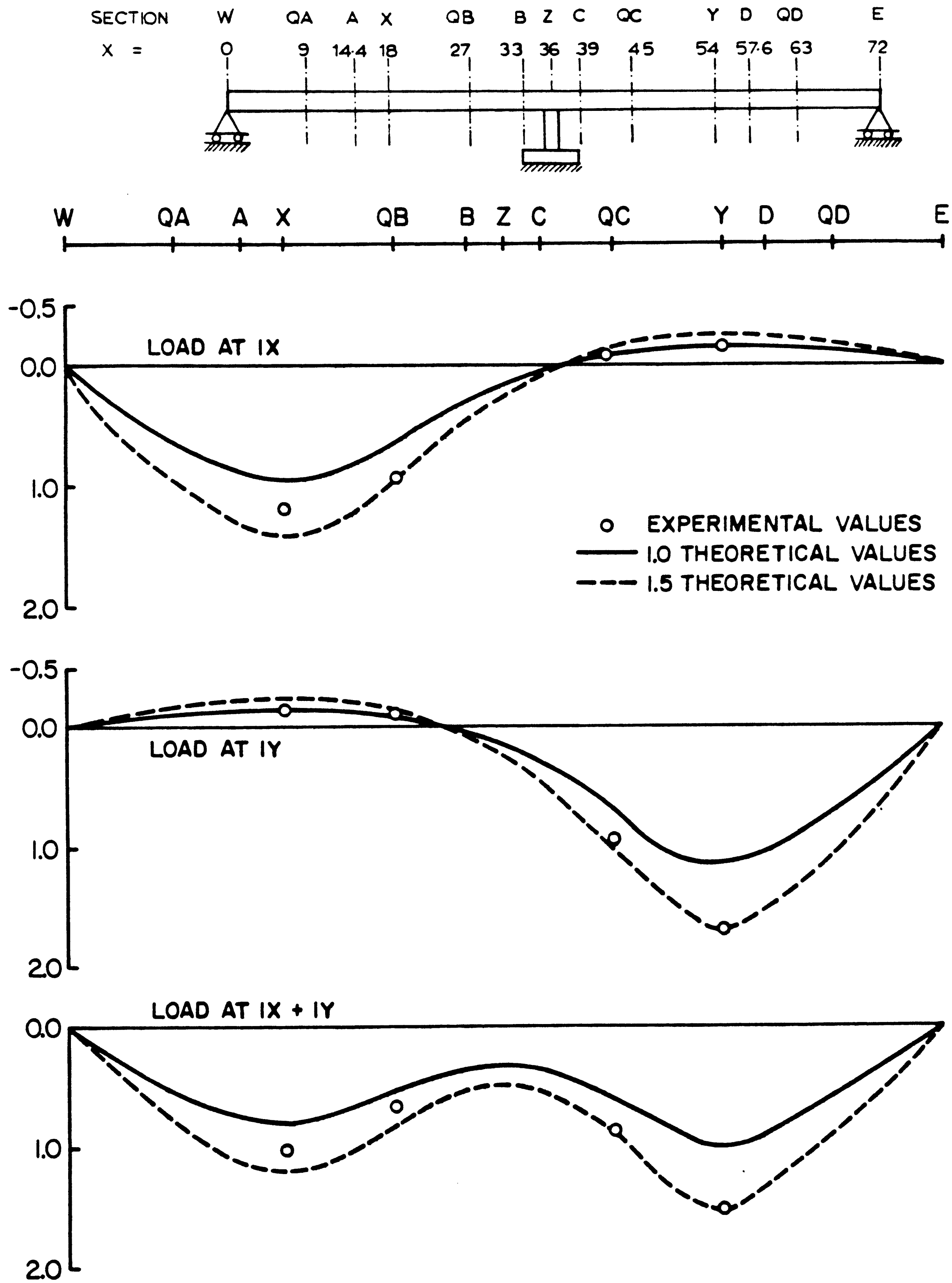

FIG. 5.1 VERTICAL DEFLECTIONS (INCHES) ALONG INNER GIRDER 1
FOR 100 KIP LOADS AT 1X, 1Y, 1X + 1Y

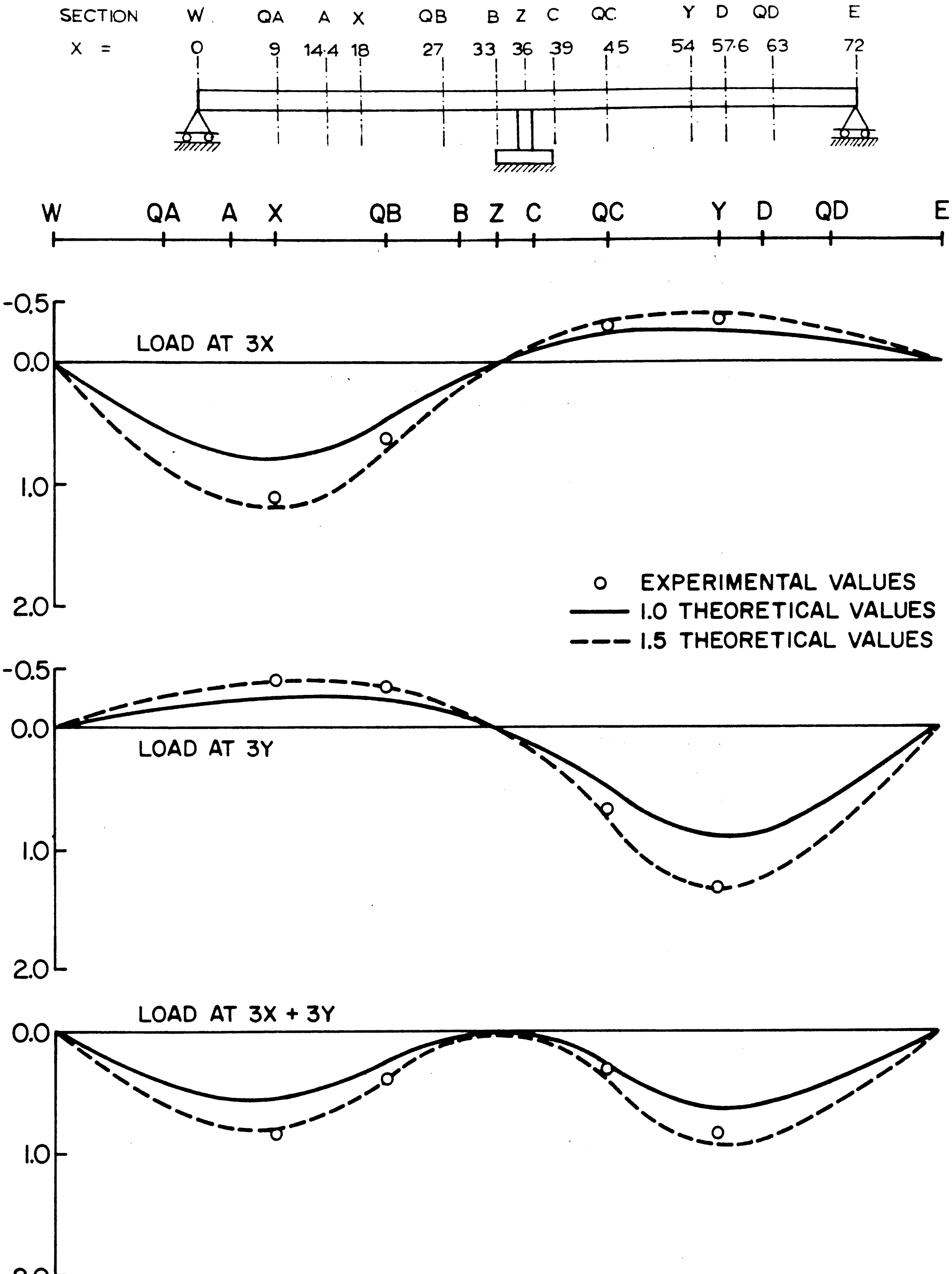

FIG. 5.2 VERTICAL DEFLECTIONS (INCHES) ALONG CENTER GIRDER 3 FOR 100 KIP LOADS AT 3X, 3Y, 3X+3Y

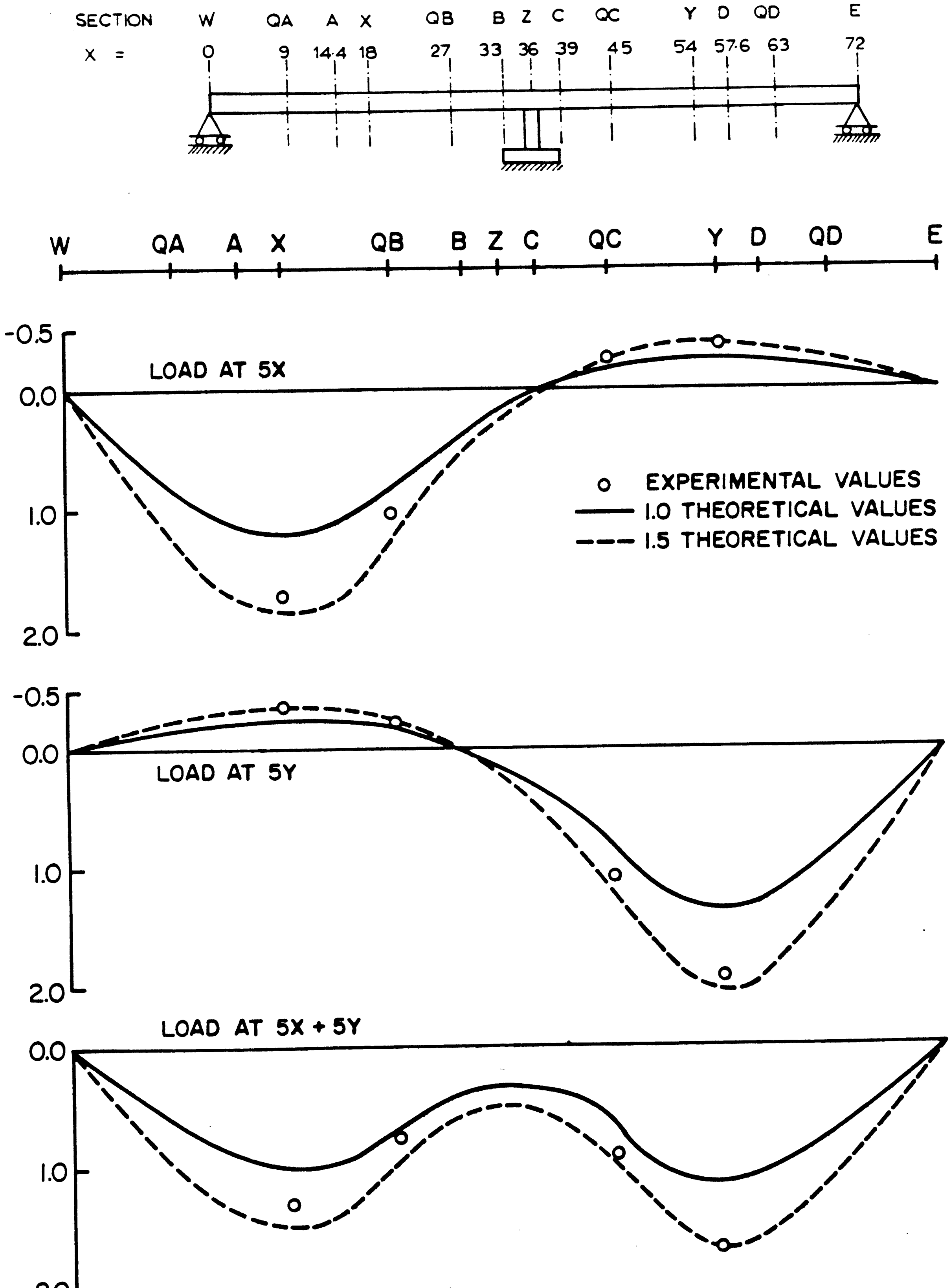

FIG. 5.3 VERTICAL DEFLECTIONS (INCHES) ALONG OUTER GIRDER 5
FOR 100 KIP LOADS 5X, 5Y, 5X + 5Y

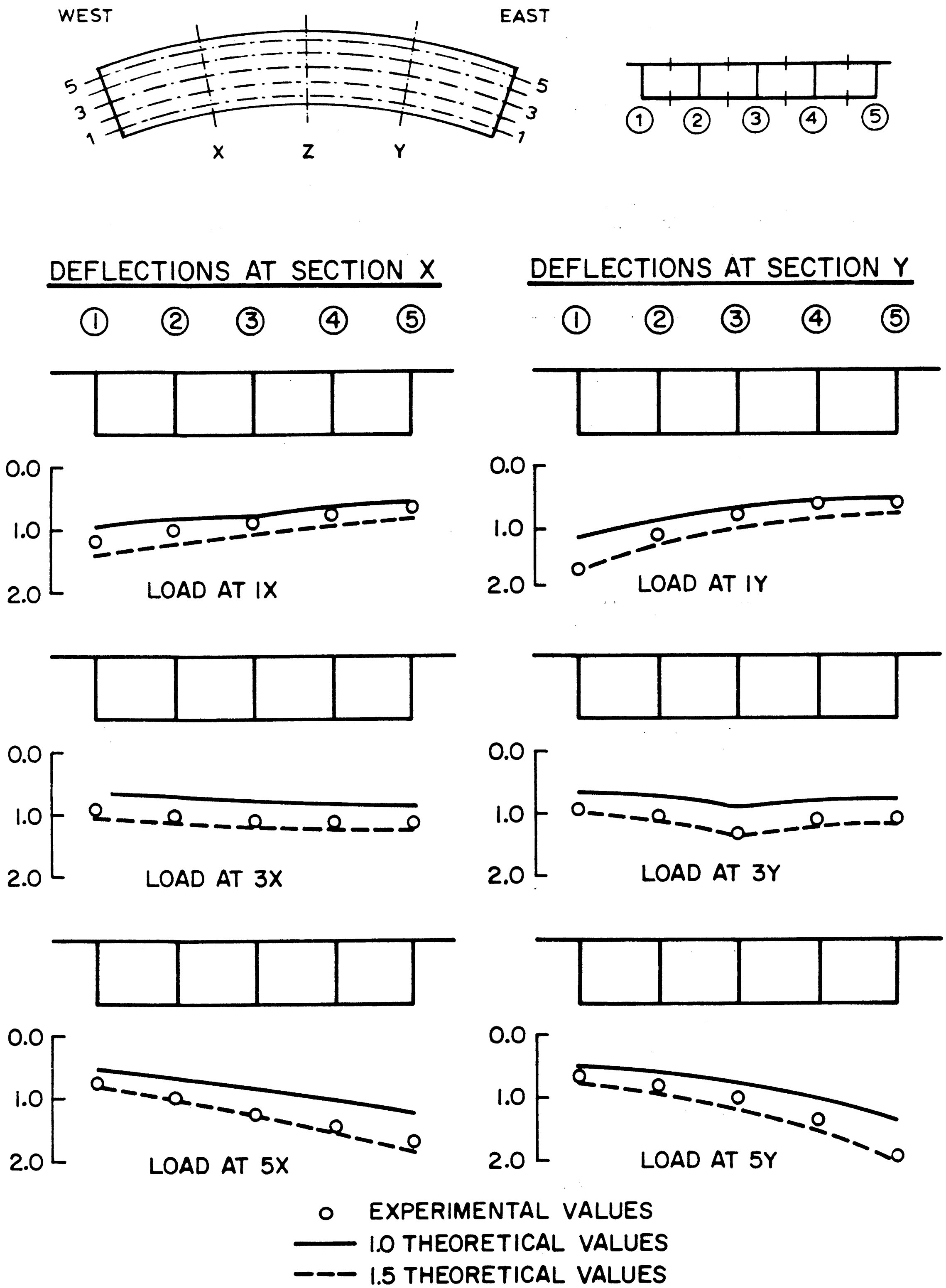

FIG. 5.4 VERTICAL DEFLECTIONS (INCHES) AT TRANSVERSE SECTIONS X AND Y FOR 100 KIP LOADS AT 1X, 1Y, 3X, 3Y, 5X, 5Y

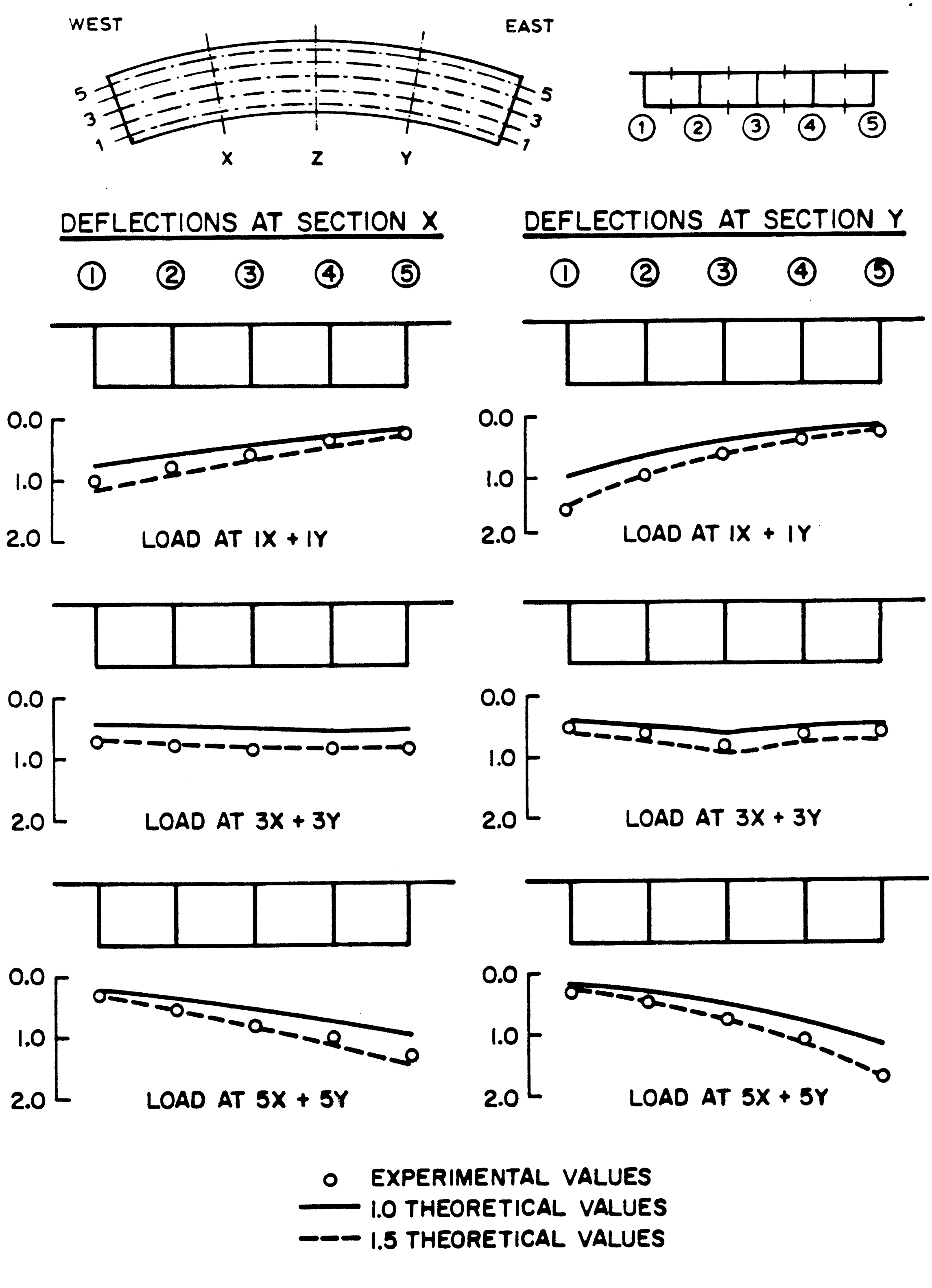

FIG. 5.5 VERTICAL DEFLECTIONS (INCHES) AT TRANSVERSE SECTIONS X AND Y FOR 100 KIP LOADS AT 1X+1Y, 3X+3Y, 5X+5Y

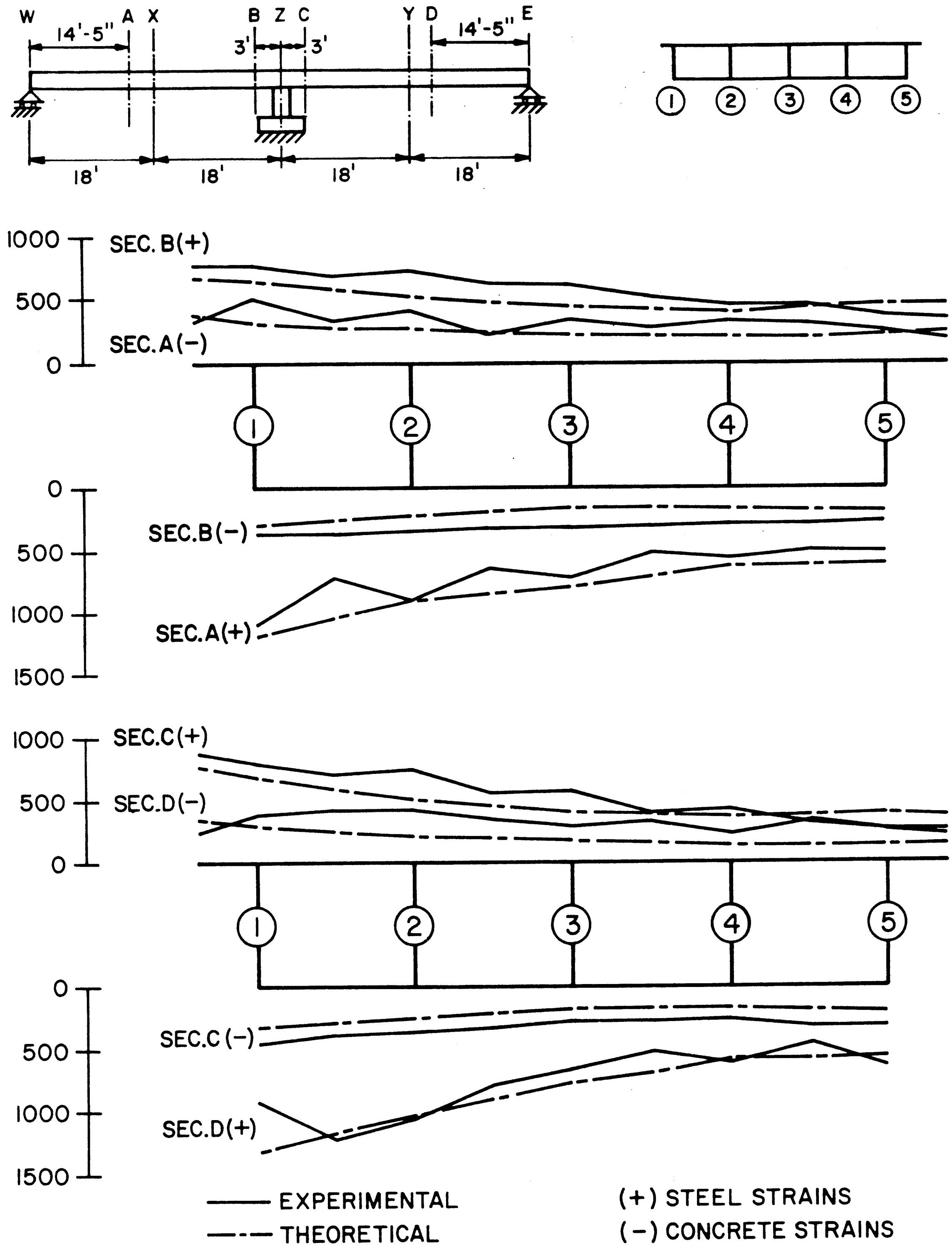

FIG. 5.6 LONGITUDINAL STRAINS (MICRO-INCH/INCH) AT TRANSVERSE SECTIONS FOR 100 KIP LOADS AT 1X + 1Y

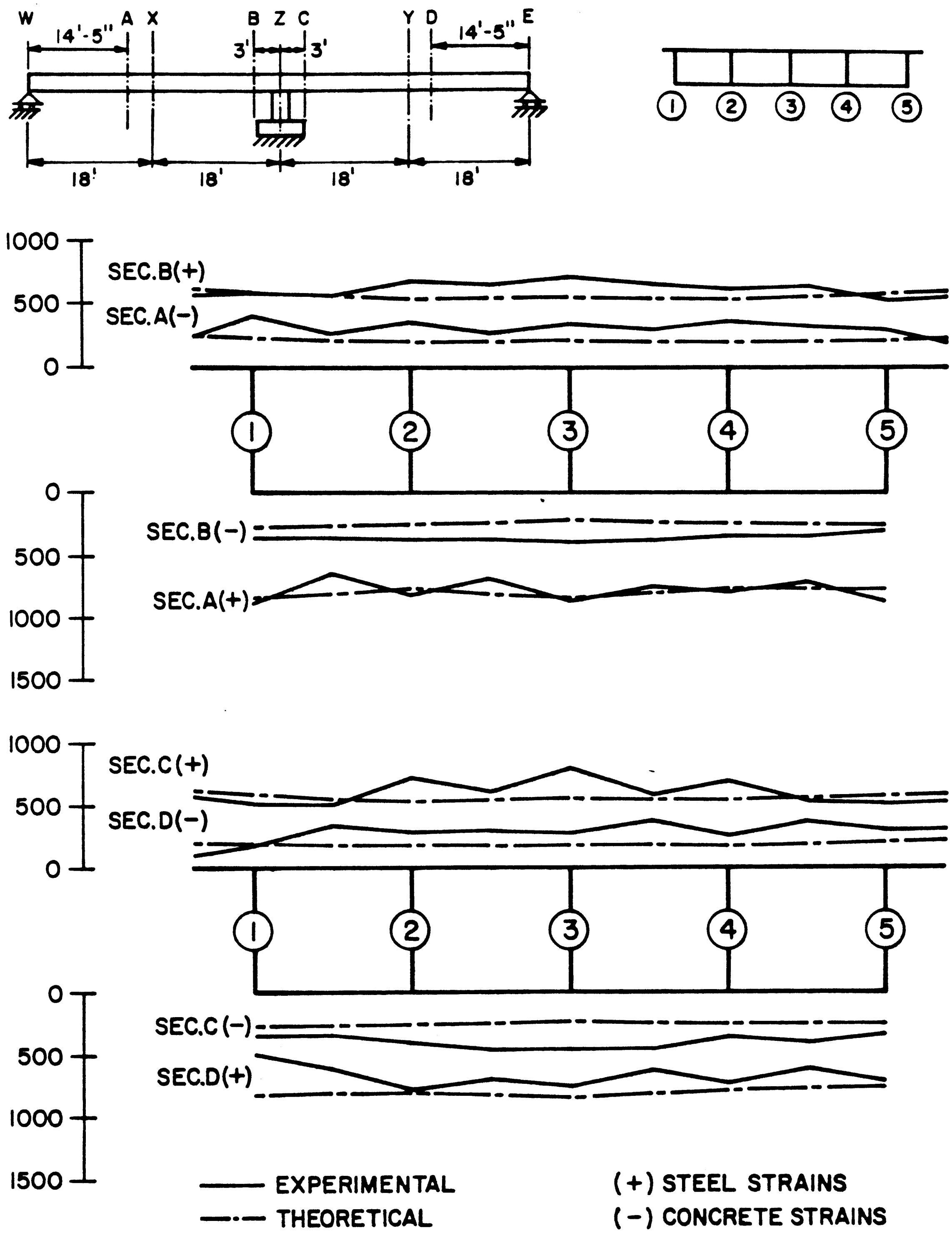

FIG. 5.7 LONGITUDINAL STRAINS (MICRO-INCH/INCH) AT TRANSVERSE SECTIONS FOR 100 KIP LOADS AT 3X+3Y

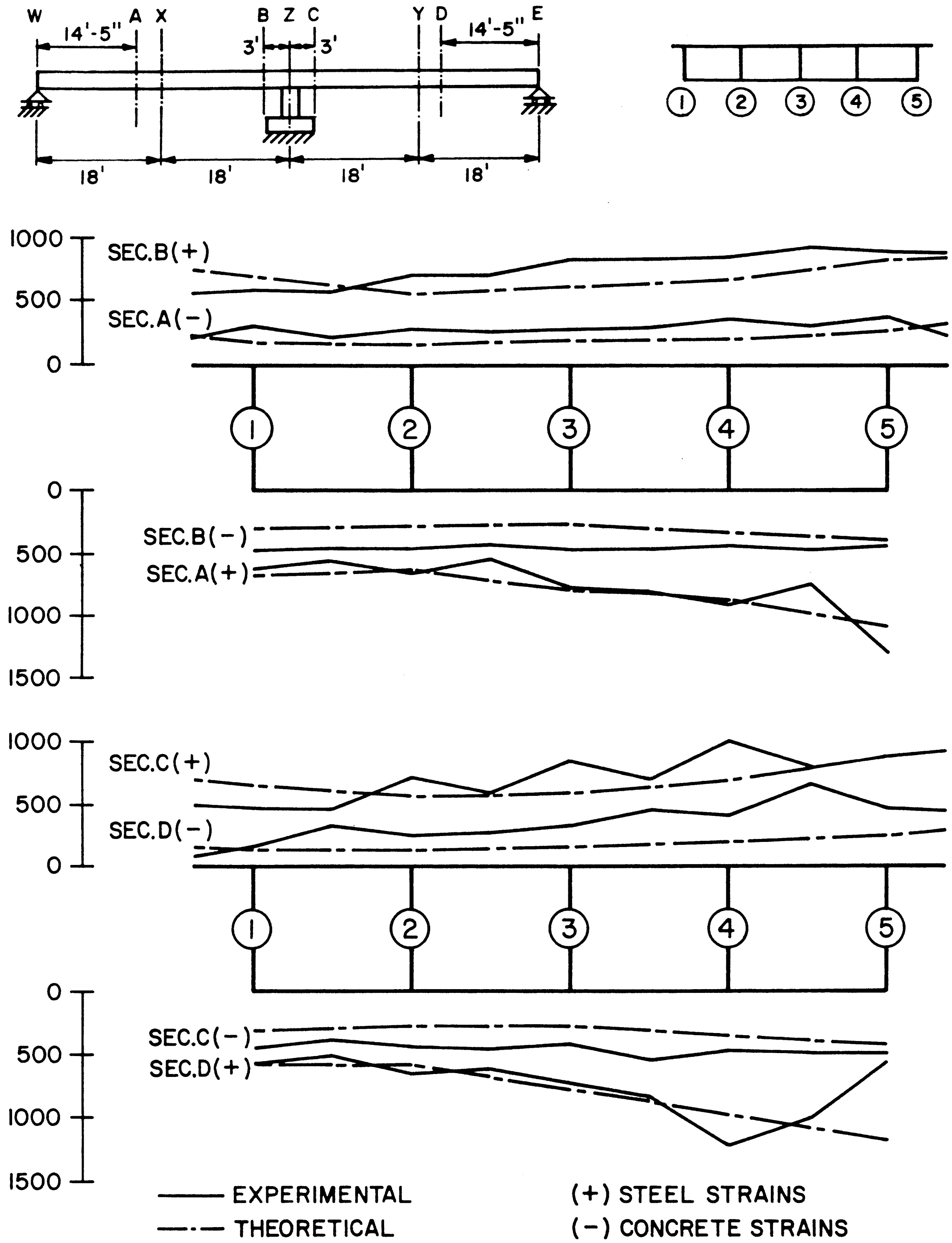

FIG. 5.8 LONGITUDINAL STRAINS (MICRO-INCH/INCH) AT TRANSVERSE SECTIONS FOR 100 KIP LOADS AT 5X + 5Y

in Figs. 5.6, 5.7, and 5.8. While there is general agreement, substantial differences exist at certain points. Theoretical strains have been obtained using the procedure described in Section 2.8 and are available only at the top and bottom of each web and thus straight lines are drawn transversely between these points. Experimental strains have been plotted over each web and also at transverse midpoints between webs and indicate that in most cases slightly higher strains existed directly over the webs than at the midpoints between webs.

The experimental steel strains are in better agreement with theory than are the experimental concrete strains. The experimental concrete strains appear to be consistently higher than theoretical values. As discussed in Section 3.9 this is due to uncertainty regarding the proper modulus of elasticity of the concrete to be used in converting theoretical concrete stresses to strains.

5.2.4 Moments

A comparison is given is Figs. 5.9, 5.10 and 5.11 of the theoretical and experimental longitudinal distributions of the total moments at a section. All values have been normalized to a 100 kip point load in the loaded spans. Moments obtained from both external reactions and an integration of the internal forces at a section are given.

First, comparing experimental values with theoretical values, the agreement for moments based on external reactions is good for positive moments at Sections A and D in the loaded spans, with most values being within 5%. For negative moments at Sections B and C and for moments in the unloaded span at Sections A and D, the agreement is not as good, however, for most load cases the agreement is within 10%. Moments at these sections are sensitive to small changes in the measured end reactions. The agreement between experiment and theory for moments based on internal forces is adequate, but variable. For moments at Sections A and D in the loaded span, the agreement is within 7%, except for load cases 1Y and 3X + 3Y where the differences are 14 and 12% respectively. For negative moments at Sections B and C and for moments in the unloaded span at Sections A and D the agreement is not as good with differences ranging from 0 to 25%. Agreement is best for cases where both Sections X and Y are loaded simultaneously.

Second, comparing moments based on internal forces to those based on external reactions, which should give indentical results, it is evident from Figs. 5.9, 5.10 and 5.11 that the agreement for theoretical results is excellent, generally within 1%. For experimental values, the difference between external and internal moments at Sections A and D in the loaded span ranges from 1 to 9%, except for load case 1Y where the difference is 11%. For negative moments at Sections B and C, when both spans are loaded the differences range from 1 to 11%. When only one span is loaded, the differences between external and internal experimental negative moments at Sections B and C and in the unloaded span at Sections A and D became much larger for some cases and range from 1 to 40%.

As discussed in Sec. 3.9, all experimental results for moments based on internal forces shown in Figs. 5.9, 5.10 and 5.11 have been determined using the modification factors for internal forces from the 30 ksi conditioning load case. Since this common set of factors was used for all point load cases, perfect agreement between experimental external and internal moments could not be expected. The range of differences cited above is undoubtedly partially due to the fact that the relation between measured strain and internal force is not a constant for a particular section, but is dependent on the position in the section where the strain is being measured, as well as the load position and stress level. Stress reversals encountered in unloaded spans for point load cases also can change the relation between measured strain and internal force significantly due to cracks opening or closing.

The transverse distribution of the total positive moments at Section A for loading 1X, 3X, 5X and at Section D for loadings 1Y, 3Y, 5Y and of the total negative moment at Section B for loadings 1X + 1Y, 3X + 3Y and 5X + 5Y are illustrated in Figs. 5.12, 5.13 and 5.14. The percentages shown may be compared with the best possible distributions of 16.5, 22.4, 22.4, 22.4 and 16.5%, for girders 1 to 5 respectively, which would be obtained for a uniform distribution of stress across the entire section. The closer one gets to these optimum values, the better the load distribution properties of the bridge. From Figs. 5.12, 5.13 and 5.14 the following observations may be made.

(1) The agreement between theory and experiment is generally good, with differences in most cases being of the order of 1 to 2%. A maximum difference of 3.6% occurs for girder 4 for a load at 5Y.

(2) As the loadings move from girder 1 to 3 to 5, a corresponding shift of the distribution of the total moment from inner to outer girders occurs. This shift is most pronounced for the positive moment at Section D of the undiaphragmed span under loads at Section Y, Fig. 5.13, and least pronounced for the negative moment at Sections B, under loads at Sections X + Y, Fig. 5.14.

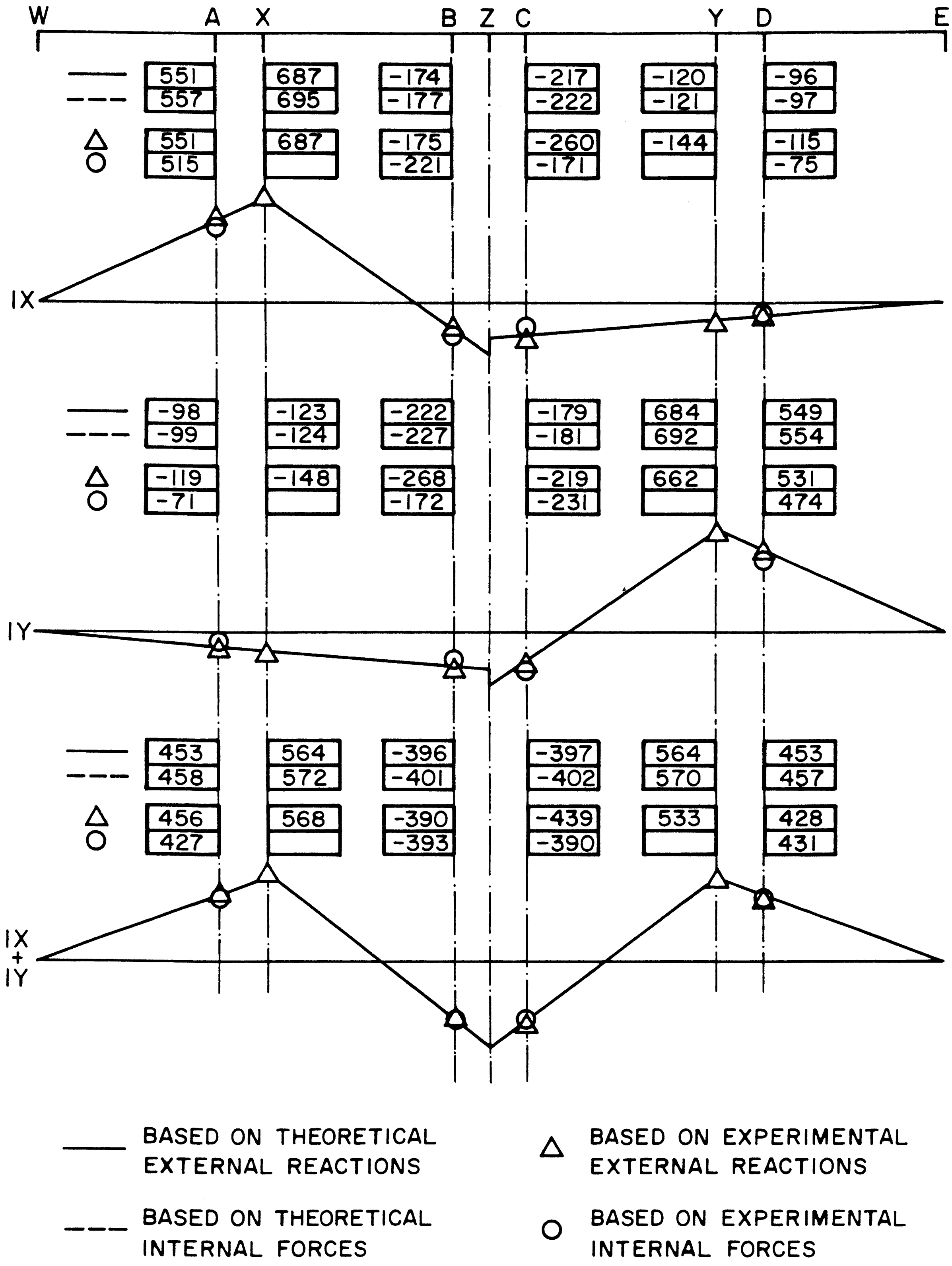

FIG. 5.9 TOTAL MOMENTS KFT-KIPS) AT A SECTION FOR NORMALIZED 100 KIP POINT LOADS AT 1X, 1Y, 1X + 1Y

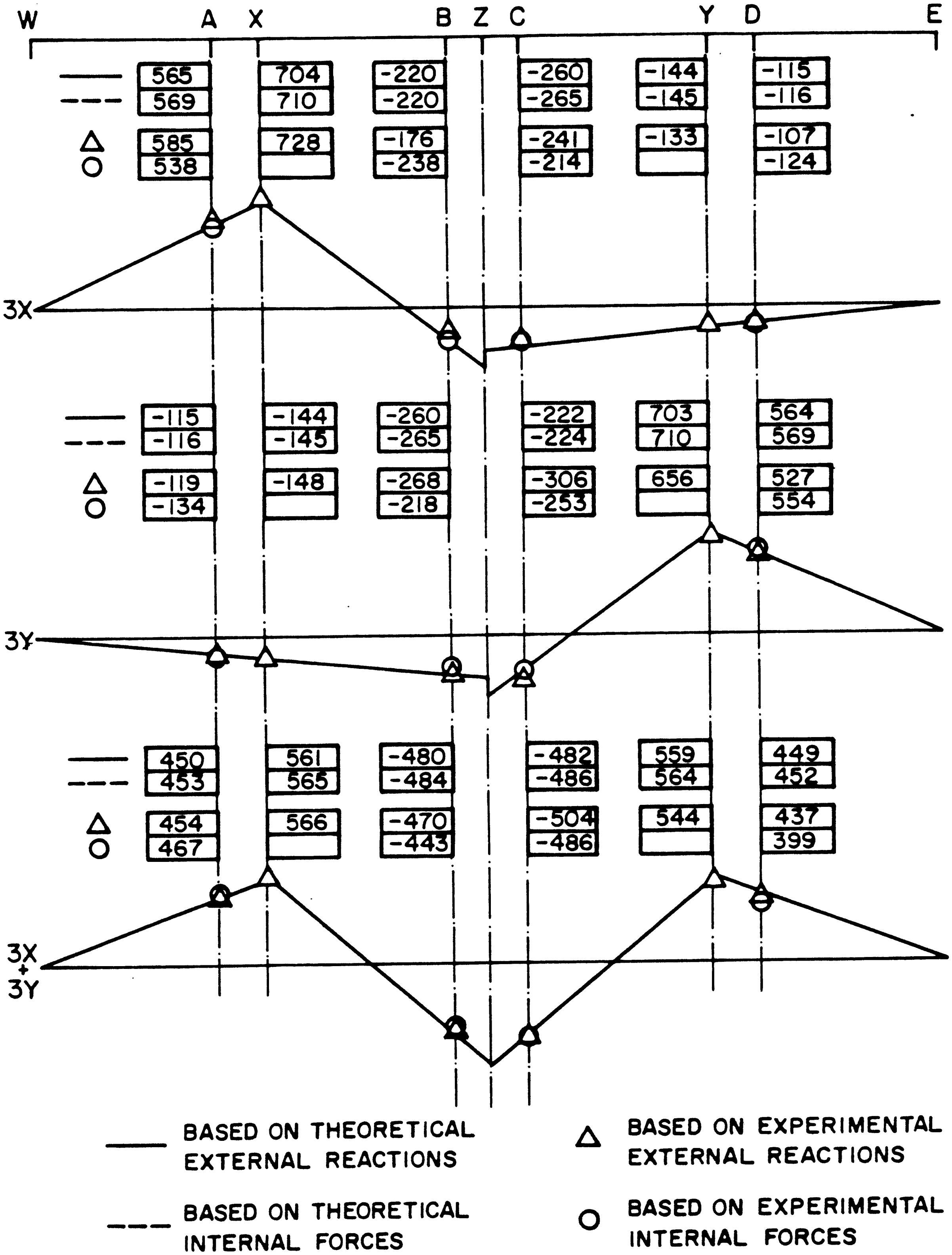

FIG. 5.10 TOTAL MOMENTS (FT-KIPS) AT A SECTION FOR NORMALIZED 100 KIP POINT LOADS AT 3X, 3Y, 3X + 3Y

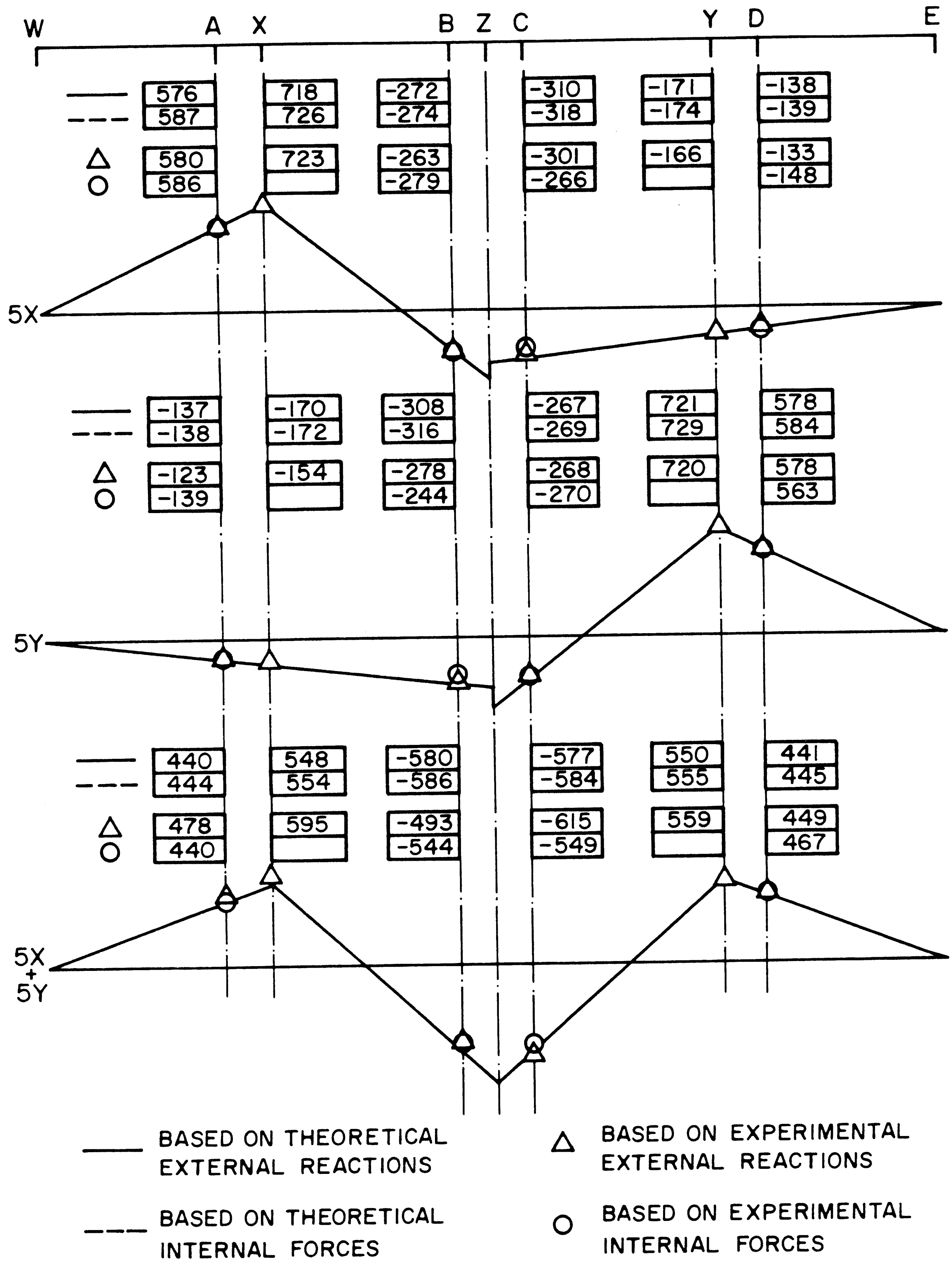

FIG. 5.11 TOTAL MOMENTS (FT-KIPS) AT A SECTION FOR NORMALIZED 100 KIP POINT LOADS AT 5X, 5Y, 5X + 5Y

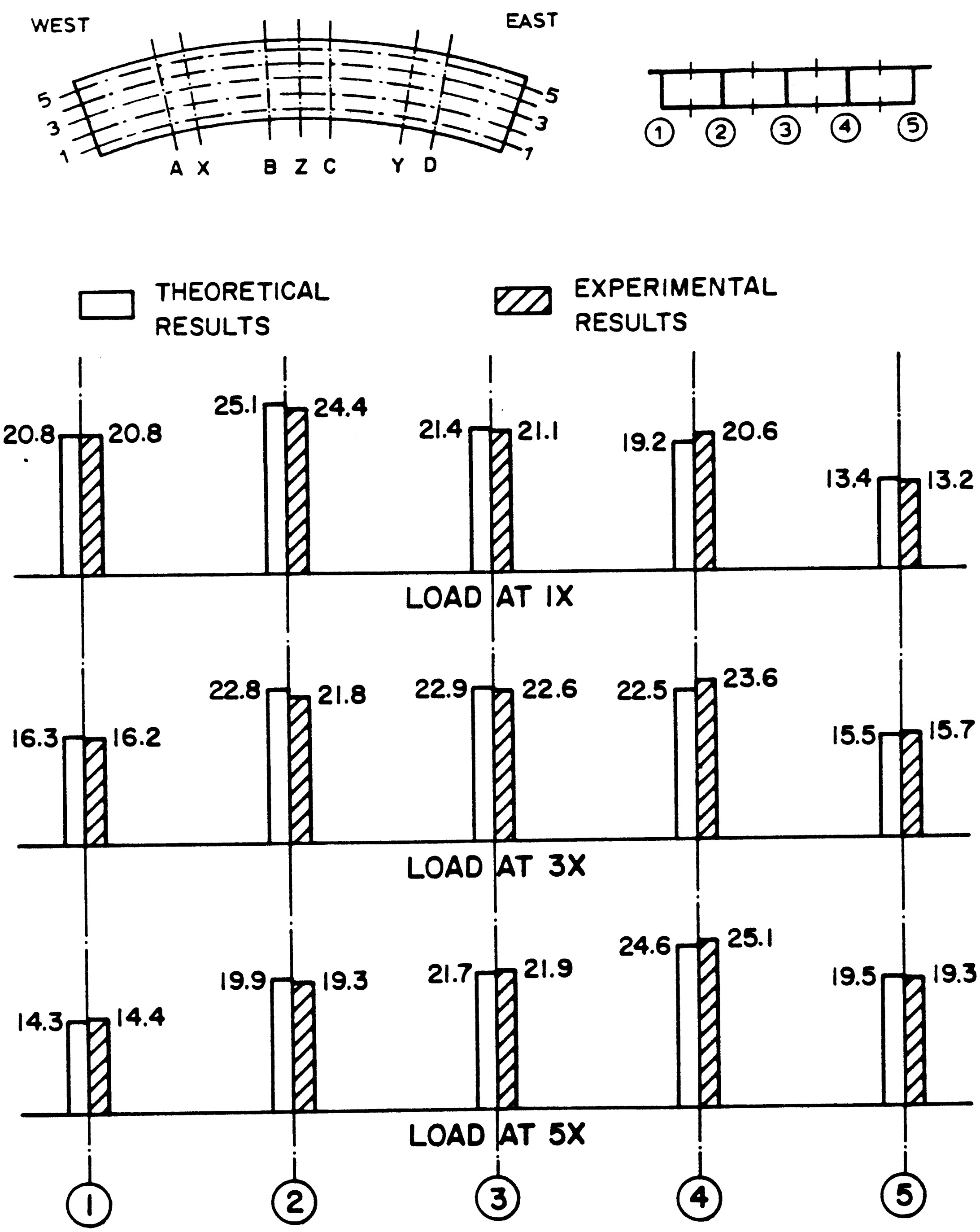

FIG. 5.12 PERCENTAGES OF TOTAL MOMENT AT SECTION A CARRIED BY EACH GIRDER FOR 100 KIP LOADS AT 1X, 3X, 5X

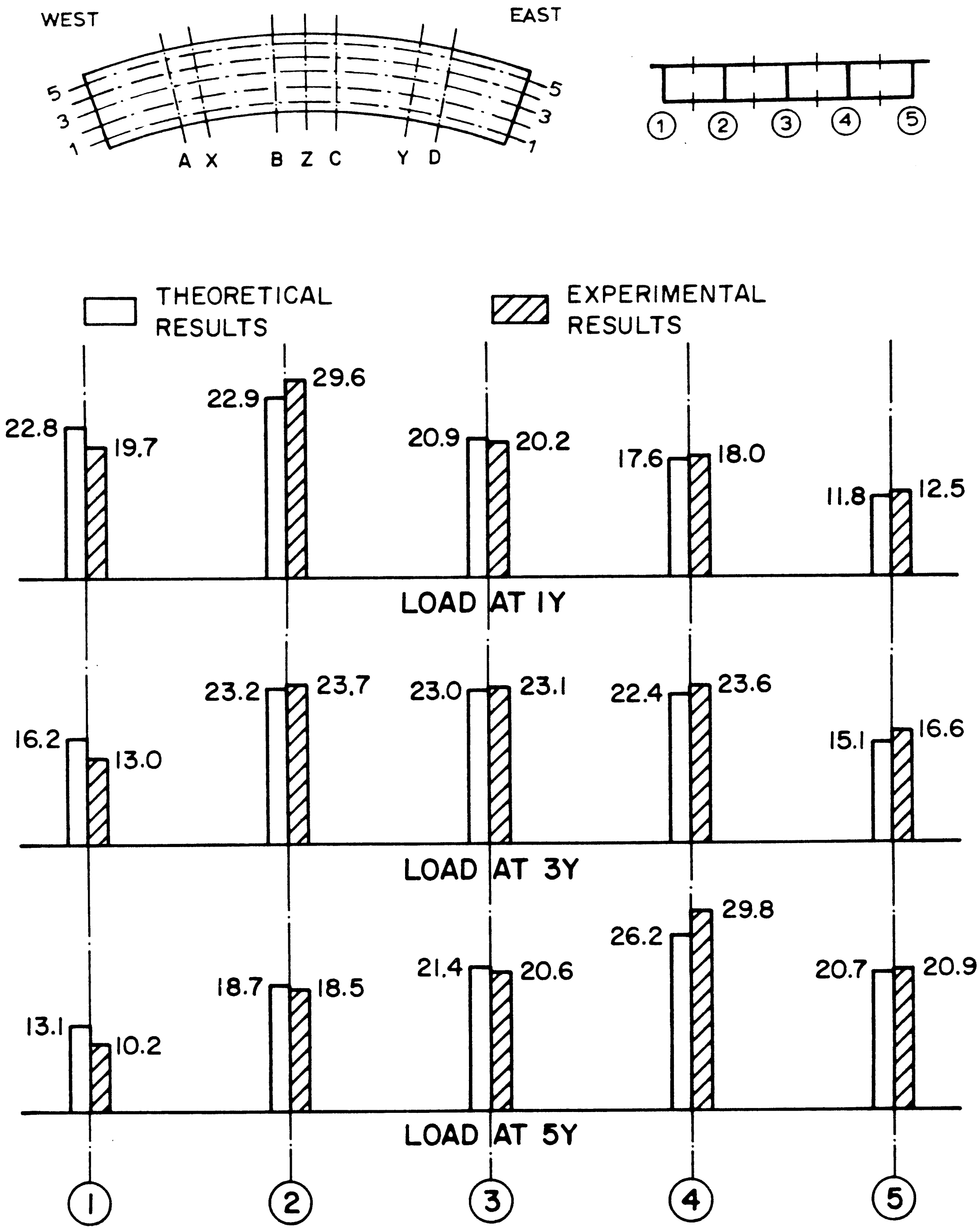

FIG. 5.13 PERCENTAGES OF TOTAL MOMENT AT SECTION D CARRIED BY EACH GIRDER FOR 100 KIP LOADS AT 1Y, 3Y, 5Y

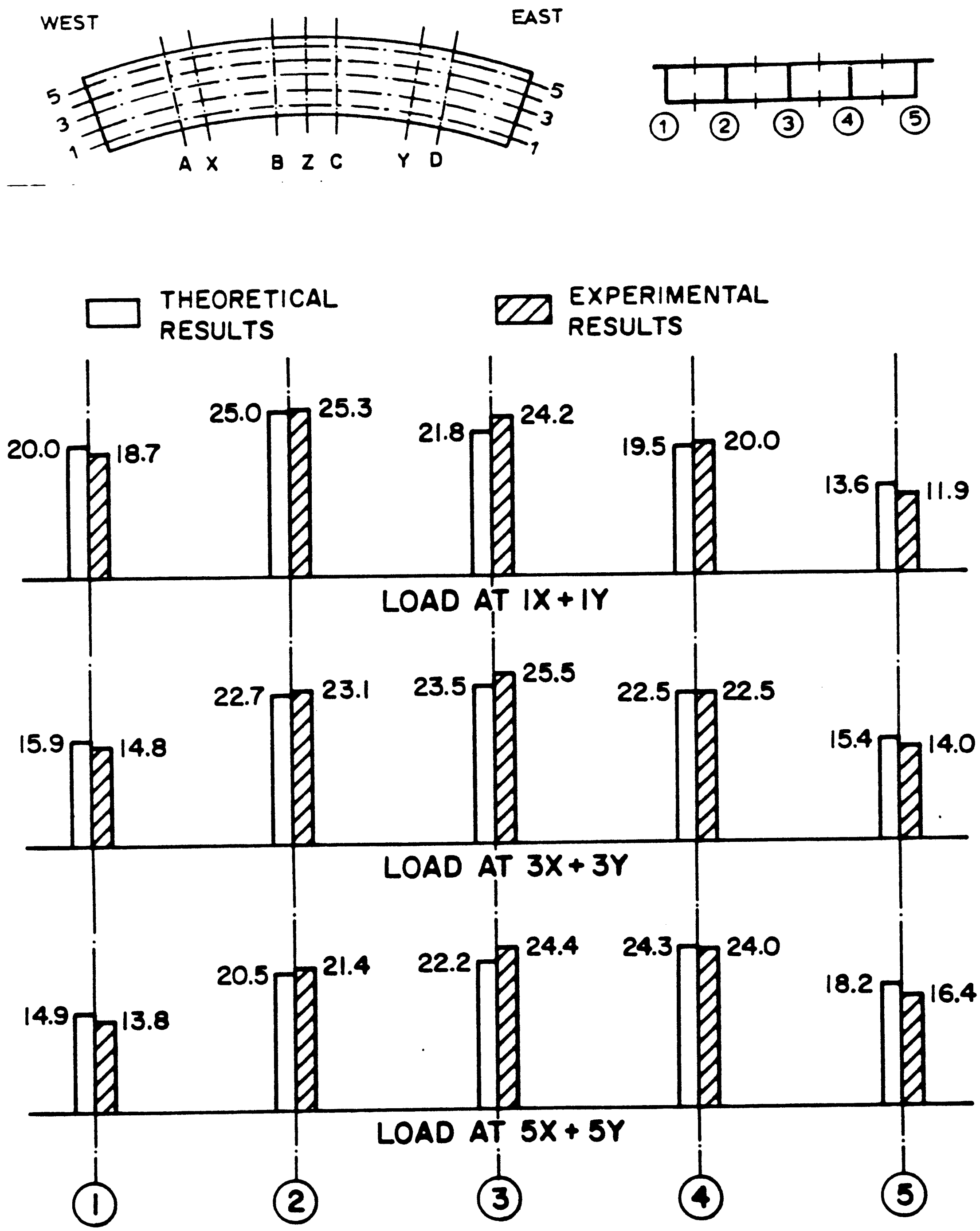

FIG. 5.14 PERCENTAGES OF TOTAL MOMENT AT SECTION B CARRIED BY EACH GIRDER FOR 100 KIP LOADS AT 1X + 1Y, 3X + 3Y, 5X + 5Y

(3) For point loads on center girder 3, (load cases 3X, 3Y and 3X + 3Y) the distributions approach the optimum values given above.

5.3 Effect of Support Restraints

As described in detail in Vol. I, most of the experimental program was carried out for the bridge model with what has been termed normal support restraints. These consisted of simply supported end abutments and the center bent being supported by a single central column as shown in Figs. 1.2 and 1.3. However, in order to investigate the effect of torsional restraint at the center bent and longitudinal restraint at the two end diaphragms, 10 of the 19 point load cases (1X, 1Y, 1X + 1Y, 3X, 3Y, 3X + 3Y, 5X, 5Y, 5X + 5Y and 1X + 5Y) were repeated for the 30 ksi working phase for each of these additional two support conditions.

Torsional restraint at the center bent was provided by adding vertical supports under girders 1 and 5 at center section Z. Longitudinal restraint at the end diaphragms was provided by adding three horizontal reaction supports at each end directly below girders 1, 3, 5. The horizontal reactions were located at a vertical distance of 3.42 ft. below the top surface of the bridge, which is equivalent to 2.73 ft. below the gross neutral axis of the bridge. Details of these support conditions are given in Figs. 5.2 and 5.3 of Vol. I.

Detailed tabulation of experimental results for only selected point load cases for the torsional and longitudinal restraint cases are given in Vol. III. In this section comparisons of experimental results will be made for the three support conditions: (1) Normal Restraint;

(2) Torsional Restraint; and (3) Longitudinal Restraint.

5.3.1 Reactions

Table 5.2 compares experimental reactions for each of the three support restraints under normalized 100 kip loads at 1X, 1X + 1Y, 3X, 3X + 3Y, 5X, 5X + 5Y. Comparison relative to the normal restraint case can then be made.

The torsional restraint has little effect on the two vertical end reactions, R_W and R_E, while the vertical reaction at the center footing, R_F, decreases by the amount which is transferred to the vertical supports at the center bent under girder 1 and 5, which is not recorded. The longitudinal restraint increases R_W and R_E and decreases R_F. This is due to the negative moment reaction developed at the two ends of the bridge under this support condition.

Considering the external torsional reactions, T_W, T_F and T_E, Table 5.2 shows that there is a substantial decrease in these reactions for the torsional restraint case for eccentric loadings on girders 1 or 5. This is due to the vertical reactions developed under these girders at the center bent support, which aid in carrying the torque. For the longitudinal restraint case, there is a decrease in the torsional reactions for loads on girder 1, but an increase for loads on girder 5. Looking at the external longitudinal moment reaction under the center footing, M_F, Table 5.2 shows that substantial changes occur in the magnitude and sign of this reaction, depending upon which of the three support restraints exist. Maximum values of M_F occur under the longitudinal restraint when only one span is loaded (1X, 3X, 5X).

TABLE 5.2 EXPERIMENTAL REACTIONS FOR DIFFERENT SUPPORT RESTRAINTS

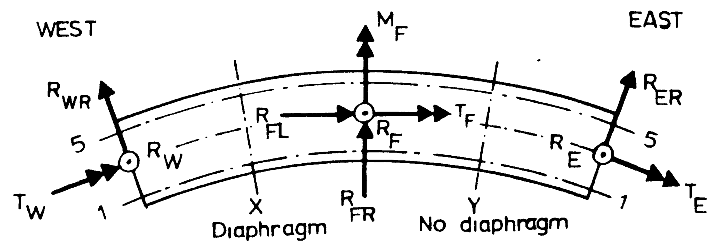

LOAD CASE	SUPPORT RESTRAINT	REACTIONS (KIPS AND FT-KIPS)								LOADS (KIPS)		
		WEST END		CENTER FOOTING			EAST END		TOTAL	SEC X	SEC Y	TOTAL
		R_W	T_W	R_F	M_F	T_F	R_E	T_E	R	P_X	P_Y	P
1X	NORMAL	41.2	-280	68.1	24	-78	-7.1	-96	102.2	100.0	-0.1	99.9
	TORSIONAL	40.3	-210	45.2	7	-19	-7.7	-35	77.8	100.0	0.0	100.0
	LONGIT.	46.4	-265	60.2	-217	11	-3.7	-80	103.0	100.0	0.0	100.0
1X + 1Y	NORMAL	35.5	-381	132.5	-54	-149	33.2	-346	201.3	100.0	99.1	199.1
	TORSIONAL	33.4	-247	75.1	- 8	-40	33.8	-242	142.3	100.0	103.4	203.4
	LONGIT.	43.1	-347	119.1	13	13	43.1	-331	205.3	100.0	101.4	201.4
3X	NORMAL	40.0	67	69.7	103	9	-7.2	-20	102.5	100.0	0.0	100.0
	TORSIONAL	40.7	76	58.7	73	16	-7.7	-17	91.7	100.0	0.0	100.0
	LONGIT.	44.6	88	64.0	-238	73	-5.5	-11	103.1	100.0	0.0	100.0
3X + 3Y	NORMAL	31.3	37	141.1	72	7	30.1	35	202.4	100.0	99.7	199.7
	TORSIONAL	31.5	48	117.3	71	18	29.8	42	178.6	100.0	99.8	199.8
	LONGIT.	39.3	77	124.4	- 2	128	36.6	58	200.3	100.0	96.8	196.8
5X	NORMAL	36.4	400	76.0	145	74	-9.7	45	102.6	100.0	0.0	100.0
	TORSIONAL	37.7	361	64.9	197	34	-9.0	-3	93.6	100.0	0.0	100.0
	LONGIT.	43.2	442	69.2	-249	133	-7.6	53	104.9	100.0	0.0	100.0
5X + 5Y	NORMAL	28.7	461	151.4	-31	162	27.1	417	207.1	100.0	103.5	203.5
	TORSIONAL	-31.2	370	91.1	33	119	29.1	331	151.3	100.0	100.4	200.4
	LONGIT.	35.7	506	135.6	8	271	35.2	462	206.5	100.0	101.2	201.2

5.3.2 Deflections

The transverse distributions of the vertical deflections at the loaded sections are presented for nine point load cases in Figs. 5.15 and 5.16 for the three support conditions. Comparing the torsional restraint results to those from the normal restraint, it can be seen that the deflections are almost identical for most load cases such that almost only one line can be shown for the results for the two support conditions. The longitudinal restraint case gives deflections which are consistently smaller than the other two support conditions, due to the decrease in the positive midspan moments for this case. However, it yields transverse deflected shapes, which are almost identical, but of smaller magnitude, to those from the normal restraint case. Comparing deflections at the undiaphragmed span Section Y to those at diaphragmed Section X, it is evident for all support conditions that there is always a greater concentration of deflection directly under the load in the former case.

5.3.3 Strains

Comparisons of the transverse distributions of experimental longitudinal strains for the different support conditions are given in Fig. 5.17 and 5.18 for a typical loading case 5X + 5Y. The type of support restraint appears to have very little effect on the compressive strains at all sections except that at support Sections B and C there is a slight increase near the loaded girder for the torsional restraint case, as should be expected.

For the tensile strains, the magnitudes and distributions for the normal and torsional restraint cases are similar. Curves for the

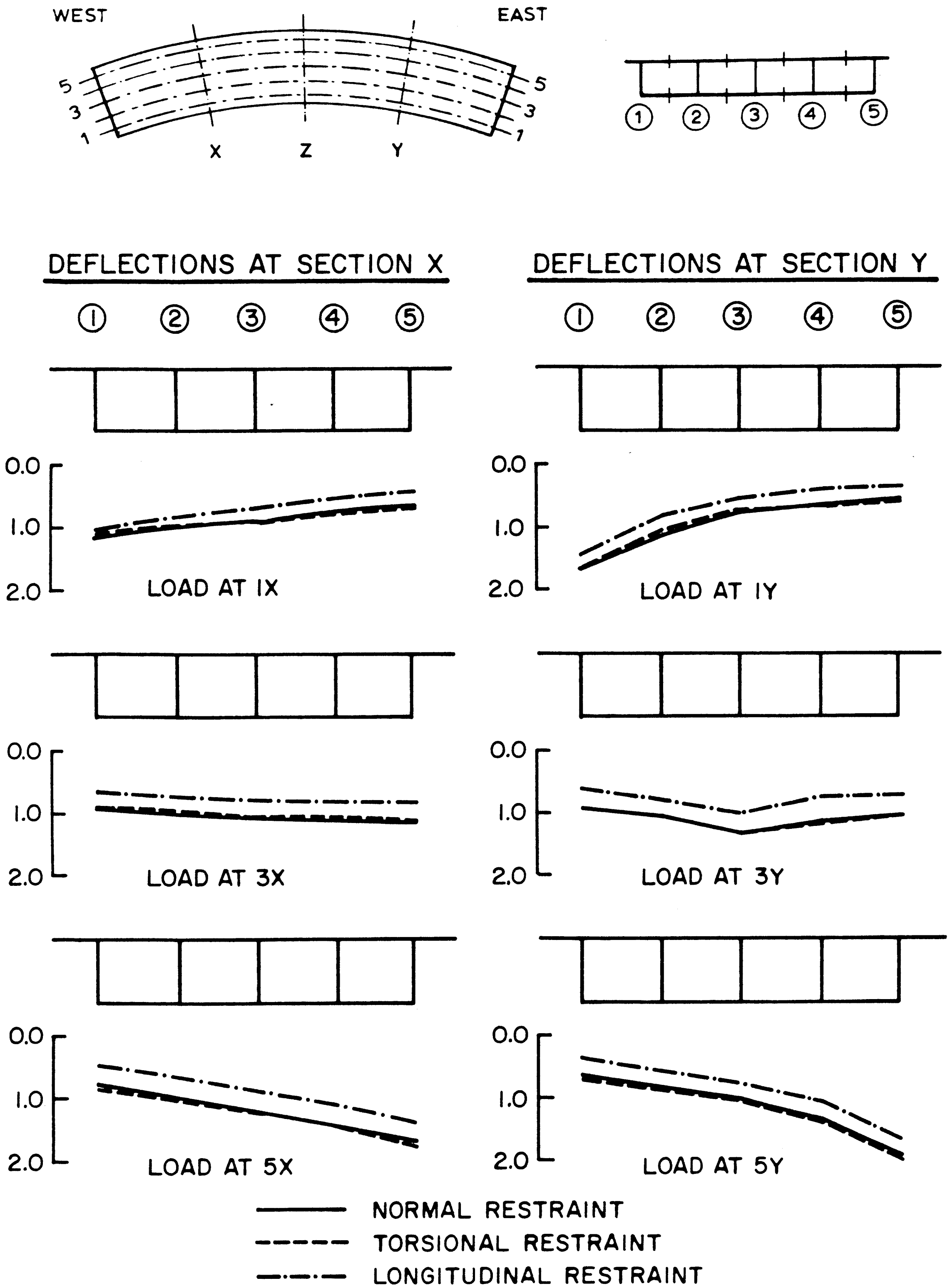

FIG. 5.15 EXPERIMENTAL DEFLECTION (INCHES) AT TRANSVERSE SECTION X AND Y WITH DIFFERENT SUPPORT RESTRAINTS FOR 100 KIP LOADS AT 1X, 1Y, 3X, 3Y, 5X, 5Y

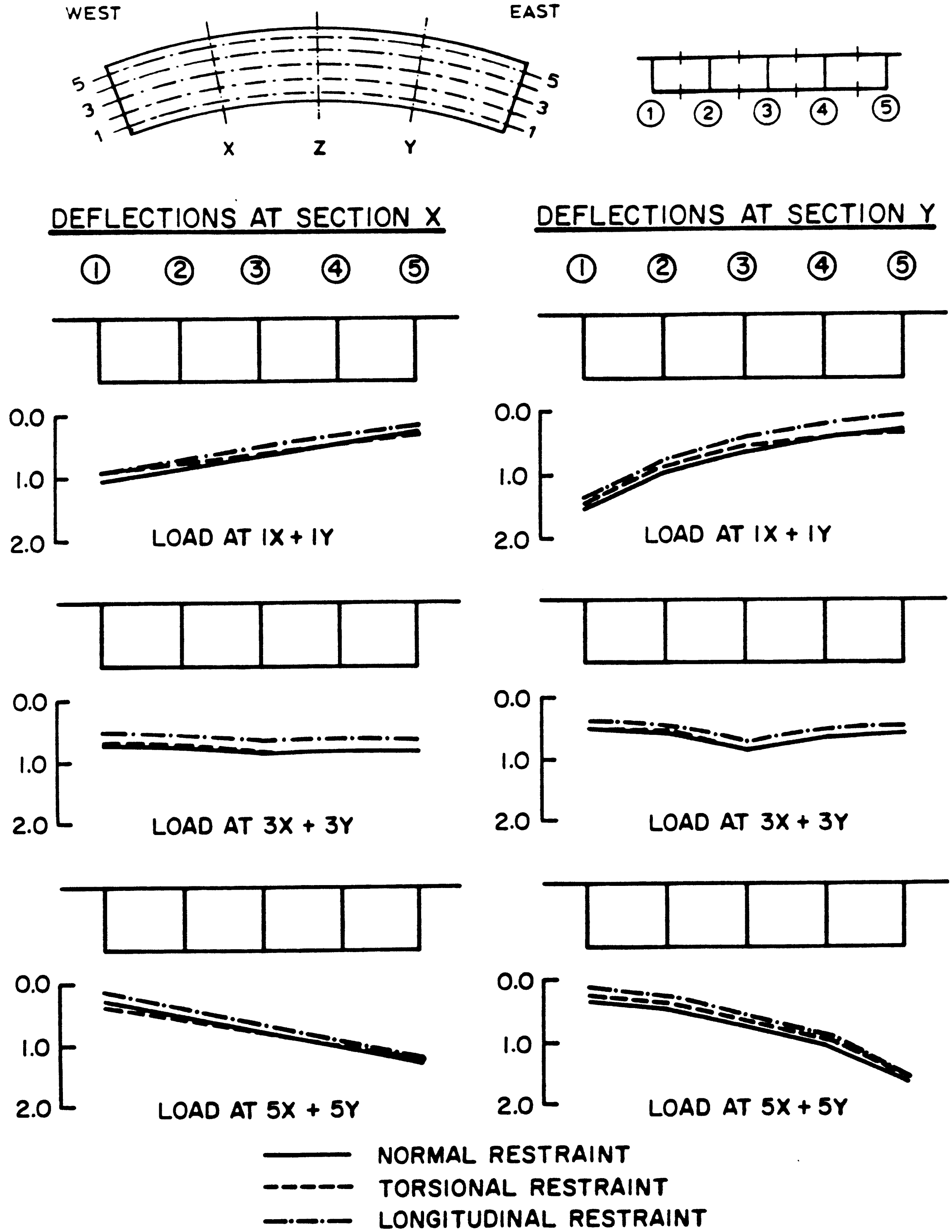

FIG. 5.16 EXPERIMENTAL DEFLECTION (INCHES) AT TRANSVERSE SECTION X AND Y WITH DIFFERENT SUPPORT RESTRAINTS FOR 100 KIP LOADS AT 1X + 1Y, 3X + 3Y, 5X + 5Y

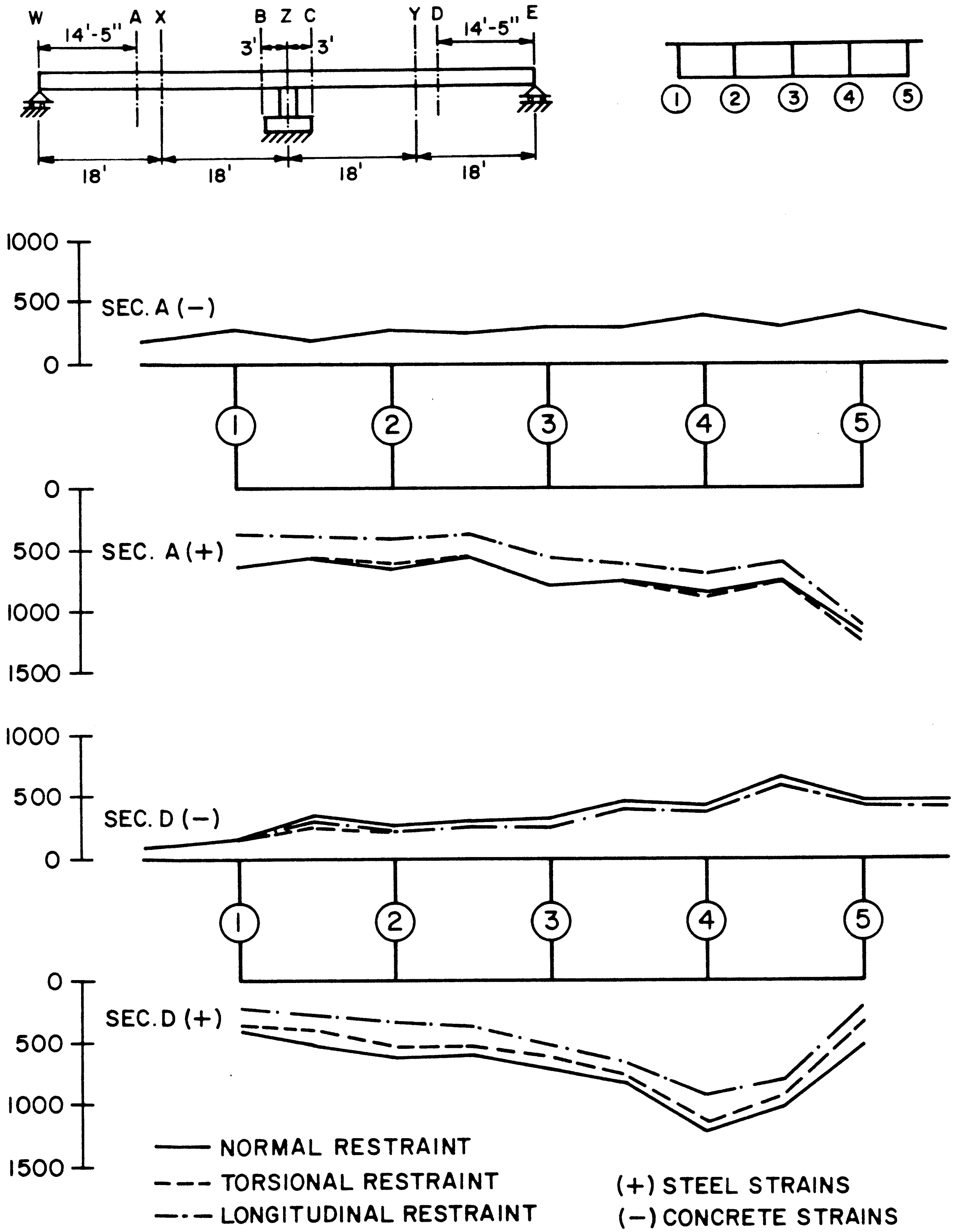

FIG. 5.17 EXPERIMENTAL LONGITUDINAL STRAINS (MICRO-INCH/INCH) IN TOP AND BOTTOM SLABS AT SECTIONS A AND D FOR DIFFERENT SUPPORT RESTRAINTS UNDER 100 KIP LOADS AT 5X+5Y

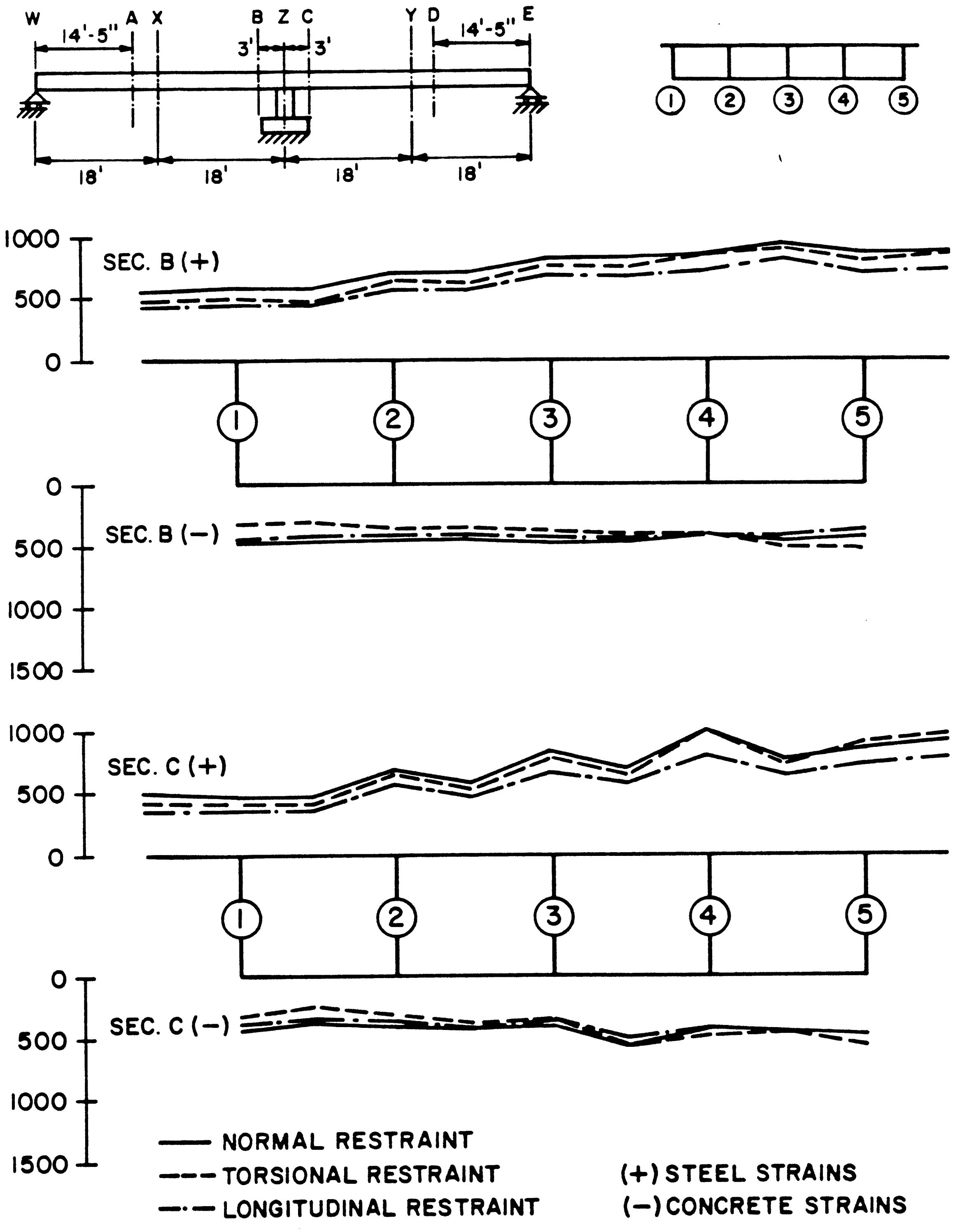

FIG. 5.18 EXPERIMENTAL LONGITUDINAL STRAINS (MICRO-INCH/INCH) IN TOP AND BOTTOM SLABS AT SECTIONS B AND C FOR DIFFERENT SUPPORT RESTRAINTS UNDER 100 KIP LOADS AT 5X+5Y

longitudinal restraint case, while similar in shape to the other restraint cases, have values which are substantially smaller in magnitude. This is due to the combined additive effects at each section of a decrease in moment and the introduction of a longitudinal compressive axial force produced by the longitudinal reactions at the supports. Note that for the compressive strains these effects tend to cancel each other resulting in little change as mentioned above.

5.3.4 Moments

The total moments at Sections A, B, C and D for different support conditions are given in Table 5.3 for load cases 1X, 1Y, 1X + 1Y, 3X, 3Y, 3X + 3Y, 5X, 5Y, 5X + 5Y. The moments shown are based on experimental internal forces found from the strains.

Comparing the values in Table 5.3 to ascertain the effect of support restraints, the results for the normal and torsional restraints are quite similar especially for loadings on center girder 3. For eccentric loadings on girders 1 or 5 the differences are slightly greater, but for practical design purposes, the differences would be considered negligible. Results for the longitudinal restraint case, however, indicate considerably lower positive moments in the loaded spans than the other cases. This decrease is due to the negative moment developed at the end supports by the longitudinal restraint and it should be taken into account where it exists. For loadings in both spans simultaneously (X + Y), the negative moments at Sections B and C are also substantially lower for the longitudinal restraint case. For loads in only one span (X or Y), the moments in the unloaded span also decrease for this longitudinal restraint case, however, the negative moment in the loaded span increases slightly.

TABLE 5.3 COMPARISON OF EXPERIMENTAL TOTAL INTERNAL MOMENTS (FT-KIPS) AT A SECTION FOR DIFFERENT SUPPORT RESTRAINTS

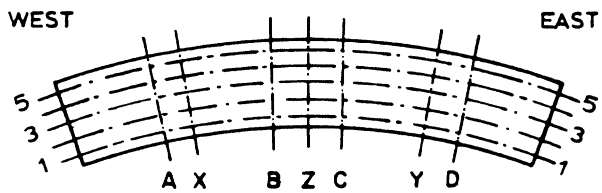

LOAD CASE	SUPPORT RESTRAINT	MOMENT AT SECTION			
		A	B	C	D
1X	NORMAL	515	-221	-171	-75
	TORSIONAL	502	-236	-186	-72
	LONGIT.	424	-225	-100	-59
1Y	NORMAL	-65	-172	-231	474
	TORSIONAL	-72	-184	-241	463
	LONGIT.	-56	-97	-232	380
1X + 1Y	NORMAL	427	-393	-390	431
	TORSIONAL	413	-413	-431	399
	LONGIT.	355	-322	-337	329
3X	NORMAL	539	-238	-214	-123
	TORSIONAL	525	-240	-212	-107
	LONGIT.	423	-263	-131	-67
3Y	NORMAL	-134	-218	-253	554
	TORSIONAL	-134	-216	-248	537
	LONGIT.	-71	-127	-280	407
3X + 3Y	NORMAL	467	-443	-486	398
	TORSIONAL	465	-447	-492	391
	LONGIT.	372	-392	-405	323
5X	NORMAL	586	-278	-266	-148
	TORSIONAL	604	-261	-265	-153
	LONGIT.	450	-308	-172	-78
5Y	NORMAL	-139	-244	-270	563
	TORSIONAL	-115	-245	-279	550
	LONGIT.	-77	-168	-312	426
5X + 5Y	NORMAL	440	-544	-549	467
	TORSIONAL	441	-489	-513	416
	LONGIT.	379	-482	-490	379

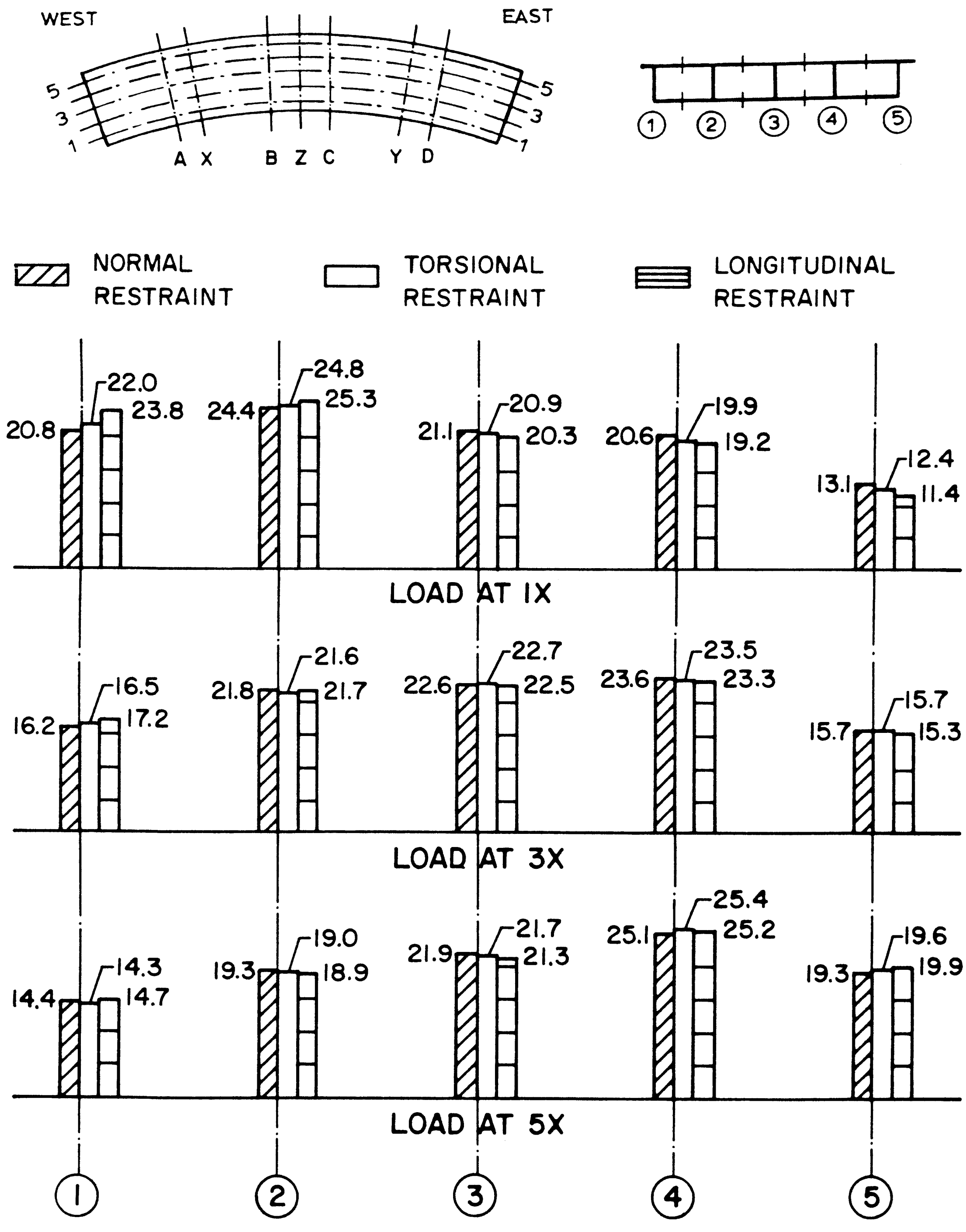

FIG. 5.19 PERCENTAGES OF TOTAL MOMENT AT SECTION A CARRIED BY EACH GIRDER FOR 100 KIP LOADS AT 1X, 3X, 5X

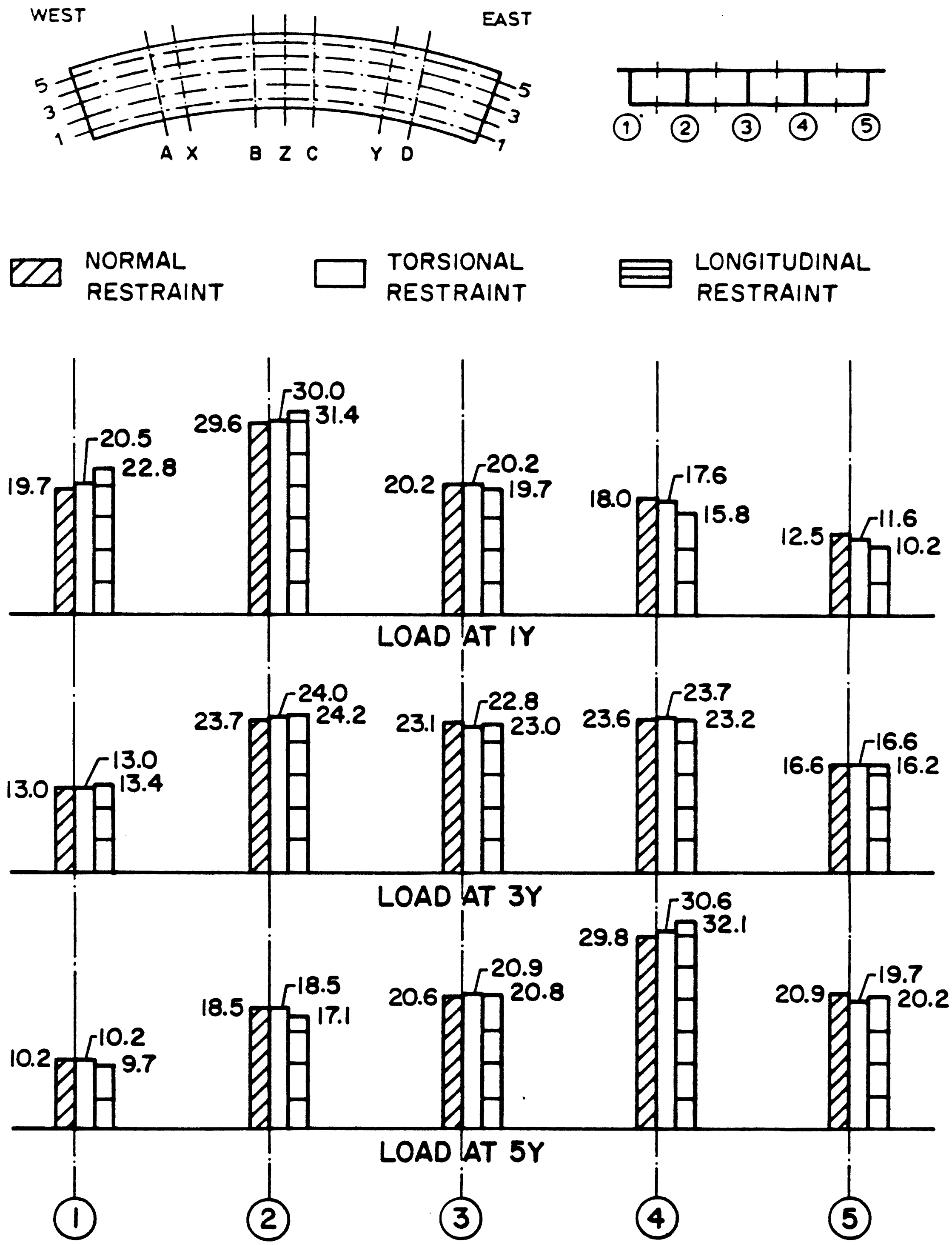

FIG. 5.20 PERCENTAGES OF TOTAL MOMENT AT SECTION D CARRIED BY EACH GIRDER FOR 100 KIP LOADS AT 1Y, 3Y, 5Y

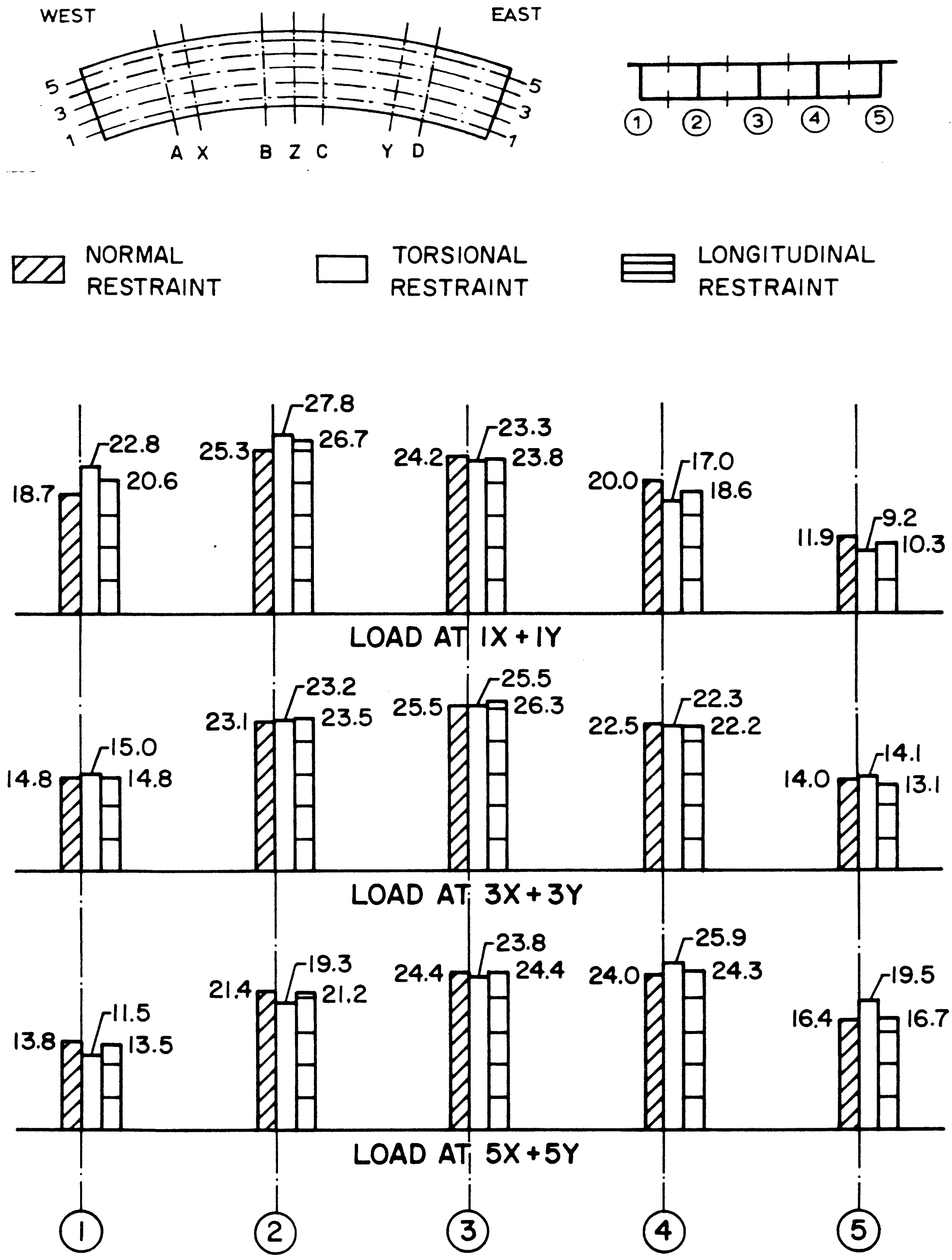

FIG. 5.21 PERCENTAGES OF TOTAL MOMENT AT SECTION B CARRIED BY EACH GIRDER FOR 100 KIP LOADS AT 1X+1Y, 3X + 3Y, 5X+5Y

Results for moments from theoretical analyses using the SAP program, not shown here, verify all of the trends for changes in experimental moments due to the support restraints cited above.

The transverse distributions of the total positive moment at Section A for loadings 1X, 3X, 5X and at Section D for loadings 1Y, 3Y, 5Y and of the total negative moment at Section B for loading 1X + 1Y, 3X + 3Y and 5X + 5Y are illustrated in Figs. 5.19, 5.20 and 5.21 for the different support conditions. From these figures the following may be stated

(1) For loads in one span only, Figs. 5.19 and 5.20, no significant changes in the distribution of the positive moment in the loaded span occur due to different support conditions.

(2) For loads in both spans, Fig. 5.21, the distribution of the negative moment at Section B is essentially the same for the normal and longitudinal restraint cases, but for the torsional restraint case there is a larger concentration of moment near the loaded girder for the eccentric loadings on girders 1 or 5. The latter is due to the vertical supports under girders 1 and 5 at the center bent for the torsional restraint case.

5.4 Summary of Moments for all Point Load Cases

As described in Vol. I a total of 19 different point load combinations were applied to the bridge. Detailed tabulations of theoretical and experimental result for reactions, deflections, strains and moments for each of these cases are given in Vol. III. All results have been normalized for purposes of comparison to loads of 100 kips per span. Theoretical values were obtained using CELL. In this section, the total moments at instrumented Sections, A, B, C, D and the transverse distribution of these total moments will be summarized and discussed for all 19 point load cases used with normal support restraints.

5.4.1 Total Moments at a Section

Table 5.4 summarizes the total moments at Sections A and D, near the diaphragmed and undiaphragmed midspan Sections X and Y respectively, for each of the 19 point load cases. Theoretical and experimental moments are given, first, based on the external reactions, and second, based on an integration of the internal longitudinal forces at the section times the appropriate lever arm to the gross-section neutral axis. A study of Table 5.4 reveals the following regarding the moments at Sections A and D.

(1) For point loads in one span only (X or Y) the moment increases gradually as the transverse position of the point load moves from inner girder 1 to outer girder 5. Contrary to this, for loads in both spans (X + Y) on the same girder, the moment is essentially independent of transverse position of the point loads.

(2) Comparing external and internal moments, which should be equal, the static checks between theoretical values are almost perfect. For experimental values, the agreement is more variable. The important moments, from a design standpoint at these sections are the positive moments in the loaded spans and here the differences range from 1 to 10%.

TABLE 5.4 SUMMARY OF THEORETICAL AND EXPERIMENTAL TOTAL MOMENTS (FT-KIPS) AT SECTIONS A AND D FOR ALL POINT LOAD (100 KIPS) POSITIONS

SECTION A					SECTION D				
100K LOAD AT	BASED ON EXTERNAL REACTIONS		BASED ON INTERNAL FORCES		100K LOAD AT	BASED ON EXTERNAL REACTIONS		BASED ON INTERNAL FORCES	
	THEO.	EXPT.	THEO.	EXPT.		THEO.	EXPT.	THEO.	EXPT.
1X	551	551	557	515	1Y	549	531	554	474
2X	559	573	563	526	2Y	557	526	562	536
3X	565	585	569	538	3Y	564	527	569	554
4X	571	588	576	544	4Y	572	534	577	572
5X	576	580	582	586	5Y	578	578	584	563
1Y	-98	-119	-99	-71	1X	-96	-115	-97	-75
2Y	-107	-111	-108	-123	2X	-106	-96	-107	-112
3Y	-115	-119	-116	-134	3X	-115	-107	-116	-124
4Y	-126	-132	-127	-143	4X	-126	-117	-127	-132
5Y	-137	-123	-138	-139	5X	-138	-133	-139	-148
1X + 1Y	453	456	458	427	1X + 1Y	453	428	457	431
2X + 2Y	452	475	455	434	2X + 2Y	451	423	455	386
3X + 3Y	450	454	453	467	3X + 3Y	449	437	452	399
4X + 4Y	446	452	449	470	4X + 4Y	446	443	450	424
5X + 5Y	440	478	444	440	5X + 5Y	441	449	445	467
1X + 5Y	415	432	419	393	1Y + 5X	412	432	415	384
2X + 4Y	433	457	436	418	2Y + 4X	431	399	435	362
1Y + 5X	478	520	483	477	1X + 5Y	482	483	487	453
2Y + 4X	464	501	468	450	2X + 4Y	466	484	471	453

TABLE 5.5 SUMMARY OF THEORETICAL AND EXPERIMENTAL TOTAL MOMENTS (FT-KIPS) AT SECTIONS B AND C FOR ALL POINT LOAD (100 KIPS) POSITIONS

SECTION B					SECTION C				
100K LOAD AT	BASED ON EXTERNAL REACTIONS		BASED ON INTERNAL FORCES		100K LOAD AT	BASED ON EXTERNAL REACTIONS		BASED ON INTERNAL FORCES	
	THEO.	EXPT.	THEO.	EXPT.		THEO.	EXPT.	THEO.	EXPT.
1X	-174	-175	-177	-221	1Y	-179	-219	-181	-231
2X	-196	-163	-199	-222	2Y	-200	-270	-203	-236
3X	-220	-176	-220	-238	3Y	-222	-306	-224	-253
4X	-245	-207	-246	-255	4Y	-243	-325	-243	-265
5X	-272	-263	-274	-279	5Y	-267	-268	-269	-270
1Y	-222	-268	-227	-172	1X	-217	-260	-222	-171
2Y	-241	-250	-247	-200	2X	-238	-217	-245	-191
3Y	-260	-268	-265	-218	3X	-260	-241	-265	-214
4Y	-283	-298	-291	-237	4X	-284	-264	-291	-232
5Y	-308	-278	-316	-244	5X	-310	-301	-318	-266
1X + 1Y	-396	-390	-401	-393	1X + 1Y	-397	-439	-402	-390
2X + 2Y	-437	-384	-442	-409	2X + 2Y	-438	-447	-442	-429
3X + 3Y	-480	-470	-484	-433	3X + 3Y	-482	-504	-486	-486
4X + 4Y	-528	-514	-532	-490	4X + 4Y	-527	-548	-533	-531
5X + 5Y	-580	-493	-586	-544	5X + 5Y	-577	-615	-584	-549
1X + 5Y	-482	-443	-487	-446	1Y + 5X	-489	-491	-487	-485
2X + 4Y	-480	-426	-484	-457	2Y + 4X	-484	-480	-490	-468
1Y + 5X	-494	-399	-499	-454	1X ± 5Y	-484	-484	-490	-453
2Y + 4X	-486	-402	-491	-439	2X + 4Y	-481	-488	-485	-474

(3) Comparing experimental and theoretical moments based on external reactions, the agreement is very good for the positive moments in the loaded spans, with differences ranging from 1 to 8%.

(4) Comparing experimental and theoretical internal moments, for the positive moments in the loaded spans, the differences again range from 1 to 8% except for a few load cases.

(5) For the negative moments in the unloaded spans, where the moments are much smaller, the magnitude of the moment differences are of the same order as in (2), (3) and (4) above, but the percentage differences are, of course, larger.

Table 5.5 summarizes the total moments at Sections B and C, near the center bent support, for each of the 19 point load cases. It can be seen that negative moments are produced by all load cases. The maximum moments occur when both midspan Sections X and Y are loaded simultaneously, thus these would be considered the most important load cases from a design standpoint. Moments at Sections B and C are in a zone where the slope of the moment diagram is steep, so that small differences in measured end reactions cause large changes in moments. Experimental moments are thus sensitive in this region. A study of Table 5.5 reveals the following regarding the moments at Sections B and C.

(1) For point loads in one span only (X or Y) and also for loads in both spans (X + Y) on the same girder, the moment increases significantly as the transverse position of the point load moves from inner girder 1 to outer girder 5. The increase is much greater than that at Sections A and D,

Table 5.4.

(2) Comparing external and internal moments, the agreement for theoretical values is again almost perfect. The agreement of experimental values for the important load cases in which both spans are loaded is between 1 to 12%.

(3) Comparing experimental and theoretical moments based on external reactions, for loads in both spans the agreement is excellent at Section C, ranging from 0 to 6% except for one case. At Section B the agreement is not as good ranging from 1 to 20%.

(4) Comparing experimental and theoretical internal moments, the agreement is even better than in (3) for all cases of both spans loaded, with differences ranging from 0 to 8% except for one case.

(5) For loads in one span only the moments are smaller than those above and the percentage differences are larger than in (2), (3) and (4) above. In the loaded span, experimental external moments are consistently smaller and larger at Sections B and C respectively, than theoretical values, while the experimental internal moments are larger at both Sections B and C than theoretical values. In the unloaded span, just the reverse is true except for one value.

5.4.2 Transverse Distribution of Total Moments

Theoretical and experimental percentages of the total moments at Sections A, D, B, C carried by each girder are given in Tables 5.6, 5.7, 5.8, 5.9 respectively for all 19 point load combinations. These tables are

TABLE 5.6 SUMMARY OF THEORETICAL AND EXPERIMENTAL PERCENTAGE DISTRIBUTION OF TOTAL MOMENT AT SECTION A FOR ALL POINT LOAD POSITIONS

LOAD AT	THEORETICAL % TO GIRDERS					EXPERIMENTAL % TO GIRDERS				
	1	2	3	4	5	1	2	3	4	5
1X	21	25	21	19	13	21	24	21	21	13
2X	18	25	22	21	14	18	23	22	22	14
3X	16	23	23	23	16	16	22	23	24	16
4X	15	21	22	24	17	15	20	22	25	17
5X	14	20	22	25	20	14	19	22	25	19
1Y	16	22	22	23	17	18	22	22	22	16
2Y	16	22	22	23	17	19	20	21	23	16
3Y	17	22	22	22	16	19	20	21	23	16
4Y	17	23	22	22	16	19	20	21	23	16
5Y	17	23	22	22	16	20	21	21	22	16
1X + 1Y	22	26	21	18	13	22	25	21	20	13
2X + 2Y	19	25	22	20	14	19	24	22	22	14
3X + 3Y	16	23	23	23	15	17	22	23	24	16
4X + 4Y	15	21	23	25	18	15	20	22	25	18
5X + 5Y	13	19	22	25	21	14	19	22	25	20
1X + 5Y	22	26	21	18	13	22	25	21	20	12
2X + 4Y	19	25	22	20	14	19	24	22	22	14
1Y + 5X	14	20	22	25	20	14	19	22	26	20
2Y + 4X	15	21	23	24	18	15	20	23	25	18

TABLE 5.7 SUMMARY OF THEORETICAL AND EXPERIMENTAL PERCENTAGE DISTRIBUTION OF TOTAL MOMENT AT SECTION D FOR ALL POINT LOAD POSITIONS

LOAD AT	THEORETICAL % TO GIRDERS					EXPERIMENTAL % TO GIRDERS				
	1	2	3	4	5	1	2	3	4	5
1X	17	22	22	22	16	16	24	22	25	14
2X	17	23	22	22	16	14	23	21	25	17
3X	17	23	22	22	16	13	23	21	25	18
4X	17	23	22	22	16	13	23	21	25	19
5X	17	23	22	22	16	13	22	21	25	20
1Y	23	27	21	18	12	20	30	20	18	13
2Y	20	25	23	19	13	17	26	22	21	14
3Y	16	23	23	22	15	13	24	23	24	17
4Y	14	20	23	24	19	11	20	23	27	20
5Y	13	19	21	26	21	10	19	21	29	21
1X + 1Y	24	28	21	17	11	20	30	20	18	13
2X + 2Y	21	26	23	19	12	18	27	22	19	14
3X + 3Y	16	23	23	23	15	13	24	23	24	17
4X + 4Y	13	19	23	25	20	10	19	23	27	21
5X + 5Y	12	17	21	28	22	10	18	21	32	20
1X + 5Y	12	18	21	27	22	10	18	21	31	20
2X + 4Y	13	20	23	25	19	10	19	23	27	21
1Y + 5X	25	28	21	16	11	22	32	20	17	11
2Y + 4X	21	26	23	18	12	19	28	22	19	13

TABLE 5.8 SUMMARY OF THEORETICAL AND EXPERIMENTAL PERCENTAGE DISTRIBUTION OF TOTAL MOMENT AT SECTION B FOR ALL POINT LOAD POSITIONS

LOAD AT	THEORETICAL % TO GIRDERS					EXPERIMENTAL % TO GIRDERS				
	1	2	3	4	5	1	2	3	4	5
1X	16	24	30	20	11	18	25	28	19	10
2X	14	23	31	21	12	15	25	29	20	11
3X	13	22	30	22	13	13	23	29	22	13
4X	12	21	29	24	14	12	22	28	23	15
5X	12	20	28	24	16	11	21	27	23	17
1Y	23	26	16	20	16	21	27	18	20	14
2Y	21	26	17	21	16	19	26	21	21	14
3Y	18	23	18	23	17	17	23	23	23	15
4Y	17	21	18	25	19	16	21	22	25	16
5Y	17	21	17	25	20	16	21	21	25	16
1X + 1Y	20	25	22	20	14	19	25	24	20	12
2X + 2Y	18	25	23	21	14	17	25	25	21	13
3X + 3Y	16	23	24	23	15	15	23	26	23	14
4X + 4Y	15	21	23	24	17	14	22	25	24	16
5X + 5Y	15	21	22	24	18	14	21	24	24	16
1X + 5Y	17	22	22	23	17	17	23	25	23	13
2X + 4Y	16	22	23	23	16	16	23	25	23	14
1Y + 5X	17	23	23	22	16	15	23	24	22	16
2Y + 4X	17	23	23	22	15	15	24	25	22	15

TABLE 5.9 SUMMARY OF THEORETICAL AND EXPERIMENTAL PERCENTAGE DISTRIBUTION OF TOTAL MOMENT AT SECTION C FOR ALL POINT LOAD POSITIONS

LOAD AT	THEORETICAL % TO GIRDERS					EXPERIMENTAL % TO GIRDERS				
	1	2	3	4	5	1	2	3	4	5
1X	21	25	17	21	16	17	24	20	23	17
2X	20	24	17	22	17	16	24	21	23	16
3X	19	23	18	23	18	16	23	21	24	17
4X	18	22	18	24	19	15	23	21	24	17
5X	17	21	18	24	20	15	22	21	24	18
1Y	22	27	28	16	7	27	29	23	14	8
2Y	16	27	30	18	9	17	30	28	17	9
3Y	12	22	32	22	11	11	23	33	22	11
4Y	10	19	30	26	16	9	18	30	28	16
5Y	10	18	27	26	19	10	18	28	27	18
1X + 1Y	22	26	22	19	13	22	27	22	18	12
2X + 2Y	18	25	23	20	13	17	27	25	20	12
3X + 3Y	16	23	24	22	15	13	23	27	23	14
4X + 4Y	15	21	23	25	17	12	21	26	26	16
5X + 5Y	14	20	22	25	19	12	20	24	26	17
1X + 5Y	16	21	22	23	18	12	21	25	25	17
2X + 4Y	15	22	23	24	16	12	21	26	26	16
1Y + 5X	19	23	21	21	15	20	25	21	20	13
2Y + 4X	17	24	23	22	15	16	26	24	20	13

essentially influence tables, which at a glance enable one to determine the load distributing properties of the bridge. It should be kept in mind that for a uniform stress distribution across the entire section, the percentage distributions to girders 1 to 5 respectively would be 16.5, 22.4, 22.4, 22.4 and 16.5%.

Maximum total moments are produced at Section A for loads in Span I at Section X only; at Section D for loads in Span II at Section Y only; and at Sections B and C near the center bent for loads in both Spans I and II at Sections X and Y. Restricting attention in Tables 5.6, 5.7, 5.8 and 5.9 to these critical loading cases the following observations may be made.

(1) Differences between theoretical and experimental values in almost all cases range from 0 to 2% of the total moment at the section.

(2) The maximum percentages found in the tables for single loads over any girder at Sections X and/or Y for the critical loading cases are as follows.

	Theoretical		Experimental	
	Interior girder	Exterior girder	Interior girder	Exterior girder
Section A	25	21	25	21
Section B	25	20	25	19
Section C	26	22	27	22
Section D	27	23	29	21

As can be seen above, experimental values are equal to or only slightly larger than theoretical values for the interior girder, while the reverse is true for the exterior girder.

(3) Actual design live loads consist of two or three lanes of trucks on the bridge and for such conditions the average percentage taken by an individual girder would approach the uniform stress distribution values of 22.4% and 16.5% for interior and exterior girders respectively.

5.4.3 Maximum Number of Wheel Loads Carried by an Interior or Exterior Girder

As described in Vol. I, the AASHO Specifications require that each girder be designed as a separate member by applying to it a certain fraction of a single longitudinal line of wheels from a standard AASHO HS 20-44 truck. This fraction known as the number of wheel loads N_{WL}, is given by the relations

$N_{WL} = S/7$ for interior girders

$N_{WL} = S_1/7$ for exterior girders

S is the flange width in feet of the interior girder, which is also equal to the average width of the cell, and S_1 is the top flange width in feet of the exterior girder, which is also equal to half the cell width plus the cantilever overhang. For the prototype of the bridge model, $S = 7.25$ ft. and $S_1 = 6.12$ ft., which gives N_{WL} values of 1.04 and 0.88 for interior and exterior girders. Because of similitude, these same values of N_{WL} are applicable to the model. The most important variable unaccounted for in the AASHO formulas is the number of traffic lanes on the bridge.

To study this problem, Table 5.10 has been prepared to give the maximum number of wheel loads to be carried by an interior girder or an exterior girder at Sections A, B, C and D. Line (1) gives the AASHO values from above. The remaining lines give values for two lanes of trucks (total of 4 wheel lines on bridge) and for three lanes of trucks (total of 6 wheel lines on bridge). The uniform stress values, lines (2) and (5) are obtained by multiplying the total number of wheel lines on the bridge by 22.4 and 16.5% for an interior and exterior girder respectively. Lines (3), (4), (6) and (7) are found by using the values in Tables 5.6 to 5.9 as influence ordinates. Each truck is assumed to occupy a 10 ft. traffic lane and has wheels spaced transversely at 6 ft. For simplicity, only a single transverse series of wheels at midspan are considered. These are shifted laterally to give maximum effects. Finally lines (8), (9) and (10) are given since AASHO specifies a 10% reduction for three lanes of loading. It is important to note in using the S/7 AASHO empirical formula, no reduction should be made for more than two lanes of loading, since this is assumed to have been already included in the development of the formula.

A study of Table 5.10 reveals several interesting facts for the bridge under consideration.

(1) The AASHO formulas are conservative for the two lane truck loading, but unconservative for the three lane truck loading on the bridge. The latter is especially true for interior girders, even with the 10% reduction, where AASHO underestimates the load by about 13 to 22%.

(2) Comparing theoretical and experimental values, experimental values are 0 to 7% higher for interior girders. For exterior girders at Sections A and D, the values are essentially the same, while at Sections B and C,

TABLE 5.10 MAXIMUM NUMBER OF WHEEL LOADS TO BE CARRIED BY AN INTERIOR OR AN EXTERIOR GIRDER

GIRDER	LINE	LOAD CASE	SECTION A	SECTION B	SECTION C	SECTION D
INTERIOR	1	AASHO Specifications	1.04	1.04	1.04	1.04
	2	Two Lane (Uniform Stress)	0.90	0.90	0.90	0.90
	3	Two Lane (Theoretical)	0.97	0.97	0.98	0.99
	4	Two Lane (Experimental)	0.98	0.97	1.02	1.06
	5	Three Lane (Uniform Stress)	1.34	1.34	1.34	1.34
	6	Three Lane (Theoretical)	1.33	1.39	1.39	1.39
	7	Three Lane (Experimental)	1.41	1.41	1.44	1.48
	8	.90 x Three Lane (Unif. Stress)	1.21	1.21	1.21	1.21
	9	.90 x Three Lane (Theor.)	1.20	1.25	1.25	1.25
	10	.90 x Three Lane (Exper.)	1.27	1.27	1.30	1.33
EXTERIOR	1	AASHO Specifications	0.88	0.88	0.88	0.88
	2	Two Lane (Uniform Stress)	0.66	0.66	0.66	0.66
	3	Two Lane (Theoretical)	0.73	0.71	0.74	0.78
	4	Two Lane (Experimental)	0.73	0.67	0.68	0.77
	5	Three Lane (Uniform Stress)	0.99	0.99	0.99	0.99
	6	Three Lane (Theoretical)	1.03	1.02	1.04	1.06
	7	Three Lane (Experimental)	1.03	0.96	0.93	1.05
	8	.90 x Three Lane (Unif. Stress)	0.89	0.89	0.89	0.89
	9	.90 x Three Lane (Theor.)	0.93	0.92	0.94	0.95
	10	.90 x Three Lane (Exper.)	0.93	0.86	0.84	0.94

experimental values are 0 to 11% lower than theoretical values.

(3) Comparing both theoretical and experimental values with the uniform stress values, the former are 1 to 13% higher than the latter, with the three lane truck loading being the closest.

5.5 Truck and Construction Vehicle Loads

As described in Vol. I, the model was loaded by scaled down versions of the standard AASHO HS 20-44 truck (total load = 72 kips) and a proposed overload construction vehicle class II (total load = 330 kips). All linear dimensions were reduced by the scale factor 1:2.82 and details of wheel positions in the model vehicles can be found in Vol. I. Similitude required that the loads be reduced by a factor of 1:8 to produce the same stresses in the model as in the prototype. Thus for the model the total load for each truck was 9.0 kips and for each construction vehicle was 41.25 kips. Using these loads, a study could be made of the bridge response due to actual design truck live loads placed at various positions on the bridge.

Figure 5.22 shows the positions and directions of the truck and construction vehicle loads on the bridge. As described in Vol. I, a total of 11 combinations of two lane truck loadings, 3 combinations of three lane truck loadings, and 8 combinations of construction vehicle loading were used. Because each vehicle had six wheels and the front wheels had smaller loads than the rear wheels, exact symmetry of loading about the bridge longitudinal and transverse centerlines was not maintained, Fig. 5.22.

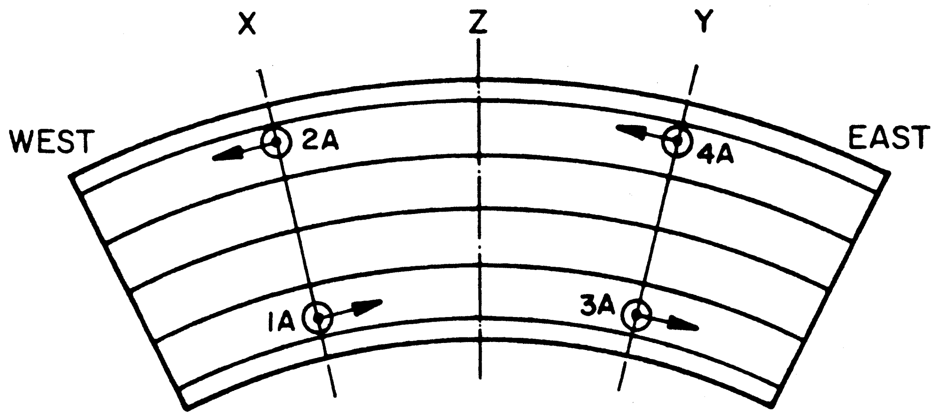

(a) TWO LANE TRUCK LOADING (EACH TRUCK = 9.0 KIPS NOMINAL)

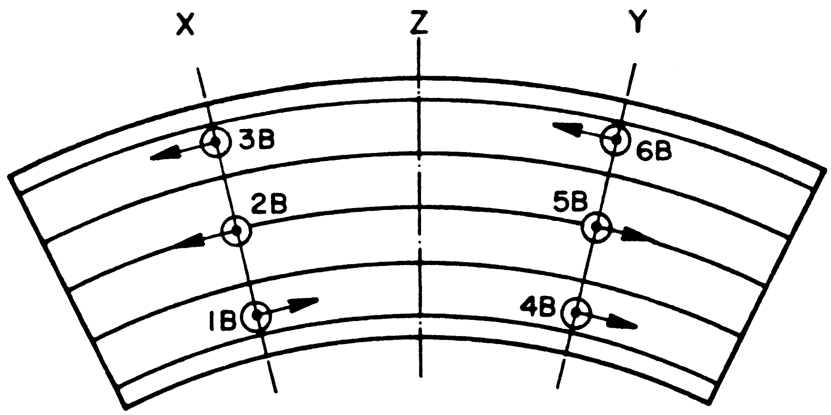

(b) THREE LANE TRUCK LOADING (EACH TRUCK = 9.0 KIPS NOMINAL)

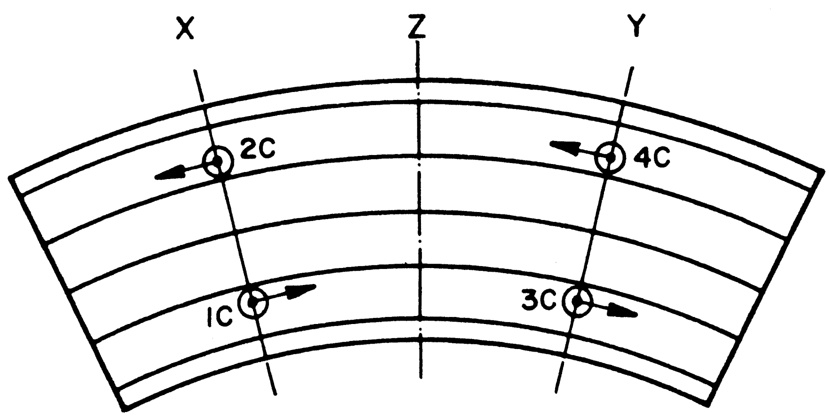

(c) CONSTRUCTION VEHICLE LOADING (EACH TRUCK = 41.25 KIPS NOMINAL)

FIG. 5.22 POSITIONS AND DIRECTIONS OF TRUCK (9.0K) AND CONSTRUCTION VEHICLE (41.25K) LOADS ON THE BRIDGE

Detailed tabulations of theoretical and experimental results related to reactions, deflections, strains and moments for these loadings are given in Vol. III. Theoretical values were obtained from computer analyses using CELL. Selected results will be discussed in the following sections.

5.5.1 Reactions

A summary of theoretical and experimental reactions is given in Table 5.11 for various vehicle loadings. Excellent agreement exists between experiment and theory for the vertical reactions, R_W, R_F and R_E. The same is true for the torsional and moment reactions T_W, T_F and T_E and M_F except in a couple of places. Once again it is evident that the theoretical analysis by CELL can be used to accurately predict the reactions.

5.5.2 Deflections

Experimental deflections are shown in Fig. 5.23 for vehicle loadings producing maximum values at diaphragmed Section X and undiaphragmed Section Y. For the two and three lane truck cases, the loading is relatively uniform across the width of the bridge, Fig. 5.22, resulting in a uniform distribution of deflection also. For the construction vehicle, only one lane is loaded, Fig. 5.22, resulting in a larger deflection under girder 5. By comparing results at Sections X and Y, these loadings also demonstrate the effect of the diaphragm.

It is of interest to compute the maximum deflection to span ratios for each of these design live loadings, since they would be the same in a full scale prototype structure because of similitude. For the two lane truck, three lane truck and construction vehicle loading the

TABLE 5.11 COMPARISON OF THEORETICAL AND EXPERIMENTAL REACTIONS (KIPS AND FT - KIPS) UNDER TRUCK (9 KIPS) AND CONSTRUCTION VEHICLE (41.25 KIPS) LOADS

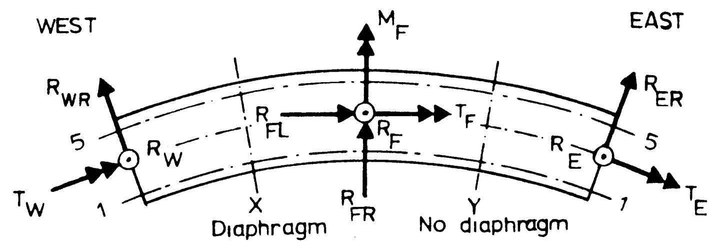

LOAD TYPE	LOAD CASE	SOLUTION	REACTIONS (KIPS & FT-KIPS)								LOAD (KIPS)		
			WEST END		CENTER FOOTING			EAST END		TOTAL	SEC X	SEC Y	TOTAL
			R_W	T_W	R_F	M_F	T_F	R_E	T_E	R	P_X	P_Y	P
TWO LANE TRUCK LOADING	4A	THEORY	-0.9	4	6.5	-11	6	3.4	-31	9.0	0.0	-9.0	-9.0
		EXPER.	-0.9	4	6.3	5	8	3.4	-12	8.9	0.0	-9.0	-9.0
	3A + 4A	THEORY	-1.4	-4	12.3	-21	-1	7.0	-6	18.0	0.0	-18.0	-18.0
		EXPER.	-1.4	-4	12.6	-13	2	7.0	-11	18.2	0.0	-18.0	-18.0
	2A + 4A	THEORY	2.5	33	13.0	0	12	2.5	-35	18.0	-9.0	-9.0	-18.0
		EXPER.	2.7	35	12.8	0	15	2.8	-32	18.3	-9.0	-9.1	-18.1
	1A + 2A +3A + 4A	THEORY	5.9	7	24.5	0	-1	5.6	-3	36.0	-18.0	-18.0	-36.0
		EXPER.	5.8	7	24.9	10	3	5.7	-6	36.5	-18.0	-18.0	-36.0
THREE LANE TRUCK LOADING	4B+5B+6B	THEORY	-2.1	-5	18.5	-31	0	10.6	-15	27.0	0.0	-27.0	-27.0
		EXPER.	-2.1	-6	18.8	-41	1	9.9	-13	26.5	0.0	-27.0	-27.0
	1B+2B+3B +4B+5B+6B	THEORY	8.5	10	37.0	0	0	8.5	-10	54.0	-27.0	-27.0	-54.0
		EXPER.	8.4	8	37.9	13	2	8.6	-10	54.8	-27.0	-27.7	-54.7
CONSTR. VEHICLE LOADING	4C	THEORY	-3.5	16	28.9	-47	24	15.9	-117	41.3	0.0	-41.3	-41.3
		EXPER.	-3.5	11	29.8	-63	27	15.1	-102	41.4	0.0	-41.3	-41.3
	2C + 4C	THEORY	12.3	134	57.8	0	48	12.4	-134	82.5	-41.2	-41.2	-82.5
		EXPER.	13.0	131	58.4	3	53	12.3	-109	83.6	-41.2	-41.3	-82.5

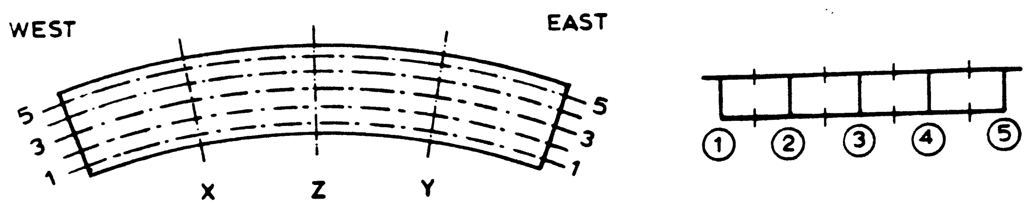

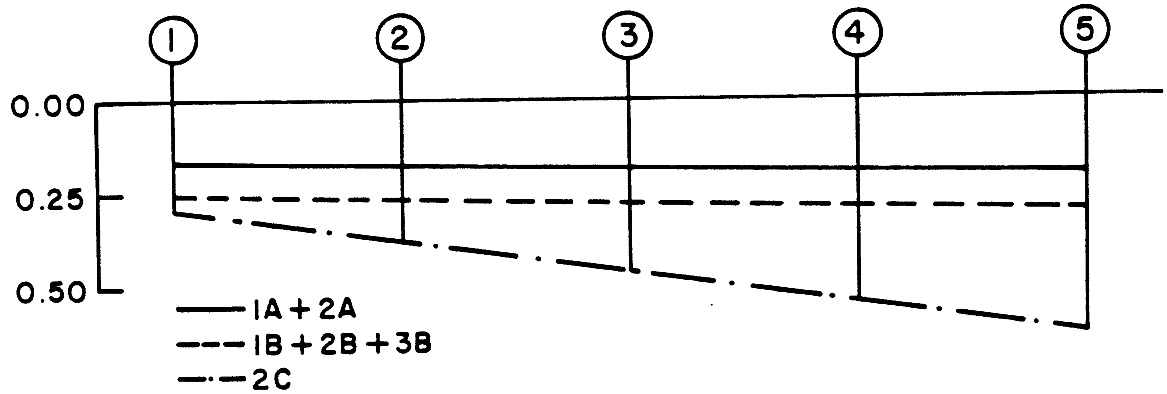

DIAPHRAGMED SECTION X

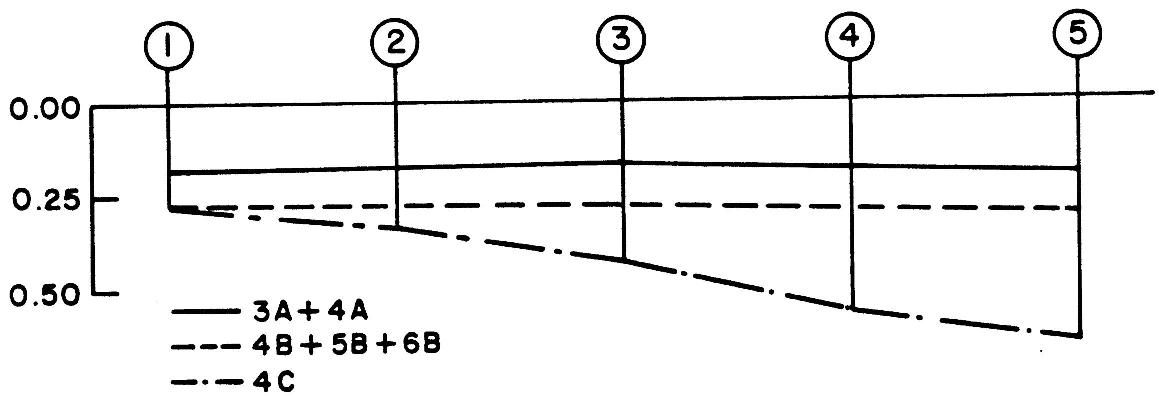

UNDIAPHRAGMED SECTION Y

FIG. 5.23 EXPERIMENTAL DEFLECTIONS (INCHES) AT TRANSVERSE SECTIONS FOR DIFFERENT VEHCILE LOADINGS maximum deflections are respectively 0.20, 0.31, and 0.64 in. which when divided by the span of 432 in. (36 ft.) give deflection to span ratios of 1/2160, 1/1400, and 1/680, all of which are quite small.

5.5.3 Loadings for Maximum Girder Moments

Table 5.12 summarizes the experimental girder moments for a variety of load combinations on the bridge involving 1, 2, 3, 4 or 6 vehicles on the bridge. Vehicle locations can be identified from Fig. 5.22. If one searches Table 5.12 for maximum moments in interior girders 2, 3, 4 and exterior girders 1 and 5 certain conclusions can be immediately reached regarding critical design loadings.

(1) As would be expected the maximum moments get progressively larger as one proceeds from the two lane truck, to the three lane truck to the construction vehicle loading.

(2) Considering positive moment Sections A and D maximum moments are produced when loading only one span with as many vehicles as possible across the width of the bridge. Single vehicles in one span in an extreme eccentric position do not produce maximum effects.

(3) Considering negative moment Sections B and C maximum moments are produced when both spans are loaded, again with as many vehicles as possible across the width of the bridge.

(4) Considering two lane truck, three lane truck and construction vehicle loadings respectively, the ratios of the maximum moment for an exterior girder 1 or 5 to an interior girder 2, 3 or 4 for the critical loadings are

TABLE 5.12 EXPERIMENTAL GIRDER MOMENTS (FT-KIPS) UNDER CRITICAL TRUCK (9.0 KIPS) AND CONSTRUCTION VEHICLE (41.25KIPS) LOADS (MOMENTS ABOUT GROSS-SECTION NEUTRAL AXIS)

SECTION	GIRDER	TWO LANE TRUCK LOADING				THREE LANE TRUCK LOADING		CONSTRUCTION VEHICLE LOADING		
		2a	1a+2a	1a+4a	1a+2a +3a+4a	1b+2b+3b	1b+2b+3b +4b+5b+6b	2c	1c+4c	1c+3c
A	1	7	19	11	16	26	22	28	26	28
	2	9	21	9	17	31	26	38	32	36
	3	10	20	6	16	31	26	45	29	32
	4	12	22	6	18	32	27	55	29	32
	5	9	15	4	13	22	18	40	18	20
	Σ	47	97	36	80	142	119	206	134	148
		2a+4a	1a+2a	1a+4b	1a+2a +3a+4a	1b+2b+3b	1b+2b+3b +4b+5b+6b	2c	1c+4c	1c+3c
B	1	- 6	- 5	- 6	-12	- 8	-18	- 9	-30	-28
	2	- 9	- 9	- 9	-18	-14	-27	-20	-37	-37
	3	-10	-11	- 9	-18	-17	-28	-24	-38	-33
	4	-10	- 9	- 9	-17	-13	-26	-25	-37	-27
	5	- 7	- 6	- 5	-11	- 8	-16	-20	-23	-16
	Σ	-42	-40	-38	-75	-60	-115	-98	-165	-141
		2a+4a	1a+2a	1a+4a	1a+2a +3a+4a	4b+5b+6b	1b+2b+3b +4b+5b+6b	4c	1c+4c	1c+3c
C	1	- 5	- 6	- 5	-12	- 8	-18	- 7	-21	-31
	2	- 9	-10	- 8	-19	-14	-29	-15	-33	-42
	3	-11	-11	- 9	-19	-17	-31	-26	-40	-36
	4	-11	- 9	-10	-19	-14	-28	-27	-43	-25
	5	- 8	- 5	- 6	-12	- 8	-18	-19	-30	-17
	Σ	-44	-41	-38	-81	-61	-124	-94	-167	-151
		4a	3a+4a	1a+4a	1a+2a +3a+4a	4b+5b+6b	1b+2b+3b +4b+5b+6b	4c	1c+4c	1c+3c
D	1	4	13	4	10	19	15	21	15	34
	2	8	21	7	16	32	24	39	27	47
	3	9	18	9	14	30	23	42	32	30
	4	14	22	14	18	34	26	52	41	22
	5	11	16	11	13	25	19	36	30	15
	Σ	46	90	45	71	140	107	190	145	148

as follows:

Section A - .86, .81, .73

Section B - .67, .63, .79

Section C - .63, .59, .74

Section D - .73, .74, .69

It is of interest to compare the above ratios with the theoretical distribution for a uniform stress across the width of the bridge which gives a ratio of moment carried by an exterior girder to that by an interior girder of 16.5/22.4 = .74

5.5.4 Strains and Maximum Stresses

Transverse distributions of experimental longitudinal strains for vehicle loadings producing maximum effects are shown in Figs. 5.24 and 5.25. For the relatively uniform two and three lane truck loadings across the width of the bridge the strain distributions are also fairly uniform. For the construction vehicle case, with only one lane loaded, strains are not uniform across the width.

An estimate of the maximum design live load stresses can be obtained by multiplying the maximum strain values from Figs. 5.24 and 5.25 by the unmodified modulus of elasticity values from Tables 6.4 and 6.6 of Vol. I for this loading phase. A summary of these stresses in the concrete and the steel is given in Table 5.13.

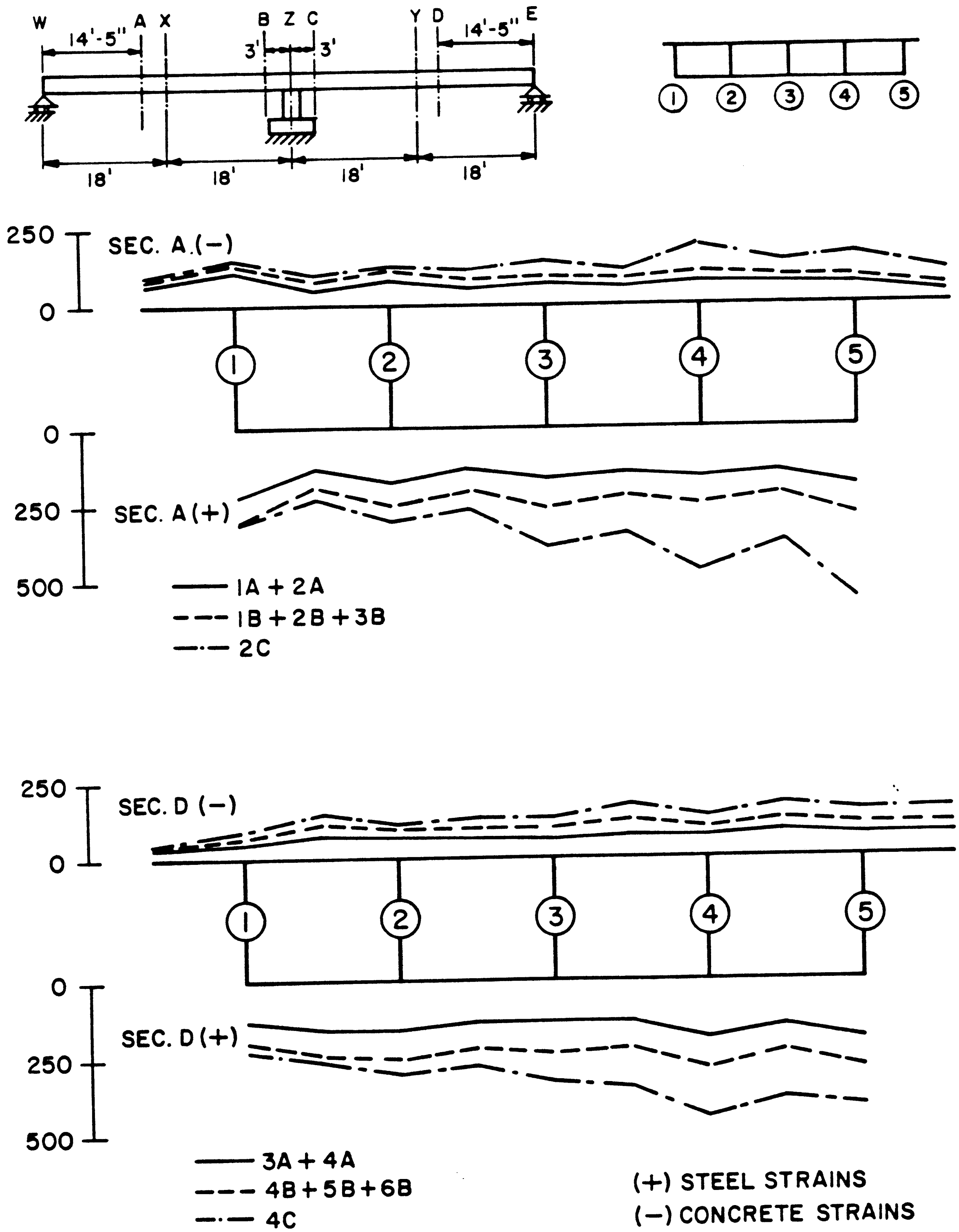

FIG. 5.24 EXPERIMENTAL LONGITUDINAL STRAINS (MICRO-INCH/INCH) IN TOP AND BOTTOM SLABS AT SECTIONS A AND D FOR DIFFERENT VEHICLE LOADINGS

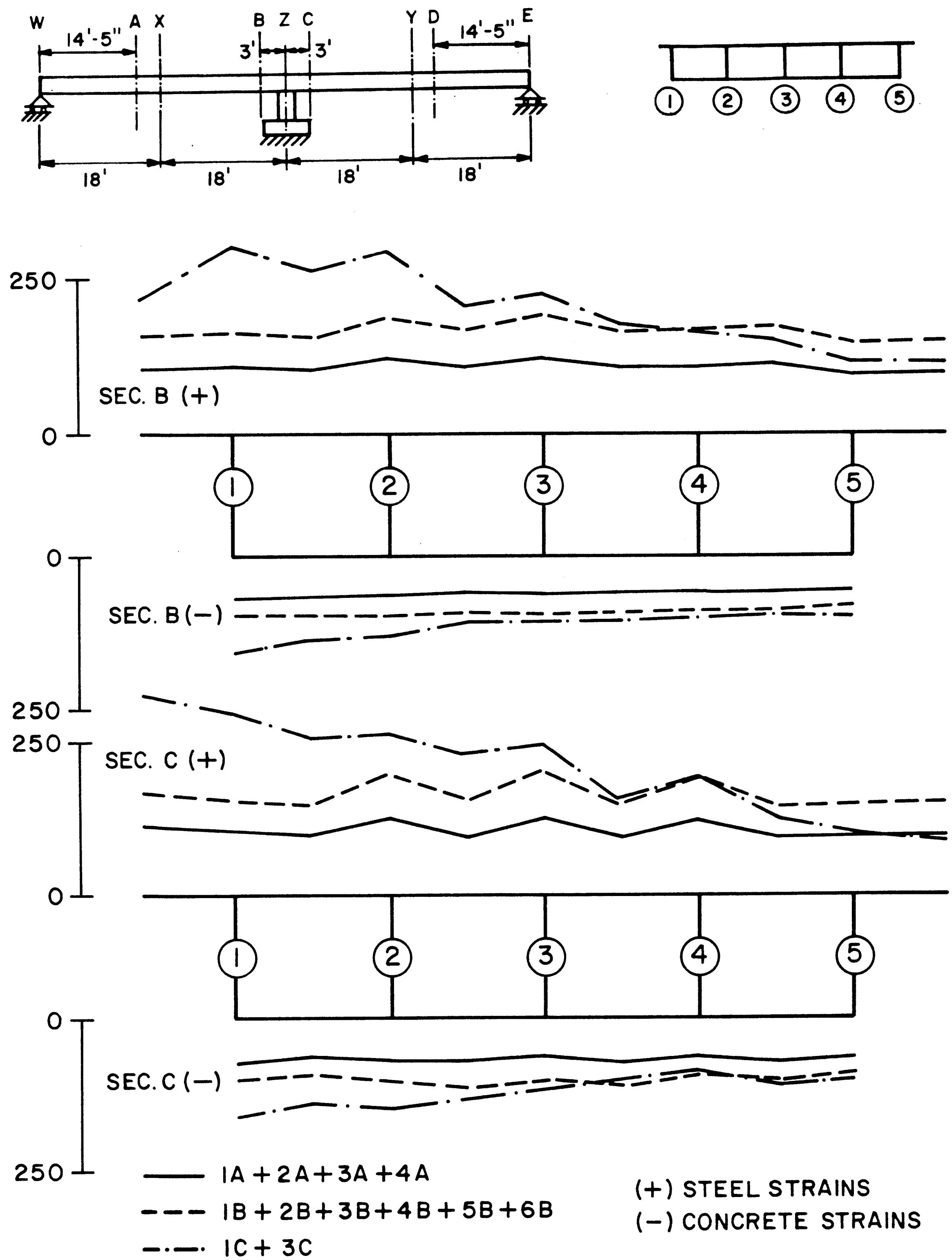

FIG. 5.25 EXPERIMENTAL LONGITUDINAL STRAINS (MICRO-INCH/INCH) IN TOP AND BOTTOM SLABS AT SECTIONS B AND C FOR DIFFERENT VEHCILE LOADINGS

TABLE 5.13 MAXIMUM LIVE LOAD EXPERIMENTAL STRESSES (PSI) UNDER TRUCK AND CONSTRUCTION VEHICLE LOADS

MATERIAL	SECTION	TWO LANE TRUCK LOADING	THREE LANE TRUCK LOADING	CONSTRUCTION VEHICLE LOADING
CONCRETE	A	297	373	516
	B	178	263	408
	C	186	292	411
	D	254	387	543
STEEL	A	6,080	8,420	15,500
	B	3,380	5,360	8,330
	C	3,440	5,500	8,910
	D	5,420	7,980	12,400

If one adds to the live load stresses for the steel in Table 5.13, the nominal calculated dead load steel stresses of 12,900 psi at Sections A and D and 8,900 psi at Sections B and C, it can be seen that the total steel stresses for the two lane and three lane truck loadings would be below the allowable value of 24,000 psi. For the construction vehicle loading a maximum calculated total steel stress of about 28,000 psi occurs.

It should be recognized that total stresses at midspan Sections X and Y would be about 10% higher than those at Sections A and D, each of which are 3.55 ft. away from midspan Sections X and Y respectively, likewise the total stresses near the edge of the center bent diaphragm would be about 30% higher than those at Sections B and C which are 3 ft. away from the centerline of the center bent diaphragm.

Live load concrete stresses in Table 5.13 are quite low and would be well within the allowable when added to the nominal dead load stresses.

5.6 Moving Fork Lift Truck Load

A fork lift truck with two concrete blocks on the fork was used as a total moving load of about 10.3 kips. Three longitudinal passes were made from west to east and static readings were taken at 11 different transverse sections, in order to obtain an approximately continuous record from which experimental influence ordinates could be determined. Details on the truck dimensions, wheel loads, loading paths and transverse sections at which measurements were taken may be found in Sections 5.5 and 5.6.1 of Vol. I.

5.6.1 Influence Lines

Figs. 5.26 to 5.29 show theoretical influence lines obtained using the SAP frame analysis program and plotted experimental points for the three passes of the fork lift truck. In each figure results are given for a pass near outer girder 5, a pass near center girder 3 and a pass near inner girder 1. In each case the experimental influence ordinates are plotted for the front wheels of the fork lift truck at the given position on the bridge.

The theoretical curves are obtained from results of analyses using SAP in which the four wheel loads were placed in identical positions to those occupied during the experimental passes. The eccentricity of the truck with respect to the longitudinal axis of the bridge for passes near girders 5 and 1 has been taken into account in the analyses. Theoretical values have been scaled so that the experimental and theoretical ordinates at a selected location are identical. In this way a comparison between the shapes of the experimental and theoretical influence lines can be made directly.

Fig. 5.26 depicts the influence lines for the East end reaction. Theoretical values have been scaled to the experimental values at Section QD indicated on the figure. The scaling factors were 1.03, 1.01 and 0.98 for the passes near girders 5, 3 and 1 respectively. As can be seen in Fig. 5.26 excellent agreement exists between theory and experiment.

Fig. 5.27 illustrates the influence lines for the deflection at 5Y. Theoretical values have been scaled to the experimental values at Section Y indicated on the figure. The scaling factors were 1.62, 1.32 and 1.20 for the passes near girders 5, 3 and 1 respectively, indicating that these are a function of which girder is loaded. The agreement between experimental and scaled theoretical influence lines is excellent.

As discussed in Chapter 2, the SAP analysis on which the theoretical values are based idealizes the curved bridge as a simple three dimensional frame made up of one dimensional beam and column members. The horizontally curved bridge is idealized by dividing it along its longitudinal centerline into 24 straight segments lying in a horizontal plane. The section properties of each of these one dimensional members are calculated by considering the entire four cell bridge cross-section as an uncracked concrete section.

The theoretical values of deflections at 5Y for the influence lines in Fig. 5.27 from the SAP analysis were found by taking the sum of the vertical deflection at the frame centerline at Section Y plus the torsional rotation times a lever arm from the longitudinal centerline to girder 5. It is evident that the simple frame analysis used in the

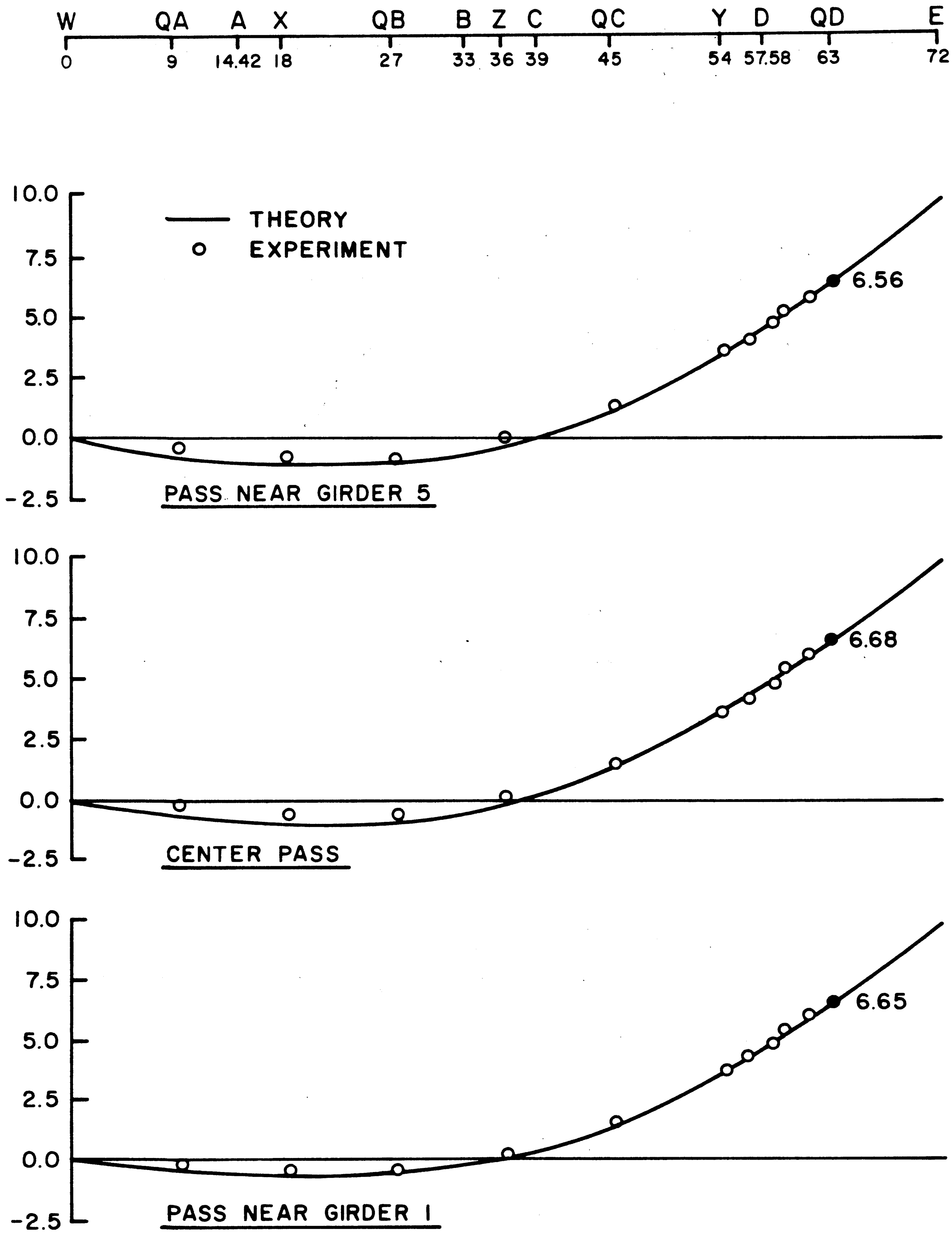

FIG. 5.26 INFLUENCE LINES FOR END REACTION (KIPS) UNDER MOVING FORK LIFT TRUCK LOAD

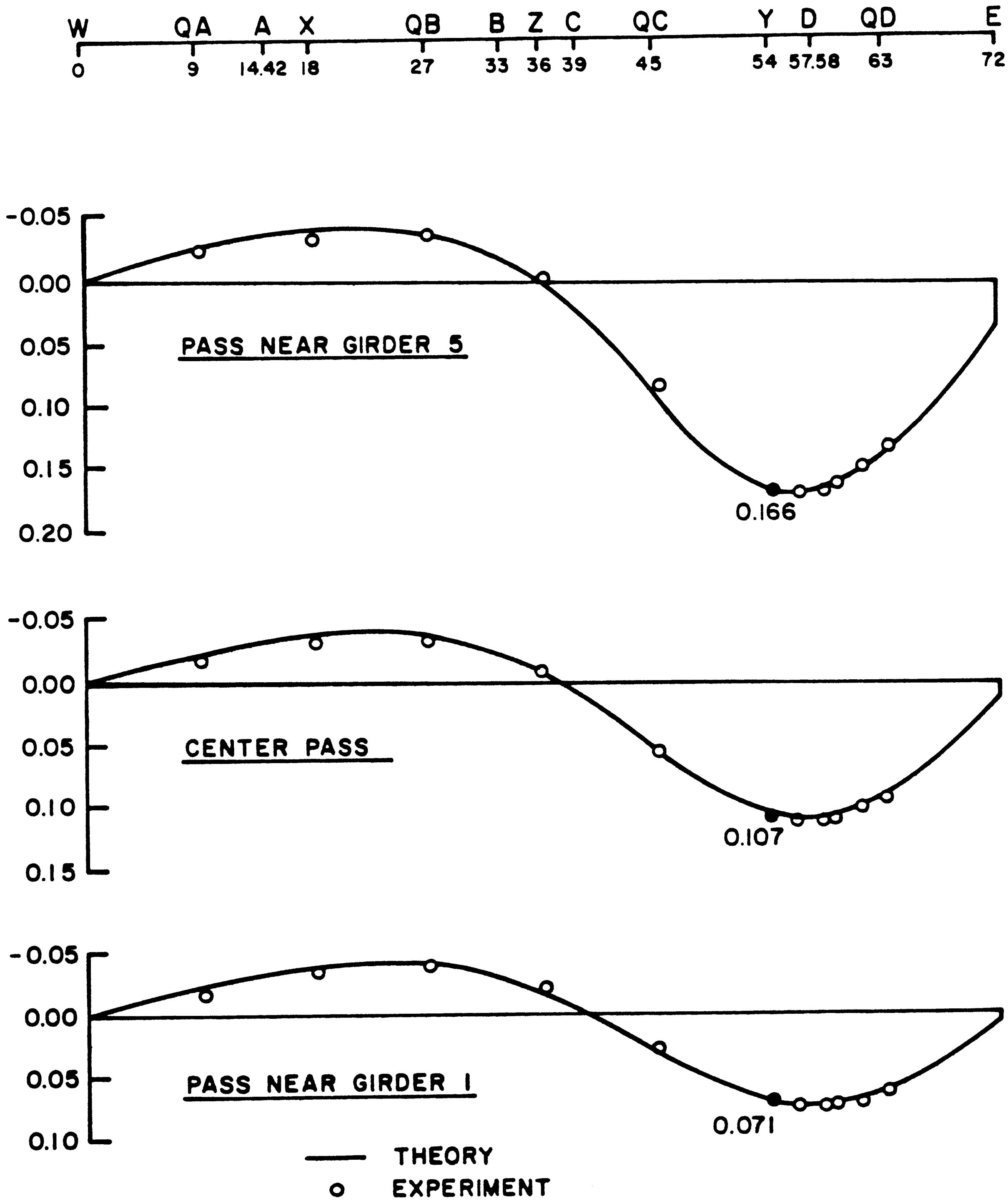

FIG. 5.27 INFLUENCE LINES FOR DEFLECTION (INCHES) AT 5Y UNDER MOVING FORK LIFT TRUCK LOAD

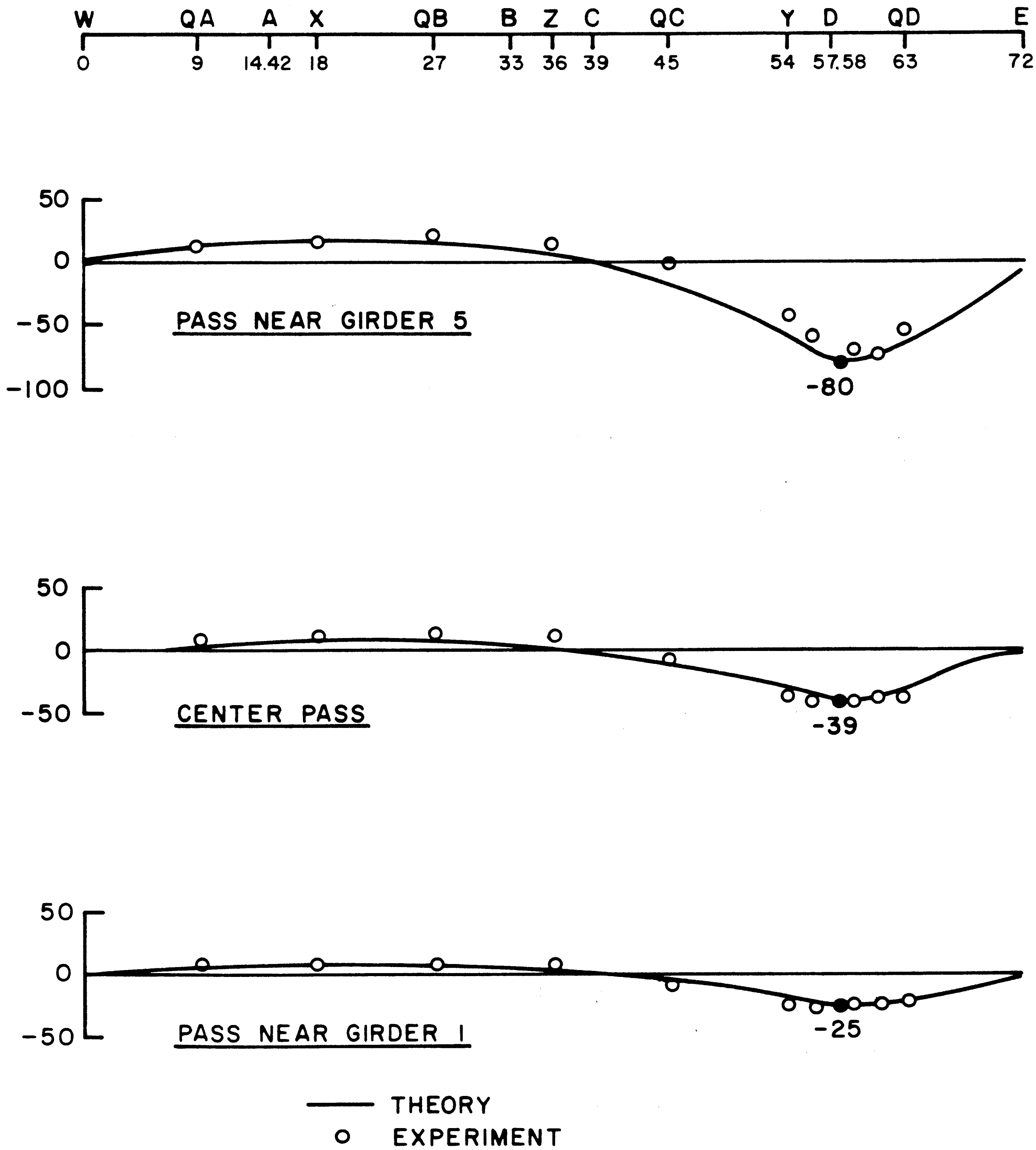

FIG. 5.28 INFLUENCE LINES FOR LONGITUDINAL CONCRETE STRAINS (MICRO-INCH/INCH) AT 5D UNDER MOVING FORK LIFT TRUCK LOAD

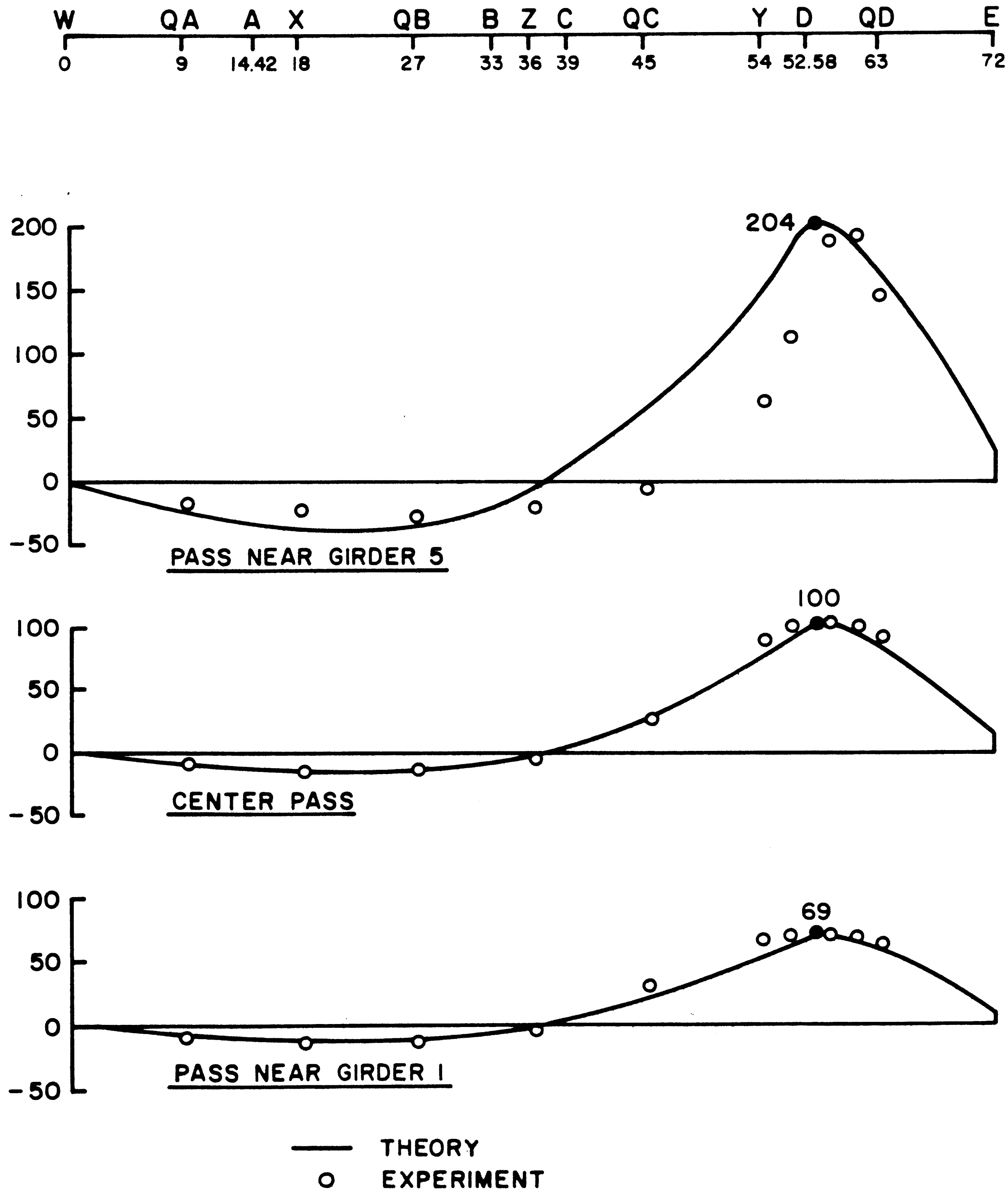

FIG. 5.29 INFLUENCE LINES FOR LONGITUDINAL STEEL STRAINS (MICRO-INCH/INCH) AT 5D UNDER MOVING FORK LIFT TRUCK LOAD

SAP program, unlike the CELL program, cannot capture the deflection due to the local bending when the load is at 5Y. A check of the results for point load deflections, Section 5.2.2, in which CELL was used to obtain the theoretical values indicates a ratio of experimental to theoretical deflections of 1.41 for the deflection at 5Y due to a point load at 5Y, which can be compared to the 1.62 value found for the influence lines for the pass near girder 5. This tends to confirm the point made above.

Figs. 5.28 and 5.29 give influence lines for concrete and steel strains at 5D. The shape of the scaled theoretical curve is identical in all cases and was taken to be the same as the theoretical influence line for the bending moment at Section D found in the SAP analyses. Scaling factors were then obtained at 5D to plot each influence line. Agreement is quite good for the center pass near girder 3 and the pass near girder 1. For the pass near girder 5, the simple theoretical approach used above cannot capture the local bending effects occuring when the fork lift truck is near the instrumented location 5D.

5.7 Comparison of Results for Straight and Curved Bridge Models

Comparing results found for the curved bridge model with those of the straight bridge model [10, 11] for the 30 ksi working load phase, it can be concluded that the general response of the two models was similar.

In this section a comparison will in general only be made of the experimental results for the straight and curved bridge model. Comparisons of theoretical results have already been made and discussed in Chapter 2.

A comparison of experimental reactions under point loadings is given in Table 5.14. It can be seen that for the straight bridge, the

TABLE 5.14 COMPARISON OF EXPERIMENTAL REACTIONS (KIPS & FT-KIPS) FOR STRAIGHT AND CURVED BRIDGE MODELS DUE TO 100 KIPS POINT LOADS

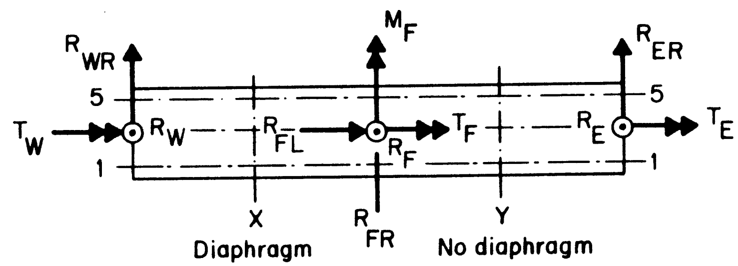

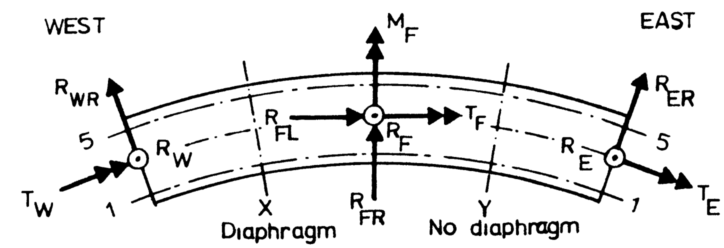

LOAD CASE	BRIDGE MODELS	REACTION (KIPS AND FT-KIPS)								LOAD (KIPS)		
		WEST END		CENTER FOOTING			EAST END		TOTAL	SEC X	SEC Y	TOTAL
		R_W	T_W	R_F	M_F	T_F	R_E	T_E	R	P_X	P_Y	P
1X	STRAIGHT	38.0	-300	69.0	135	-66	-8.3	-122	98.7	100.0	0.0	100.0
	CURVED	41.2	-280	68.1	24	-78	-7.1	-96	102.2	100.0	-0.1	99.9
1Y	STRAIGHT	-8.0	-86	70.1	-126	-69	38.3	-343	100.5	0.0	100.0	100.0
	CURVED	-7.2	-110	68.9	-15	-84	39.5	-256	101.2	0.3	100.0	100.3
IX+IY	STRAIGHT	30.1	-374	139.2	14	-140	30.4	-458	199.7	100.0	99.7	199.7
	CURVED	35.5	-381	132.5	-54	-149	33.2	-346	201.3	100.0	99.1	199.1
3X	STRAIGHT	38.1	5	70.3	135	3	-8.3	-2	100.1	100.0	0.0	100.0
	CURVED	40.0	67	69.7	103	9	-7.2	-20	102.5	100.0	0.0	100.0
3Y	STRAIGHT	-8.0	-2	70.9	-125	3	38.4	2	101.3	0.0	100.0	100.0
	CURVED	-8.0	-27	71.3	-146	-3	36.1	54	99.4	-0.1	100.0	99.9
3X+3Y	STRAIGHT	29.7	2	138.4	9	5	30.5	1	198.8	100.0	100.2	202.2
	CURVED	31.3	37	141.1	72	7	30.1	35	202.4	100.0	99.7	199.7
5X	STRAIGHT	37.9	306	69.5	128	72	-8.3	116	99.1	100.0	0.0	100.0
	CURVED	36.4	400	76.0	145	74	-9.7	45	102.6	100.0	0.0	100.0
5Y	STRAIGHT	-8.4	79	69.7	-131	69	39.0	347	100.2	0.0	100.0	100.0
	CURVED	-9.2	59	72.2	-130	98	36.6	366	99.6	0.1	100.0	100.1
5X+5Y	STRAIGHT	30.3	389	140.2	-2	144	31.5	468	201.9	100.0	101.3	201.3
	CURVED	28.7	461	151.4	-31	162	27.1	417	207.1	100.0	103.5	203.5

total vertical reactions at the two end supports and the center support remain essentially unchanged as the loads moves from girder 1 to 3 to 5, the applied torque created by the eccentric loads being taken by the torsional reactions T_W, T_F and T_E. Comparing the results for the curved bridge to these, it can be seen that the vertical reactions do change as the loads move from girder 1 to 3 to 5 and that the applied torque is taken partially by the torsional reactions and partially by the couples formed by the changing vertical reactions. The differences in the vertical reactions R_W, R_F and R_E for the two bridge models, however, is not significant. For loads on center girder 3 all reactions for the two bridges are of similar magnitude.

The transverse distributions of experimental deflections at Sections X and Y for nine point load cases are given in Figs. 5.30 and 5.31. No modifications have been made in the plotted experimental results to reflect the fact that the curved bridge had concrete which had a somewhat lower modulus of elasticity through out, than that of the straight bridge. For the straight bridge all girders had the same length, while for the curved bridge girders 5, 3, and 1 were respectively longer, equal and shorter in length than the corresponding girder in the straight bridge. Keeping these facts in mind the results depicted in Figs. 5.30 are quite reasonable and similar for the straight and curved bridge models.

Table 5.15 gives a comparison of experimental total maximum moments at Sections A, B, C and D under point loadings. Maximum positive moments at Sections A and D are produced by point loads at Sections X and Y respectively. Maximum negative moments at Sections B and C are both produced by point loads at both Sections X and Y simultaneously. For the straight bridge it is evident that the moments at each section are

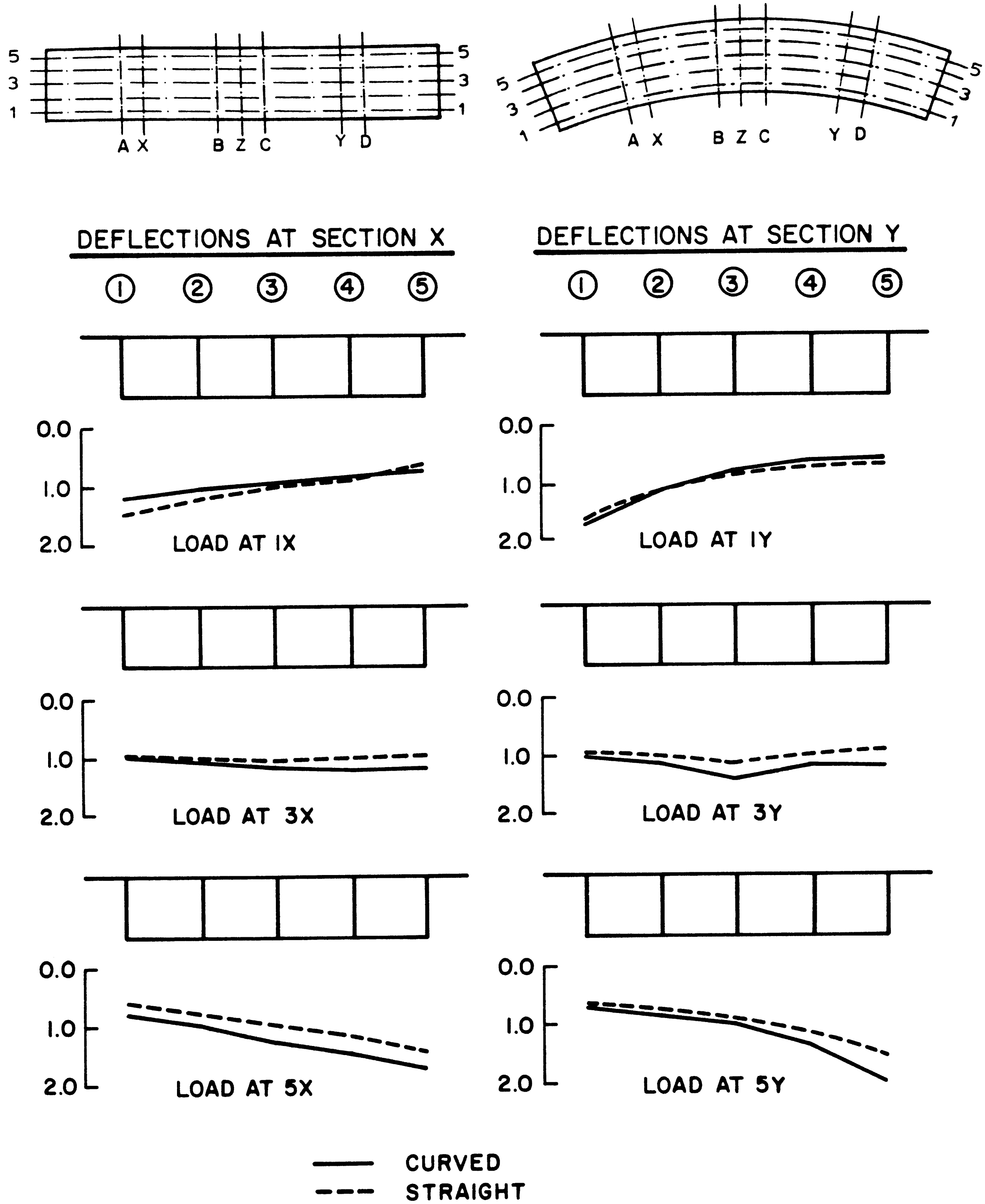

FIG. 5.30 COMPARISON OF EXPERIMENTAL VERTICAL DEFLECTIONS (INCHES) AT TRANSVERSE SECTIONS X AND Y FOR STRAIGHT AND CURVED BRIDGE MODELS DUE TO 100 KIP POINT LOADS AT 1X, 1Y, 3X, 3Y, 5X, 5Y

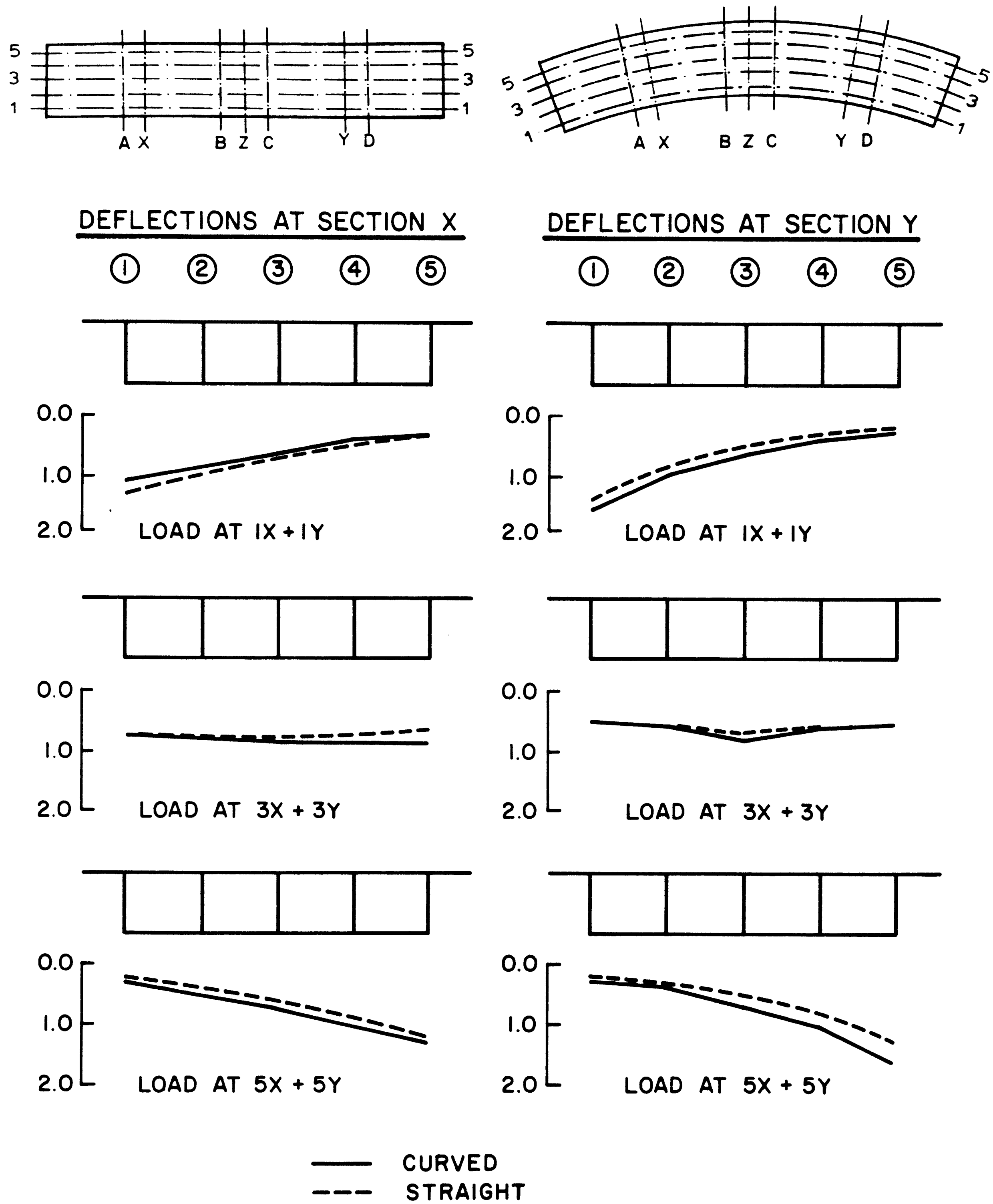

FIG. 5.31 COMPARISON OF EXPERIMENTAL VERTICAL DEFLECTIONS (INCHES) AT TRANSVERSE SECTIONS X AND Y FOR STRAIGHT AND CURVED BRIDGE MODELS DUE TO 100 KIP POINT LOADS AT 1X+1Y, 3X+3Y, 5X+5Y

TABLE 5.15 COMPARISON OF EXPERIMENTAL MAXIMUM TOTAL MOMENTS (FT-KIPS) AT A SECTION FOR STRAIGHT AND CURVED BRIDGE MODELS DUE TO 100 KIP POINT LOADS

100 K LOAD AT	BASED ON EXTERNAL REACTIONS		BASED ON INTERNAL FORCES		100 K LOAD AT	BASED ON EXTERNAL REACTIONS		BASED ON INTERNAL FORCES	
	STR	CUR	STR	CUR		STR	CUR	STR	CUR
	MAXIMUM AT SECTION A					MAXIMUM AT SECTION D			
1X	546	551	524	515	1Y	553	531	572	474
2X	547	573	525	526	2Y	544	526	586	536
3X	550	585	535	538	3Y	553	527	574	554
4X	547	588	532	544	4Y	558	534	581	572
5X	546	580	542	586	5Y	562	578	598	563
	MAXIMUM AT SECTION B					MAXIMUM AT SECTION C			
1X+1Y	-508	-390	-500	-393	1X+1Y	-496	-439	-500	-390
2X+2Y	-503	-384	-519	-409	2X+2Y	-457	-447	-540	-429
3X+3Y	-521	-470	-498	-433	3X+3Y	-494	-504	-490	-486
4X+4Y	-498	-514	-517	-490	4X+4Y	-474	-548	-498	-531
5X+5Y	-500	-493	-500	-544	5X+5Y	-461	-615	-495	-549

essentially independent of transverse load position, while for the curved bridge there is a general increase as the load moves transversely from inner girder 1 to outer girder 5. This latter increase is more pronounced for the negative moment, Sections B and C, than for the positive moment, Sections A and D. Comparing the range of percentage differences between the maximum moments for the straight and curved bridges for the same load position, Table 5.15 shows a range of differences of 0 to 8% for positive moments at Sections A and D except for one case, and of 1 to 25% for negative moments at Sections B and C.

From the above, it can be concluded that the effect of bridge curvature is more important in the negative moment region over the center bent support than it is in the midspan positive moment regions. As discussed in Section 5.5 critical design live loading will occur with all lanes loaded across the width of the bridge. For such a loading case the differences in maximum moments between the straight and curved bridge will be much smaller than the values cited above for point loads.

Table 5.16 compares the distribution of the experimental total section moments to the individual girders for the straight and curved bridge models for various point loads. Most corresponding values are within 1 or 2% of each other, however, the range of differences for Sections A, B, C and D respectively are 0 to 1, 0 to 4, 1 to 6 and 0 to 5% of the total section moment. The changes in distribution as the point loads move transversely from girder 1 to 5 seem to be quite similar for the two bridges. The values for point loads on center girder 3 are generally very close for corresponding values in the two bridges. For design loads across the entire width of the bridge, even better agreement could be expected.

TABLE 5.16 COMPARISON OF EXPERIMENTAL PERCENTAGE DISTRIBUTION OF TOTAL MAXIMUM MOMENTS AT A SECTION FOR STRAIGHT AND CURVED BRIDGE MODELS DUE TO 100 KIPS POINT LOADS.

100 K LOAD AT	STRAIGHT BRIDGE % TO GIRDERS					CURVED BRIDGE % TO GIRDERS				
	1	2	3	4	5	1	2	3	4	5
	DISTRIBUTION OF MAXIMUM MOMENT AT SECTION A									
1X	21	24	23	21	12	21	24	21	21	13
2X	18	23	23	22	13	18	23	22	22	14
3X	17	22	23	23	15	16	22	23	24	16
4X	14	20	23	25	18	15	20	22	25	17
5X	13	18	23	26	20	14	19	22	25	19
	DISTRIBUTION OF MAXIMUM MOMENT AT SECTION B									
1X+1Y	17	24	21	23	15	19	25	24	20	12
2X+2Y	16	23	21	25	14	17	25	25	21	13
3X+3Y	15	23	23	25	15	15	23	26	23	14
4X+4Y	14	21	22	28	16	14	22	25	24	16
5X+5Y	14	21	21	26	18	24	21	24	24	16
	DISTRIBUTION OF MAXIMUM MOMENT AT SECTION C									
1X+1Y	18	26	21	20	14	22	27	22	18	12
2X+2Y	15	25	22	22	15	17	27	25	20	12
3X+3Y	14	24	23	231	15	13	23	27	23	14
4X+4Y	13	23	20	25	19	12	21	26	26	16
5X+5Y	13	22	22	25	18	12	20	24	26	17
	DISTRIBUTION OF MAXIMUM MOMENT AT SECTION D									
1Y	16	29	23	20	12	20	30	20	18	13
2Y	16	25	27	21	11	17	26	22	21	14
3Y	13	25	24	25	13	13	24	23	24	17
4Y	11	22	26	25	16	11	20	23	27	20
5Y	14	18	23	28	17	10	19	21	29	21

Using the method described in Section 5.4.3 the maximum number of wheel loads carried by an interior or exterior girder are calculated and compared in Table 5.17 for the straight and curved bridge models. Line (1) indicates that the AASHO specifications give the same value for the two bridges. Lines (2) and (4) show that theoretical values for the interior girder are practically the same for both bridges, while for the exterior girder the values for the curved bridge are 5 to 9% larger than those of the straight bridge. Lines (3) and (5) indicate that experimental values for both bridges are also practically the same for both bridges for the interior girder with the exception of Section B where the straight bridge values are somewhat higher. For the exterior girder, experimental values for both bridges are very close for both bridges except at Section D where the curved bridge values are somewhat higher. Summarizing these results, it appears that considering design approximations the same load distribution factors could be used for interior girders of straight or curved bridges and for exterior girders a 5 to 10% increase should be used for curved bridges as compared to straight bridges.

Comparing the results in Table 5.17 for both straight and curved bridges with AASHO specifications it is evident that AASHO is adequate or conservative for two lane loadings, but is unconservative for three lane loadings.

A final comparison of results for the straight and curved bridge models is made in Table 5.18 for maximum live load strains and stresses under the trucks and construction vehicle loads described in Section 5.5. Strains are the maximum values recorded at any point un-

TABLE 5.17 COMPARISON OF MAXIMUM NUMBER OF WHEEL LOADS CARRIED BY AN INTERIOR OR AN EXTERIOR GIRDER FOR STRAIGHT AND CURVED BRIDGE MODELS

GIRDER	LINE	LOAD CASE	BRIDGE	SECTION A	SECTION B	SECTION C	SECTION D
INTERIOR	1	AASHO Specifications		1.04	1.04	1.04	1.04
	2	Two Lane (Theory)	S C	0.96 0.97	0.95 0.97	0.99 0.98	0.99 0.99
	3	Two Lane (Experimental)	S C	0.98 0.98	1.06 0.97	1.00 1.02	1.04 1.06
	4	Three Lane (Theory)	S C	1.37 1.33	1.38 1.39	1.40 1.39	1.39 1.39
	5	Three Lane (Experimental)	S C	1.42 1.41	1.54 1.41	1.45 1.44	1.47 1.48
EXTERIOR	1	AASHO Specifications	S C	0.88	0.88	0.88	0.88
	2	Two Lane (Theory)	S C	0.67 0.73	0.67 0.71	0.71 0.74	0.71 0.78
	3	Two Lane (Experimental)	S C	0.73 0.73	0.65 0.67	0.70 0.68	0.61 0.77
	4	Three Lane (Theory)	S C	0.96 1.03	0.95 1.02	0.97 1.04	0.97 1.06
	5	Three Lane (Experimental)	S C	1.02 1.03	0.94 0.96	0.99 0.93	0.84 1.05

TABLE 5.18 COMPARISON OF MAXIMUM LIVE LOAD EXPERIMENTAL STRAINS (MICRO-INCH/INCH) AND STRESSES (PSI) FOR STRAIGHT AND CURVED BRIDGE MODELS UNDER TRUCK AND CONSTRUCTION VEHICLE LOADS

MATERIAL	SECTION	TWO LANE TRUCK LOADING		THREE LANE TRUCK LOADING		CONSTRUCTION VEHICLE LOADING	
		STR	CUR	STR	CUR	STR	CUR
		EXPERIMENTAL STRAINS (MICRO-INCH/INCH)					
CONCRETE	A	59	110	72	138	135	191
	B	81	67	123	99	176	154
	C	83	70	119	110	177	155
	D	65	83	100	127	115	178
STEEL	A	276	221	344	306	586	565
	B	128	123	202	195	352	303
	C	133	125	201	200	324	324
	D	229	197	369	290	448	450
		EXPERIMENTAL STRESS (PSI)					
CONCRETE	A	207	297	276	373	516	516
	B	235	178	351	263	510	408
	C	241	186	346	292	514	411
	D	249	254	383	387	440	543
STEEL	A	8,030	6,080	9,980	8,420	17,000	15,500
	B	3,710	3,380	5,850	5,360	10,200	8,330
	C	3,860	3,440	5,830	5,500	9,370	8,910
	D	6,640	5,420	10,700	7,980	13,000	12,400

der the loadings shown. Concrete stresses are obtained by multiplying the strains by the modulus of elasticity of the concrete at the instrumented location. As indicated in Table 6.4 of Vol. I and in Ref. [9], the modulus was not the same throughout the bridge models. Steel stresses are obtained by multiplying strains in the straight and curved bridge models by 29.0 x 10^6 and 27.5 x 10^6 psi respectively, which were the average moduli of elasticity of the no. 4 steel reinforcement in the two bridges.

Table 5.18 shows that live load concrete strains and stresses are relatively low. Generally it appears that at Sections A and D values for the curved bridge are larger, while at Sections B and C they are smaller than those for the straight bridge.

For the live load steel strains and stresses the values at Sections B and C are quite close for the two bridges, while at Sections A and D they are smaller for the curved bridge by an amount ranging from about 4 to 25% with an average difference of about 15%.

5.8 Summary

A detailed discussion of the results for working stress loads has been presented. The most important conclusions under various categories are summarized below.

1. Comparison of theoretical results from CELL with experimental results.

   a. The total reactions at the east, center and west supports are accurately predicted by theory.

   b. Theory predicts the distribution and magnitude of deflections satisfactorily (within 10 to 20%) if theoretical values based on an uncracked section are multiplied by a factor of 1.5 to account for cracking at this stress level.

c. While theory predicts the general distributions of strains, significant differences can exist with experimental values at certain points.

d. The maximum total moments at a section from a design standpoint are the positive midspan moments in the loaded span due to live load on only one span and the negative moments over the center bent support due to live load on both spans. These critical moments, as computed either from external reactions or the integration of internal stresses, are adequately predicted by theory for design purposes. Differences between theoretical and experimental values of these total moments for various transverse load positions generally range from 0 to 8% for midspan positive moments at Sections A and D and for negative moments near the center bent support at Section C; however, for the negative moments at support Section B the differences range from 1 to 14%.

e. For the transverse distribution of the total moment at a section, in terms of percentage to each girder, the maximum differences between theoretical and experimental values in almost all cases are only 0 to 2% of the total moment at the section.

2. Effect of support restraints.

   a. Comparing results from the case where torsional restraint at the center bent exists with those from the normal restraint case, the differences are small and could be ignored in a practical design problem.

   b. Comparing results from the case where longitudinal restraint exists at the end diaphragms with those from the normal restraint case, the differences are larger and should be considered in a practical design problem.

3. From the study of 19 different midspan point load combinations it can be concluded that there is a general increase in the total moment at any section as the load moves transversely from inner girder 1 to outer girder 5. This increase is much more pronounced for negative moment Sections B and C than for positive moment Sections A and D.

4. Both theoretical and experimental results show that the AASHO empirical formula $N_{WL} = S/7$ overestimates the actual value slightly for a two lane truck loading, but underestimates by as much 30%, the actual value for a three lane truck loading on the bridge.

5. Nominal calculated dead load steel stresses plus experimentally determined live load steel stresses were maximum at positive midspan Sections A and D and had the following values for design vehicles placed to produce maximum effects.

a. Two lanes of HS 20-44 trucks, 19,000 psi.

b. Three lanes of HS 20-44 trucks, 21,000 psi.

c. One lane of constructions vehicles, 27,000 psi.

6. The general response of the curved bridge model for the working load phase was similar to that of the straight model tested earlier. For design purposes it appears that the same load distribution factors could be used for interior girders of both bridges, but for exterior girders a 5 to 10% increase should be used for curved bridges as compared to straight bridges.

6. RESPONSE AT OVERLOAD STRESS LEVELS

6.1 General Remarks

As described in Vol. I, the experimental program was divided into two parts to study the response of the bridge under the following loadings:

Part 1 - Dead load and working loads

Part 2 - Overloads and loading to failure

Responses to dead load and working loads have been discussed in Chapters 4 and 5. Response to overloads will be discussed in this Chapter and loading to failure will be discussed in Chapter 8.

The overload sequence was divided into several phases, in each of which initial conditioning loads were applied to create total maximum tensile stresses in the reinforcement of 40, 50 and 60 ksi. Each of these was then followed by a detailed sequence of 10 point load cases, having magnitudes in all cases identical to those used after the 30 ksi working stress conditioning load. These point load magnitudes were chosen to produce total maximum stresses of the order of 24 to 30 ksi in the reinforcement. In this manner, the response of the bridge at working stress level could be studied assuming it had been subjected to an overload of increasing magnitude, which would accentuate the maximum amount of cracking, deflection and stress in the bridge.

Of particular interest was how much, if any, would these overloads change the distribution and magnitude of reactions, deflections, strains, total moments at a section and percentage distribution of the total moment at a section to each girder. Of additional interest was the degree of linearity of response and the change in stiffness of the bridge during and after each of the conditioning overloads.

In this chapter the results for the above will be discussed and compared for the following cases: (1) during each of the conditioning loads to bring the stress level to 24, 30, 40, 50 and 60 ksi; and (2) for a working stress point load at 1Y or 5Y after each of the conditioning loads to bring the stress level to 30, 40, 50 and 60 ksi was applied.

6.2 Results for Conditioning Loads

Detailed tabulations of theoretical and experimental results related to reactions, deflections, strains and moments for each of the conditioning loads are given in Vol. III. Conditioning loads were obtained by applying equal loads over each of the five girders at both midspan Sections X and Y. All theoretical values obtained from the computer analysis using the CELL program are for total loads of 100 kips per span. Experimental values have been normalized to a total load of 100 kips at midspan Section X. Because of small differences between the actual experimental total load at midspan Sections X and Y, the corresponding normalized total load at Section Y ranged from 96.3 to 107.4 kips.

During each of the conditioning load cases a specific sequence of loading as follows was used.

(1) Take sustained dead load readings relative to the absolute zero readings.

(2) Take zero readings on all gages and meters.

(3) Apply load in several increments to reach the full conditioning load and take readings after each increment.

(4) Remove load in several increments to reach zero load and take readings after each increment.

(5) Cycle eight times from zero to full load to zero.

(6) Take zero readings on all gages and meters.

(7) Apply full load in one increment and take readings.

(8) Unload to zero in one increment and take readings.

(9) Take sustained dead load readings relative to absolute zero readings.

A series of graphs are given in Figs. 6.1 to 6.8 for the total east reaction, deflections at 1Y and 5Y, and steel and concrete strains at 1D and 5D produced by the conditioning loads. Figs. 6.1, 6.3, 6.5 and 6.6 depict for each conditioning load separately the response for the initial complete load cycle (zero, full load, zero) as dotted lines, together with the response during the final load cycles as solid lines. These plots enable one to study the linearity of response and the permanent sets encountered in each conditioning load sequence. Fig. 6.2 superimposes on a single plot the response for the final load cycle only, for all conditioning loads. The same procedure is used also for Figs. 6.4, 6.7 and 6.8, where this information is given for both inner girder 1 and outer girder 5. These plots permit an evaluation of change in response to load for increasing values of maximum conditioning load.

6.2.1 Reactions

Table 6.1 gives a comparison of theoretical and experimental total reactions for conditioning loads normalized to 100 kips at Section X. One set of theoretical values applies for all conditioning

TABLE 6.1 COMPARISON OF EXPERIMENTAL AND THEORETICAL REACTIONS (KIPS AND FT - KIPS) FOR CONDITIONING LOADS

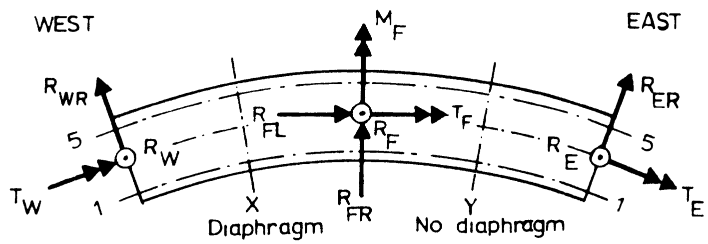

LOAD CASE	SOLUTION	REACTIONS (KIPS AND FT-KIPS)								LOADS (KIPS)		
		WEST END		CENTER FOOTING			EAST END		TOTAL	SEC X	SEC Y	TOTAL
		R_W	T_W	R_F	M_F	T_F	R_E	T_E	R	P_X	P_Y	P
ALL CASES	THEORY	30.8	39	138.4	0	-1	30.8	39	200.0	100.0	100.0	200.0
24 KSI	EXPER.	31.2	42	139.4	9	11	30.2	38	200.8	100.0	97.8	197.8
30 KSI	EXPER.	31.5	41	138.7	10	3	29.1	35	199.3	100.0	96.3	196.3
40 KSI	EXPER.	30.0	37	136.4	-1	2	29.1	34	195.5	100.0	100.0	200.0
50 KSI	EXPER.	31.8	40	144.8	-8	-2	30.2	30	206.8	100.0	107.4	207.4
60 KSI	EXPER.	30.0	28	139.2	-2	-4	29.2	29	198.5	100.0	102.8	202.8

load levels. The horizontal reactions R_{WR}, R_{FL}, R_{FR} and R_{ER} are zero in all cases and thus are not tabulated. Table 6.1 shows that for vertical reactions R_W, R_F and R_E experimental values for all conditioning load levels are very close to theoretical values with maximum percentage differences being 3.1, 4.4 and 5.8% respectively. Values for external torsional and moment reactions T_W, T_F, T_E and M_F are quite small, but even here the agreement between experimental and theroretical values is generally good.

Figures 6.1 and 6.2 depict graphically the results for the total east reaction in which the values have not been normalized. Fig. 6.1 indicates that this reaction is linearly related to load for all load levels and little difference exists between the first and last cycle of loading. Fig. 6.2 shows that there is a very slight decrease in the reaction per unit load response under increasing load levels. It is also seen that theory accurately predicts this reaction response.

6.2.2 Deflection at 1Y and 5Y

Figure 6.3 indicates that some residual deflection exists at 5Y after the first cycle of loading in each case due to an increased level of cracking. Comparing the unloading path during the first cycle with the loading path during the final cycle of loading, indicates that the slopes are almost identical and little additional permanent deflection occurs between the first cycle and the last (tenth) cycle of loading.

Fig. 6.4 shows that the structural stiffness decreases under increasing conditioning loads due to the larger amount of cracking.

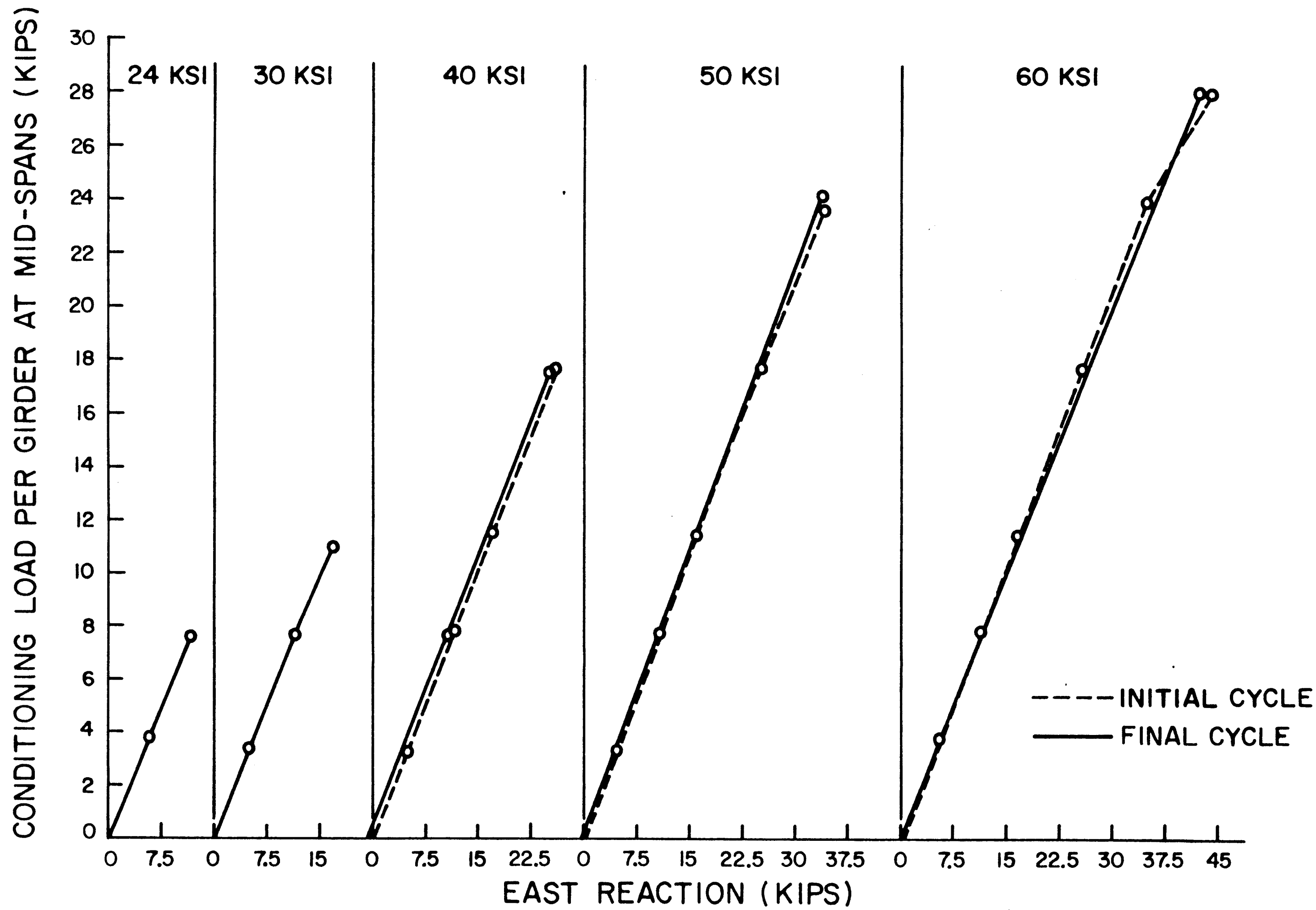

FIG. 6.1 EXPERIMENTAL TOTAL EAST REACTIONS (KIPS) DURING CONDITIONING LOAD CYCLES

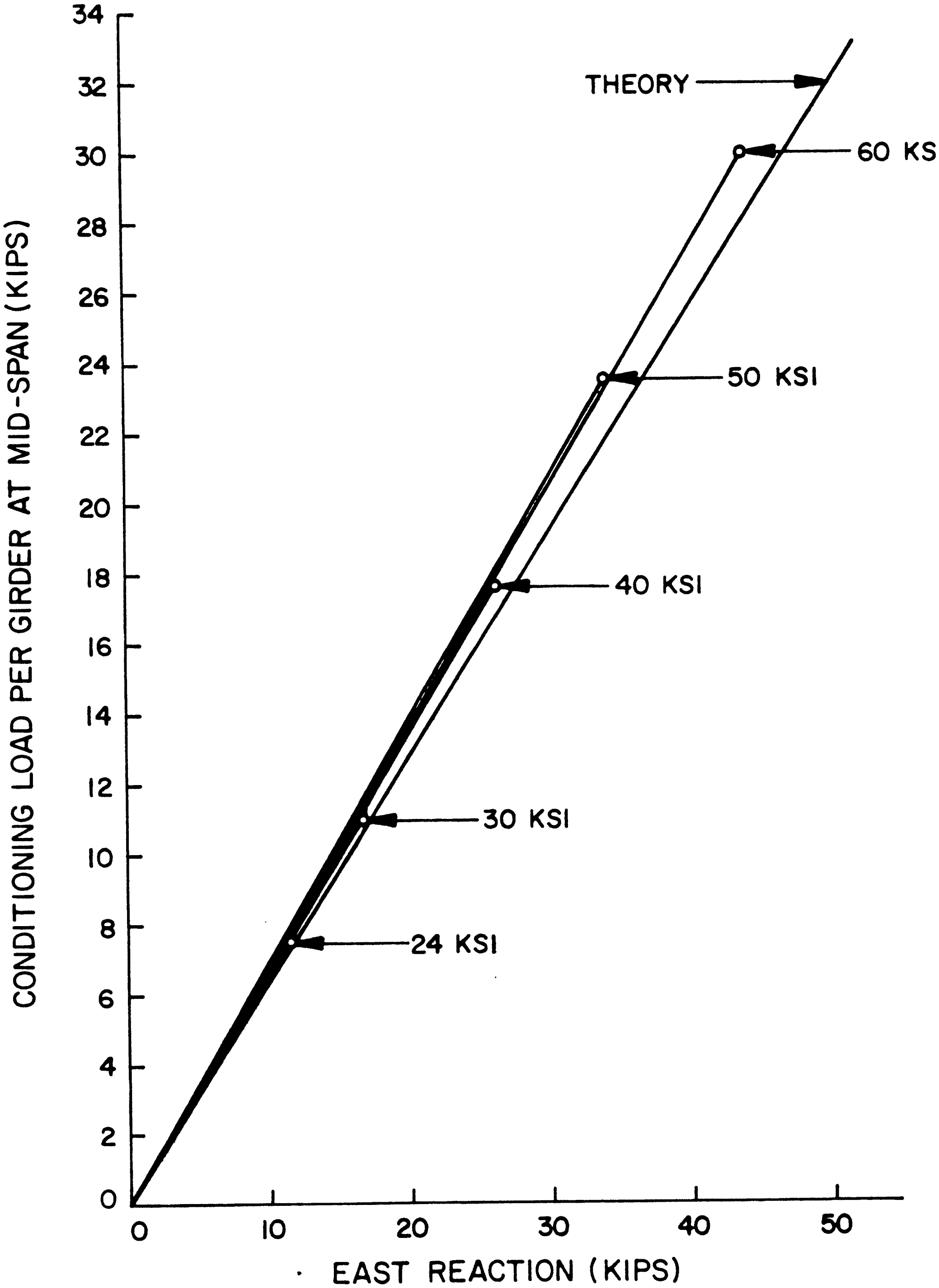

FIG. 6.2 TOTAL EAST REACTION (KIPS) DURING CONDITIONING LOAD CYCLES

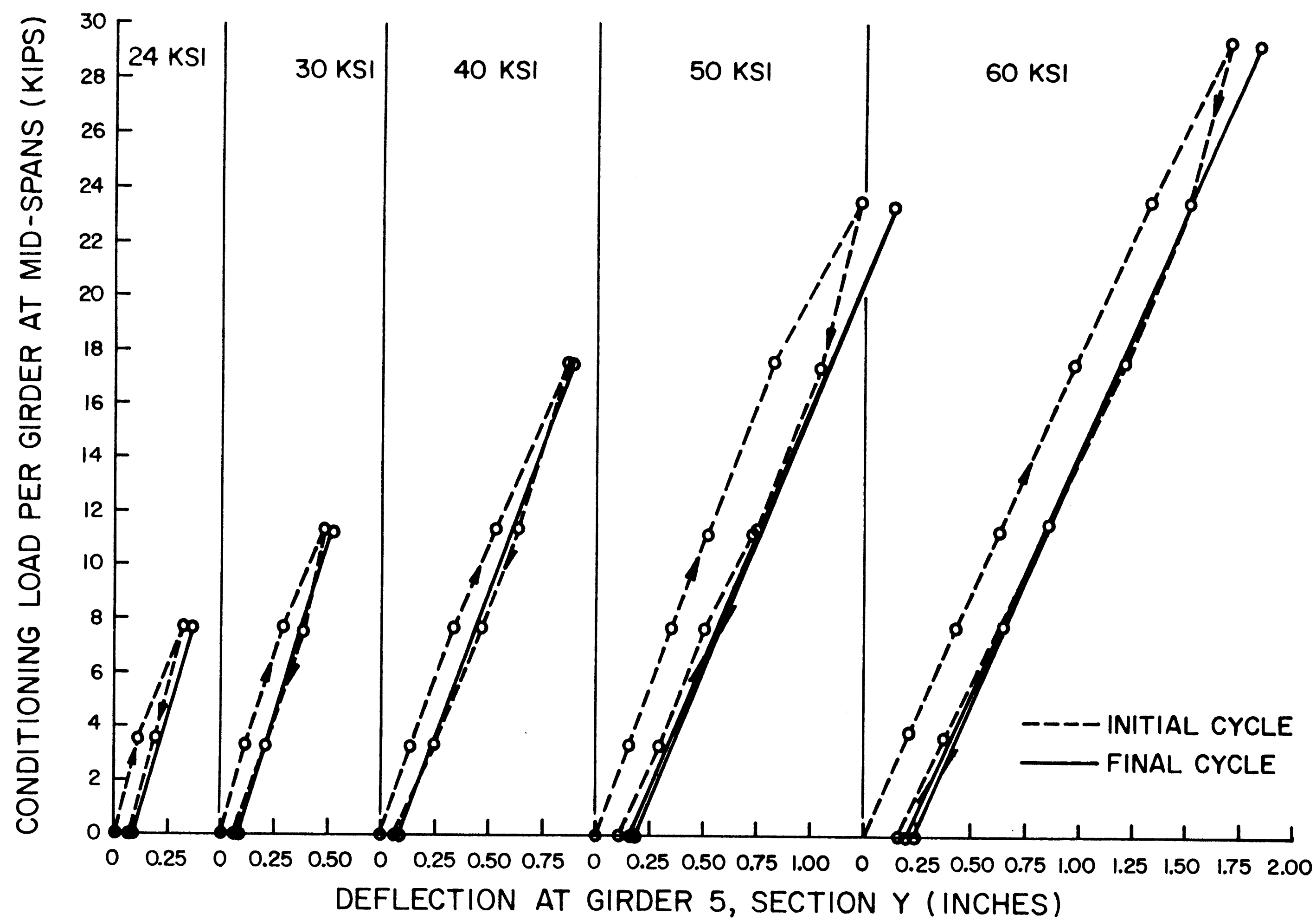

FIG. 6.3 EXPERIMENTAL DEFLECTIONS (INCHES) AT 5 Y DURING CONDITIONING LOAD CYCLES

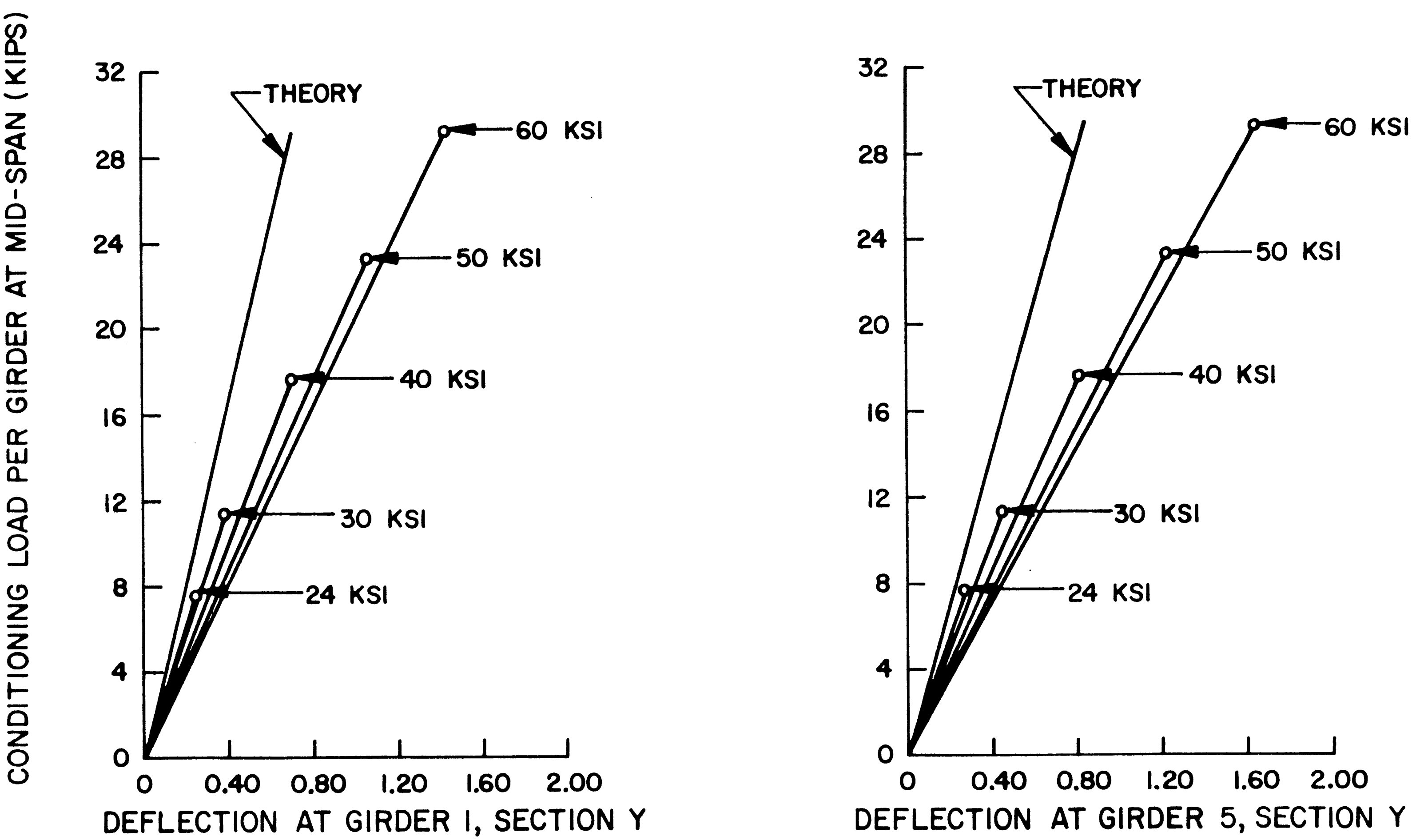

FIG. 6.4 DEFLECTIONS (INCHES) AT 1Y AND 5Y DURING CONDITIONING LOAD CYCLES.

Comparing the experimental values with those from theory based on an uncracked section, one finds that the ratio of experimental to theoretical deflections is about the same for both girders 1 and 5 for all conditioning load levels. These ratios are approximately 1.3, 1.4, 1.6, 1.9 and 2.0 for the 24, 30, 40, 50 and 60 ksi conditioning loads respectively.

6.2.3 Steel and Concrete Strains at 1D and 5D

As indicated in Figs. 6.5 and 6.6, steel and concrete strains at 5D exhibit a similar response to that of deflection with respect to linearity and residual deformation. Linearity appears to be quite good even at high load levels.

Fig. 6.7 shows that the response for the concrete strains per unit load is constant at all load levels, both for girders 1 and 5. However, Fig. 6.8 indicates that the steel strain per unit load for girder 1 increases with higher levels of conditioning loads while the response is essentially constant for girder 5.

6.2.4 Moments

The experimental longitudinal variation of the total moments at a section for each conditioning load normalized to 100 kips per span are compared to theoretical values in Fig. 6.9. Moments obtained from both external reactions and integration of internal forces at the sections are given.

First, comparing experimental values with theoretical values, the agreement for moments based on external reactions is good for all load levels for the positive moment sections near the midspans. The values are between 1 to 4% and 1 to 6% of each other for Sections A

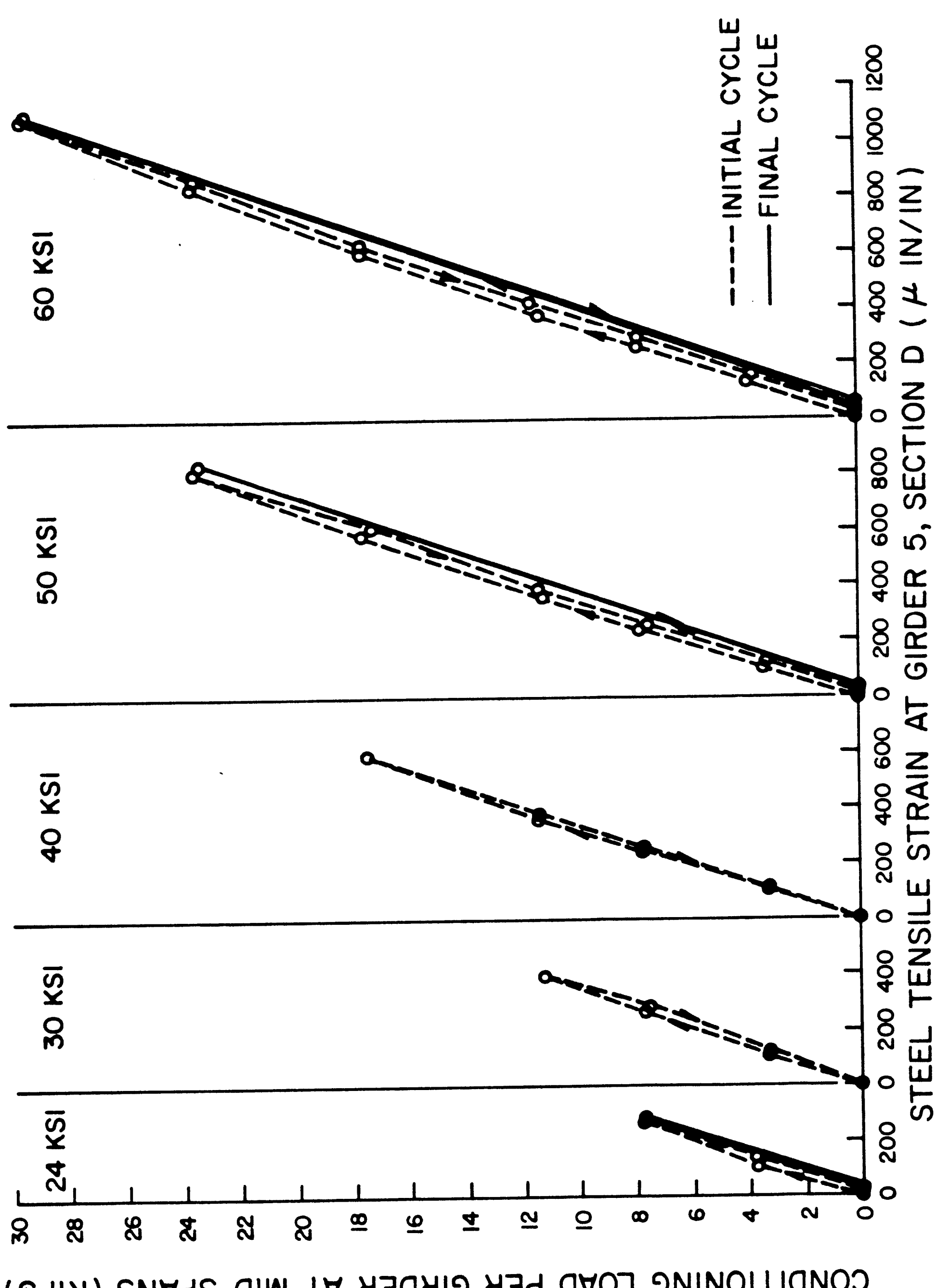

FIG. 6.5 EXPERIMENTAL LONGITUDINAL STEEL TENSILE STRAINS (MICRO-INCH/INCH) AT 5 D DURING CONDITIONING LOAD CYCLES

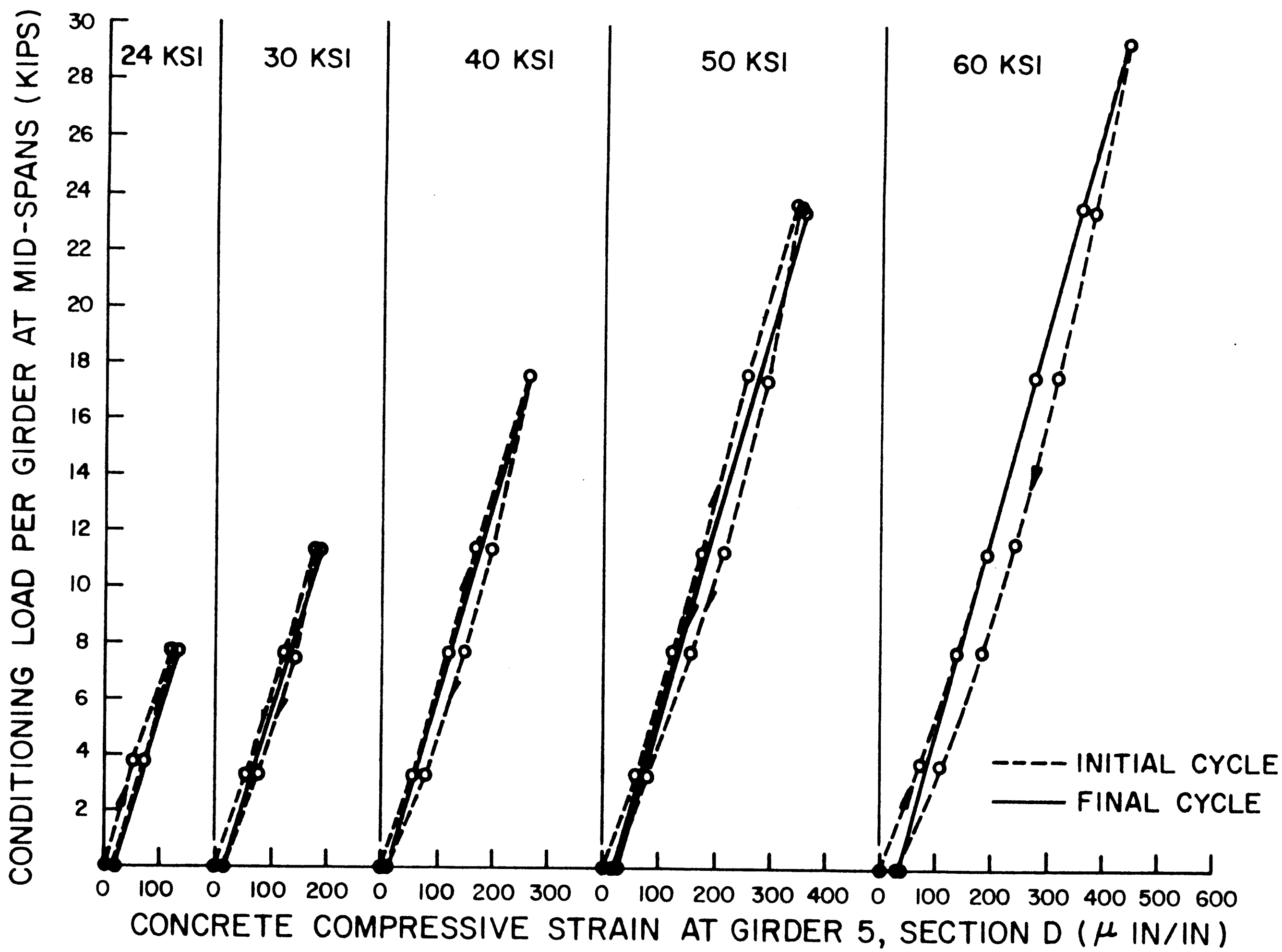

FIG. 6.6 EXPERIMENTAL LONGITUDINAL CONCRETE COMPRESSIVE STRAINS (MICRO-INCH/INCH) AT 5 D DURING CONDITIONING LOAD CYCLES

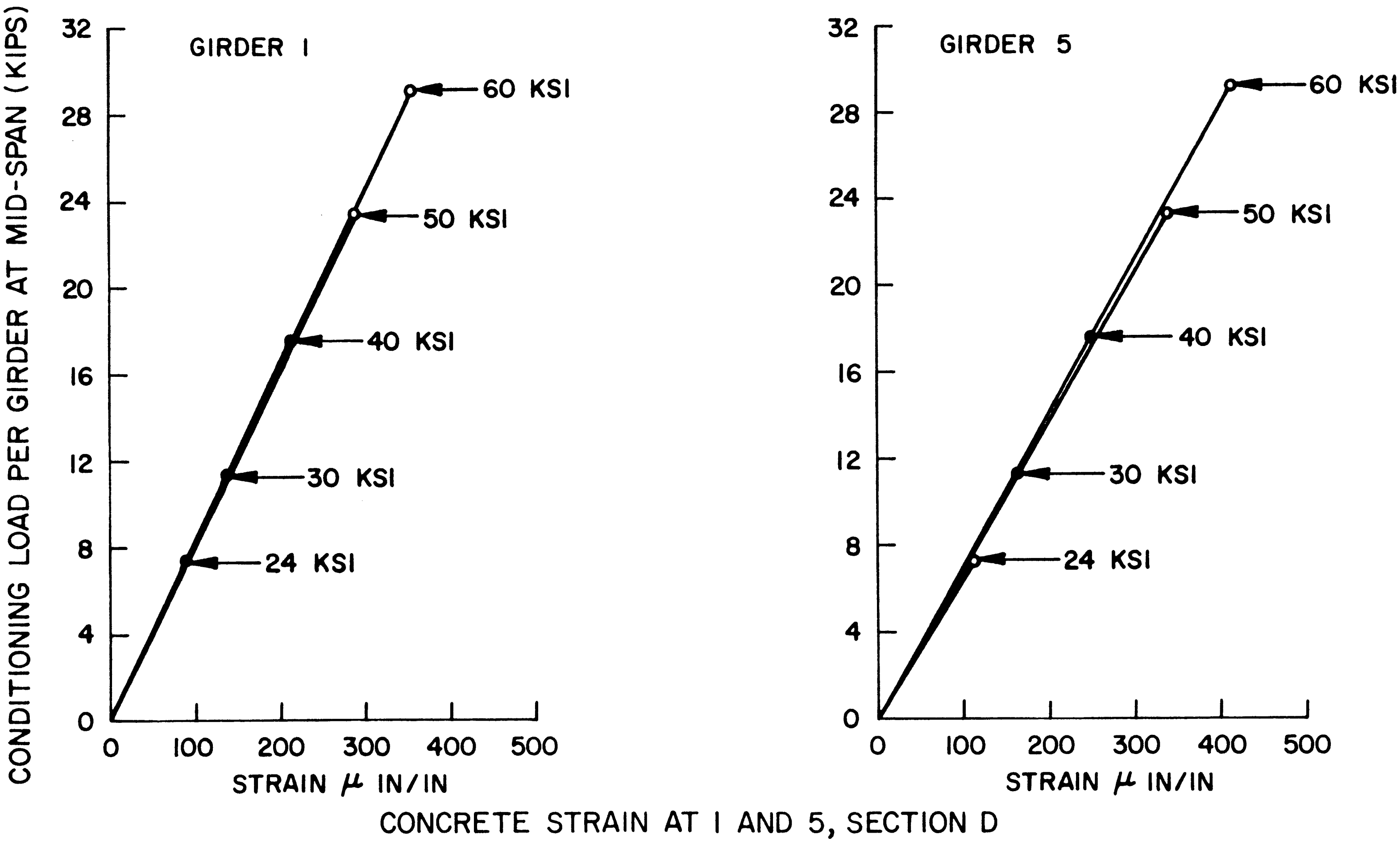

FIG. 6.7 EXPERIMENTAL LONGITUDINAL CONCRETE COMPRESSIVE STRAINS (MICRO-INCH/INCH) AT 1D AND 5D DURING CONDITIONING LOAD CYCLES

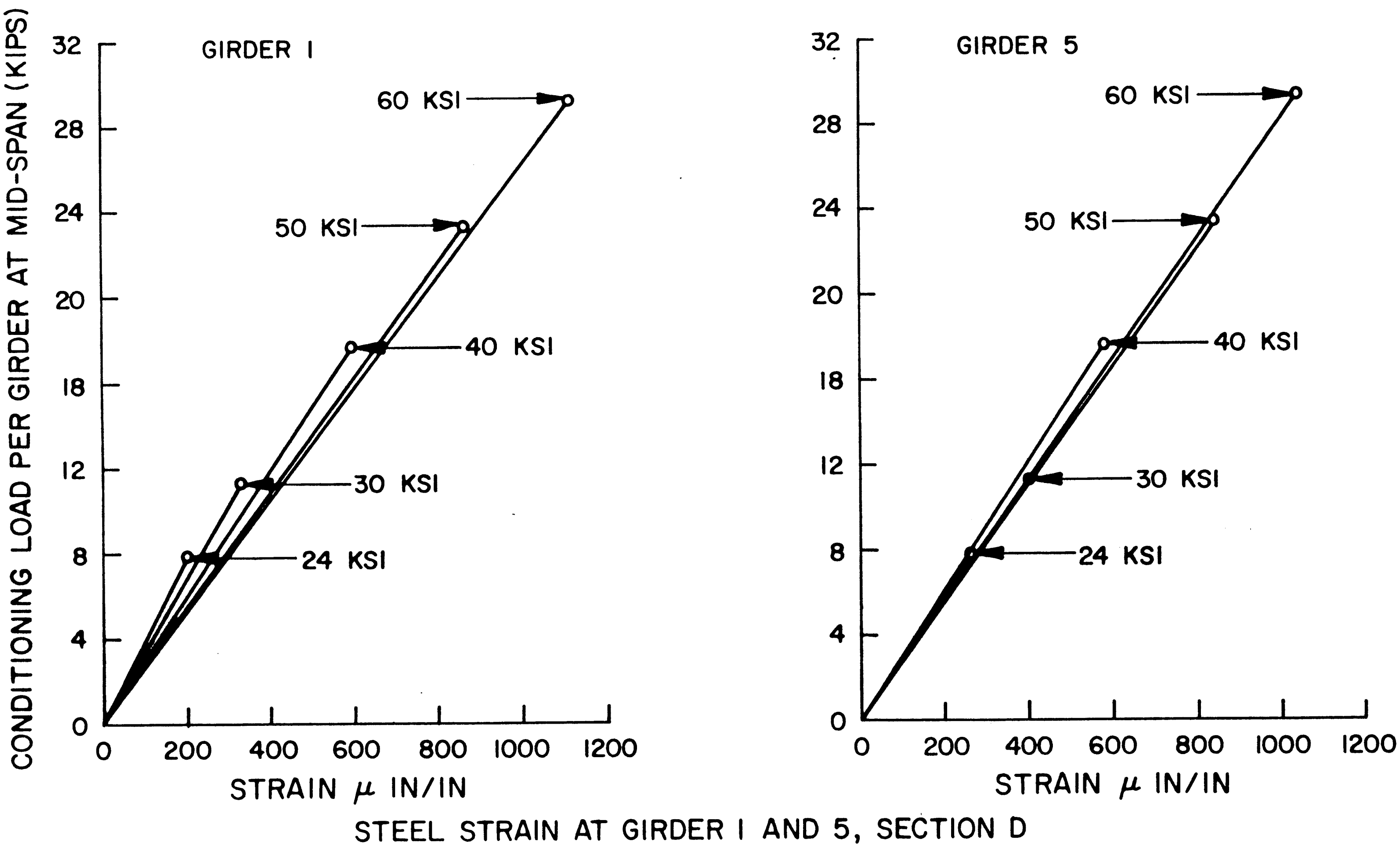

FIG. 6.8 EXPERIMENTAL LONGITUDINAL STEEL TENSILE STRAINS (MICRO-INCH/INCH) AT 1D ABD 5D DURING CONDITIONING LOAD CYCLES

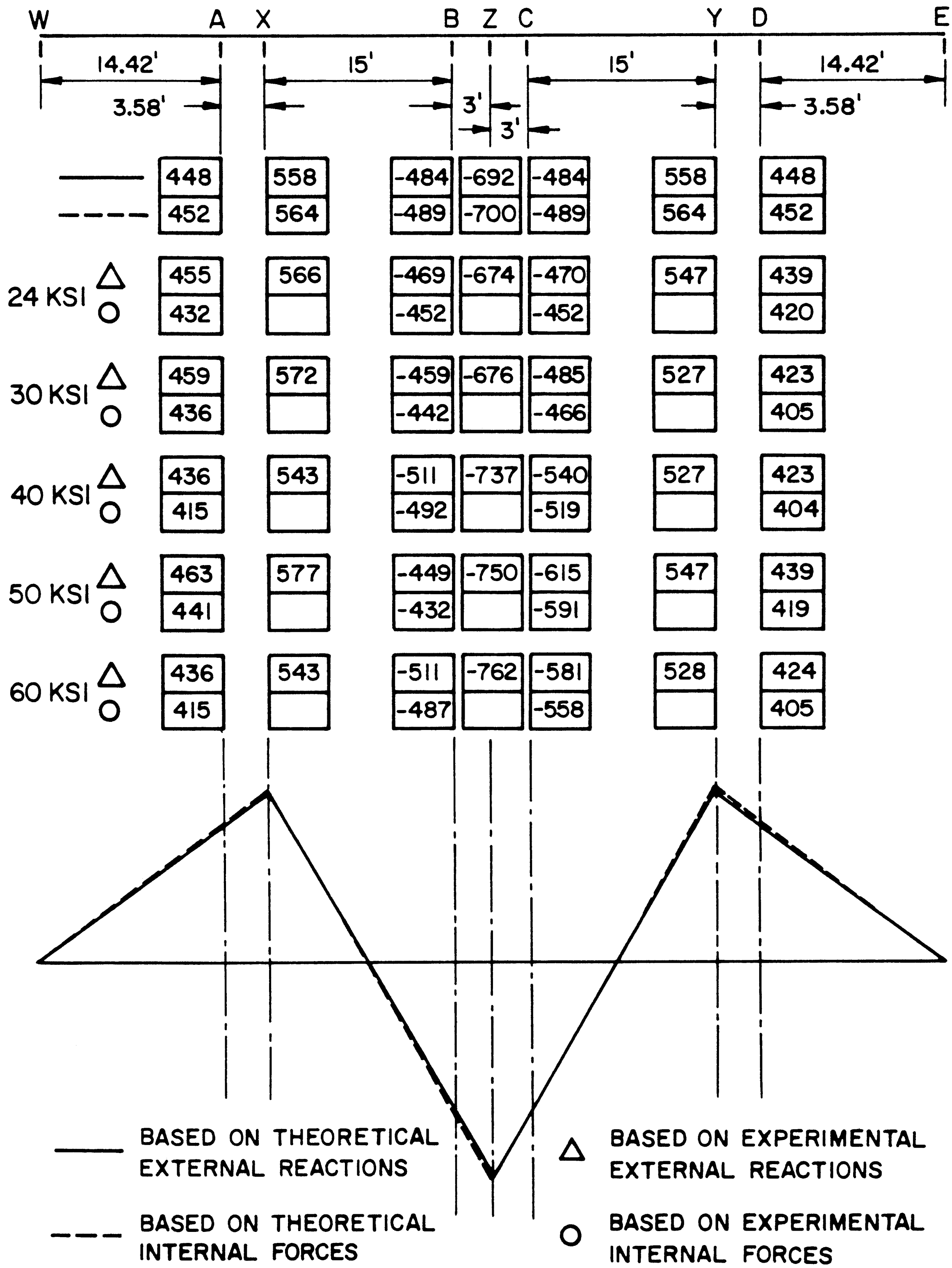

FIG. 6.9 TOTAL MOMENTS (FT-KIPS) FOR CONDITIONING LOADS OF 100 KIPS PER SPAN CAUSING NOMINAL MAXIMUM STEEL TENSIL STRESSES AS SHOWN

and D respectively. At the negative moment sections near the center bent support the differences at Section B are similar, being 2 to 6%, but are somewhat larger at Section C for the higher load levels, of 40 ksi and above, reaching a maximum difference of 20% for the 60 ksi conditioning load. The agreement between experiment and theory for moments based on internal forces is adequate, but variable with no systematic pattern of differences being discernible. Range of differences for Sections A, B, C and D respectively are 2 to 8%, 1 to 14%, 4 to 18% and 5 to 11%. In general the agreement is better at the lower conditioning load levels.

Second, comparing moments based on internal forces to those based on external reactions, which should give identical results, it is evident from Fig. 6.9 that for theoretical results, the agreement is excellent with differences of about 1% at all sections. For experimental values the agreement between external and internal moments is also close as should be expected. This is due to the modification procedure, described in Section 3.9, which was used to modify the experimental internal forces to approximately satisfy equilibrium with external forces and reactions.

The transverse distributions of the total moments at Sections A, B, C and D are illustrated in Fig. 6.10. Recalling that a theoretical distribution of 16.5, 22.4, 22.4, 22.4 and 16.5% for girders 1 to 5 would be obtained for a uniform stress distribution across the entire section, it can be seen that theoretical values and experimental values for all conditioning load levels shown in Fig. 6.10 approach this distribution. Agreement between theory and experiment is generally within 1 to 2% of the total moment for the percentage taken by any girder.

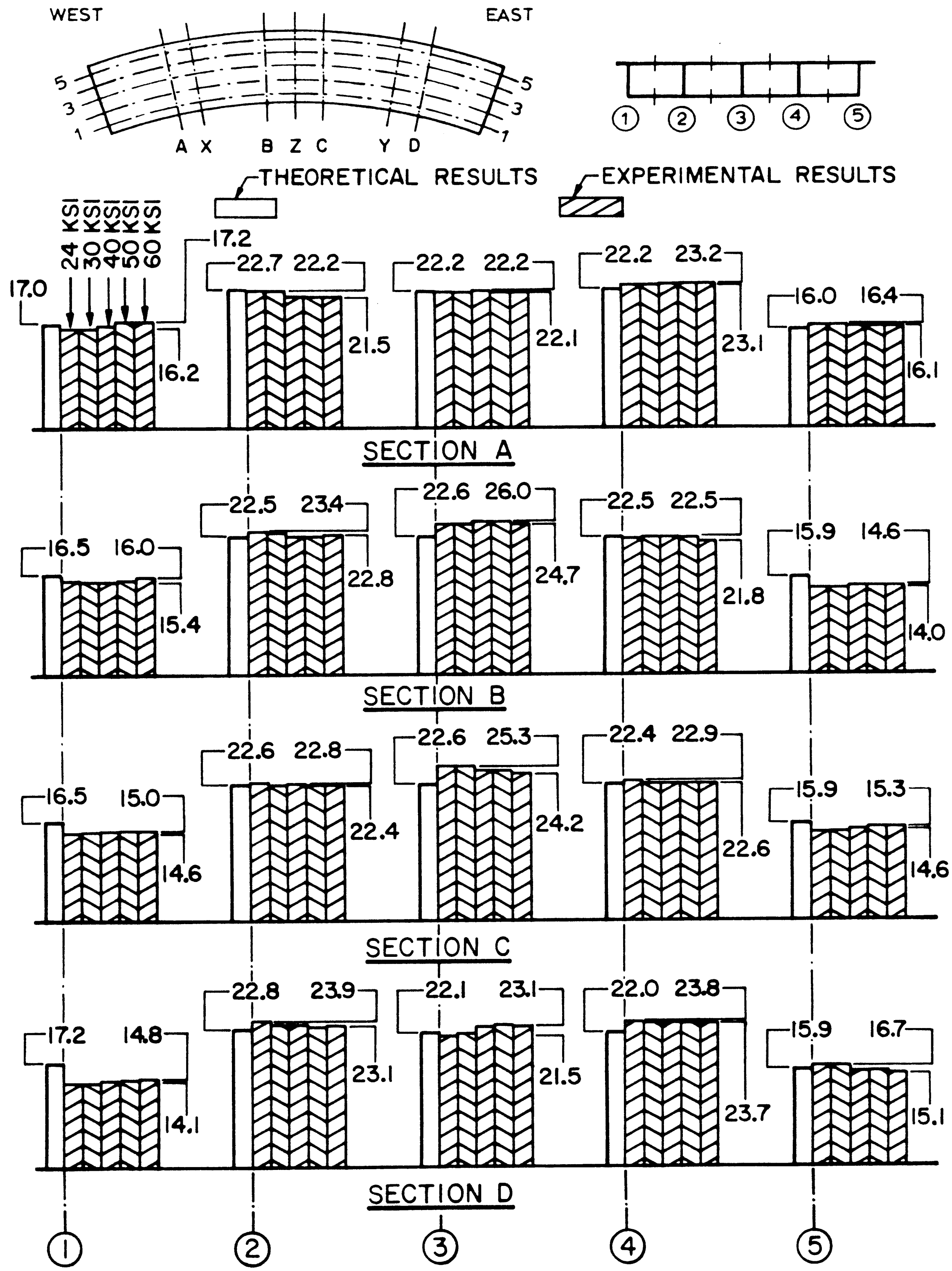

FIG. 6.10 PERCENTAGES OF TOTAL MOMENT AT A SECTION CARRIED BY EACH GIRDER FOR CONDITIONING LOADS (MOMENTS TAKEN ABOUT GROSS CROSS-SECTION NEUTRAL AXIS)

Little change in the experimental distribution occurs as the conditioning load level is increased from the 24 to the 60 ksi cases.

6.3 Results for Point Loads After Conditioning Overloads

Detailed tabulation of theoretical and experimental results related to reactions, deflections, strains and moments are given in Vol. III for the ten basic point load combinations shown in Fig 5.11 of Vol. I (same as Fig 2.1 of Vol. III). These point loads were designed to give a total maximum stress of 24 to 30 ksi in the reinforcement in each case, subsequent to the application of the conditioning loads which brought the maximum stress level to 24, 30, 40, 50 and 60 ksi. All theoretical and experimental values have been normalized for purposes of comparison to total loads of 100 kips per span.

During each of the cases of application of a total point load at 1Y or at 5Y following the 24, 30, 40, 50 and 60 ksi conditioning loads a special sequence was followed (See Fig. 5.11 of Vol. I).

(1) Take zero readings on all gages and meters.

(2) Apply load in four increments (1/4, 1/2, 3/4, 1) to reach the full load and take readings after each increment.

(3) Remove full load in one increment to reach zero load and take readings.

For the above cases of point loading at 1Y or at 5Y, a series of graphs are given in Figs. 6.11 to 6.20 for the total east and center reactions, the deflections at 1Y and 5Y, and steel and concrete strains at 1D and 5D. Figs. 6.11, 6.12, 6.14, 6.15, 6.17 and 6.19 depict in separate graphs the response for each complete point load cycle after the 30, 40, 50 and 60 ksi conditioning loads. Figs. 6.13, 6.16, 6.18 and 6.20 superimpose on single plots the response for all of the point load cycles.

6.3.1 Total East and Center Reactions

Figures 6.11 and 6.12 indicate that the east and center reactions are linearly related to load for all cases shown and little difference exists between the results for the cycles after 30 and 60 ksi conditioning loads.

Figure 6.13 shows that the relation between reactions and applied point load remains essentially unchanged after all conditioning overloads up to 60 ksi. It can also be seen that theory accurately predicts the reactions.

6.3.2 Deflections at 1Y and 5Y

Figures 6.14 and 6.15 indicate that very little permanent deflection exists after each cycle of loading. Only slight nonlinearities occur in a few of the cycles.

Figure 6.16 shows that the deflections directly under a point load of 19.3 kips at 5Y or at 1Y increase if the load is applied after successively higher conditioning loads. This is due to the larger amount of cracking produced by the higher conditioning loads. Comparing the experimental values with those from theory based on an uncracked section, Fig. 6.16 indicates that the ratio of experimental to theoretical deflections is about the same for the deflection at 5Y due to a point load at 5Y, as it is for the deflection at 1Y due to a point load at 1Y. These ratios are for the former, 1.4, 1.8, 2.0, 2.2 and for the latter, 1.5, 1.9, 2.1, 2.2, for the point load of 19.3 kips applied

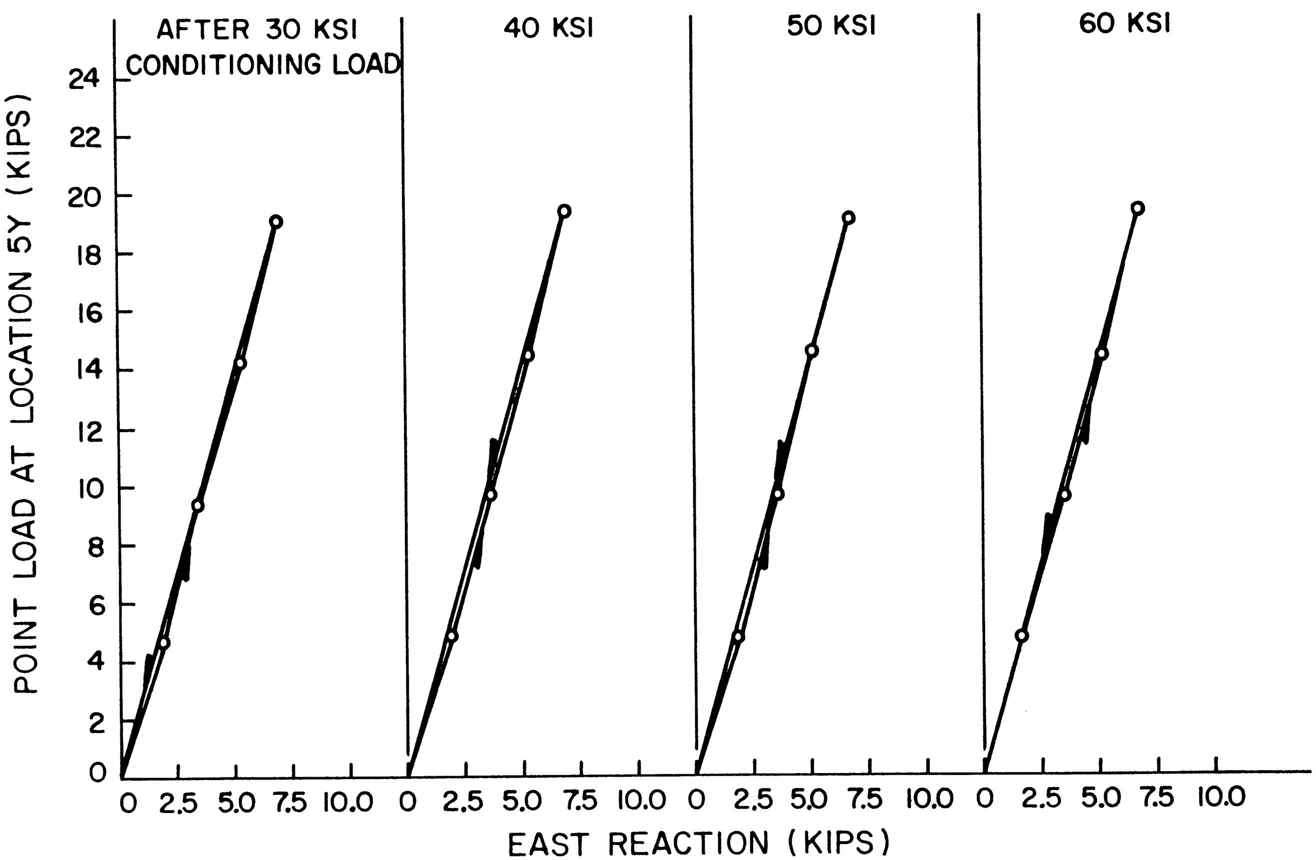

FIG. 6.11 EXPERIMENTAL TOTAL EAST REACTIONS (KIPS) DUE TO POINT LOAD AT 5 Y AFTER CONDITIONING LOADS

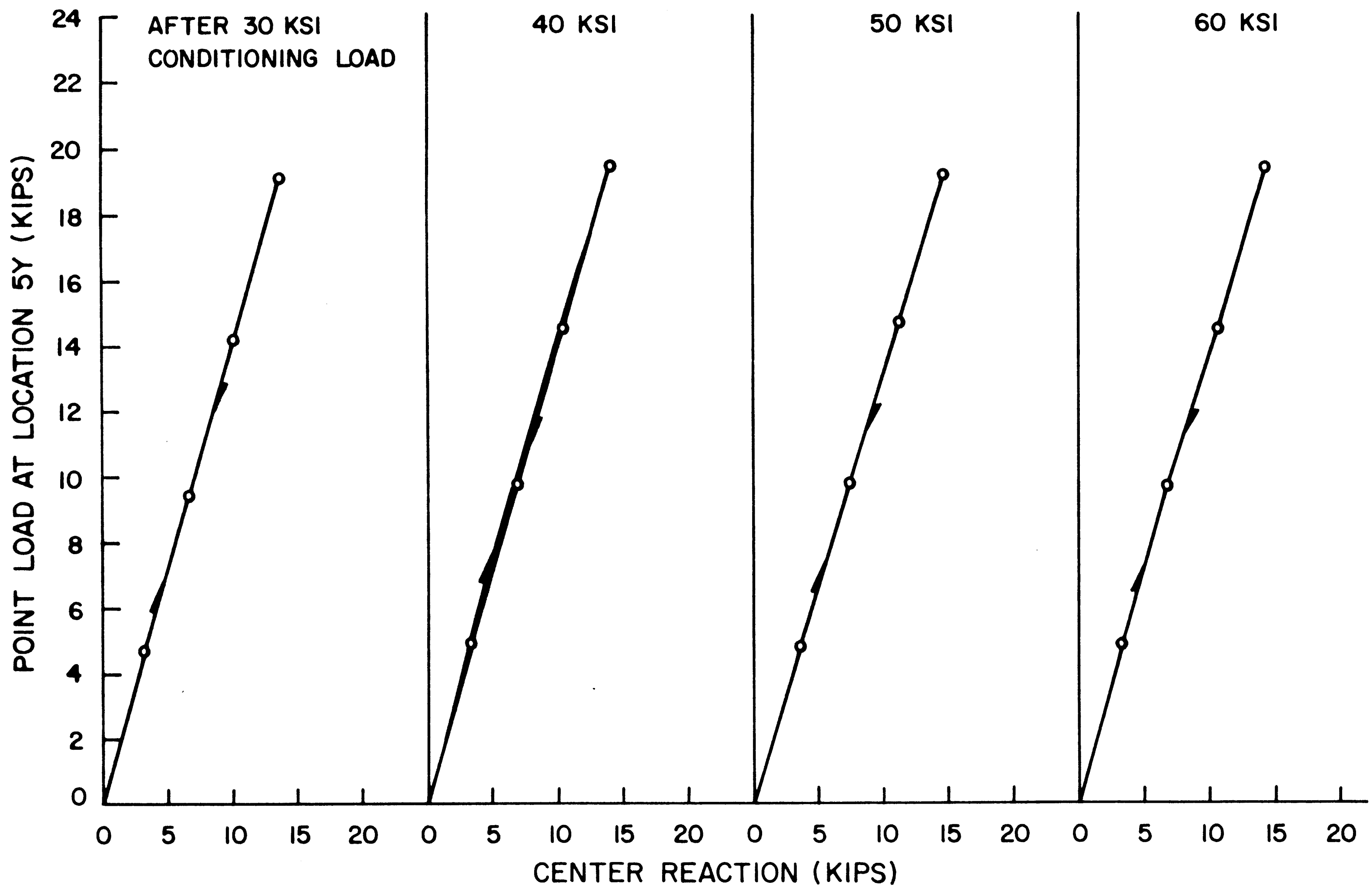

FIG. 6.12 EXPERIMENTAL TOTAL CENTER REACTIONS (KIPS) DUE TO POINT LOAD AT 5 Y AFTER CONDITIONING LOADS

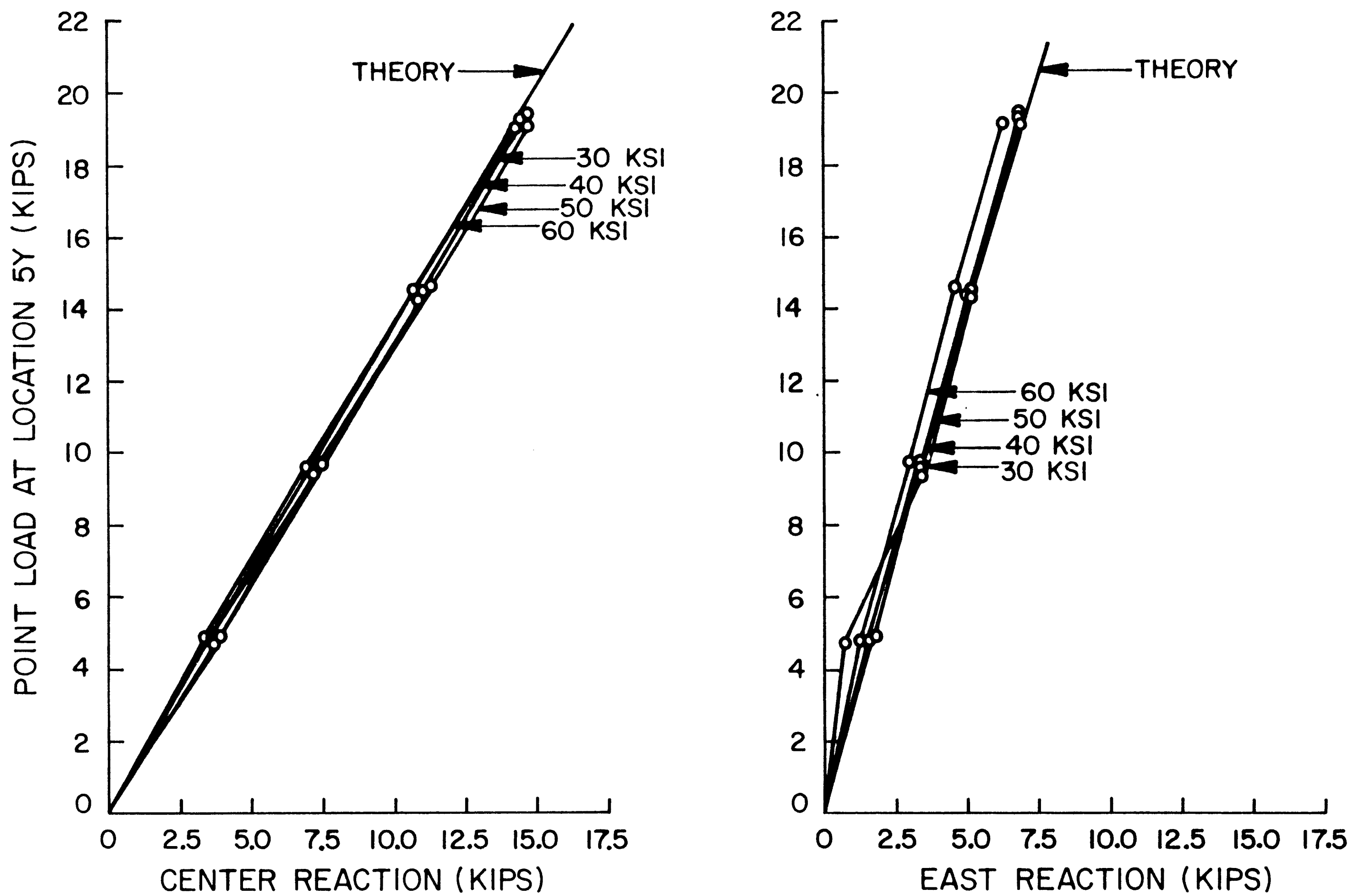

FIG. 6.13 CENTER AND EAST REACTIONS (KIPS) DUE TO POINT LOAD AT 5Y AFTER CONDITIONING LOADS

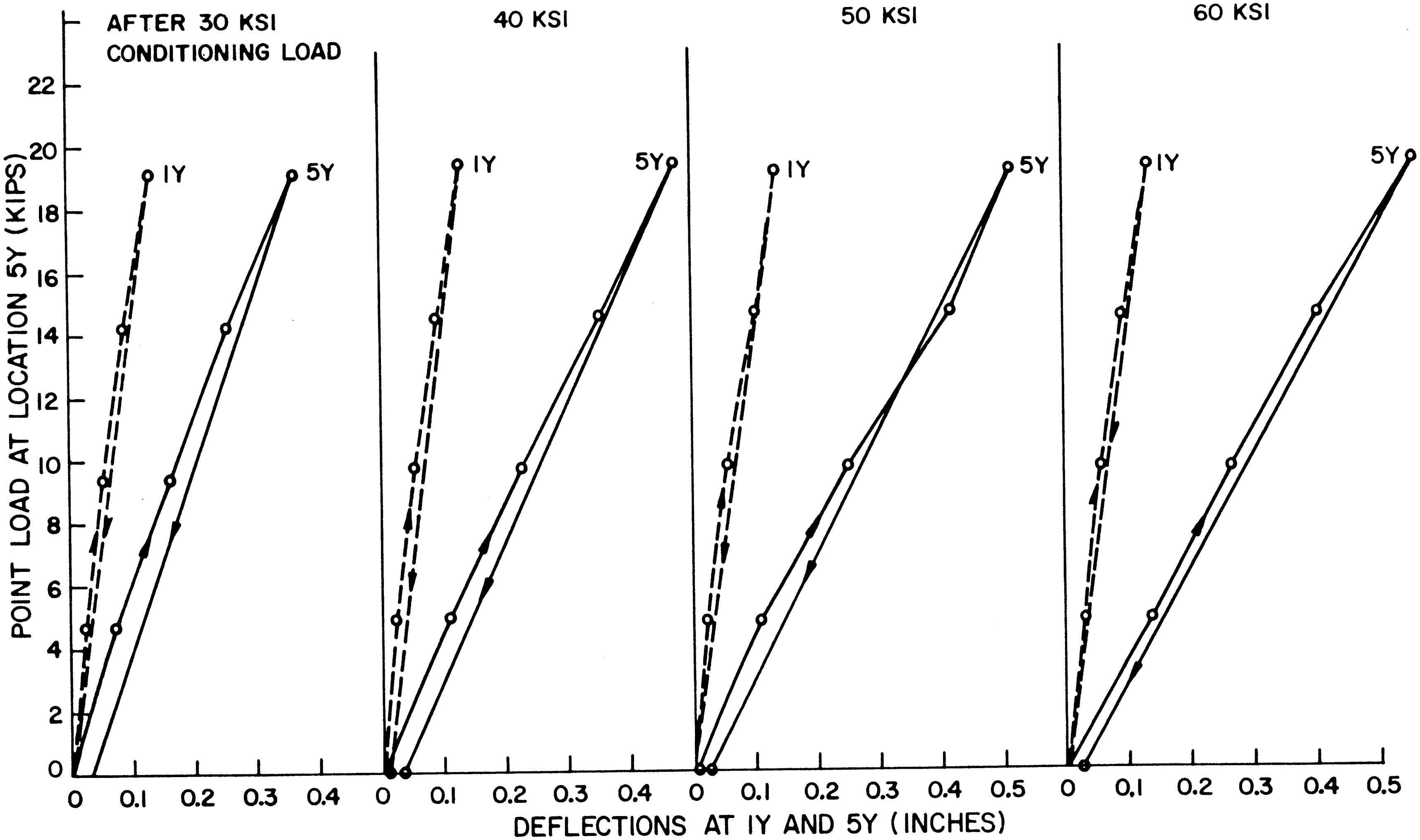

FIG. 6.14 EXPERIMENTAL DEFLECTIONS (INCHES) AT 5Y AND 1Y DUE TO POINT LOAD AT 5Y AFTER CONDITIONING LOADS

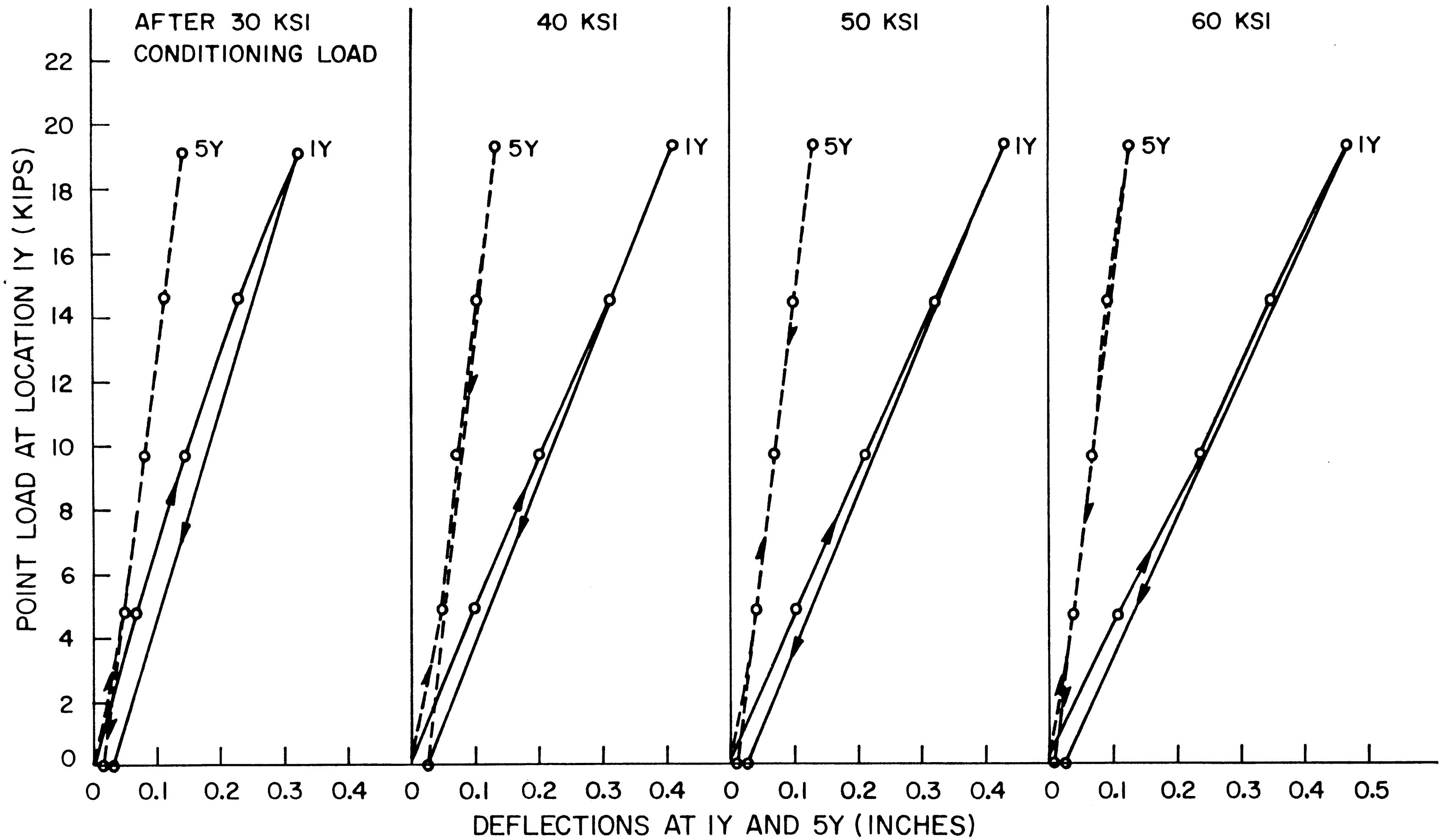

FIG. 6.15 EXPERIMENTAL DEFLECTIONS (INCHES) AT 1Y AND 5Y DUE TO POINT LOAD AT 1Y AFTER CONDITIONING LOADS

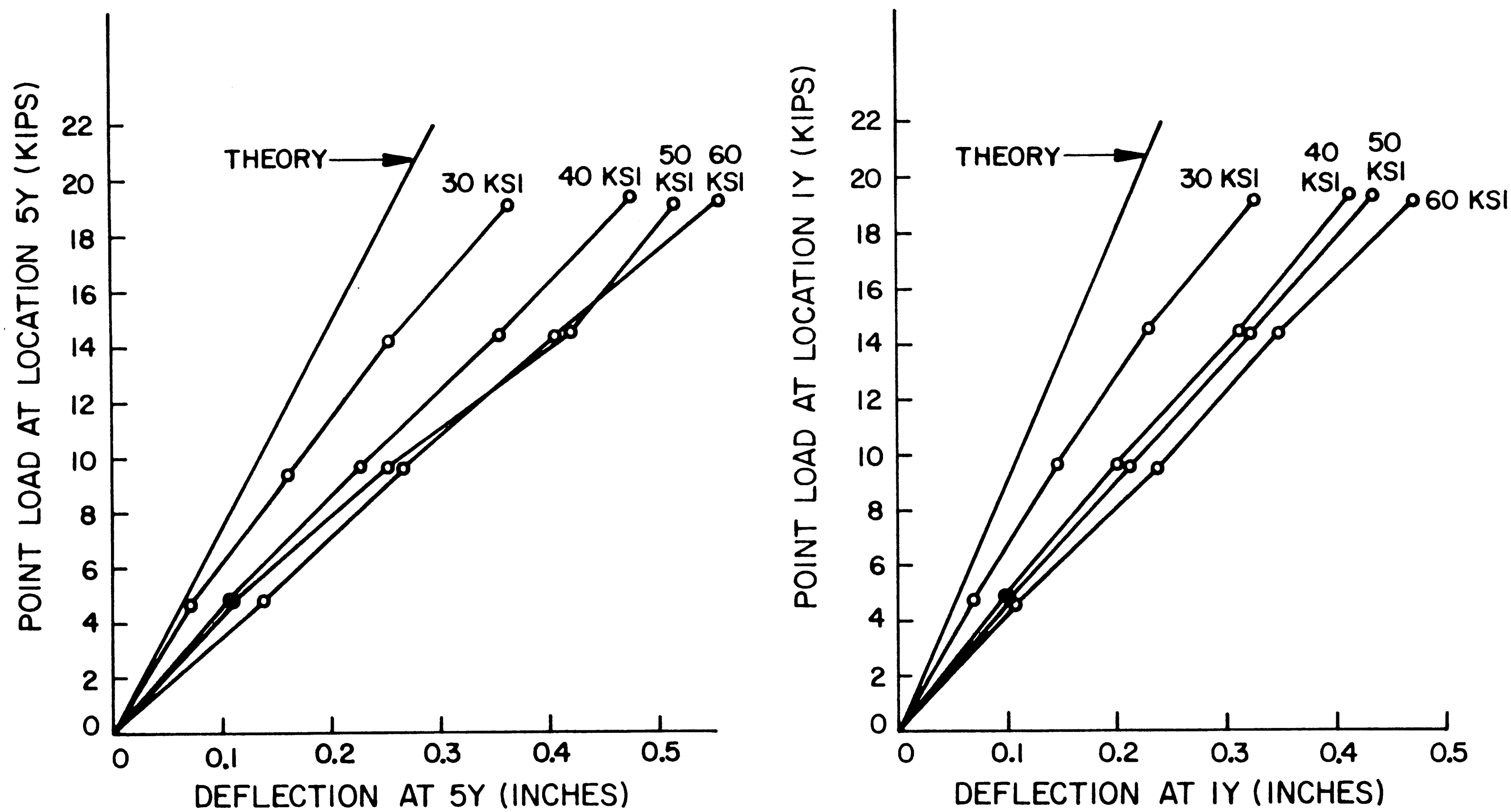

FIG. 6.16 DEFLECTIONS (INCHES) AT 5Y DUE TO POINT LOAD AT 5Y AND AT 1Y DUE TO POINT LOAT AT 1Y AFTER CONDITIONING LOADS

after the 30, 40, 50 and 60 ksi conditioning loads respectively. This increase in deflection, however, does not occur for the deflection at 1Y due to a point load at 5Y or the deflection at 5Y due to a point load at 1Y. This is shown clearly in Figs. 6.14 and 6.15, where the former deflection remains at about 0.11 in. and the latter remains at about 0.13 in. for point loads applied after all conditioning loads. These give ratios of experimental to theoretical deflections of about 1.1 and 1.3 respectively.

From the above, it may be concluded that after the 30 ksi working stress conditioning load, the theory based on uncracked section gives an acceptable prediction of the transverse distribution of deflections under point loads, with experimental values being 10 to 50% higher than theoretical values. However, after higher and higher conditioning overloads, the theory can no longer be used to predict the transverse distribution of deflections. As indicated above, after the 60 ksi conditioning load, the experimental deflection may be anywhere from 10% higher than theoretical values, at points some distance away from the point load, to 120% higher, at points directly under the point load.

6.3.3 Steel and Concrete Strains at 1D and 5D

For point loadings at 1Y, Figs. 6.17 to 6.20 depict the strains at 1D, near the point load, and at 5D, near the opposite edge of the bridge.

Figs. 6.17 and 6.18 indicate for the steel strains that some slight nonlinearities with load and some residual defermations occur at 1D near the point load, but at the opposite edge 5D, these are essentially negligible. In Fig. 6.18, it can be also seen that an increase

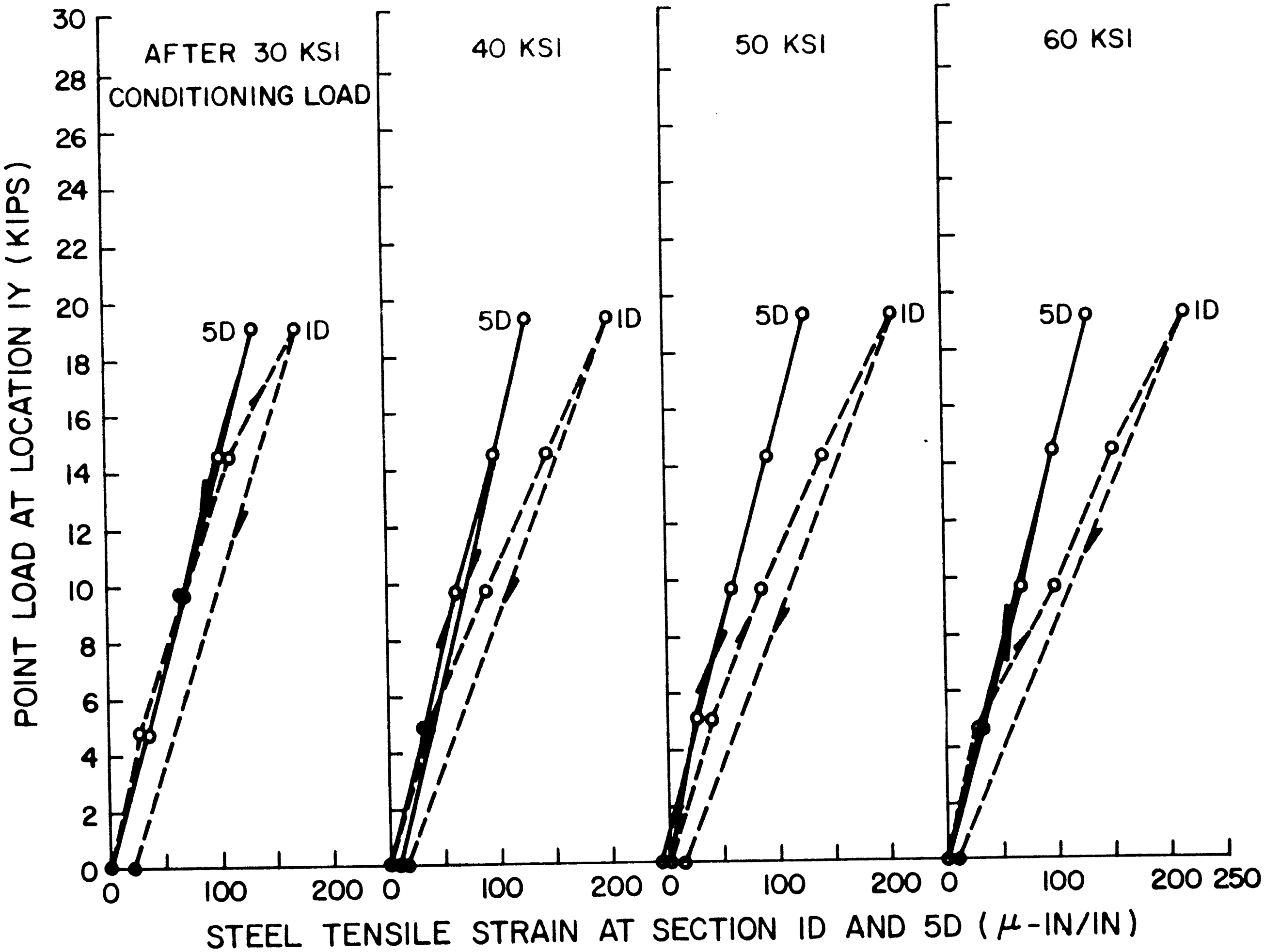

FIG. 6.17 EXPERIMENTAL STEEL TENSILE STRAINS (MICRO-INCH/INCH) AT 1 D AND 5 D DUE TO POINT LOAD AT 1 Y AFTER CONDITIONING LOADS

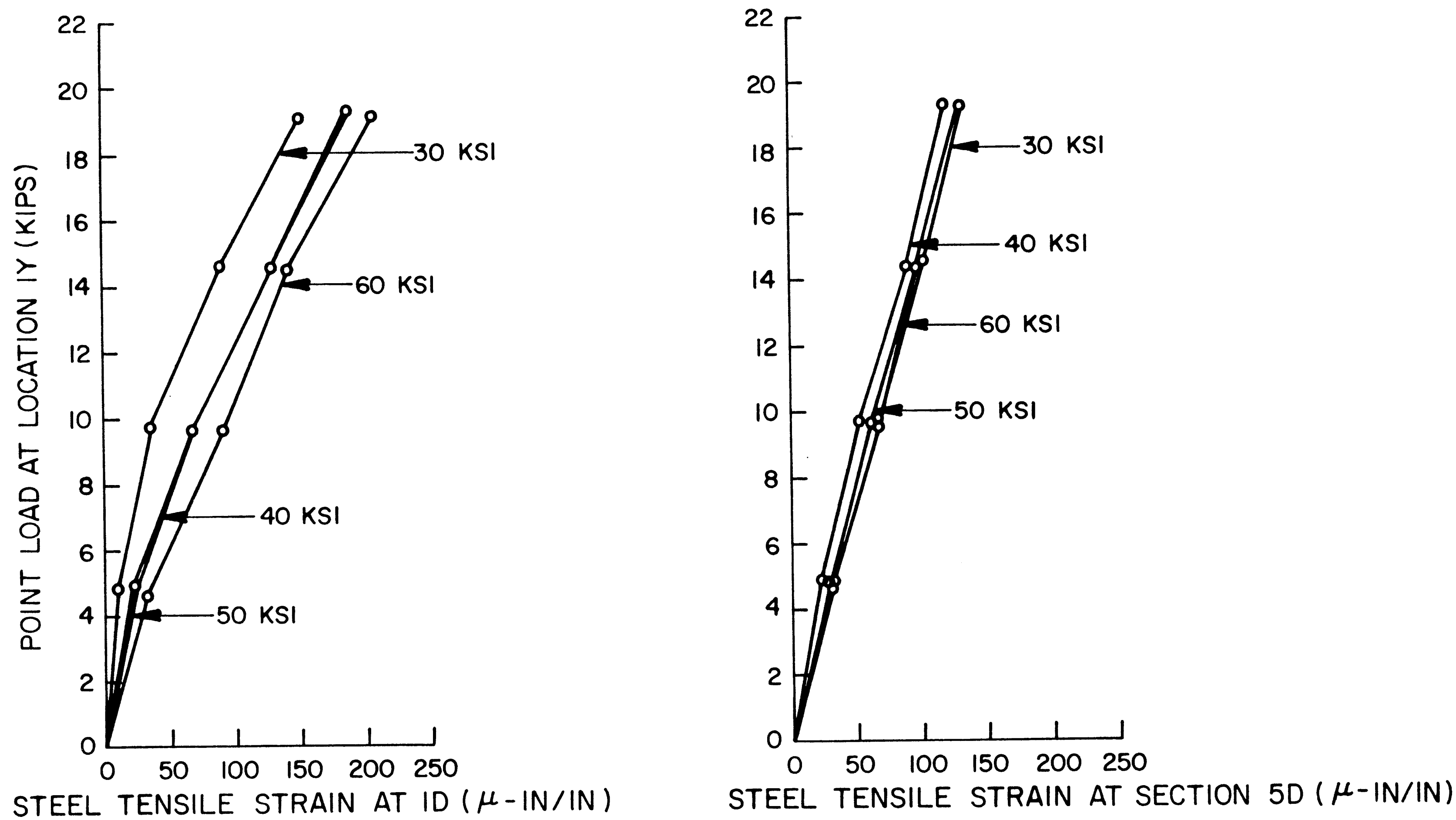

FIG. 6.18 EXPERIMENTAL STEEL TENSILE STRAINS (MICRO-INCH/INCH) AT 1D AND 5D DUE TO POINT LOAD AT 1Y AFTER CONDITIONING LOADS

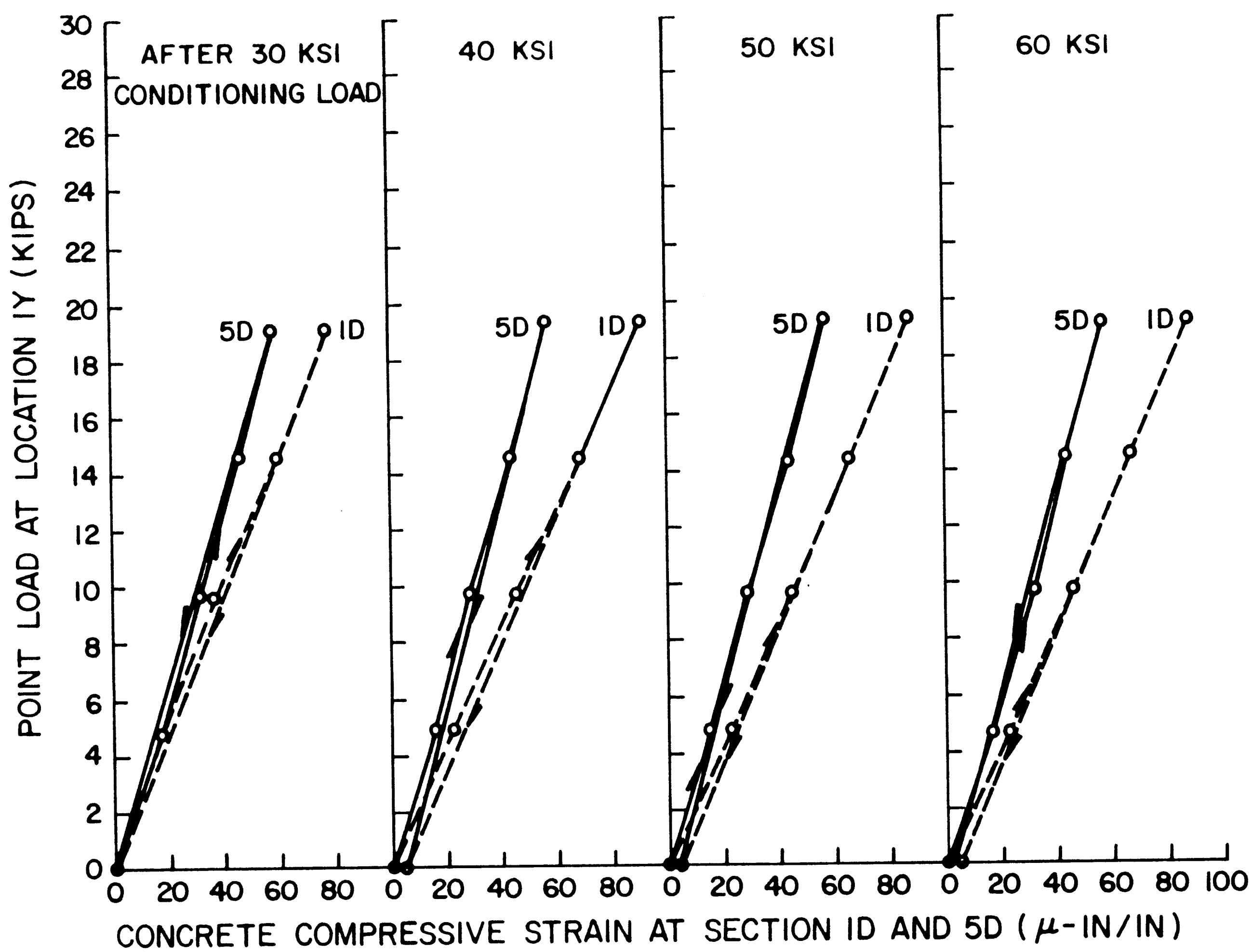

FIG. 6.19 EXPERIMENTAL CONCRETE COMPRESSIVE STRAINS (MICRO-INCH/INCH) AT 1 D AND 5 D DUE TO POINT LOAD AT 1 Y AFTER CONDITIONING LOADS

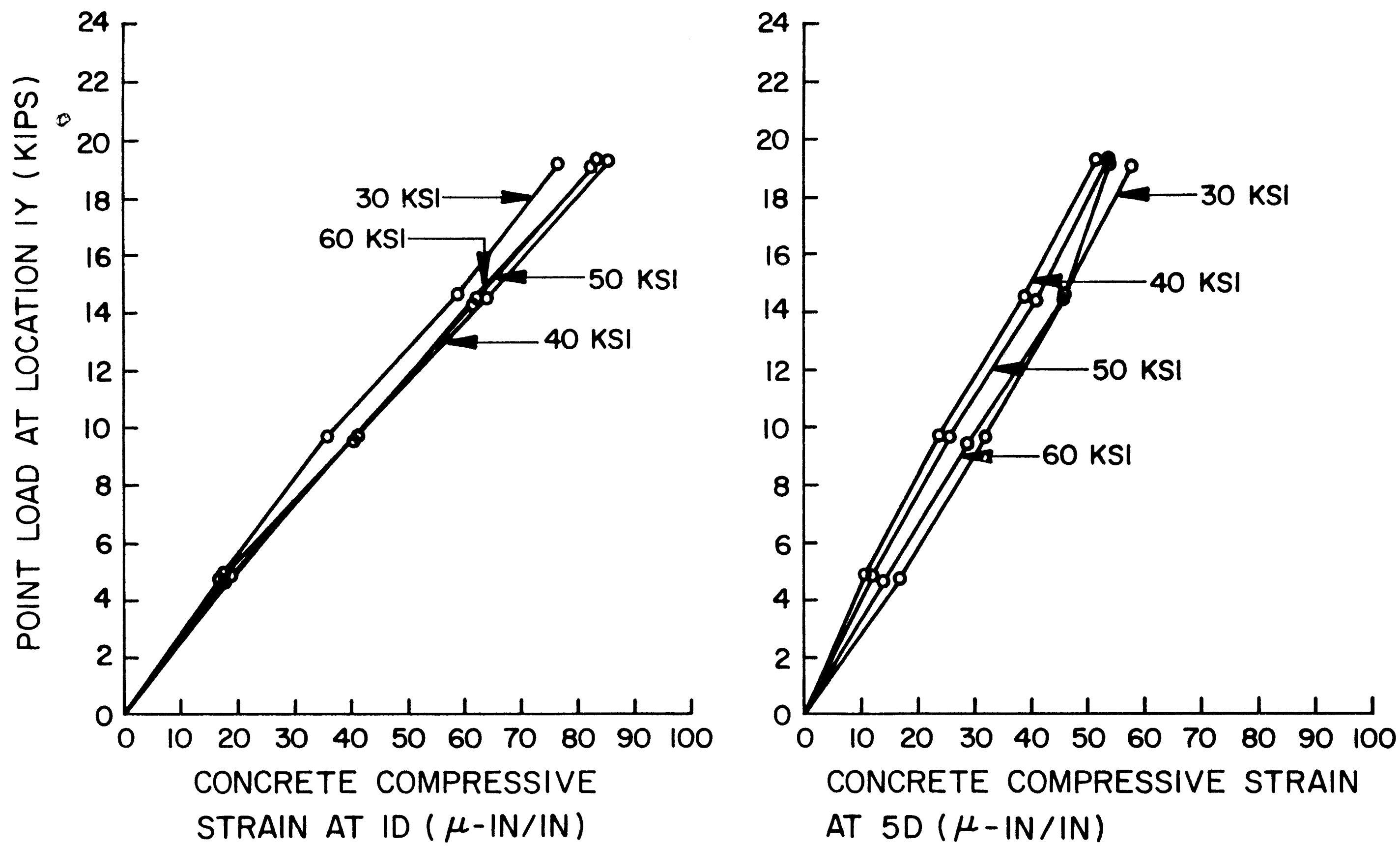

FIG. 6.20 EXPERIMENTAL CONCRETE COMPRESSIVE STRAINS (MICRO-INCH/INCH) AT 1 D AND 5 D DUE TO POINT LOAD AT 1 Y AFTER CONDITIONING LOADS

in steel strain per unit load occurs at 1D after higher conditioning loads, while at 5D this relationship remains practically unchanged and essentially linear.

Figs. 6.19 and 6.20 for the concrete strains, indicate that nonlinearities with load and residual deflections are small both at 1D and 5D for a point load applied at 1Y after all conditioning loads. In Fig. 6.20, it can be seen that the concrete strain per unit load at both 1D and 5D remains relatively constant after all conditioning load levels.

6.3.4 Moments

A comparison is given in Fig. 6.21 of the theoretical and experimental longitudinal distributions of the total moments at a section for a point load at 5Y designed to give a total maximum stress of 24 to 30 ksi in the reinforcement in each case, subsequent to the application of conditioning loads which brought the maximum stress level to 24, 30, 40, 50 and 60 ksi. All values have been normalized to a 100 kip point load at 5Y. Moments obtained from both external reactions and an integration of the internal forces at a section are given.

First, comparing experimental values with theoretical values, the agreement for moments based on external reactions is very good (within 1 to 4%) at Sections Y and D of the loaded span for point loads applied after all conditioning loads. But at Section C in the loaded span, where the external moment is very sensitive to changes in the measured east reaction, this agreement (1 to 4%) holds only until after the 40 ksi conditioning load level. After the 50 and 60 ksi conditioning loads the differences are much larger (10 and 20%). For the unloaded span at Sections A, X, B, the agreement between experimental and theoretical moments based on external reactions is within 10% for all cases except after the 50 ksi conditioning load. The agreement between experiment and theory for moments based on internal forces is adequate, but variable, with no systematic pattern of differences being discernible. Ranges of differences for Sections A and B in the unloaded span and C and D in the loaded span respectively are 1 to 19%, 3 to 25%, 1 to 15% and 1 to 13%.

Second comparing moments based on internal forces to those based on external reactions, which should give identical results, it is evident from Fig. 6.21, that the theoretical results are excellent with differences of about 1% at all sections except B where the difference is about 3%. For experimental values, the agreement between external and internal moments, at Sections C and D in the loaded span is generally quite good, within 1 to 3%, except for a few cases. At Sections A and B in the unloaded span, the differences are larger and more variable, reflecting the sesitivity of these experimental values.

The transverse distribution of the total moments at Sections A, B, C and D are illustrated in Fig. 6.22 for a point load at 5Y. At Section D, nearest the loaded midspan Section Y, the changes in the experimental distribution to each girder, after successively higher conditioning overloads, range from 1.0 to 2.3% of the total moment at the section. In terms of individual girder moments, the maximum percentage changes are 8% for interior girders and 10% for exterior girders. Theoretical values at Section D for girders 2, 3 and 5 are in good agreement with all experimental values generally differing by only 1 to 2% of the total moment on the section. However, for girders 1 and 4,

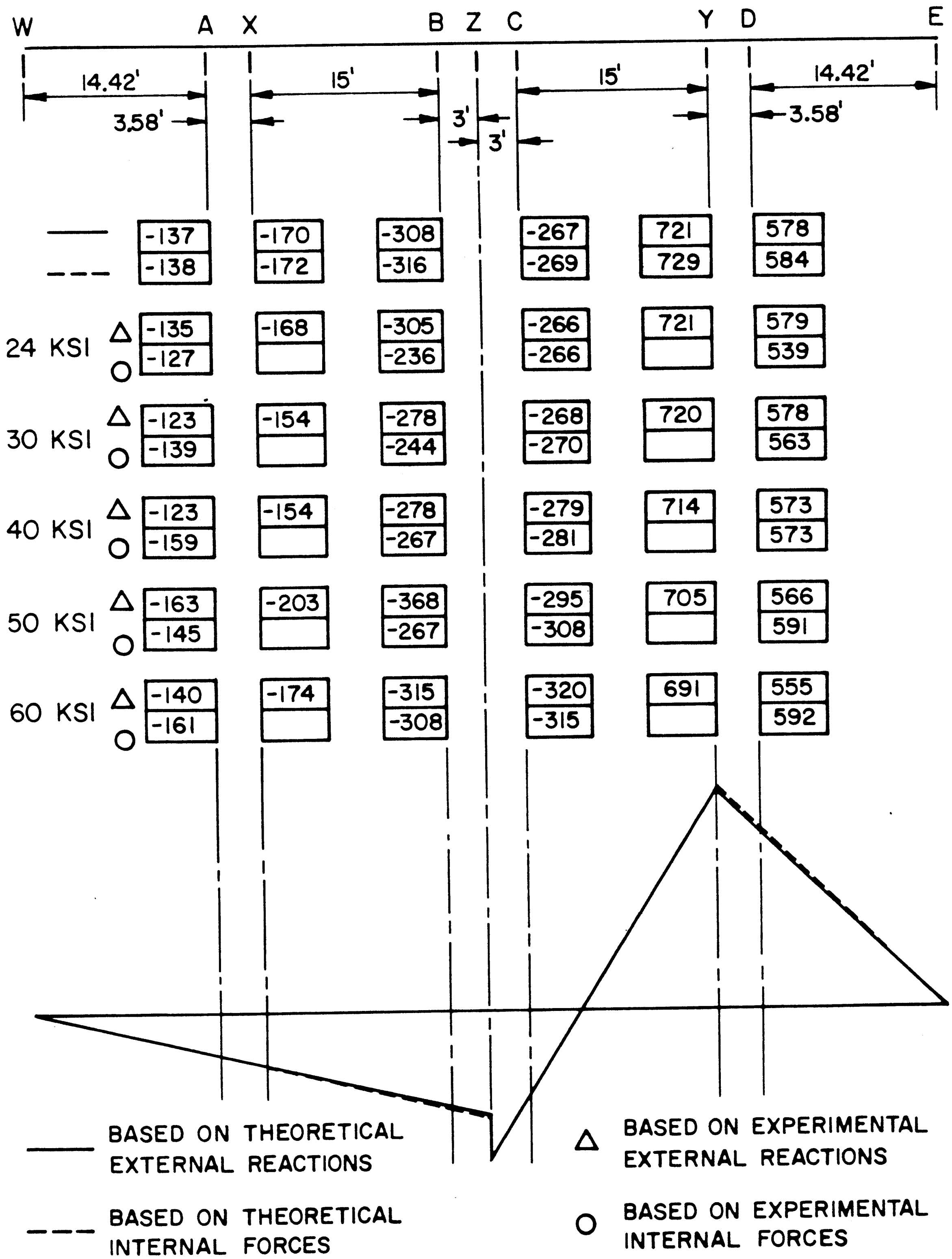

FIG. 6.21 TOTAL MOMENTS (FT-KIPS) AT A SECTION FOR NORMALIZED 100 KIP LOAD AT 5Y APPLIED AFTER CONDITIONING LOADS CAUSED NOMINAL MAXIMUM STEEL TENSILE STRESSES AS SHOWN

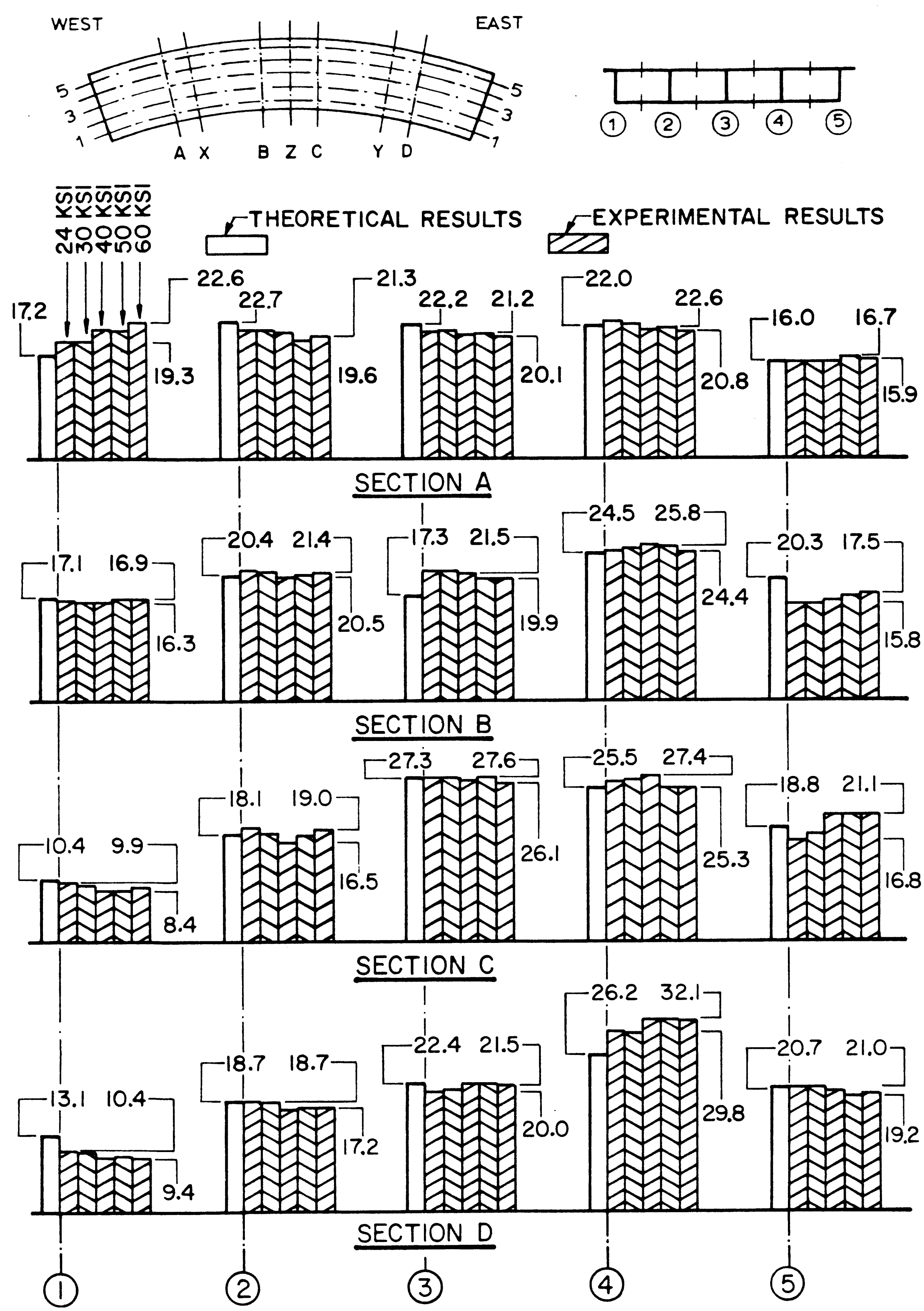

FIG. 6.22 PERCENTAGES OF TOTAL MOMENT AT A SECTION CARRIED BY EACH GIRDER FOR A POINT LOAD AT 5Y APPLIED AFTER CONDITIONING LOADS CAUSED NOMINAL MAXIMUM STEEL STRESS SHOWN (MOMENTS TAKEN ABOUT GROSS CROSS-SECTION NEUTRAL AXIS)

the maximum differences are larger, with theoretical values being 3.7% higher for girder 1 and 5.9% lower for girder 4. The same order of magnitude of changes in experimental values after successively higher conditioning loads and even smaller differences between theoretical and experimental values occur at Section C of the loaded span and at Sections A and B of the unloaded span. In general Fig. 6.22 shows that no significant differences occur in the transverse distribution of moments at each section after increasing conditioning loads have been applied.

If one considers the fact that the design for girder moments will be predicated on several wheel loads across the width of the bridge rather than a single load, it is apparent that the differences will be even smaller and approach those discussed in Section 6.2.4 for conditioning loads. Thus it would appear for practical design purposes, the theory can be used to adequately predict both the longitudinal distribution of the total moments at a section and the transverse distribution of the total moment to individual girders, even after overload conditions producing stresses of 30, 40 or 50 ksi.

6.4 Comparison of Results for Straight and Curved Bridge Models

Comparing results found for the curved bridge model with those of the straight bridge model [10, 11] for reactions, deflections, strains and distribution of moments for overload stress levels produced by increasing conditioning loads and for working stress point loads applied after each succesively higher conditioning load, it can be concluded that the general response of the two models was similar.

The total reaction at one end and the deflection at 5Y for the 30 and 60 ksi conditioning loads are presented in Fig. 6.23 for straight vs. curved bridge models. For the end reactions the theoretical values are almost identical. Experimental values for the straight bridge are very close to theory, while for the curved bridge, experimental values for the 60 ksi conditioning load are about 6% less than theory. Values for deflection in both Fig. 6.23 and 6.25 have not been adjusted for E_c, which averaged about 25% higher for the straight compared to the curved bridge during this loading period. Ratios of experimental to theoretical deflection for 30 ksi and 60 ksi conditioning loads are 1.6 and 2.2 for the straight bridge and 1.4 and 2.0 for the curved bridge indicating similar decreases in stiffness in the two bridges.

Percentages of total moment at a section carried by each girder for conditioning loads are shown in Fig. 6.24. For experimental results, the range of values found during the 24, 30, 40, 50 and 60 ksi conditioning loads is given. For both the straight and curved bridge models, experimental rsults are close to theoretical results and approached the 16.5, 22.4, 22.4, 22.4 and 16.5% for girders 1 to 5, which would be obtained for a uniform stress distribution across the entire cross-section.

The total reaction at one end and the deflection at 1Y due to a point load applied at 1Y after the 30 and 60 ksi conditioning loads are shown in Fig. 6.25 for straight and curved bridge models. The end reaction for the curved bridge is slightly higher, about 5%, than that for the straight bridge, as would be expected, due to the curvature of the bridge. Experimental values of end reactions for both bridges agree very well with theory. Ratios of experimental to theoretical deflection for point loads applied after the 30 and 60 ksi conditioning loads,

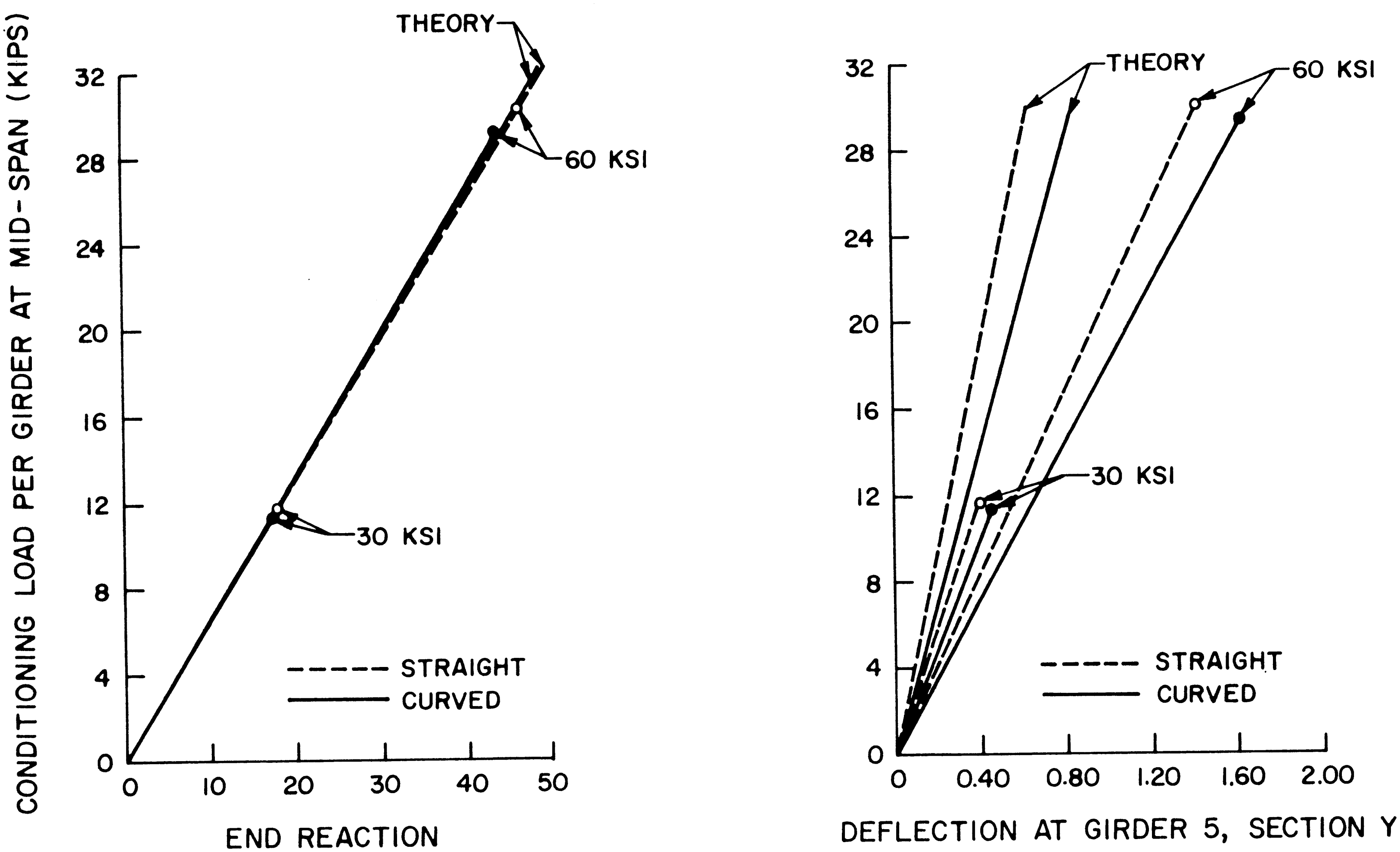

FIG. 6.23 END REACTION (KIPS) AND DEFLECTION (INCHES) AT 5Y FOR 30. AND 60 KSI CONDITIONING LOADS - STRAIGHT VS. CURVED BRIDGE MODELS

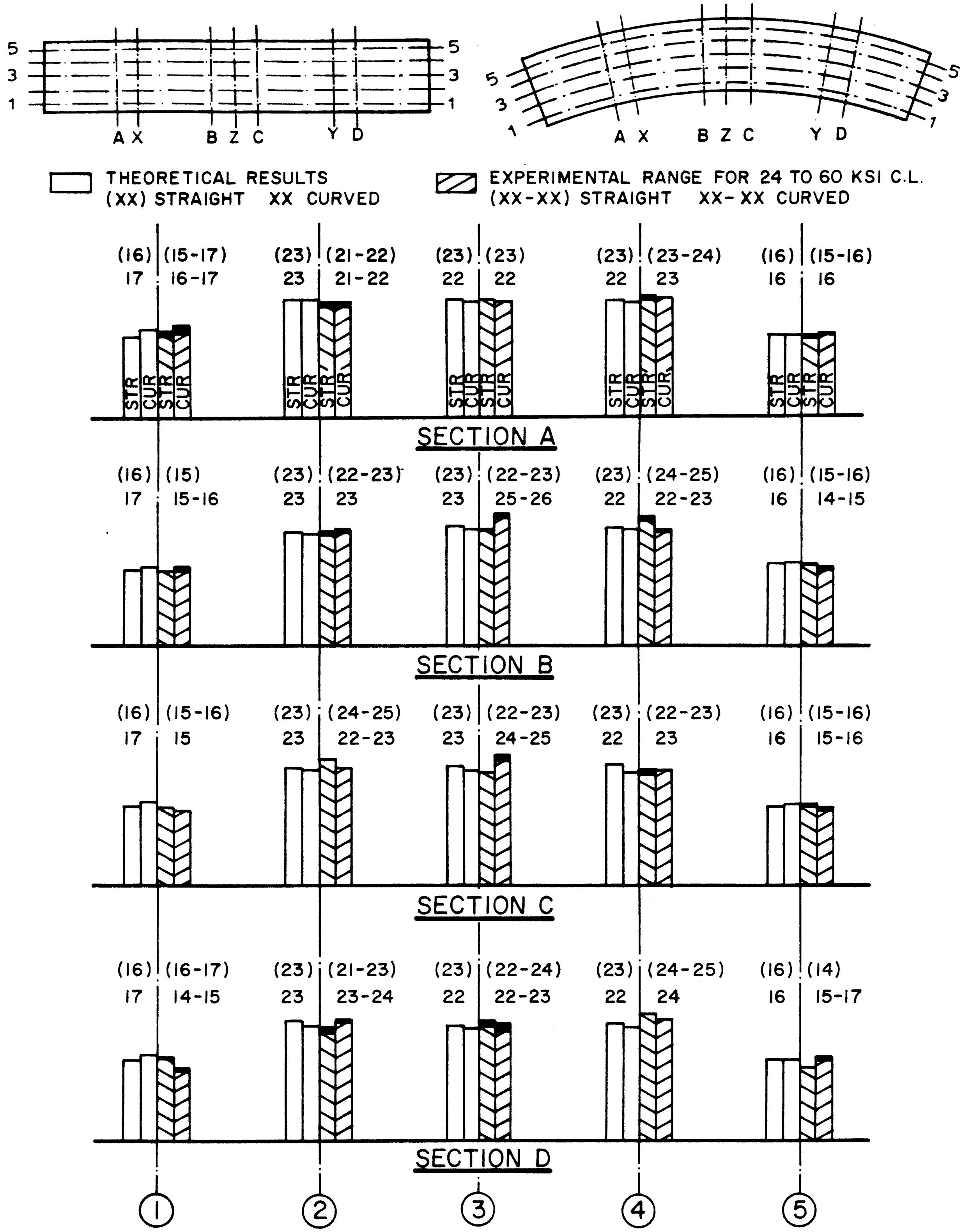

FIG. 6.24 PERCENTAGES OF TOTAL MOMENT AT A SECTION CARRIED BY EACH GIRDER FOR CONDITIONING LOADS -- STRAIGHT VS. CURVED BRIDGE MODELS

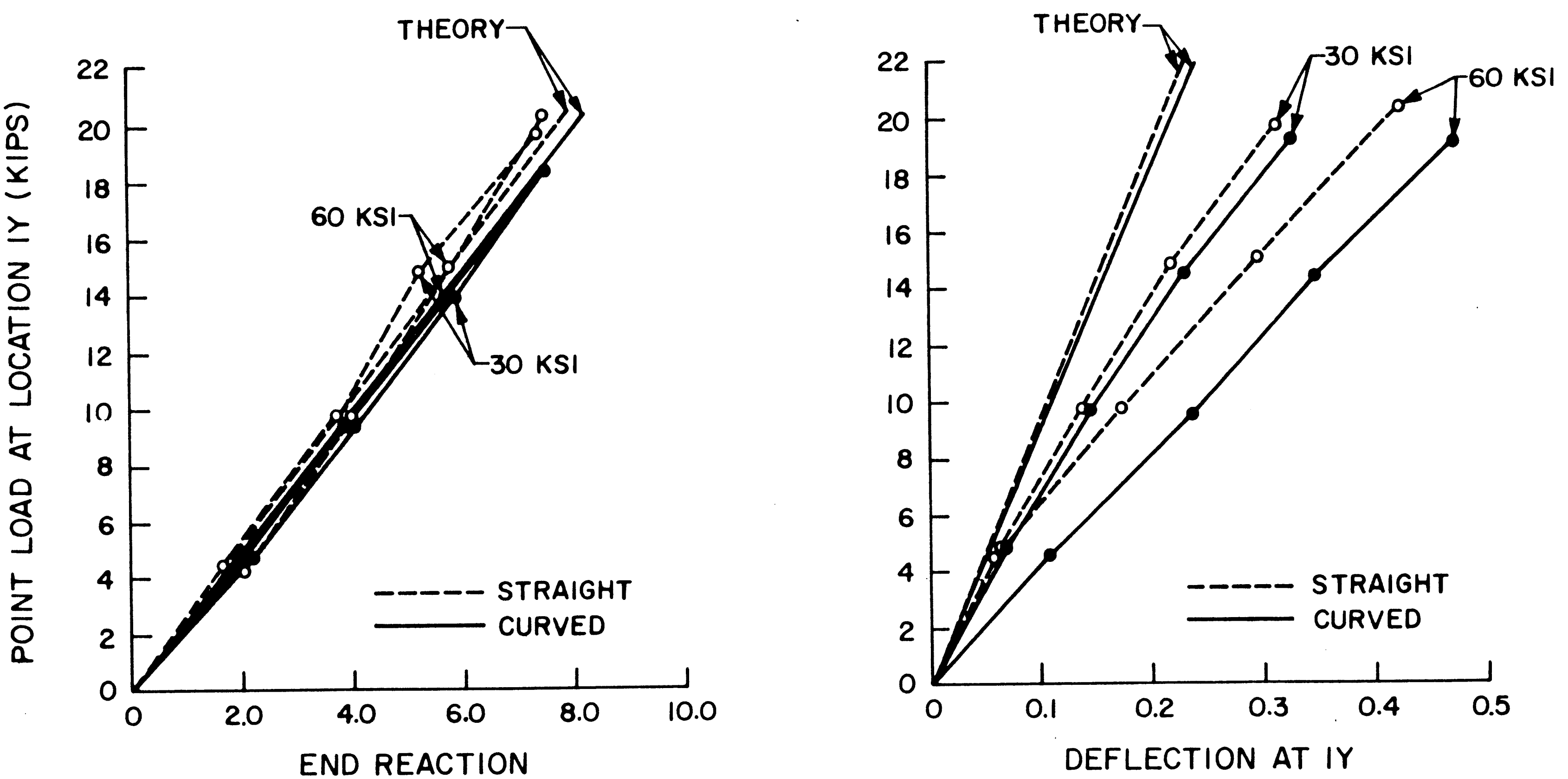

FIG. 6.25 END REACTION (KIPS) AND DEFLECTION (INCHES) AT 1Y FOR A POINT LOAD AT 1Y APPLIED AFTER 30 AND 60 KSI CONDITIONING LOADS -- STRAIGHT VS. CURVED BRIDGE MODELS

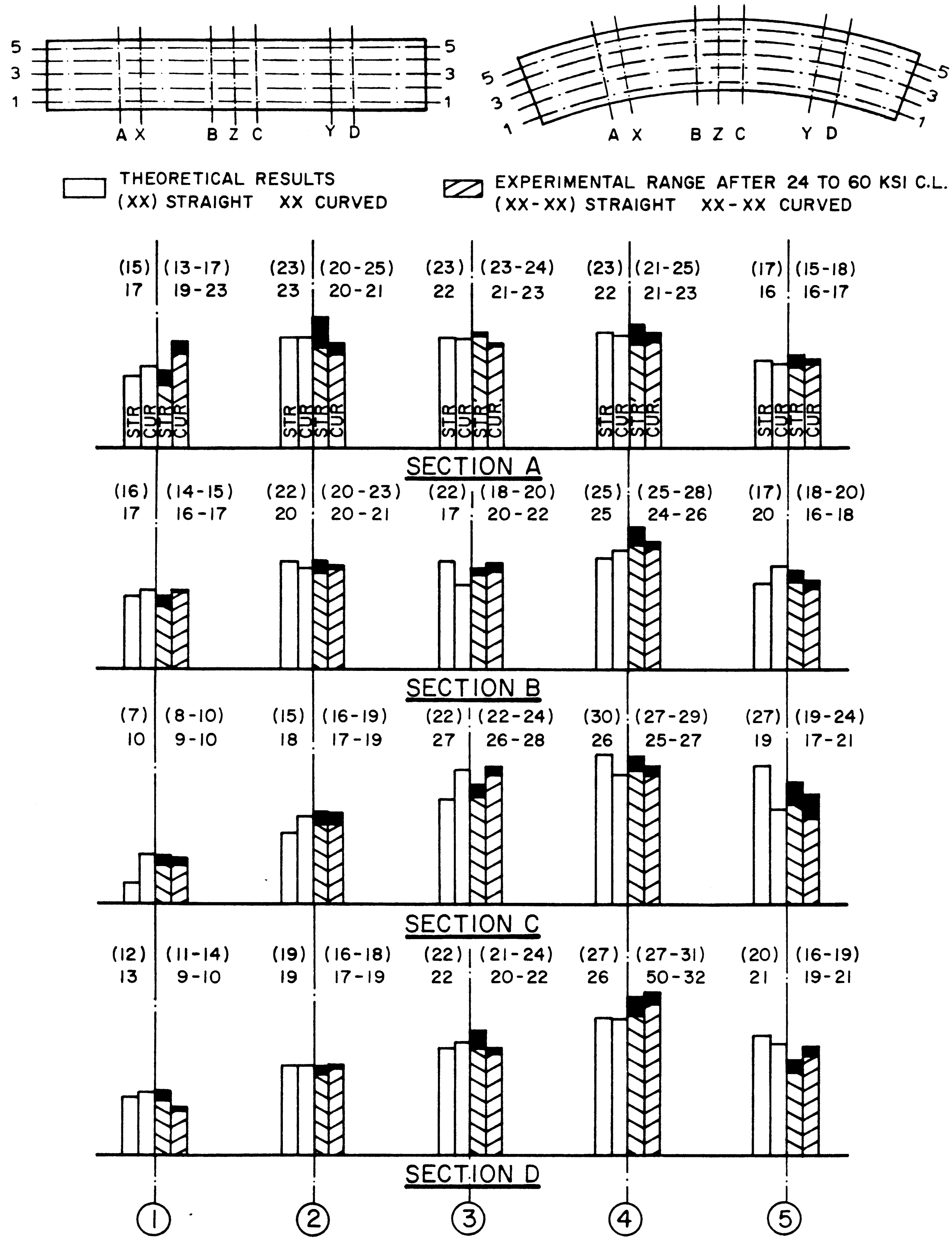

FIG. 6.26 PERCENTAGES OF TOTAL MOMENT AT A SECTION CARRIED BY EACH GIRDER FOR A POINT LOAD AT 5Y AFTER 24 TO 60 KSI CONDITIONING LOADS -- STRAIGHT VS. CURVED BRIDGE MODELS

Fig. 6.25, are 1.5 and 2.1 for the straight bridge and 1.5 and 2.2 for the curved bridge. These are similar to the values found for the conditioning loads, Fig. 6.23.

Percentages of total moment at a section due to a point load applied at 5Y after the 24, 30, 40, 50 and 60 ksi conditioning loads are given in Fig. 6.26. Experimental results appear to generally range within 1 or 2% of theoretical results except at 4B, 5C, 4D and 5D for the straight bridge. The maximum percentage of the total moment at a section taken by an individual girder, occurs at 4C in the straight bridge and close by at 3C in the curved bridge.

6.5 Summary

Detailed discussions of the results for the overload stress levels produced by increasing conditioning loads and for working stress point loads applied after each successively higher conditioning load have been presented. The most important conclusions for the curved bridge model studied are summarized below.

1. Total measured vertical reactions at the west end, center column and east end of the bridge are predicted by theory within 1 to 6% for all load levels.
2. Theory adequately predicts the magnitude ($\pm$ 20%) and distribution of deflections for loadings at the 30 ksi working stress level provided theoretical values based on an uncracked section are multiplied by a factor of about 1.4 to account for cracking.
3. At or after higher stress levels of 40, 50, or 60 ksi the deflections for a given load at some locations can

increase to a value as high as 2.2 times the theoretical value. In addition the theory can no longer be used to accurately predict the distribution of deflections under point loads. After the 60 ksi conditioning load, values ranging from 1.1 to 2.2 times the theoretical value were found for points some distance away and directly under the point load respectively.

4. For concrete strains, an essentially linear load vs. strain curve continues to exist at all load levels, with little change in the slope of these curves. For steel strains, an essentially linear load vs. strain curve also continues to exist at all load levels except for some small non-linearities in strains directly under single point loads. The slope of these curves tend to increase under heavier load levels, reflecting the increased cracking of the section.
5. The longitudinal distribution of total moments at a section as calculated from external reactions are adequately predicted (within 1 to 6% generally) by theory for sections A and D at all load levels. Values at Sections B and C are more sensitive to slight changes in external reactions and thus may differ from theory by larger amounts after overload stress levels of 50 ksi.
6. The longitudinal distribution of total moments at a section as calculated from internal forces indicates greater variations between experiment and theory especially after the higher conditioning load levels.
7. Changes in the transverse distribution of moments at a sec-

tion under uniform loads across the width of the bridge, such as the conditioning loads are small (less than 1% generally) for all overload stress levels. These changes are much greater for single point loads applied after the above conditioning loverloads and can range generally from 1 to 4% of the total moment at the section for individual girder moments themselves from 5 to 20%.

8. Theoretical calculations based on the CELL program predict the transverse distribution of moments under uniform loads very accurately and under point loads within the same ranges as described in 7.
9. The general response of the curved bridge model under increasing conditioning loads and for working stress point loads applied after each higher conditioning load was very similar to that observed for the straight bridge model tested earlier [10, 11].

7. REVIEW OF STRUCTURAL RESPONSE DURING LOAD HISTORY OF BRIDGE MODEL

7.1 Strain History During Construction Phase

With the intent of monitoring the concrete and steel strains during the construction phase up to the time the dead load was applied, strains in a number of selected concrete strain meters and weldable strain gages were recorded using an SR-4 strain indicator and a Carlson strain meter box. Measurements were taken for girders 1, 3 and 5 at all instrumented sections, both in top and bottom slabs. Due to problems with the instrumentation, the monitoring was not begun until 18 days after the bottom flange and webs were cast. These readings had to be discontinued three weeks prior to the removal of the shoring, in order to allow sufficient time to make the connections for all gages to the Low Speed Scanner Unit prior to the application of the dead load.

The resulting steel strain data during the construction phase for the weldable gages on the steel reinforcement are presented in Fig. 7.1. The close agreement between the results for girders 1 and 5 indicates a symmetric distribution of shrinkage strains over the cross section. At Section D the gage at girder 5 was damaged during construction and gave unreliable results. At this section the results from girder 3 are therefore plotted, and indicate a similar pattern with time, but smaller strains in the center girder 3 as compared to the two exterior girders. The same tendency was also found at Section A. The lack of absolute zero readings for Sections A and D makes it difficult to estimate the total accumulated strain at the end of the monitoring period, but it should be noted that the strain rate was significantly higher in the bottom slab at Sections A and D than in the top slab at

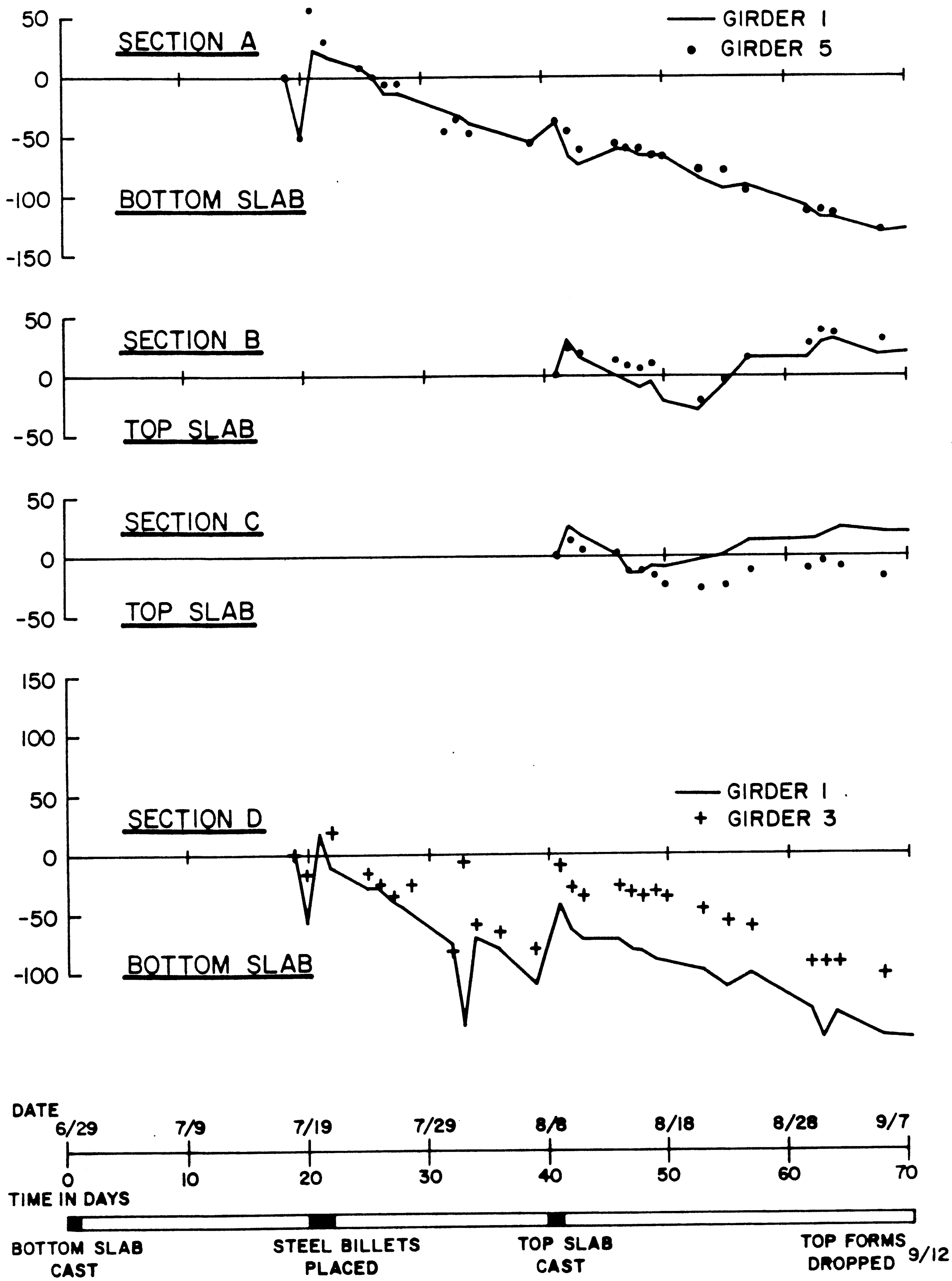

FIG. 7.1 HISTORY OF STEEL STRAINS PRIOR TO APPLICATION OF DEAD LOAD

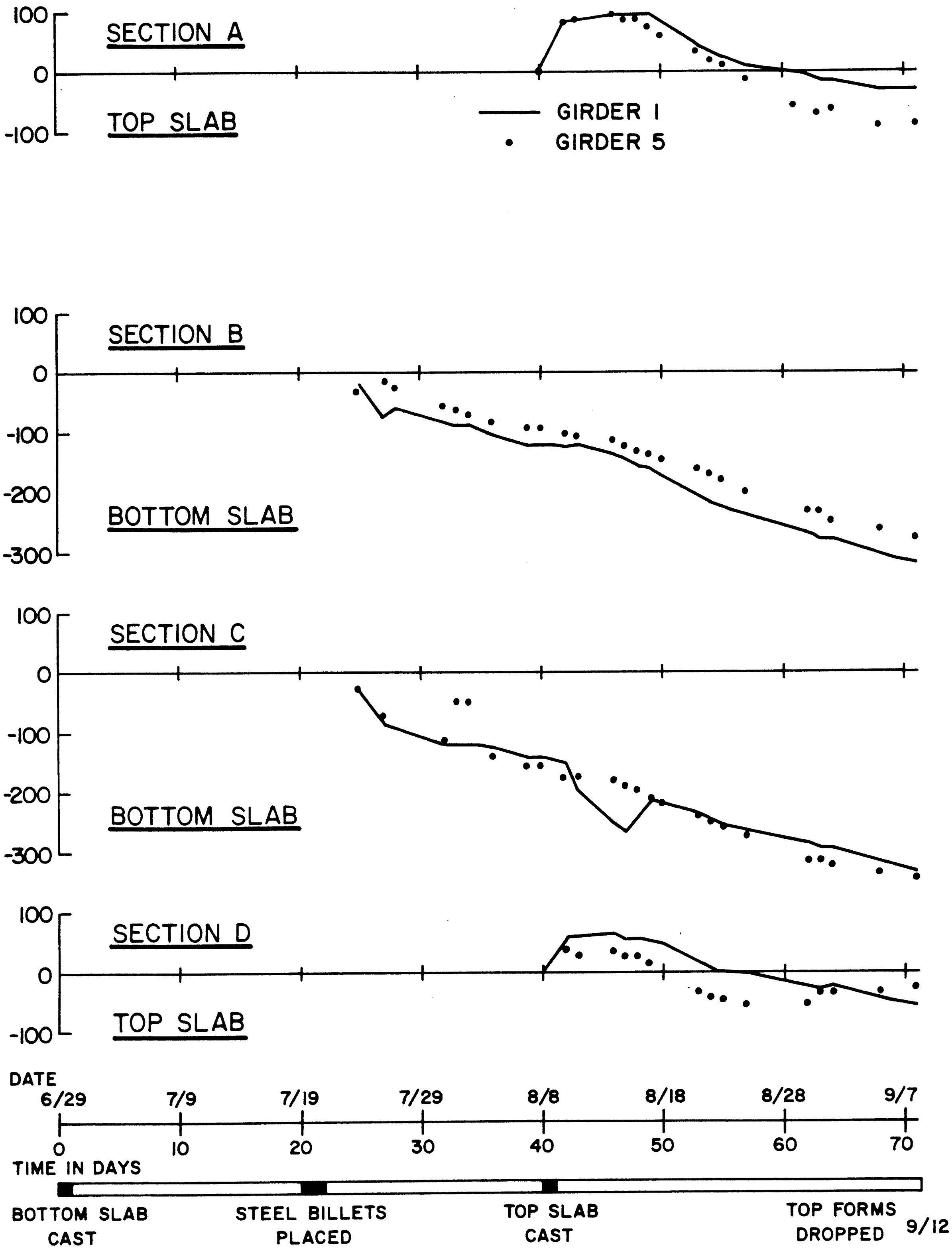

FIG. 7.2 HISTORY OF CONCRETE STRAINS PRIOR TO APPLICATION OF DEAD LOAD

Sections B and C. This is caused by the constraints imposed on the top slab by the bottom flange and webs which were cast 40 days prior to the top slab.

Fig. 7.2 gives the strain data for the concrete meters in girders 1 and 5 at all instrumented sections. Again very close agreement is found between the two girders, and a higher strain rate is again observed in the bottom slab at Sections B and C than in the top slab at Sections A and D. The maximum strain readings for the concrete, Fig. 7.2, are about twice as large as those in the steel reinforcement, Fig. 7.1.

A study of the strains in Figs. 7.1 and 7.2 seems to indicate a relatively symmetrical behavior in the two spans during the 52 day time interval covered. The effect of the transverse diaphragm at Section X does not significantly influence the strain distribution due to differential shrinkage.

7.2 Strain History Under Sustained Dead Load

While the pre-dead load behavior of the bridge model was monitored using a strain gage indicator and Carlson box, the variation of dead load strains with time was measured using the Low Speed Scanner Unit. Before and after each load phase a set of dead load readings was taken relative to the condition immediately prior to the removal of the shoring and formwork. This latter condition was taken as a reference absolute zero for all subsequent readings. Thus, total dead load strains and deflections are plotted in Figs. 7.2 to 7.8 for the entire testing period from removal of shoring to ultimate loading to failure. This occupied a total time interval of 119 days.

The steel strain data for the undiaphragmed east span are given in Fig. 7.3 for girders 1 and 5. The strain at Section D increased 75% for girder 1 and 55% for girder 5, while the increase was 60% and 105% respectively at Section C. It should be noted that most of this increase is caused by additional strains accumulated after each conditioning cycle, when the cracking gets successively more extensive and the concrete participates less and less in carrying any of the tensile stress. However, the stress redistribution in the bridge due to the creep in the concrete has little influence on the steel strains. This is clearly indicated by the near constant value of the strain between each of the conditioning load cycles.

Fig. 7.4 gives the concrete strains for girders 1 and 5, also at Sections C and D. Here the increase in strain over the test period of 119 days is significantly larger than for the steel strains. The final concrete strain values are about 2.5 to 5 times greater than the initial values. In contrast to the steel strains, the residual concrete strains caused by each of the conditioning load cycles are negligible. The major part of the increase is caused by the creep in the concrete, while the progressive cracking and deterioration of the bridge model have a much smaller influence. The increase in concrete strains with time appear to be of similar magnitude for girders 1 and 5, especially at Section D, Fig. 7.4.

It can be concluded from Figs. 7.3 and 7.4 that the rate of change of the concrete strains decreases with time, as would be expected. It should also be noted that the largest residual steel strains were observed after the 24 ksi conditioning loading, while the residual strains after the subsequent loadings were smaller and of equal

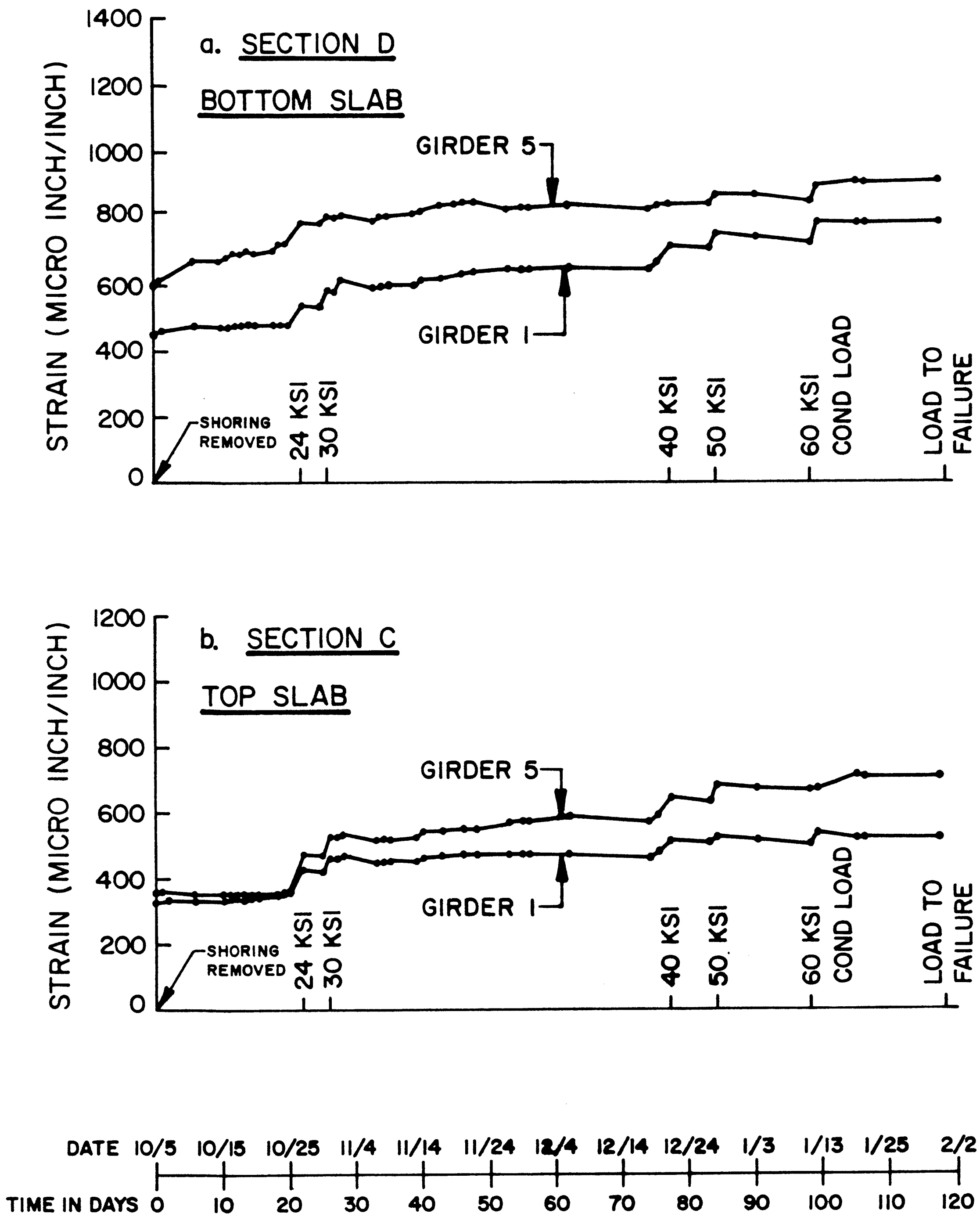

FIG. 7.3 HISTORY OF STEEL STRAINS UNDER SUSTAINED DEAD LOAD

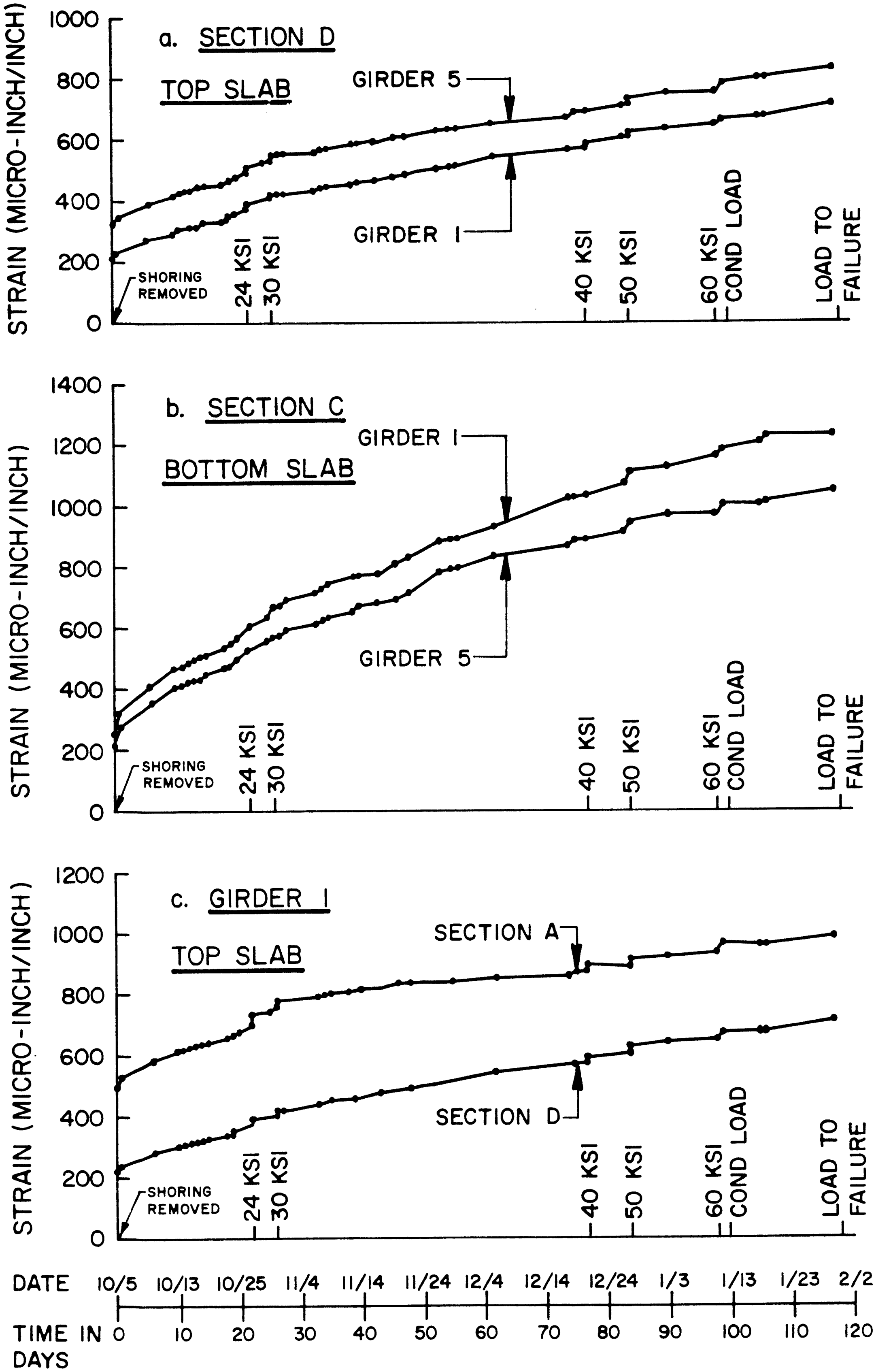

FIG. 7.4 HISTORY OF CONCRETE STRAINS UNDER SUSTAINED DEAD LOAD

magnitude. Both steel and concrete strains were larger in girder 5 than girder 1, except at Section C were the concrete strains in girder 1 exceeded those in girder 5 by about 20%.

A comparison of the behavior of the diaphragmed and undiaphragmed spans is made in Fig. 7.4 (c), giving the history for the concrete strains in girder 1. It is clear that the effect of the diaphragm has been to give a smaller initial strain level in girder 1 under dead load, while no such reduction was recorded for girder 5. However, the increases in concrete strains with time are of essentially the same magnitude in both spans as shown in Fig. 7.4 (c).

7.3 Deflections Under Sustained Dead Load

While the instantaneous deflections of the bridge model due to dead load were measured using scales and a precise surveyor's level, the deflections due to sustained dead load were measured using linear potentiometers and the Low Speed Scanner. A set of readings were taken before and after each load application for every load phase to determine any residual displacements.

The displacement data, as recorded at Sections X and Y, are presented for girders 1 and 5 in Fig. 7.5. As seen the instantaneous deflections were symmetric in the two spans, but outer girder 5 deflected more than inner girder 1. During the 22 day time interval until the first conditioning load was applied, creep caused a significant increase in the displacements. The displacement of outer girder 5 increased more rapidly at the diaphragmed midspan Section X than at the undiaphragmed midspan Section Y, while this tendency was less noticeable for inner girder 1. The average increase in displacement for the two girders was 55% over this 22 day period. The application of the 24 ksi conditioning load caused cracking of structure, which in turn resulted in residual displacement after the removal of the load. The same phenomenon was observed each time after a conditioning live load had been applied to raise the total dead and live load stresses to subsequent values of 30 ksi, 40 ksi, 50 ksi and 60 ksi. The gradual increase in deflection which can be observed from the data recorded during the 7 week period following the application of the 30 ksi conditioning load must be attributed to progressive cracking as a result of the many live load applications, and also to the continuing creep process. It is of further interest to note that the permanent displacements gradually increase with each application of a higher conditioning load cycle. This phenomenon is due to the gradual deterioration in the stiffness caused by the cracking in the concrete. The midspan displacement prior to the final loading to failure reflected a total dead load displacement of 1.5 and 1.9 inches for girders 1 and 5 respectively or about 3.8 to 4.1 times the dead load deflections recorded immediately after the removal of the shoring.

A comparison of the behavior of girders 1 and 5 in the undiaphragmed Section Y is given in Fig. 7.6. As observed, girder 5 has the largest instantaneous deflection, and also shows a slightly larger rate of increase with time.

7.4 Crack Development After Conditioning Loads

After removal of the shoring and following each application of the conditioning loads the cracks in the girders 1 and 5 (south and north side respectively) and in the top and bottom slabs were recorded

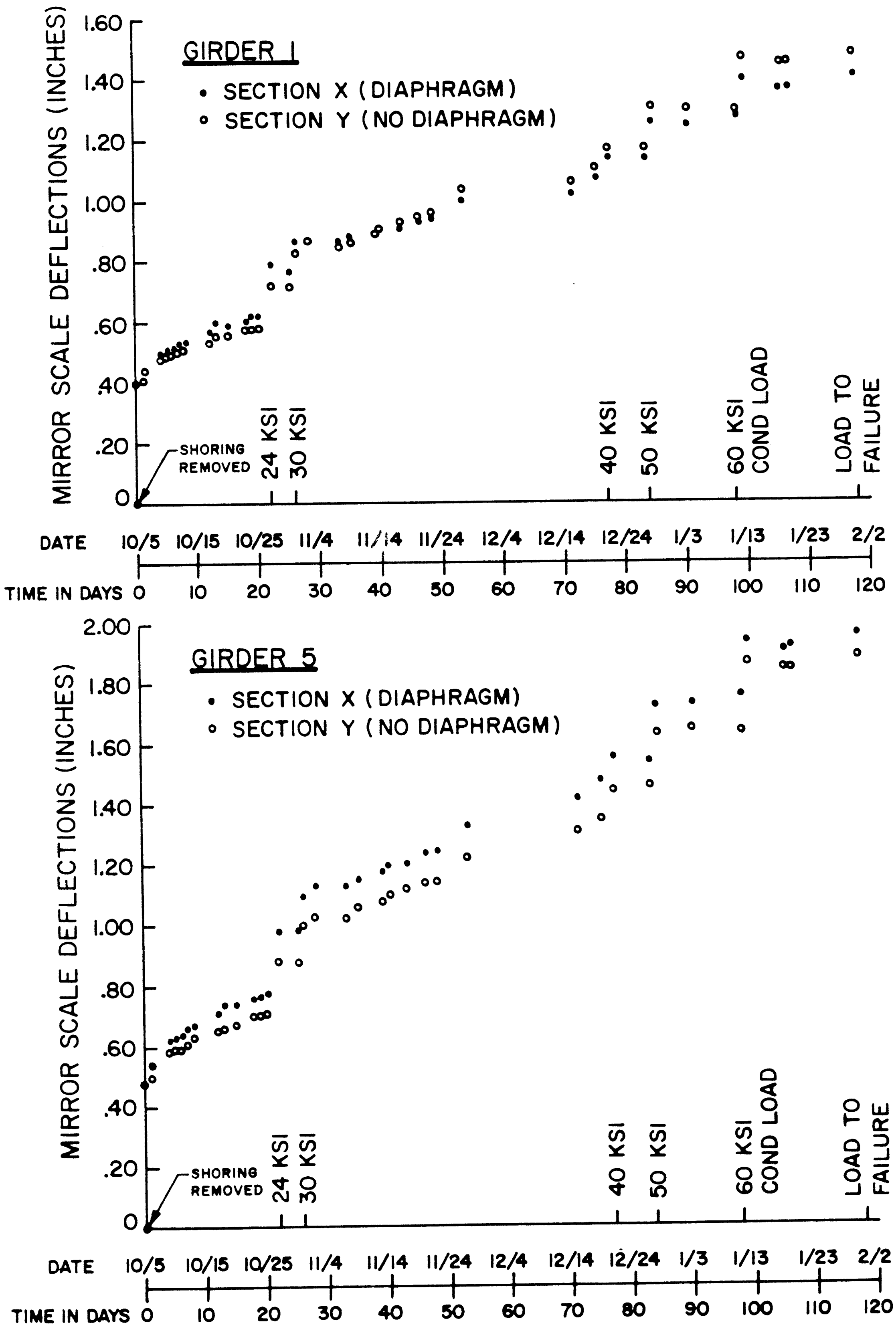

FIG. 7.5 DEFLECTION HISTORY UNDER SUSTAINED DEAD LOAD

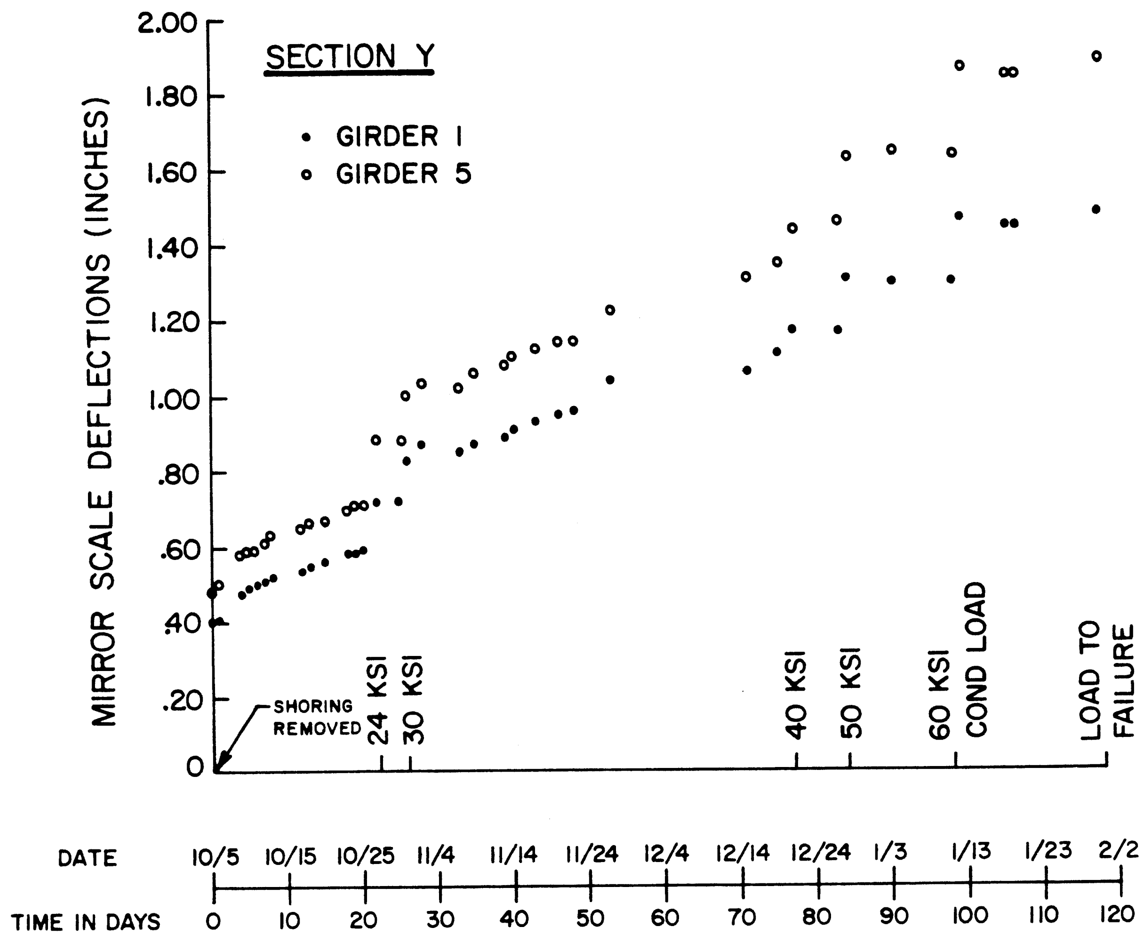

FIG. 7.6 DEFLECTION HISTORY UNDER SUSTAINED DEAD LOAD – COMPARISON BETWEEN GIRDER 1 AND 5 AT SECTION Y

and are presented in Figs. 7.7 to 7.12.

The crack patterns as presented for dead load, and the 24, 30, 40, 50 and 60 ksi conditioning loads are basically self explanatory. However, a couple of observations are particularly pertinent in evaluating the bridge model under design stress conditions and successively increasing overloads. Firstly, it is satisfying to note that under combined dead and design live loads, the crack pattern consisted virtually exclusively of hair-line cracks. After the dead load application the maximum crack width for the girders webs and the top and bottom slabs was about 0.02 in., which increased to about 0.05 in. after the 24 ksi conditioning load.

The crack patterns in the outer girder 5 and inner girder 1 webs as presented in Figs. 7.7 and 7.8 show progressively the development of bending moment cracks from the early stages of loading, followed by the development of typical shear cracks after applications of the 30 ksi conditioning loads.

The crack patterns for the bottom slab are shown in Fig. 7.9 and 7.10 and for the top slab in Fig. 7.11 and 7.12. The bottom slab shows quite extensive hair-line cracking already at the dead load stage, except for the center support region. The pattern does not change significantly until the 40 ksi stage, when the number of longitudinal cracks increases in the undiaphragmed east span. For the top slab the cracking is restricted to the center support region until 40 ksi conditioning loading, at which time the cracks propagate into the two spans and it can be seen that longitudinal, transverse and diagonal cracks develop near the supports. These are due to the increasing shear due to torisional action and load transfer between the girders.

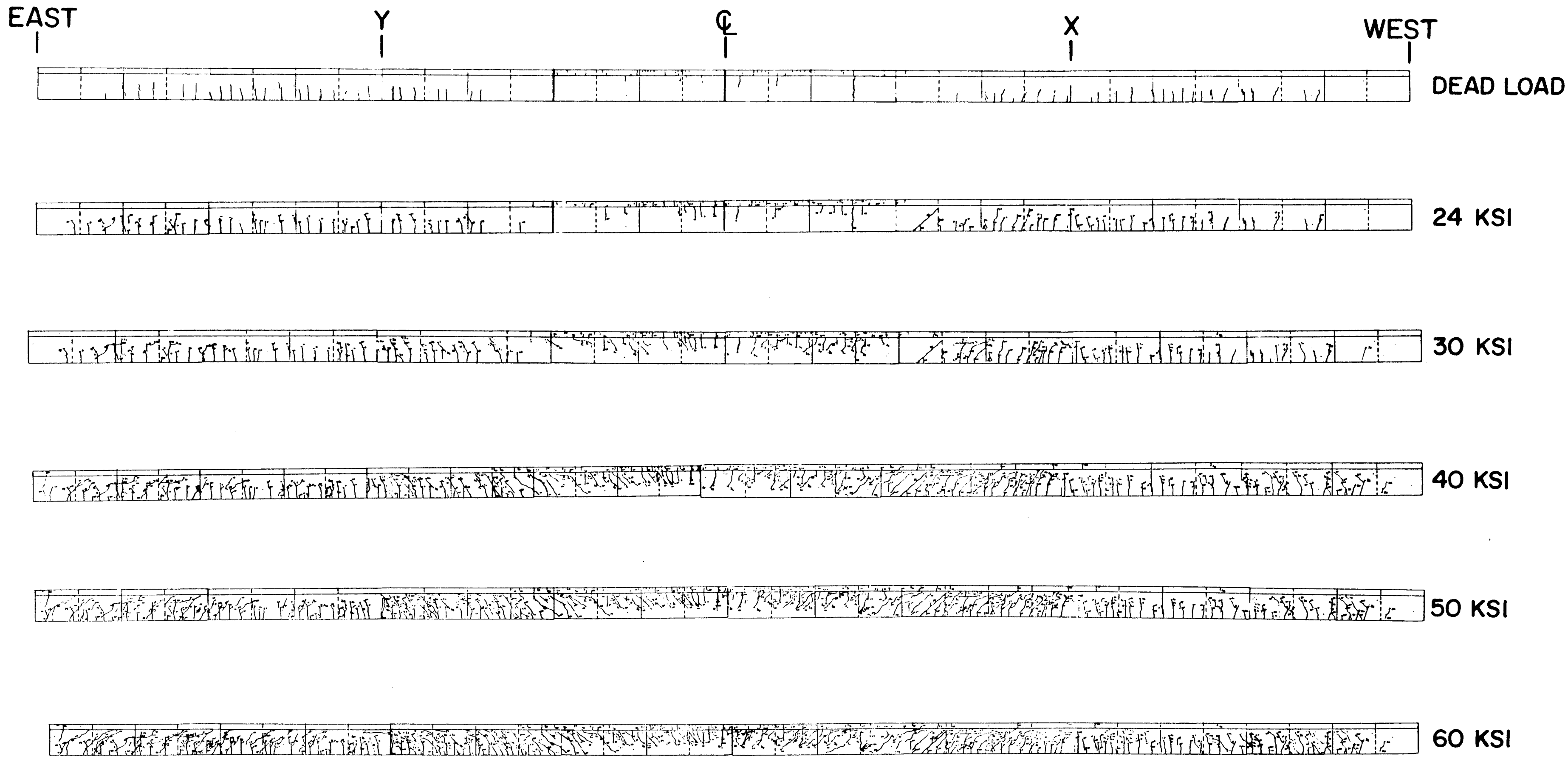

FIG. 7.7 CRACK HISTORY FOR OUTER GIRDER 5 (NORTH FACE)

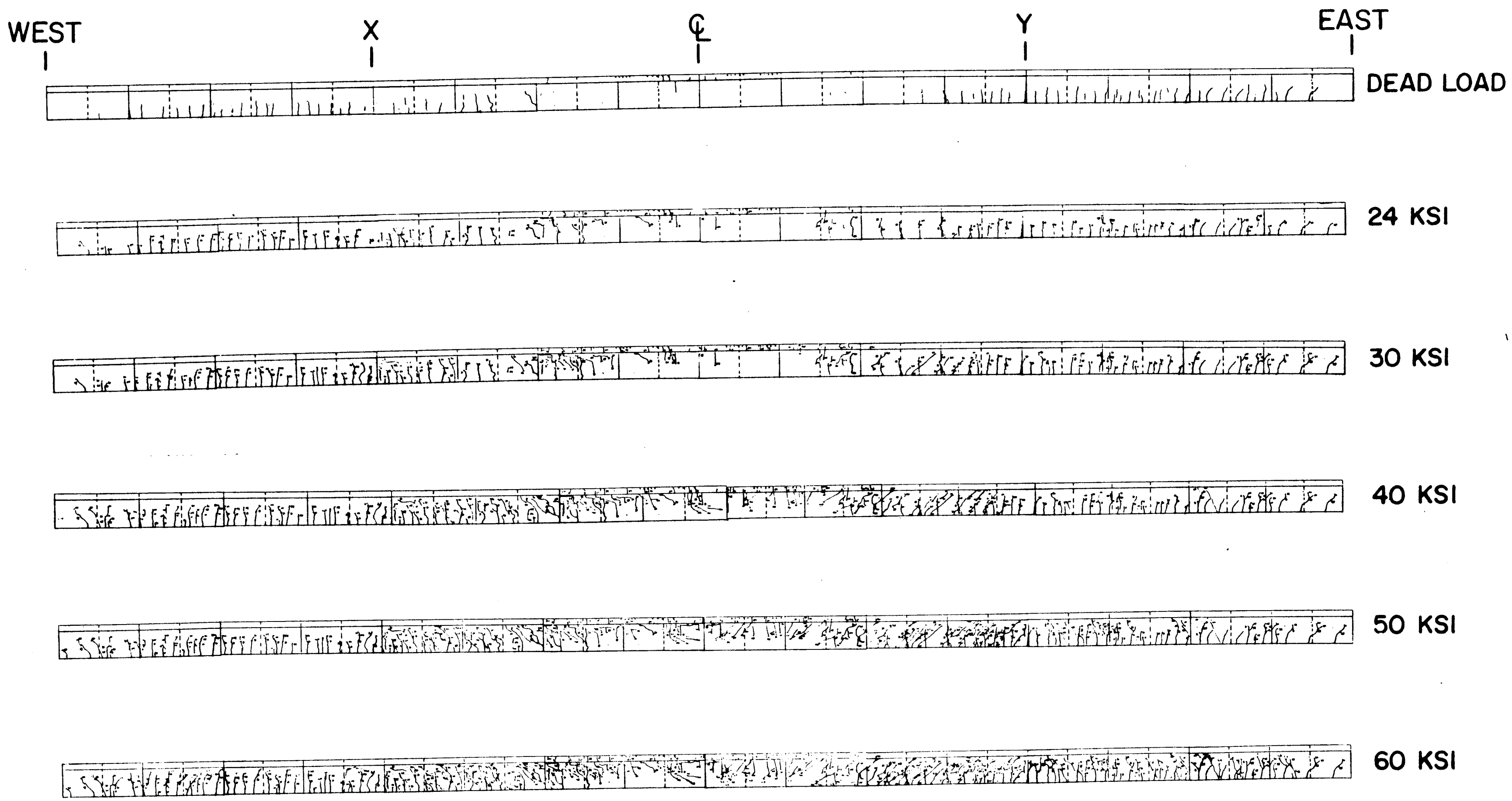

FIG. 7.8 CRACK HISTORY FOR INNER GIRDER 1 (SOUTH FACE)

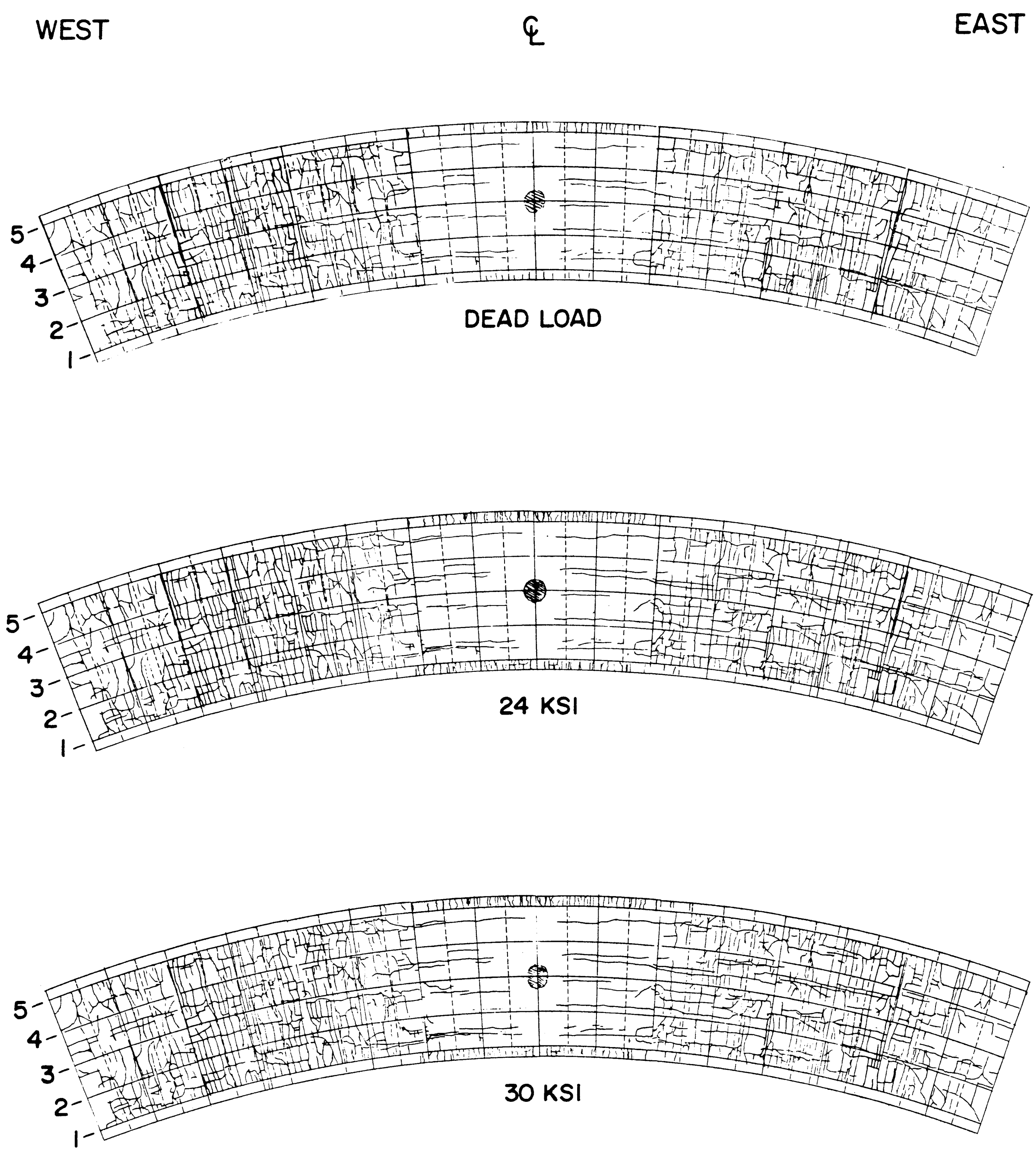

FIG. 7.9 CRACK HISTORY FOR BOTTOM SLAB

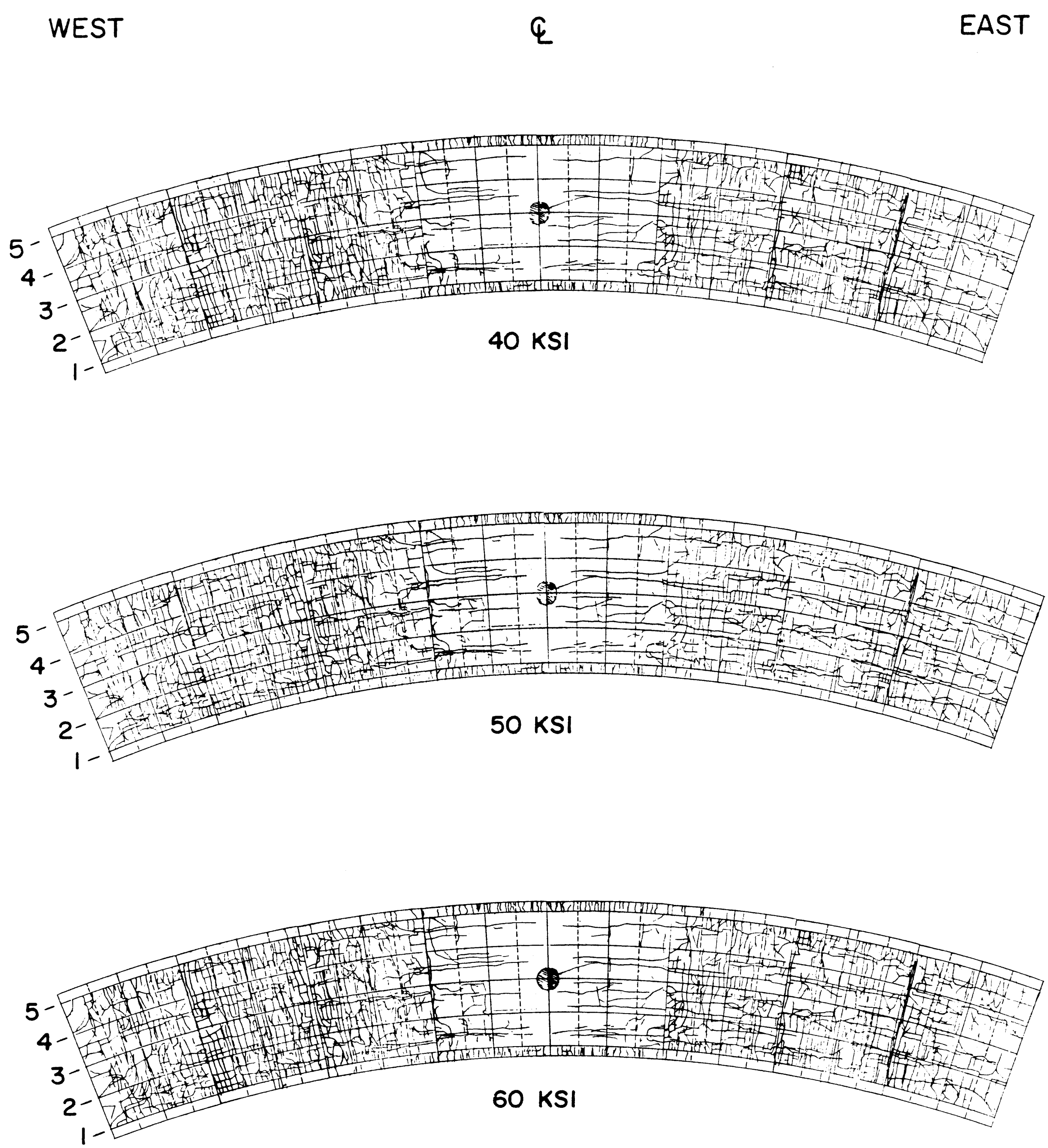

FIG. 7.10 CRACK HISTORY FOR BOTTOM SLAB

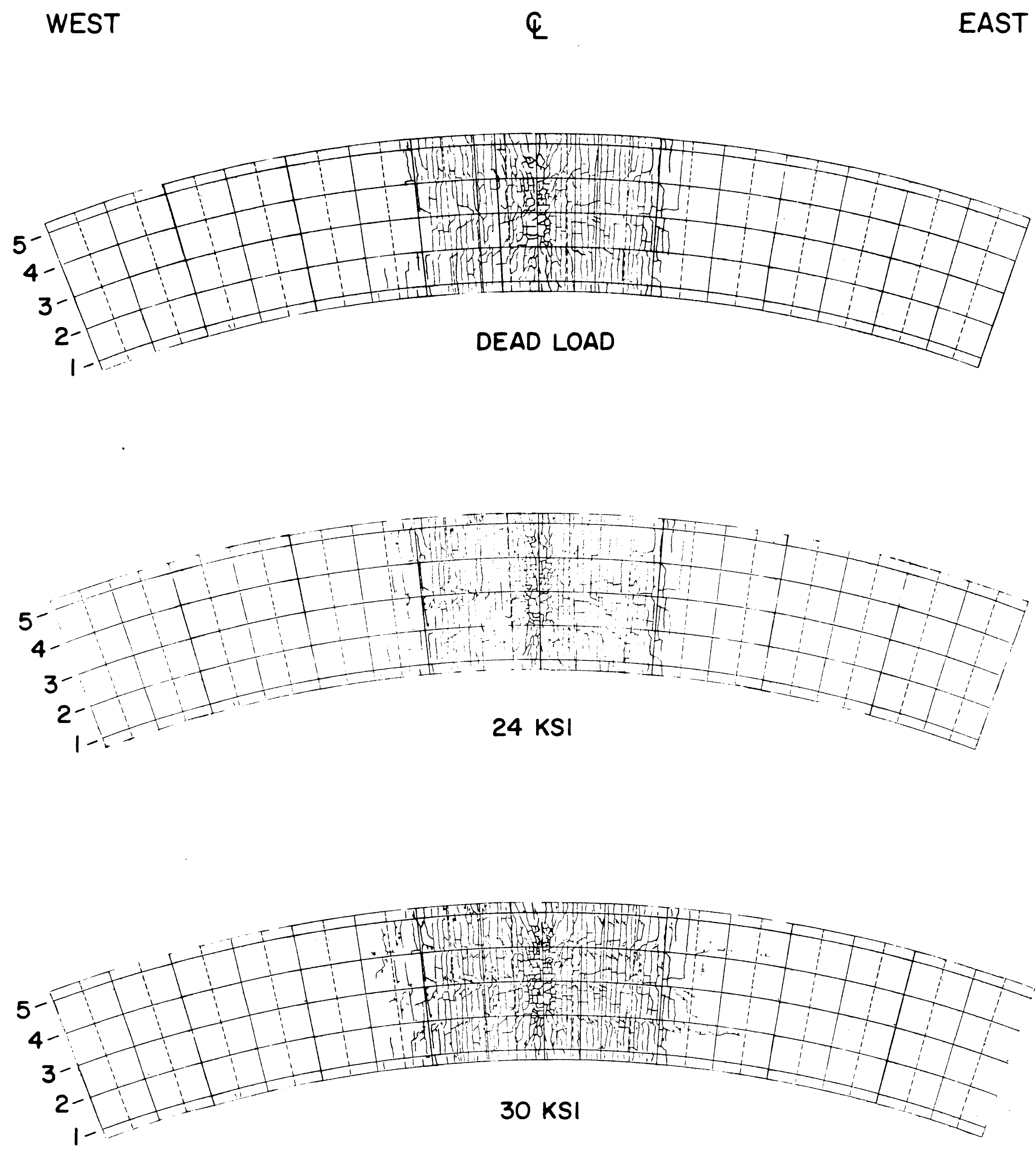

FIG. 7.11 CRACK HISTORY FOR TOP SLAB

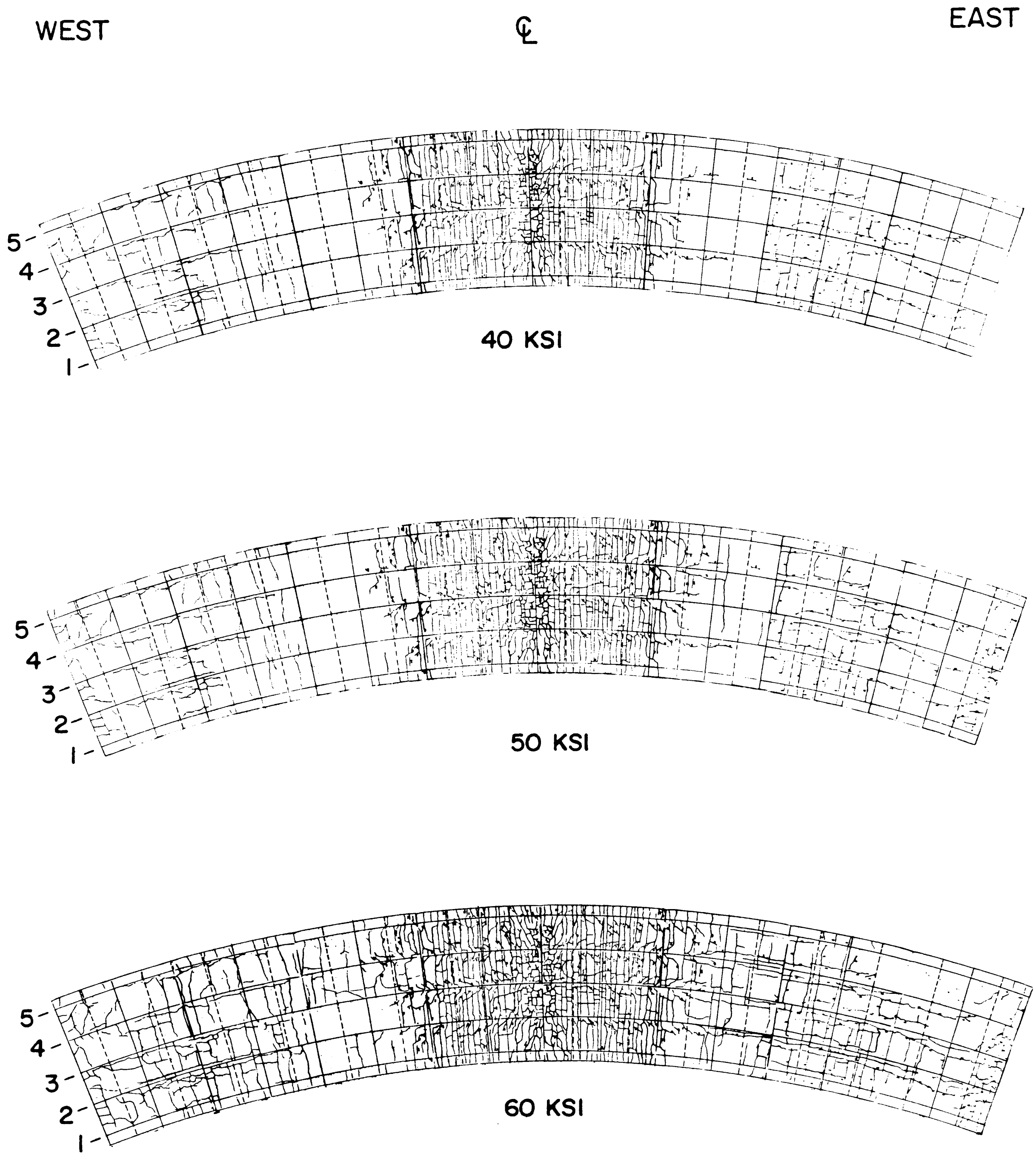

FIG. 7.12 CRACK HISTORY FOR TOP SLAB

A comparison between the patterns for the top and bottom slabs indicates a closer crack spacing for the top slab over the support as previously discussed in Section 3.9.

7.5 Comparison Between Straight and Curved Bridge Models

Due to the lack of an absolute zero reading for the strain history during the construction phase, only the deflections under sustained dead load can be compared for the two structures. While the crack patterns were of a similar nature for the two models, the records appear to indicate somewhat more extensive cracking at lower levels in the curved bridge. However, the development of cracking after each conditioning load cannot be compared directly since the crack recording schemes were quite subjective.

A comparison between the displacements of the two models is given in Fig. 7.8 for outer girder 5. It can be seen that the final total displacement of the curved bridge is about 20% larger than that of the straight one. This is of course not surprising considering the difference in this outer girder's total length in the two bridges. Considering the various parameters influencing the behavior, such as time lag between the casting of top and bottom flanges, duration of the total test program etc., there appears to be no significant differences in the way the two structures behave under sustained dead load.

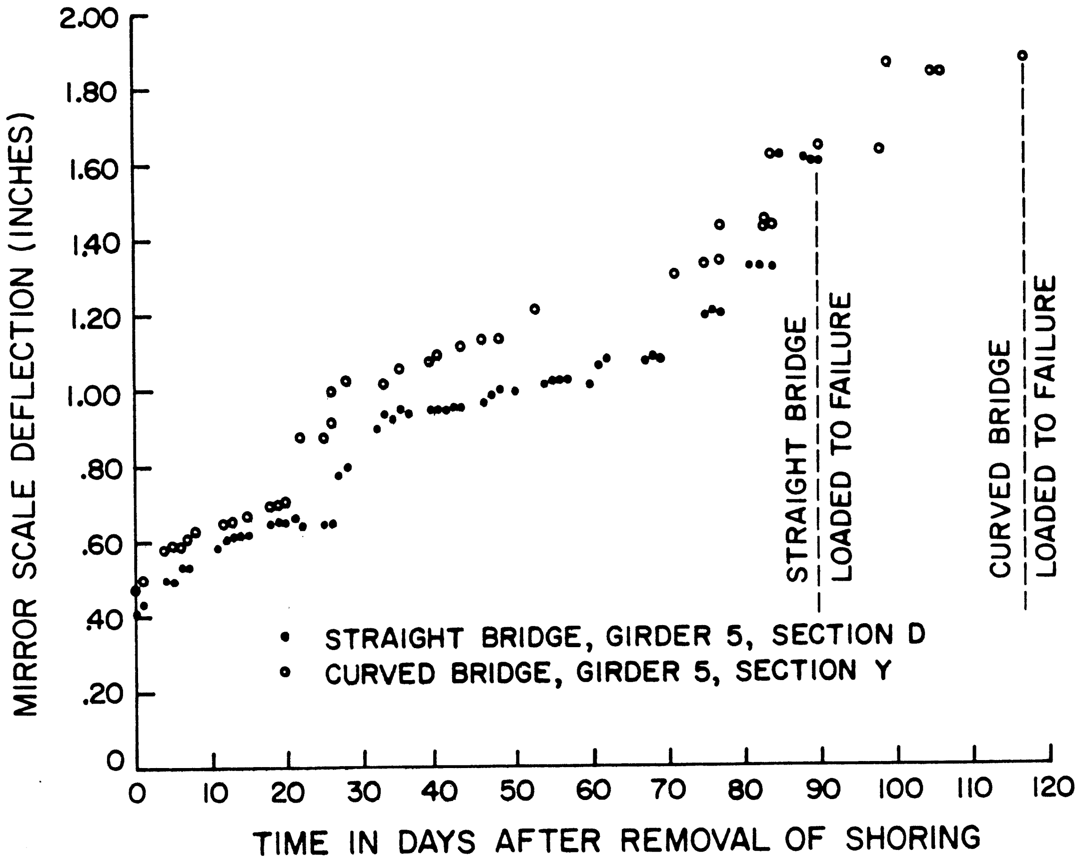

FIG. 7.13 DEFLECTION HISTORY UNDER SUSTAINED DEAD LOAD–COMPARISON BETWEEN STRAIGHT AND CURVED BRIDGE MODELS

8. LOADING OF THE BRIDGE MODEL TO FAILURE

8.1 General Remarks

To determine the bridge response under increasing loads and at failure, concentrated loads were applied simultaneously at each mid-span. The load was increased stepwise and readings were taken at each step. A general view of the bridge model before and after failure during the final load tests is given in Figs. 8.1 and 8.2. Observations during the loading procedure are given in Section 8.2. A discussion of the ultimate strength of the bridge model and a comparison with theoretically predicted values are presented in Section 8.3. Finally the behavior of the curved bridge model is compared in Section 8.4 to the behavior of the previously tested straight bridge model.

To provide a large measure of deformation in the bridge model, three large capacity loading rams were used at each of the midspans I and II, Sections X and Y. The rams had a maximum stroke of 24 in. and a maximum capacity of 200 kips (100 tons). They were centered on 10 by 12 in. thick steel plates at girders 2, 3 and 4 respectively, Fig. 8.3. Neoprene pads of one inch thickness were provided under the steel plates for better distribution of the load. The load level was measured by a pressure tranducer in each span. A calibration in terms of hydraulic pump pressure in psi versus ram load in kips was also established. In this way an independent method was provided for the measurement of the loads.

To measure the deflections of the bridge, scales and wires were mounted at Sections QA and QD in addition to the earlier mounted scales at Sections X, QB, Z, QC and Y. With this measurement arrangement it was possible to closely follow the deflections along the entire

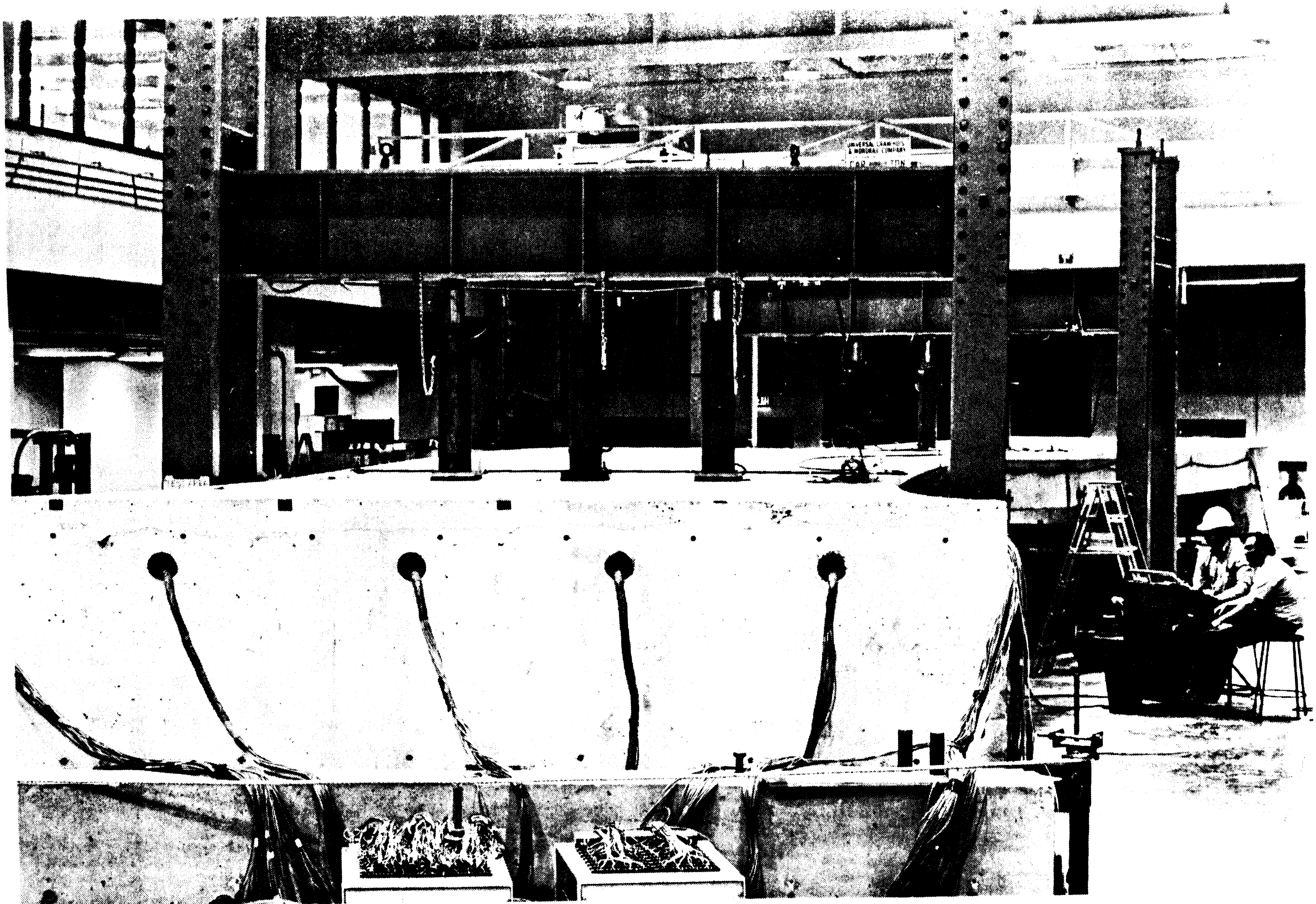

FIG. 8.1 BRIDGE MODEL BEFORE FAILURE DURING FINAL LOAD TEST

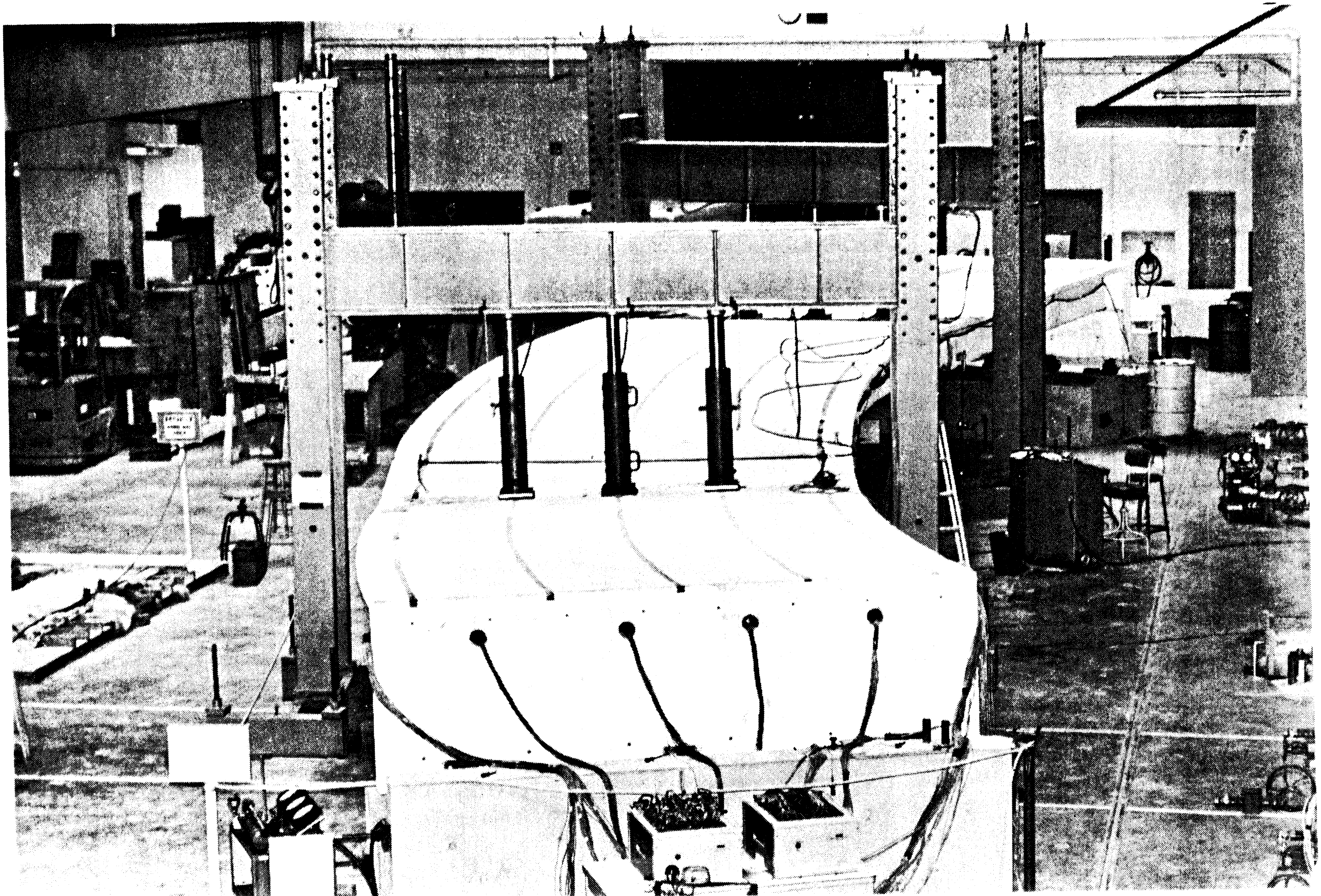

FIG. 8.2 BRIDGE MODEL AFTER FAILURE DURING FINAL LOAD TEST

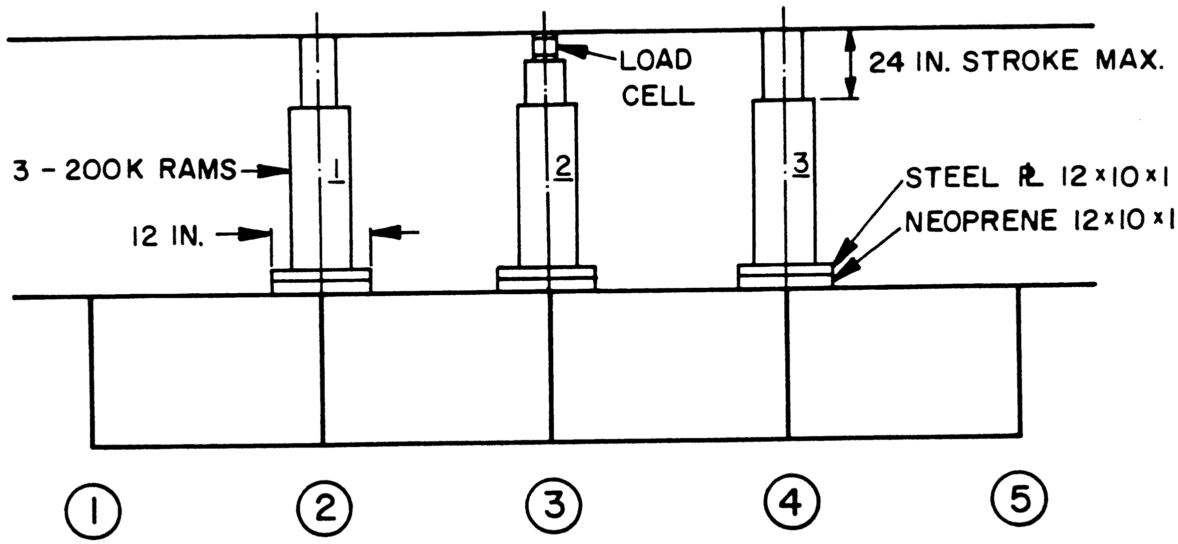

FIG. 8.3 LOAD ARRANGEMENT AT MIDSPANS I AND II FOR FINAL LOADING TO FAILURE.

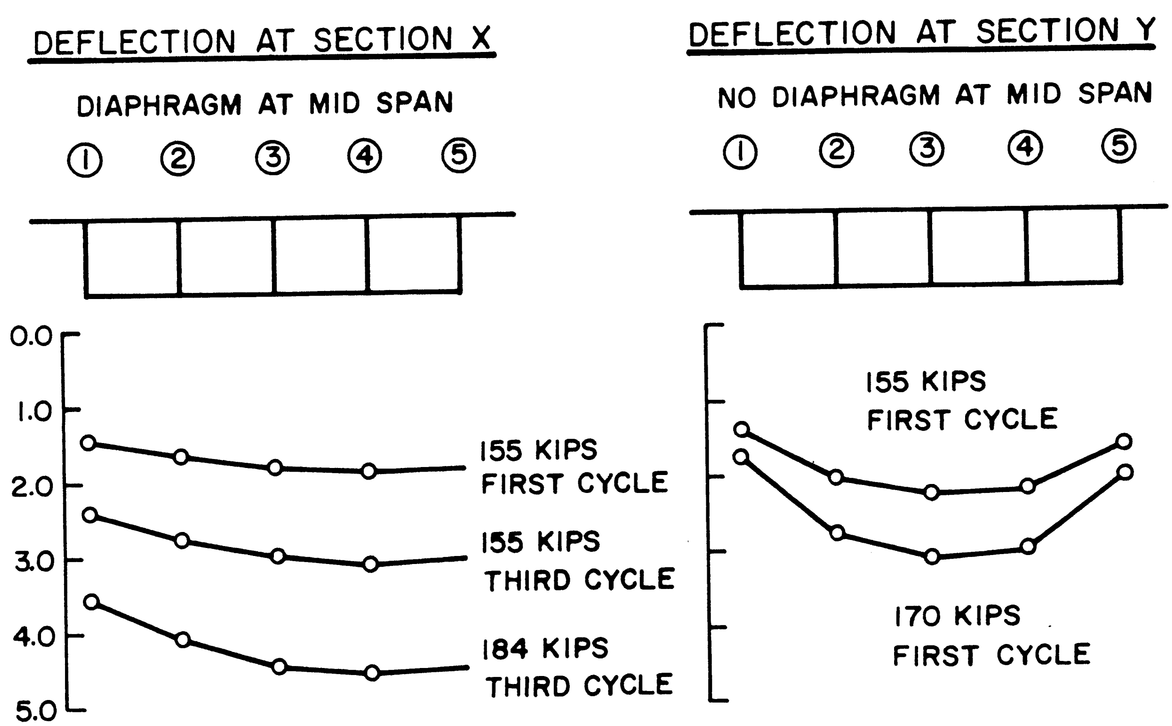

FIG. 8.4 DEFLECTIONS (INCHES) AT MIDSPAN TRANSVERSE SECTIONS X AND Y DURING FINAL LOAD CYCLES

length of the bridge model. The potentiometers at various transverse sections of the bridge model were also used as long as there was no risk of damaging them. During the final stages of the loading, the potentiometers were removed and only the scales and wires were used to measure deflections, along inner girder 1 and outer girder 5, up to ultimate failure.

8.2 Observations During Loading

8.2.1 First Loading Cycle

After taking zero readings, the three rams in each span were successively loaded to provide nominal stresses in the tensile steel at midspan Sections X and Y of 24, 30, 40, 50 and 60 ksi. In each case readings were taken by means of the data acquisition scanning unit. At the stress level of 60 ksi, each span carried a live load of 150 kips. In the next step, the load in each span was increased to 155 kips. This caused an increase in cracking and longitudinal cracks were for the first time observed in the bottom slab under girders 2 and 4 in the undiaphragmed Span II. The cracks started at midspan Section Y and progressed 5 to 7 feet towards the center bent column. No such cracks were observed in the diaphragmed Span I (Section X). The cause of the cracks seemed to be transverse bending stresses in the bottom slab. This is illustrated in Fig. 8.4 where the deformation profile across Sections X and Y can be seen for the bottom slab. There is a big change in slope under girders 2 and 4 in the undiaphragmed Section Y due to the fact that only girders 2, 3 and 4 were loaded, whereas the diaphragm obviously prevented this kind of deformation at Section X. Longitudinal shear stresses may also have contributed to the formation of the longitudinal cracks.

The load was then increased in steps to 160, 165 and 170 kips. The cracks widened during this process, especially the longitudinal cracks under girder 4 in the undiaphragmed Span II. The subsequent step called for a load increase in each span to 175 kips. However, as the load reached 173 kips a local failure occurred in the outer girder 5 of the undiaphragmed Span II near Section Y. The concrete spalled off at the bottom of the girder, the diagonal shear cracks in the girders opened up and the load dropped suddenly. The spalling of the concrete is illustrated in Fig. 8.5.

Deflections along the face of girder 5 are shown in Fig. 8.6 for some characteristic load steps, during the first loading cycle, including the maximum load of 173 kips. It can be seen from the figure that the measured deflections for girder 5 are larger in the diaphragmed Span X than in the undiaphragmed Span Y for all load steps except the last one. This is due to the fact that the diaphragm forces uniform de-deflections transversely at Section X, whereas in the undiaphragmed span at Section Y, the deflections under loaded girders 2, 3, and 4 are larger than those of girders 1 and 5, as can be seen in Fig. 8.4.

A comparison between the deflection along the inner girder 1 and the outer girder 5 is shown in Fig. 8.7 for the maximum first cycle load of 173 kips. It can be seen that outer girder 5 has about a 30% larger deflection than inner girder 1 at the diaphragmed Section X and about a 40% larger deflection at the undiaphragmed Section Y.

After the concrete spalling, the load dropped first to 168 kips and then to 164 kips. During this process longitudinal cracks also developed at the top of girder 5 near Section Y causing the beginning of

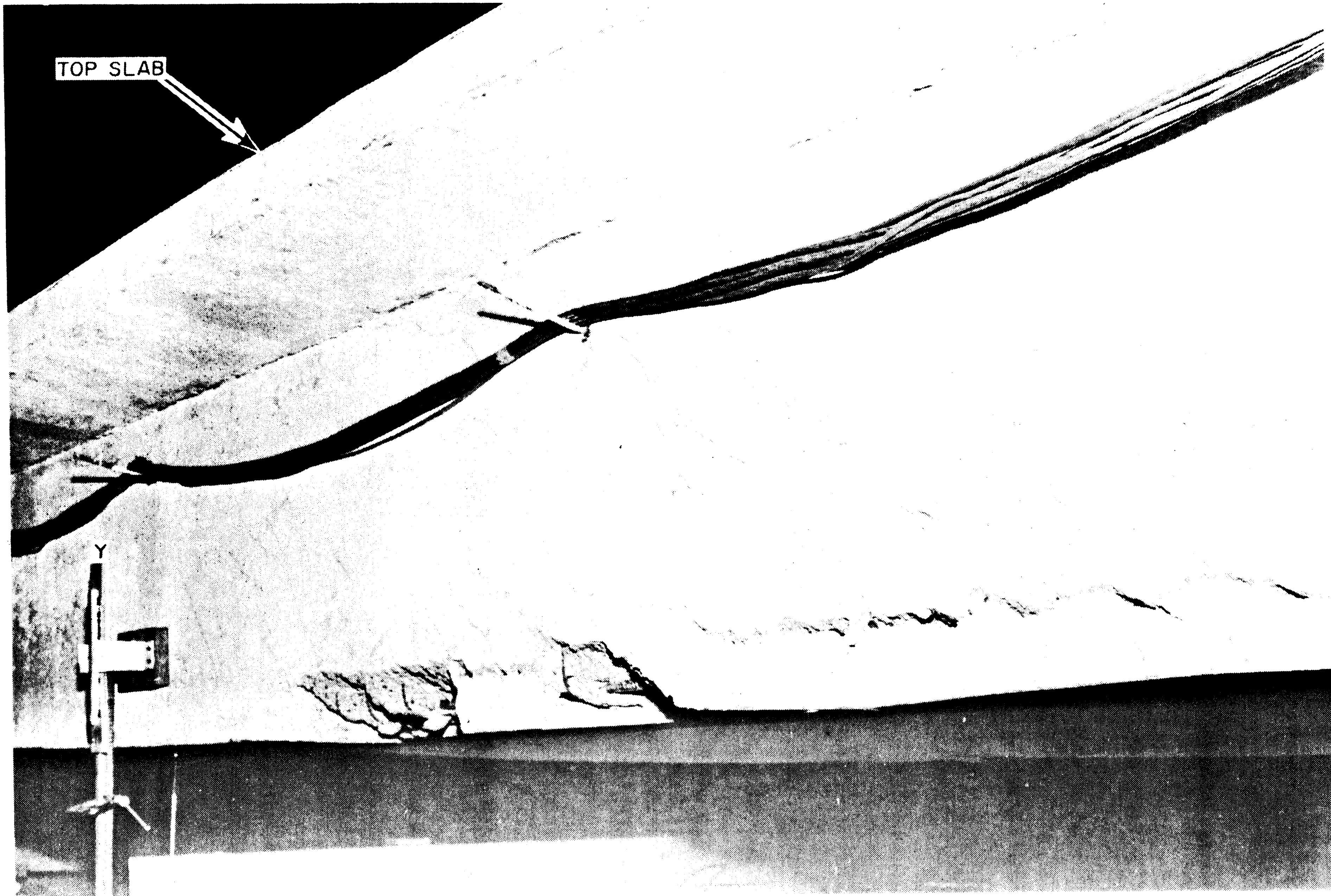

FIG. 8.5 LOCAL FAILURE AT OUTER GIRDER 5 IN UNDIAPHRAGMED SPAN II NEAR SECTION Y – FIRST LOADING CYCLE

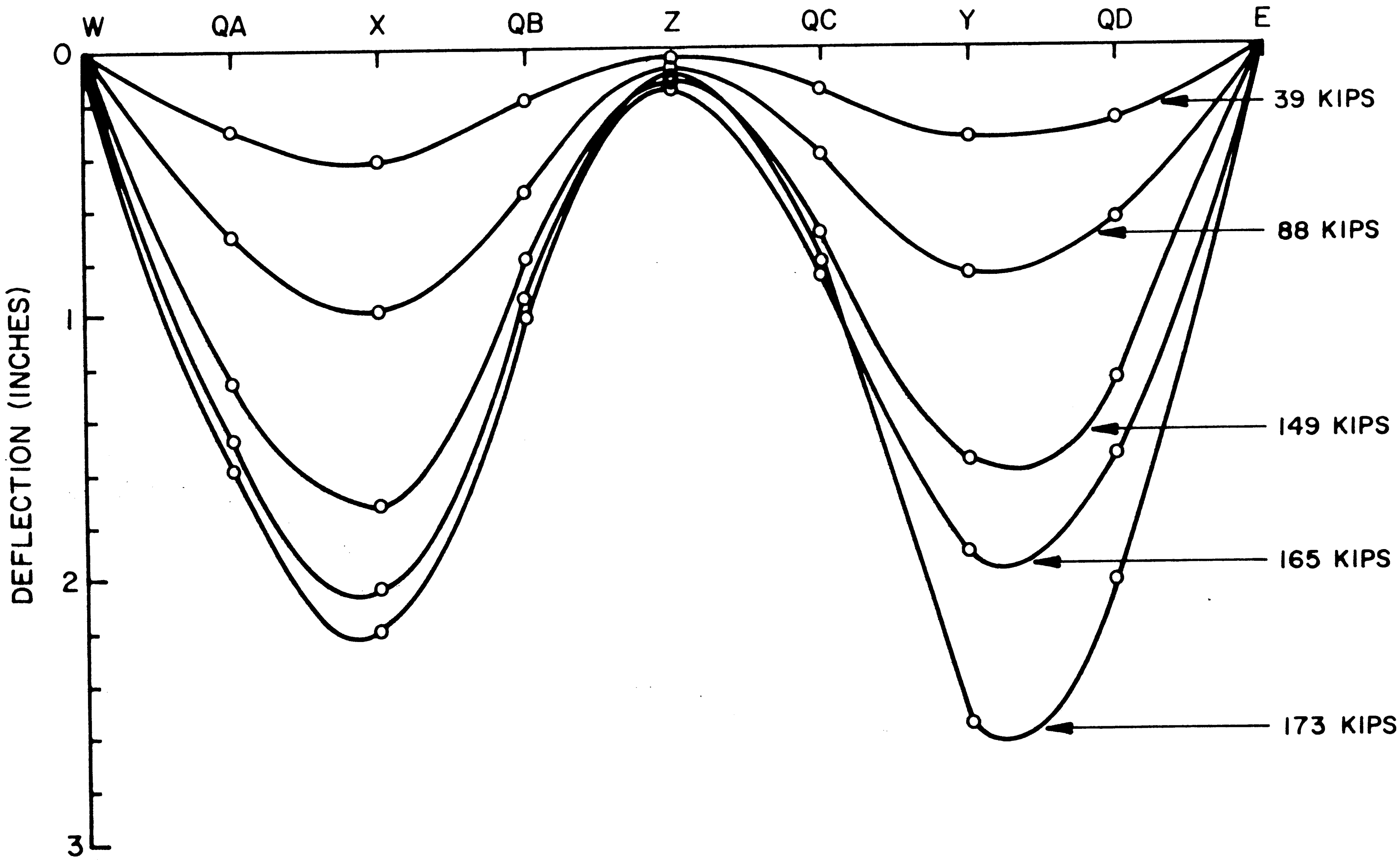

FIG. 8.6 DEFLECTION (INCHES) CURVES FOR OUTER GIRDER 5 UNDER INCREASING LOADS – FIRST LOADING CYCLE – BOTH SPANS LOADED

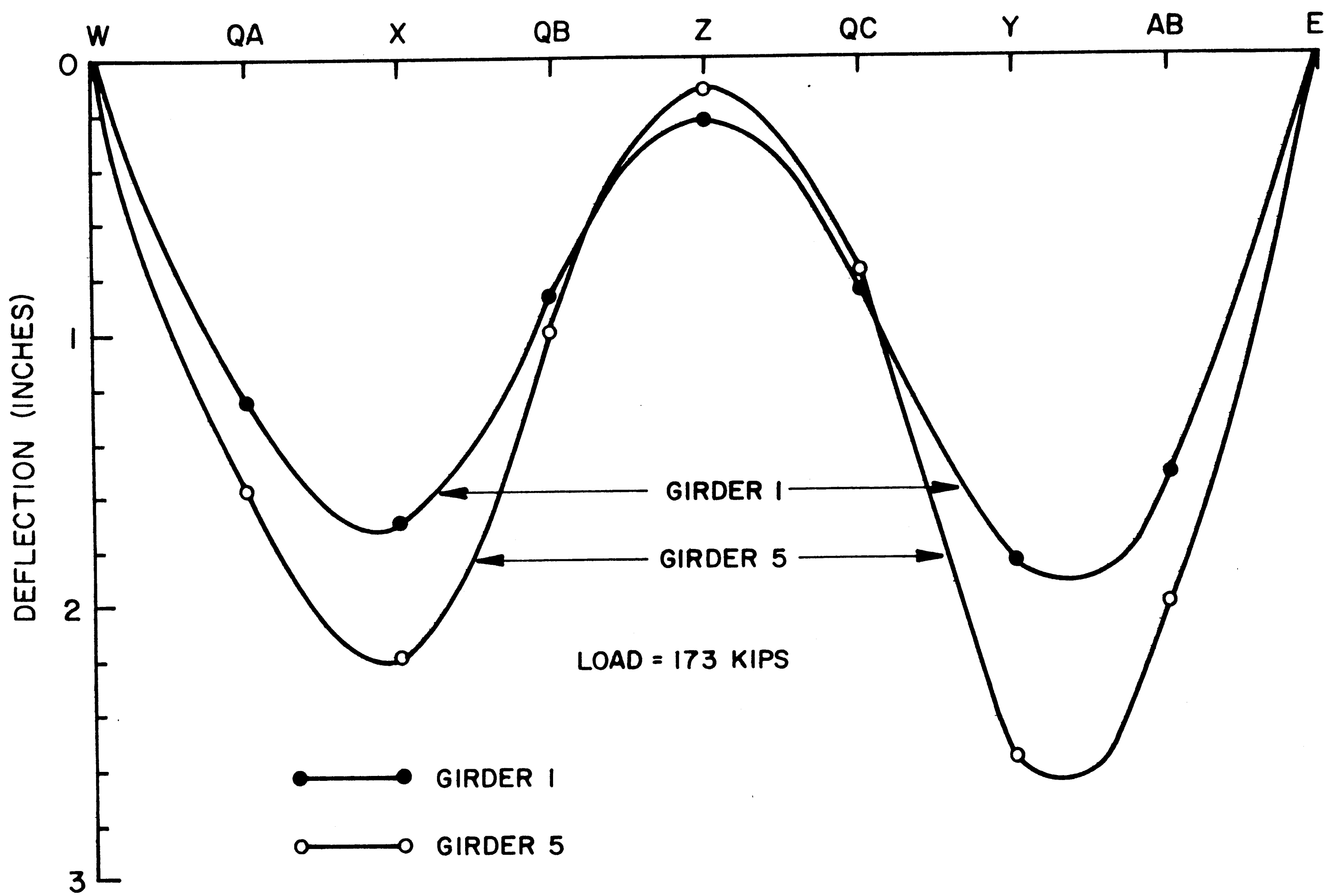

FIG. 8.7 COMPARISON OF DEFLECTION (INCHES) CURVES FOR INNER GIRDER 1 AND OUTER GIRDER 5 AT MAXIMUM FIRST CYCLE LOAD OF 173 KIPS – BOTH SPANS LOADED

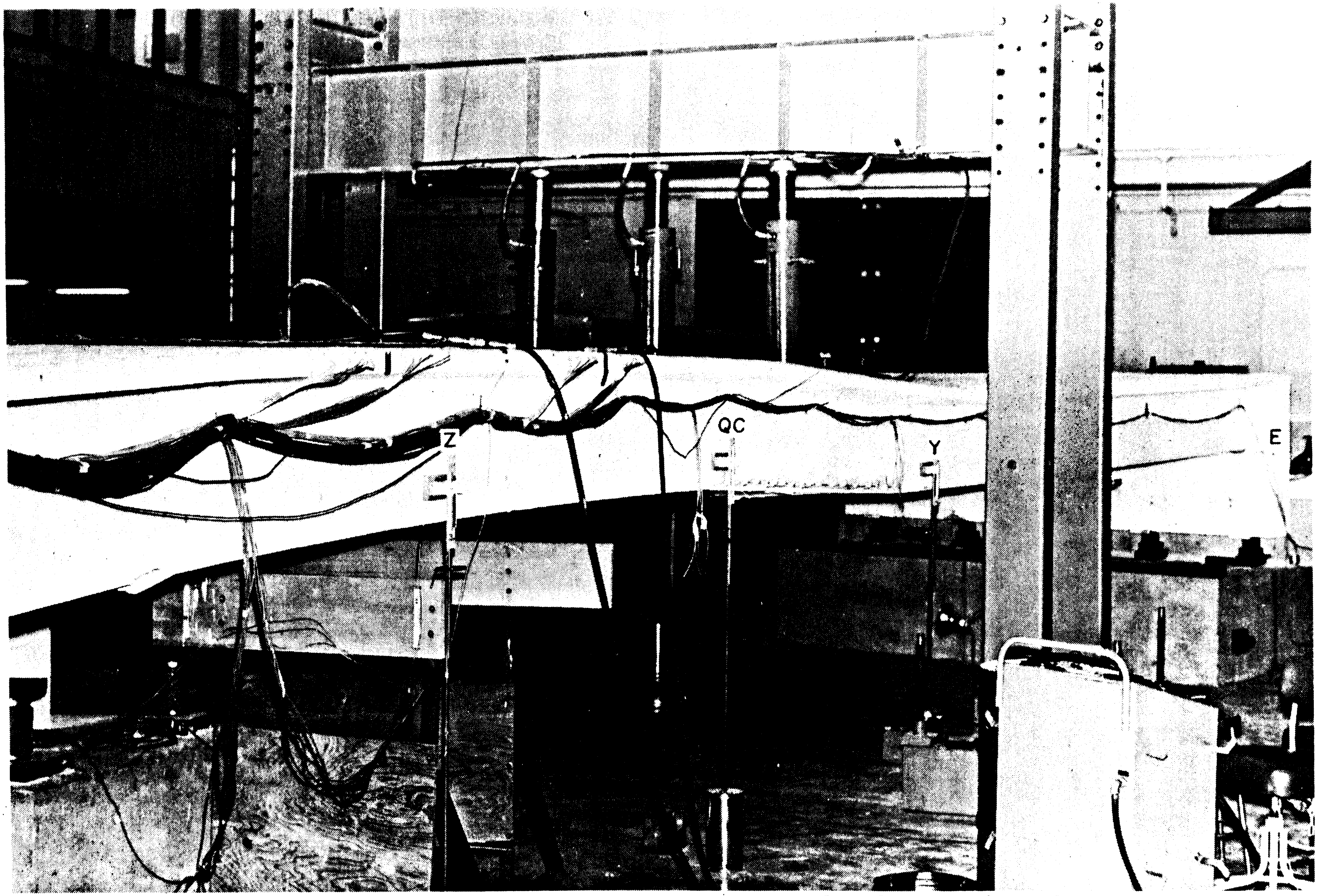

FIG. 8.9 VIEW OF FAILURE ALONG INNER GIRDER OF UNDIAPHRAGMED SPAN II AT END OF SECOND LOADING CYCLE

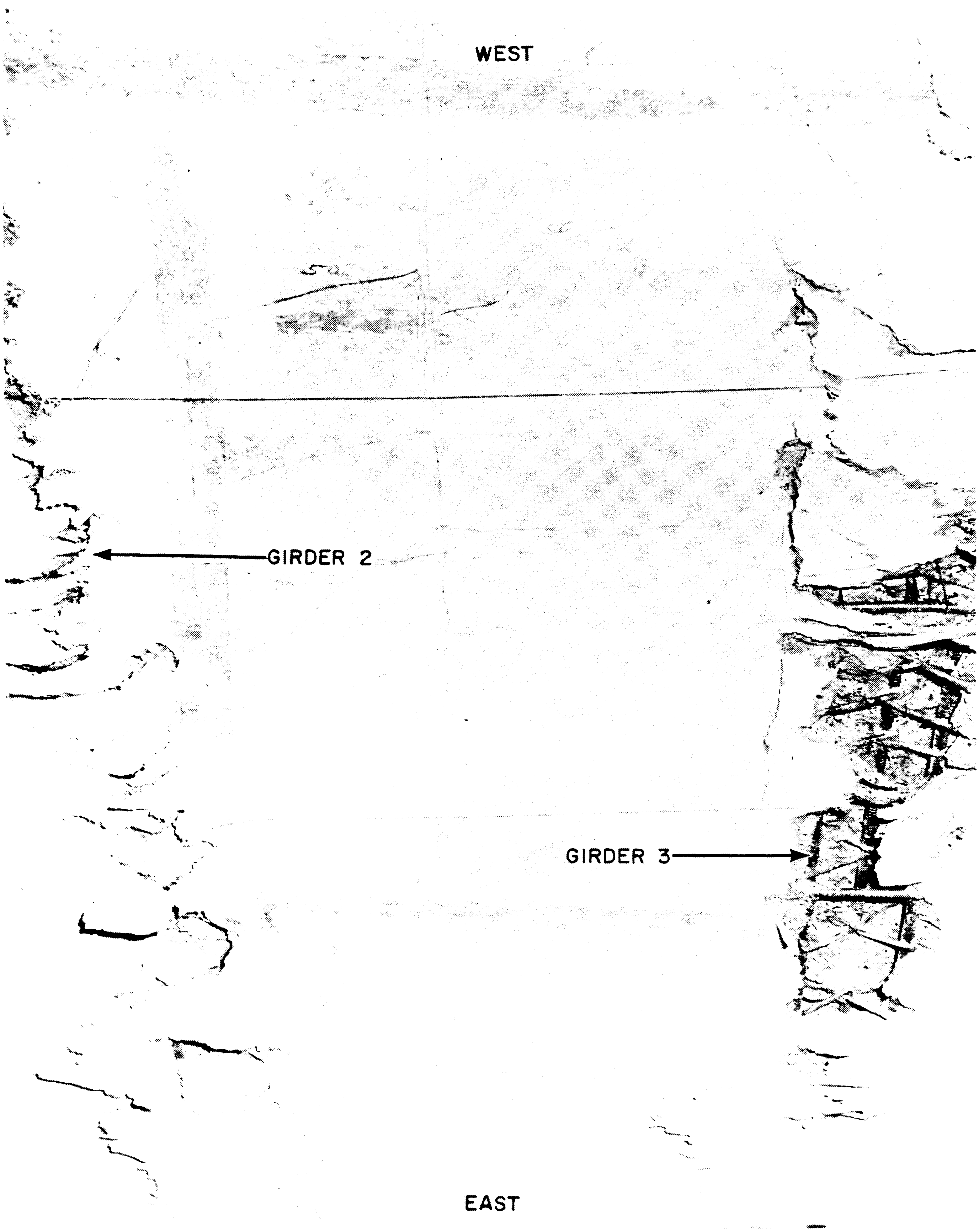

FIG. 8.10 VIEW OF BOTTOM SLAB AT END OF SECOND LOADING CYCLE SHOWING LARGE CRACKS ALONG BOTTOM OF GIRDER WEBS 2 AND 3 NEAR SECTION Y

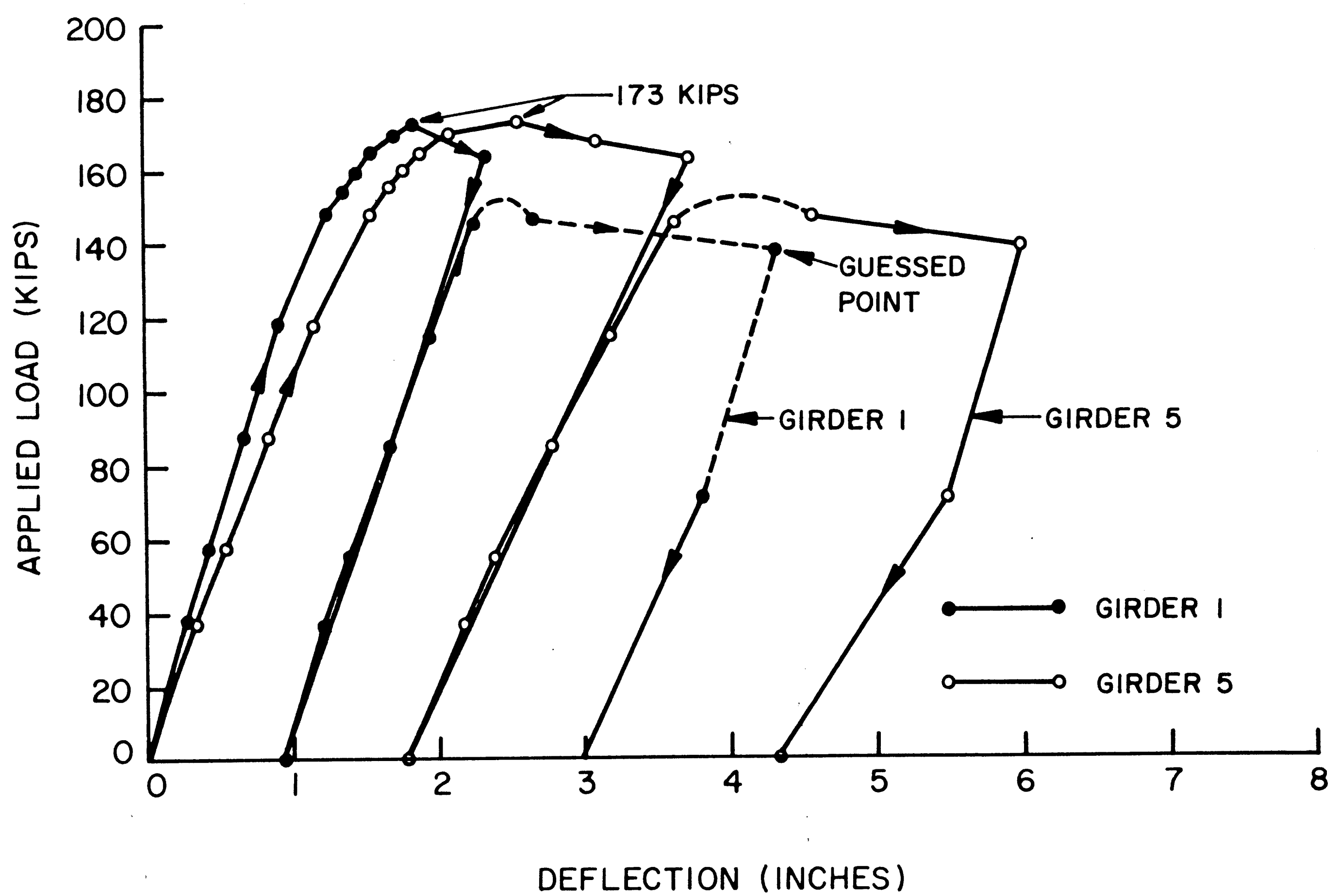

FIG. 8.11 LOAD-DEFLECTION DIAGRAM AT SECTION Y FOR GIRDERS 1 AND 5 DURING FIRST AND SECOND LOADING CYCLES -BOTH SPANS LOADED

for the first and second loading cycles. No deflection measurements were taken at the maximum load of the second loading cycle. That part of the curve has therefore been indicated with a dotted line.

During this second loading cycle no serious distress was noted in Span I which had a midspan diaphragm at Section X.

8.2.3 Third Loading Cycle

In view of the fact that the bridge model so far only had failed in the undiaphragmed Span II (Section Y), it was decided to freeze the deformations there by locking the three rams in this span. Subsequently, only the diaphragmed Span I was loaded at Section X, with readings taken at 57, 118, 149 and 155 kips. At 155 kips longitudinal cracks were observed in the bottom slab under girder 4 near Section X. Some of these cracks also extended out from the girder at an inclination of about 45° to the longitudinal axis of the bridge model. For the next load level, 160 kips, transverse cracks due to longitudinal bending were observed in the bottom slab at the diaphragmed Section X. The load was then increased in steps to 164, 170, 174, 180 and 184 kips. The transverse cracks at Section X steadily grew wider. Also a longitudinal crack at the top of girder 5, between the girder and the top slab, started to propagate from Section X towards Sections QA and QB.

During the next load increment, girder 4 punched through the bottom slab at a load of 190 kips. This was the maximum load achieved at the diaphragmed Section X. Spalling of the concrete at this time began in the bottom of girder 5 and punching also started under girder 3. The load then fell off and it was decided to let the deformations control the rest of the loading program.

The deformations were accordingly increased in steps to a maximum deflection of about 10 inches at the diaphragmed Section X at girder 5. The load dropped during this process from 159 to 26 kips. Increased punching took place under girders 2, 3 and 4 as well as spalling of the concrete in the bottom of girders 1 and 5. Also the diagonal shear cracks in the girders widened. Finally a hinge formed in outer girder 5 by the concrete crushing in the bottom of the diagonal compression struts at a point about five feet from Section X towards the center bent. In inner girder 1 no such hinge developed. Instead the deformations were spread along the girder between Sections X and QB.

Deflections along the face of girder 5 are shown in Fig. 8.12 for some characteristic load steps up to the last step before the maximum load. By the locking of the rams at the undiaphragmed Section Y it was possible to hold the deflection almost constant in Span II. It can be seen that the hinge close to Section QC in the undiaphragmed Span II has a marked influence on the deformation of the bridge model.

A comparison between the deflections for the three loading cycles is shown in Fig. 8.13 for outer girder 5. Two curves are shown for each loading cycle. One of them shows the deflection at the loading step just before, or at, the maximum load, while the other one shows the deflected shape at the most deformed stage for each loading cycle.

Load-deflection diagrams for girders 1 and 5 at the diaphragmed Section X are shown in Fig. 8.14 for all three loading cycles. The pronounced change in slope between the second and the third cycle is due to the freezing of the deflections in the undiaphragmed Span Y and to the hinge that formed close to Section QC at the end of the second loading cycle.

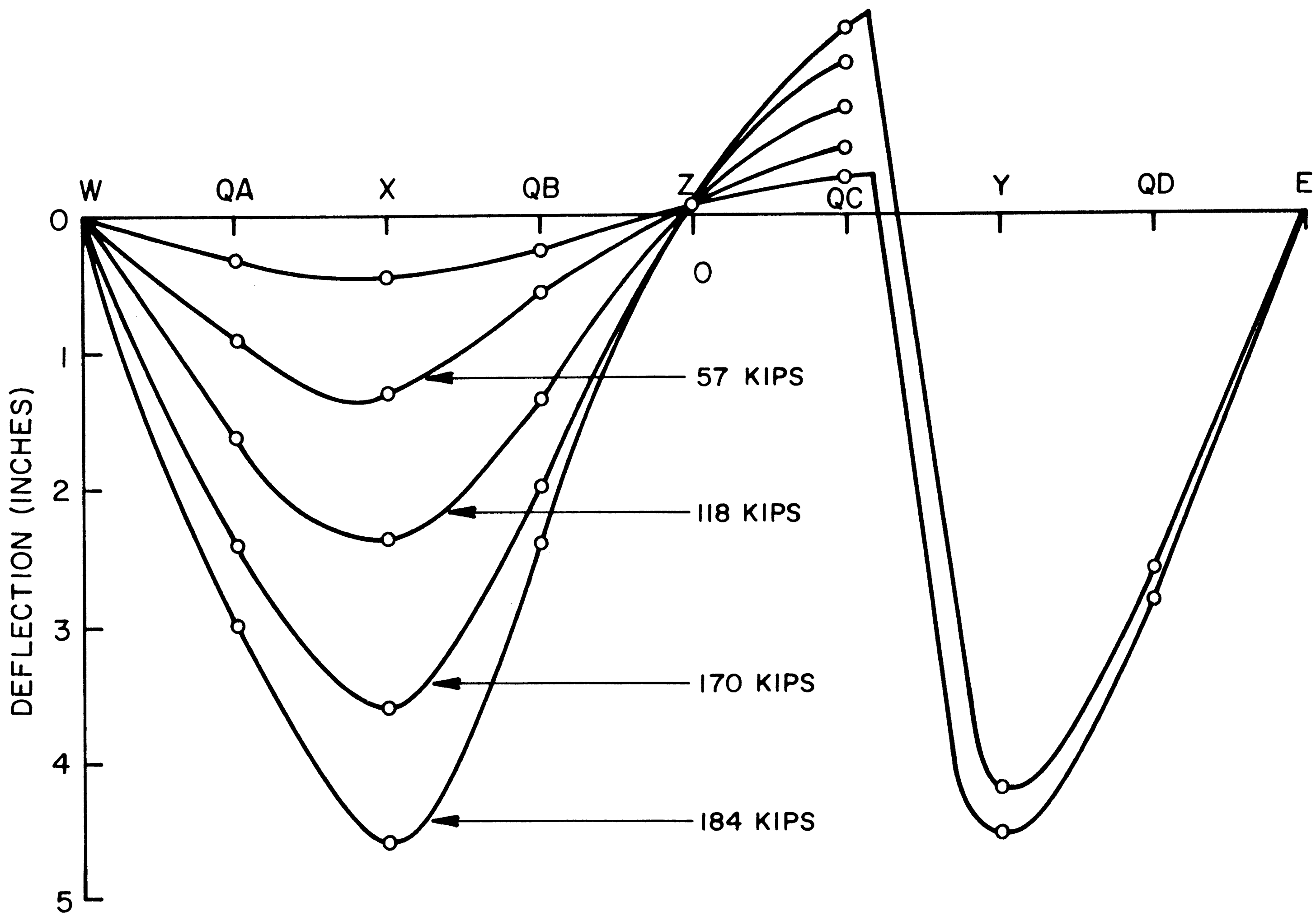

FIG. 8.12 DEFLECTION (INCHES) CURVES FOR OUTER GIRDER 5 UNDER INCREASING LOADS AT SECTION X ONLY WITH SECTION Y DEFLECTIONS LOCKED – THIRD LOADING CYCLES

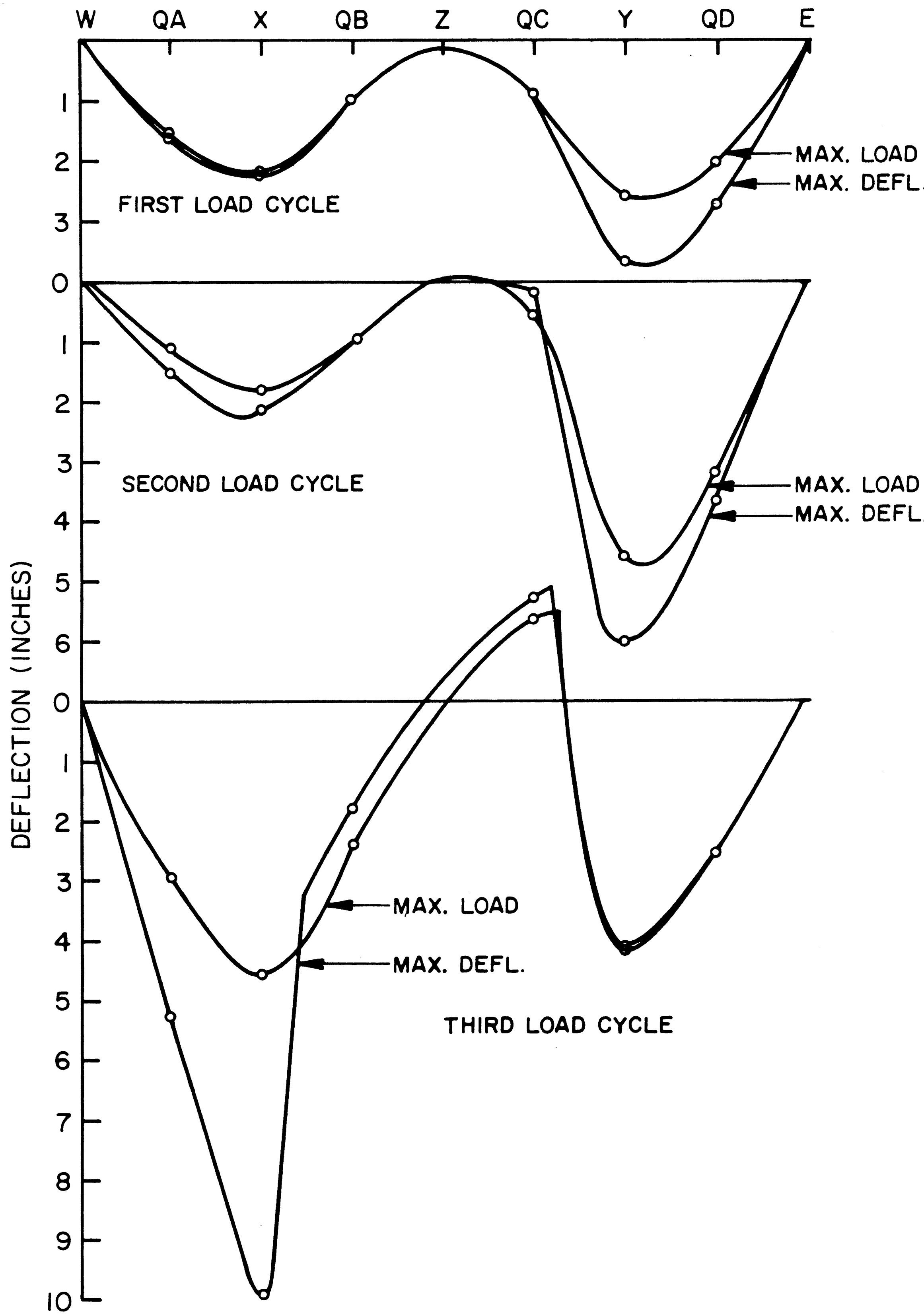

FIG. 8.13 MAXIMUM RECORDED DEFLECTION (INCHES) CURVES FOR OUTER GIRDER 5 FOR THE THREE LOADING CYCLES

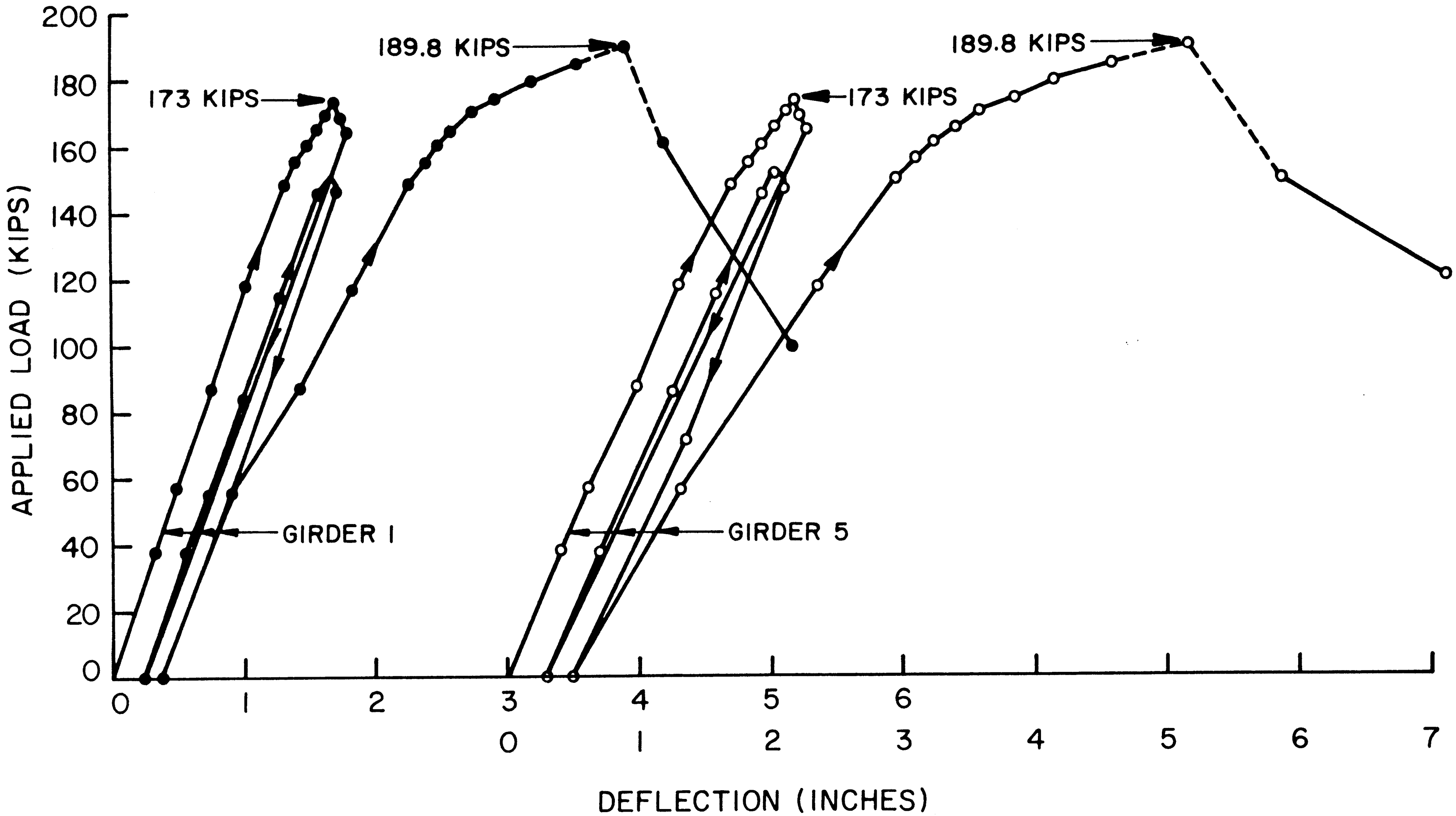

FIG. 8.14 LOAD-DEFLECTION DIAGRAMS AT SECTION X FOR GIRDERS 1 AND 5 FOR FIRST, SECOND AND THIRD LOADING CYCLES

The failure of the bridge model is illustrated in Fig. 8.15. The picture shows how girder 5 has one hinge with large bending cracks in Section X and another hinge between Sections X and QB. A close up of the failure of girder 5 at Section X is shown in Fig. 8.16. The extensive punching cracks in the bottom slab after failure are illustrated in Fig. 8.17 for girders 3 and 4. Finally, Fig. 8.18 shows an over all picture of the diaphragmed span (Section X) after failure.

8.3 Ultimate Strength Analysis

In this section analytical predictions will be discussed for the bending capacity and for the shear and torsion capacity. The predicted ultimate strengths will then be compared to the actual behavior of the bridge model as reported in Section 8.2.

8.3.1 Bending Moment Capacity

An estimate of the ultimate bending moment capacity can be obtained from an equation of moment equilibrium at failure. For the midspan Sections X and Y and the support Sections B and C, yield moment capacity has been calculated in Table 8.1. The moments have been calculated with respect to the center of the concrete compression zone. In this way only the yield forces of the longitudinal bars in the opposite slab flange and in the girder webs have to be considered. Moreover, as the contribution of the No. 3 longitudinal bars in the girder webs to the moment is very small in comparison to that of the No. 4 bars in the slab flanges, their contribution is neglected for simplicity. The moment lever arm can be taken as the distance between the longitudinal bottom bars and the center of the top slab. This distance is 1.54 feet and a safe estimate of the lever arm h is then h = 1.50 feet.

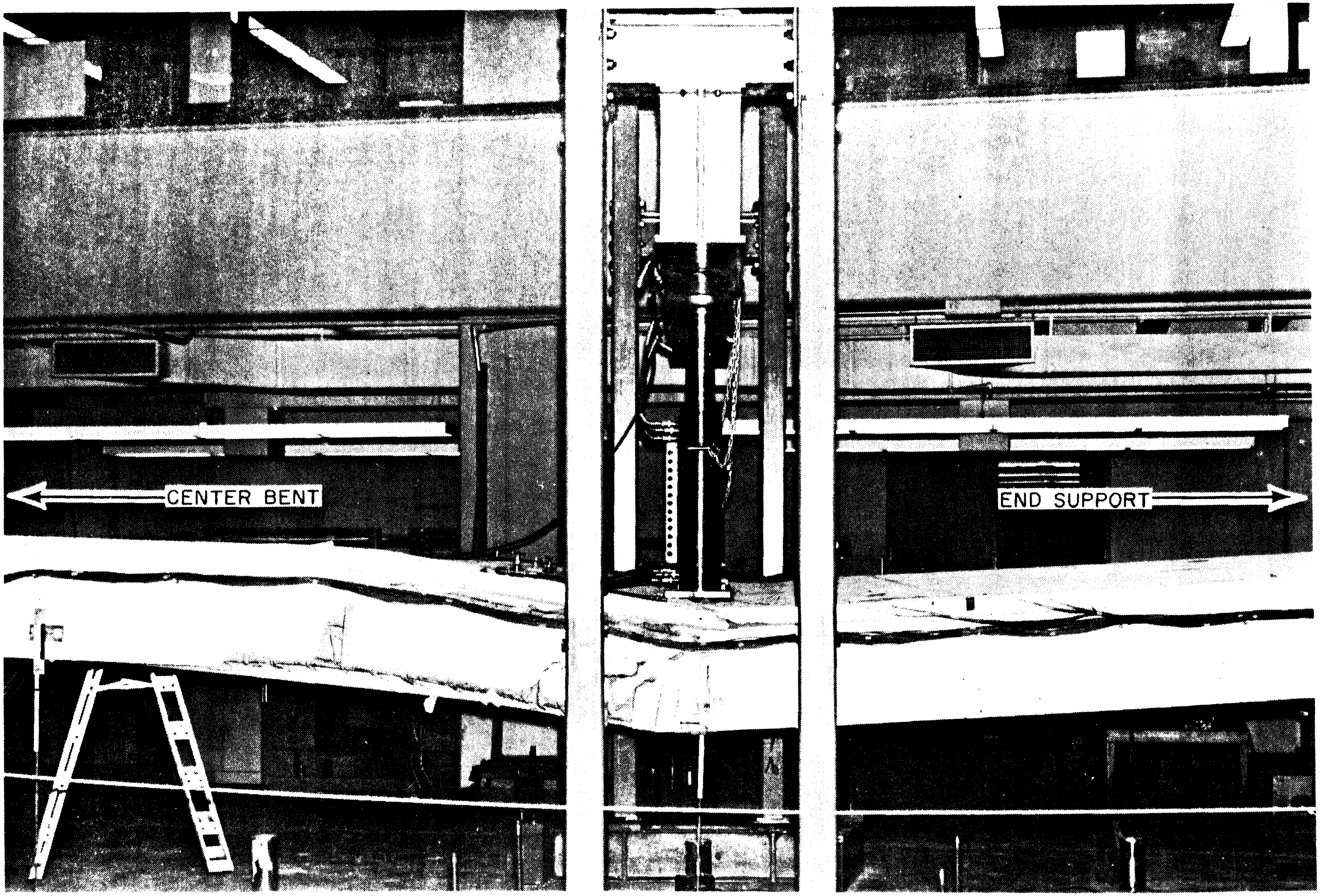

FIG. 8.15 VIEW OF FAILURE ALONG OUTER GIRDER 5 OF DIAPHRAGMED SPAN I AT END OF THIRD LOADING CYCLE

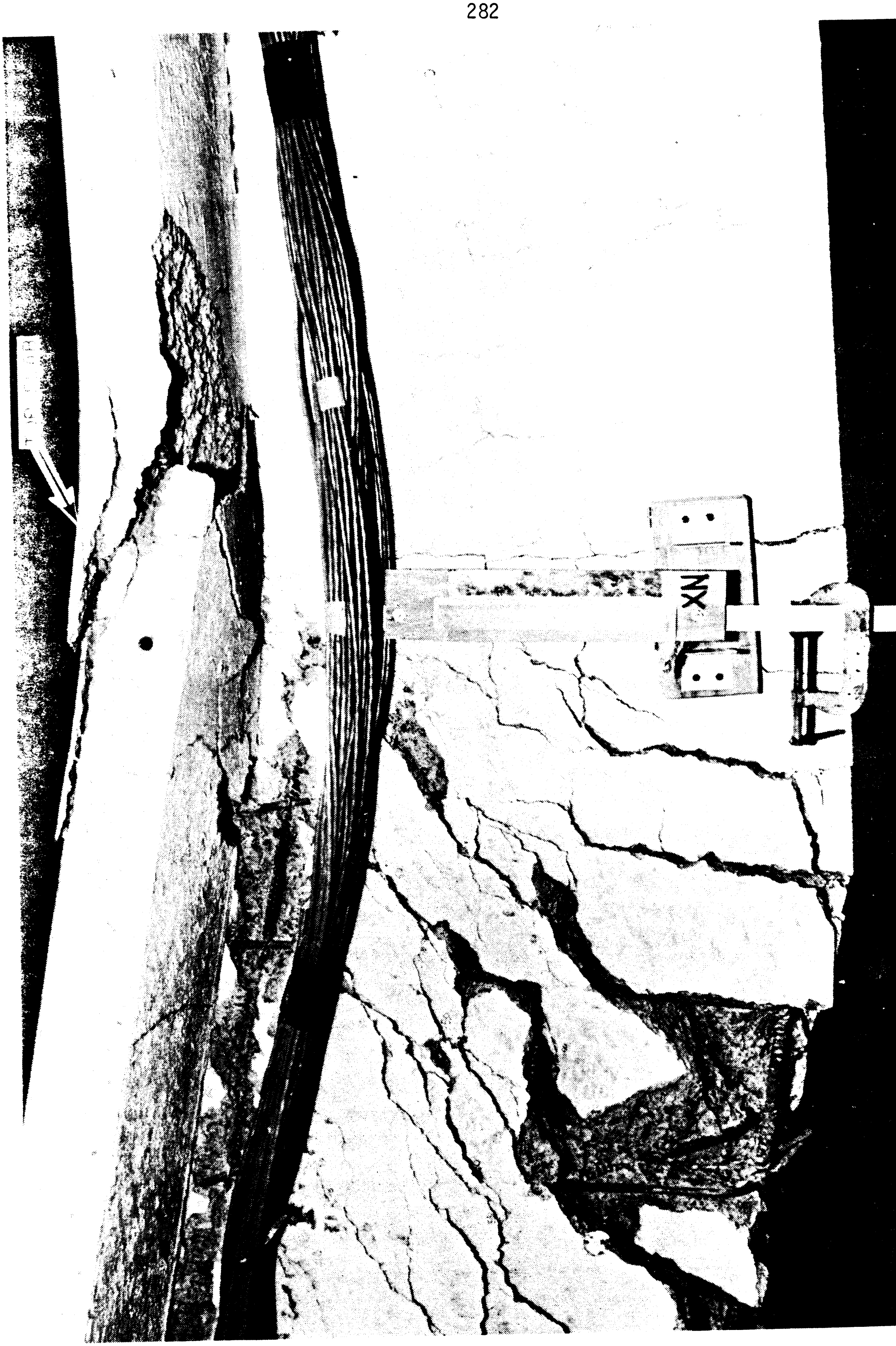

FIG. 8.16 CLOSEUP OF FAILURE OF OUTER GIRDER 5 AT DIAPHRAGMED SECTION X

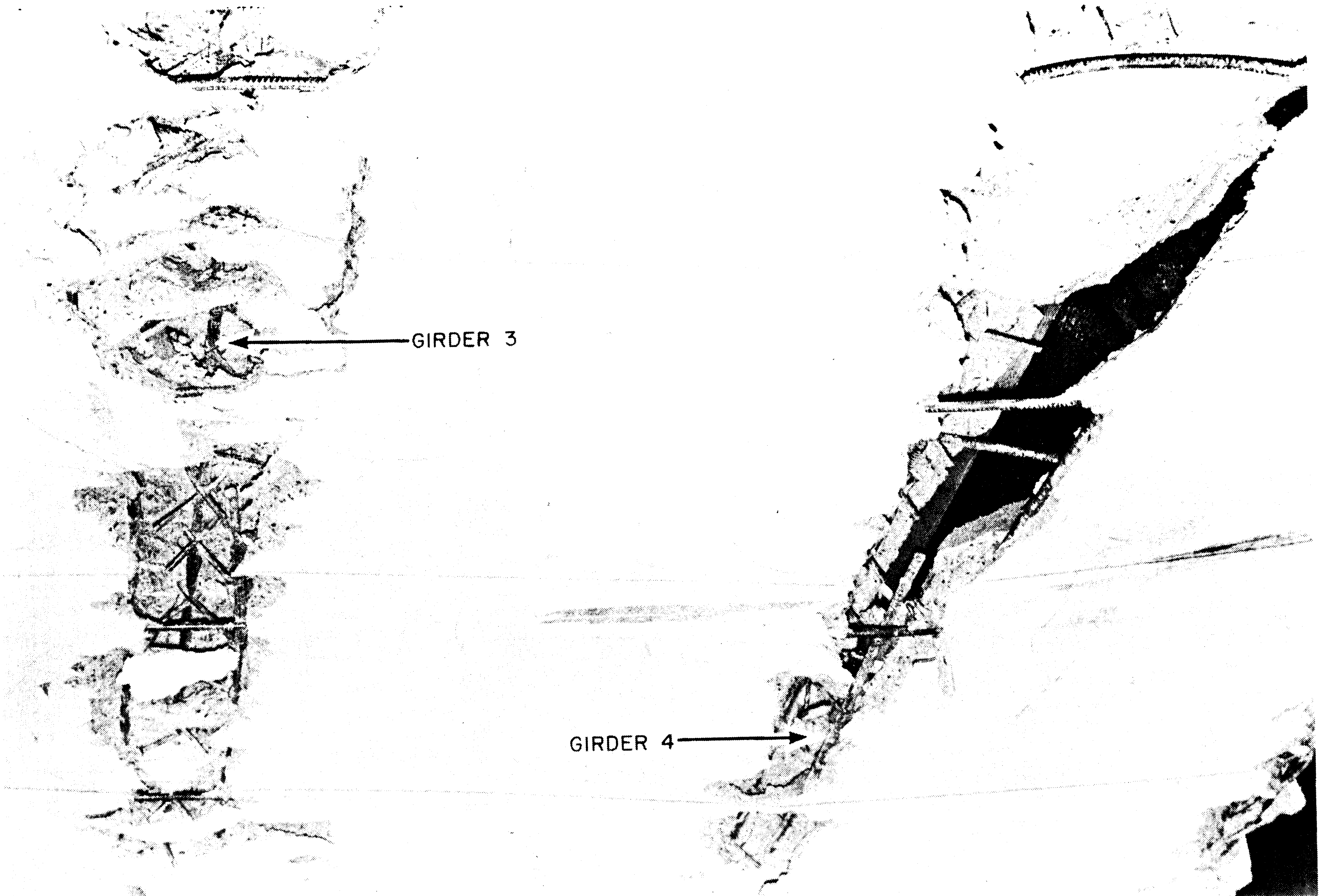

FIG. 8.17 VIEW OF BOTTOM SLAB AT END OF THIRD LOADING CYCLE SHOWING LARGE CRACKS AND PUNCHING FAILURE ALONG BOTTOM OF GIRDER WEBS 3 AND 4 NEAR SECTION X

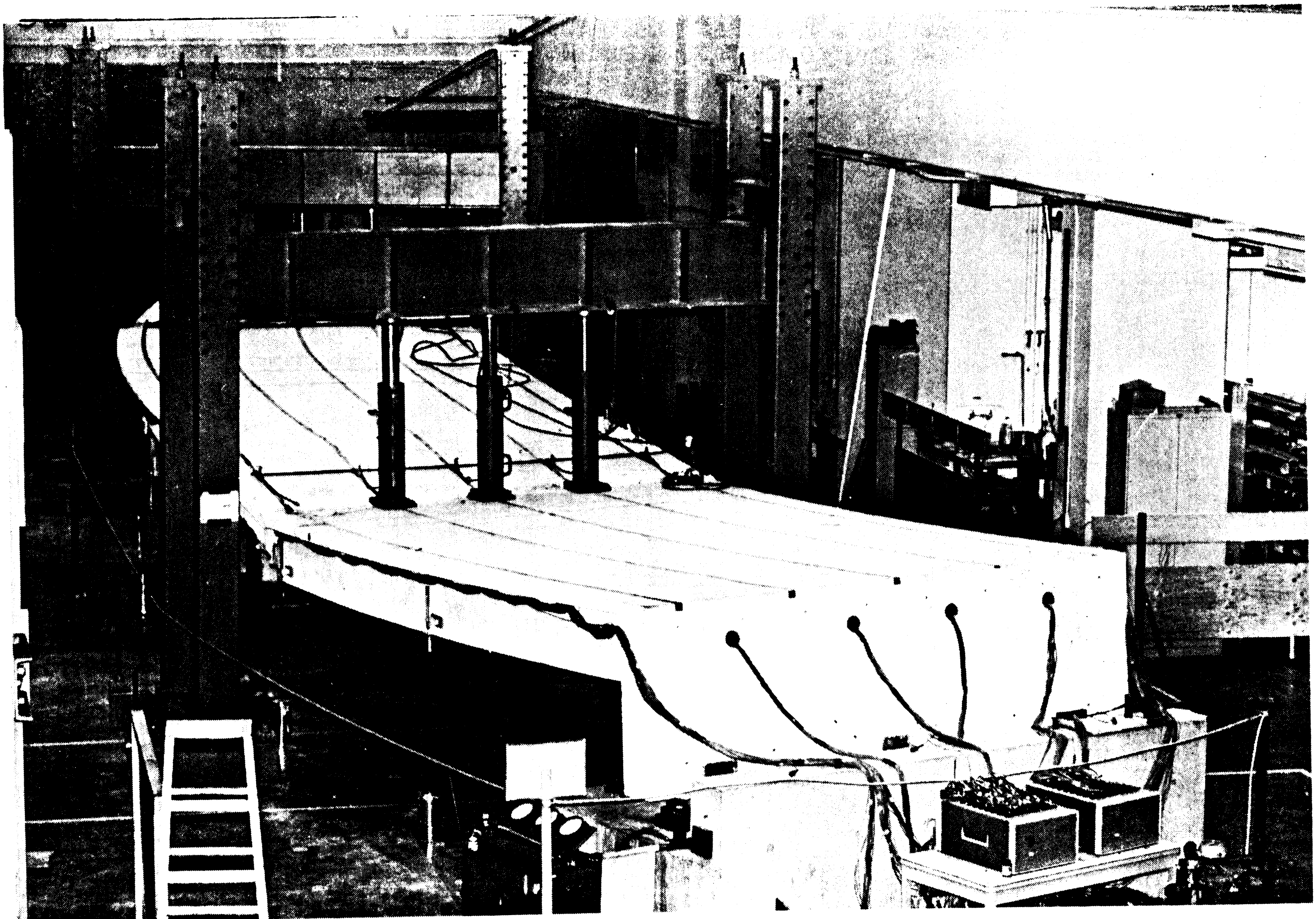

FIG. 8.18 OVERALL VIEW OF BRIDGE LOADED AFTER FINAL FAILURE

TABLE 8.1 YIELD MOMENT (FT-KIPS) CAPACITIES AT MIDSPAN AND CENTER BENT SUPPORT-SECTIONS

	SECTIONS X AND Y	SECTIONS B AND C	
Number and size of tensile bars	55-No. 4	74 No. 4	12 No. 3
Tensile reinforcement area A_s (in^2)	11.0	14.8	1.32
Yield stress f_y (ksi)	70	70	61
Yield force A_s f_y (kips)	770	1036	81
Moment lever arm h (ft)	1.5	1.5	1.5
Moment Capacity $M = A_s f_y h$ (ft-kips)	1155	1676	

TABLE 8.2 LIVE LOAD (KIPS) AT SECTIONS X AND Y TO PRODUCE YIELD MOMENTS AT SECTION X, Y OR B, C

	SECTIONS X AND Y	SECTIONS B AND C
Total moment capacity (ft-kips)	1155	1676
Dead load moment (ft-kips)	199	242
Live load moment capacity (ft-kips)	956	1434
Moment due to 1 kip load at Sections X and Y from SAP Analysis	5.63	4.75
Live Load (kips) at Sections X and Y required to produce yield moments	170	302

In Fig. 8.19 the yield moment capacity is given for all sections along the bridge model. The calculations have been done in the same manner as in Table 8.1. Each reinforcing bar has been assumed to start to carry moment one foot from its end. In the bridge model there is a slight difference in the splicing of the reinforcement bars in the top slab in the two spans. Since the difference in moment capacity at symmetrical sections is only about 5%, for simplicity in the calculations, the splicing in the undiaphragmed span has been used also for the diaphragmed span. This leads to a slight underestimation of the capacity of the diaphragmed span in sections close to the center column.

To determine the live loads at Sections X and Y required to produce yield moments at various sections, the moments due to dead load have to be considered. From the SAP frame analysis, Fig. 2.1, the moments for a distributed dead load of 2.44 kips per ft. have been drawn in Fig. 8.19. If these moments are subtracted from the total moment capacity at the different sections, an estimate of the live load bending capacity can be obtained. This is done in Table 8.2 for the two mid-span Sections X and Y and for the two support Sections B and C. Also from the SAP analysis, Fig. 2.4, influence values can be obtained for the moments due to 1 kip point loads at Sections X and Y. This information is used to get an estimate of the live loads at Sections X and Y required to produce the yield moments at Sections X, Y or B, C, assuming no redistribution of moments occurs. Table 8.2 indicates that mid-span loads of 170 kips can be carried at Sections X and Y before yielding starts in the longitudinal reinforcement in the bottom slab at Sections X and Y. It can also be seen that the negative moment capacity at support Sections B and C would permit mid-span point loads of 302 kips pro-

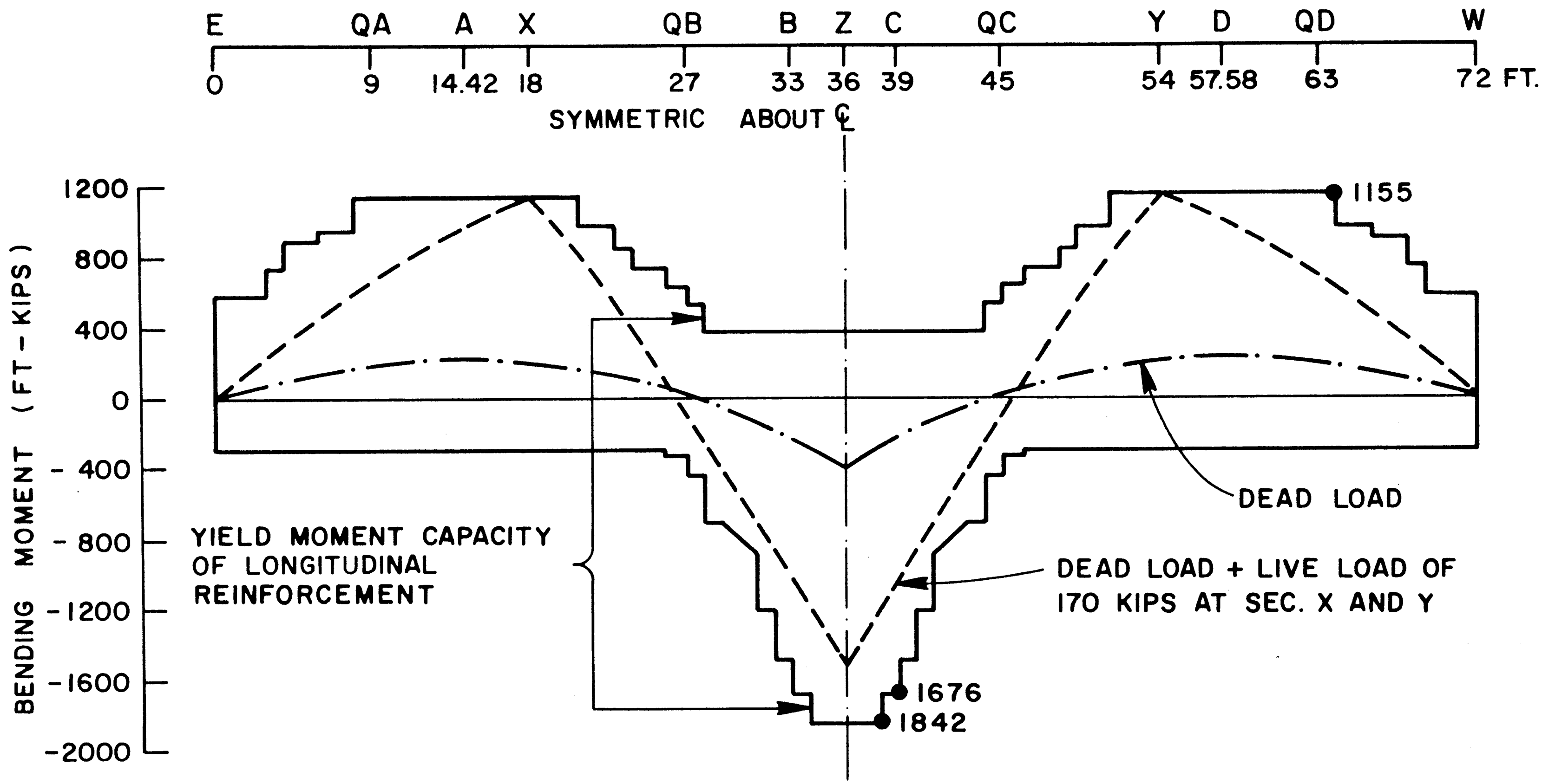

FIG. 8.19 BENDING MOMENT CAPACITY FOR BRIDGE MODEL

vided the other parts of the bridge did not yield first.

From the above calculations it is evident that initial yielding of the longitudinal steel should occur at Sections X and Y under dead load plus live loads of 170 kips at mid-span Sections X and Y. The moment diagram for this loading is plotted in Fig. 8.19. The estimated live load capacity of 170 kips is only an indication of the load when yielding first starts in the longitudinal bottom reinforcement. This estimate is conservative as various approximations have been made regarding e.g. lever arm, bar development length, and contribution from longitudinal bars in the girder webs. This implies that the real load at first yielding could be somewhat higher than 170 kips. When yielding at Sections X and Y, starts the internal forces in the bridge are redistributed. This enables the structure to carry additional loads. A flexural hinge will form at the sections where yielding first starts. After additional load increments, a second hinge will develop somewhere between the first hinge and the center bent column support of the bridge. The bridge model has then turned into a kinematically permissible failure mechanism. To study the ultimate load-carrying capacity for such a case, a failure mechanism with a first hinge at mid-span Section X and with a second hinge at support Section B will be examined. The mechanism is illustrated in Fig. 8.20. According to Table 8.2 the live load moment capacity for Section X is 956 ft. kips and for Section B it is 1434 ft. kips. The live load at Sections X and Y needed to produce the failure mechanism shown in Fig. 8.20 can now be calculated from simple equations of equilibrium. This is done in Fig. 8.20 and the load is found to be 212 kips in each span. However, this case is not necessarily the most critical one. Due to bar cutoffs, the moment capacity between the

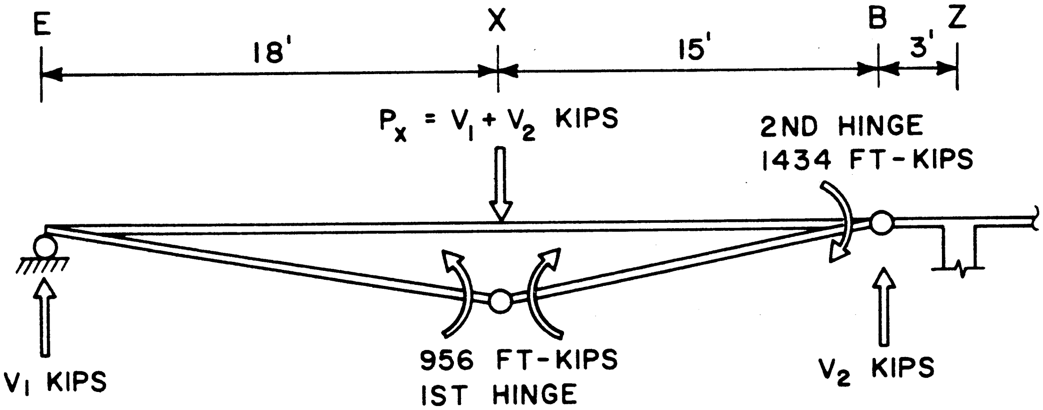

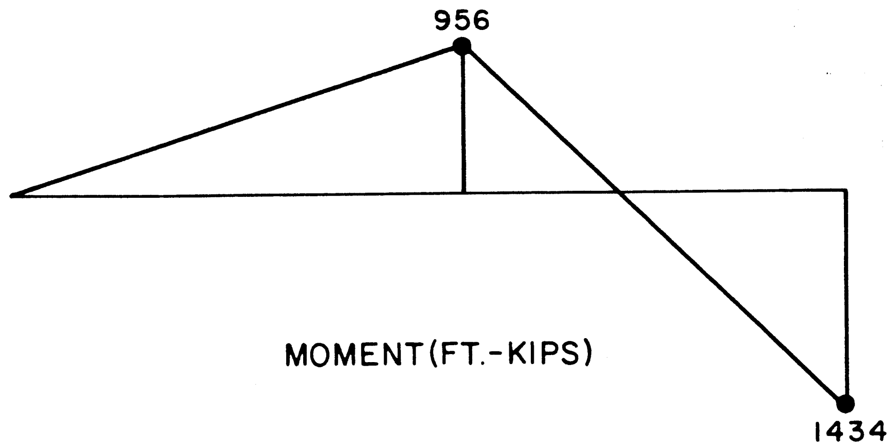

(1) FREE BODY DIAGRAM EX ; $\Sigma M_E = 0$
$V_1 (18) - 956 = 0 \quad V_1 = 956/18 = 53$ KIPS

(2) FREE BODY DIAGRAM XB ; $\Sigma M_B = 0$
$1434 + 956 - V_2 (15) = 0 \quad V_2 = 2390/15 = 159$ KIPS

(3) FREE BODY DIAGRAM EB ; $\Sigma F_Y = 0$
$P_X = V_1 + V_2 = 53 + 159 = 212$ KIPS

FIG. 8.20 LIVE LOAD CAPACITY FOR FAILURE MECHANISM WITH HINGES AT SECTION X AND B quarter Section QB and the support Section B has many abrupt steps as shown in Fig. 8.19. The yield stress and subsequent second flexural hinge may therefore occur at one of these sections along the span before a hinge has a chance to develop at the support Section B. What will happen in this regard depends very much on the bond stresses and the bond strength close to the cut off points of the longitudinal reinforcing bars.

Another pre-requisite for a complete flexural mechanism to form is that the bridge model have a sufficiently high shear and torsion capacity, so that there will be no failure in shear or torsion before the failure mechanism in flexure is fully developed. To look into this question, the shear and torsion capacity of the bridge model is studied in the next section.

8.3.2 Shear and Torsion Capacity

A useful concept in the treatment of shear forces and torsional moments in a cellular box girder system is the shear flow q. The shear flow is defined as the resultant of the shear stresses v over the thickness of a girder web. Usually the shear flow is assumed to be constant over the thickness and depth of the web. For a girder web with the shear force V and the depth h the shear flow can then be written as $q = V/h$.

The shear flow q_s that can be carried by the vertical stirrups in a girder web can be calculated from the formula

$$q_s = \frac{A_v f_v}{s} \cot \alpha$$

where A_v is the total cross-sectional area of one vertical stirrup

f_v is the stress in the stirrup

s is the longitudinal spacing of the stirrups

α is the angle of inclination of the concrete compressive struts in the girder webs.

Table 8.3 gives the size and spacing of the vertical U type stirrups used in the girder webs of the bridge model from the end support section to the center bent support section. Also shown in Table 8.3 is the shear flow capacity per girder web for the vertical stirrups at initial yielding, as calculated by the formula given above. The angle α has been assumed to be 45°.

Besides the contribution from the vertical stirrups, it is also appropriate to consider contributions to the shear-carrying capacity from other parts of the structure. These contributions may be due to the shear carried by the uncracked longitudinal concrete compression zone at the top of the bridge, interface shear transfer (also called aggregate interlock), and dowel action. According to the ACI Building Code (ACI 318-71) these effects can be lumped together to give a contribution term for the concrete. The accompanying ultimate shear stress can be calculated as $v_c = 1.9\sqrt{f'_c}$. For a concrete compression strength of $f'_c = 4000$ psi this gives $v_c = 1.9\sqrt{4000} = 120$ psi. The additional shear flow in one girder web of the bridge model would then be $q_c = v_c b = (120)(2.81)(12/1000) = 4.05$ kips/ft. In the actual bridge model the exterior girder webs were gradually thickened as they approached the supports, from 2.81 to 3.28 in. over a distance of 2 ft. 10 in. from the end support and from 2.81 to 4.28 in. over a distance of 8 ft. 6 in. from the center bent support. These thicknesses gave maximum values of q_c equal to 4.72 and 6.17 kips/ft at the end and center supports.

The shear flow capacity along the bridge model of the vertical stirrups and the concrete is plotted in Fig. 8.21. As the capacity is identical in the two spans, the stirrup and the concrete contributions are shown separately only for the left span, whereas for the right span

TABLE 8.3 SHEAR FLOW (KIPS/FT) CAPACITY PER GIRDER WEB OF VERTICAL WEB STIRRUPS AT YIELD

ZONE	DISTANCE FROM END SUPPORT (FT)	STIRRUP BAR SIZE	SPACING S (IN)	AREA A_v (IN^2)	YIELD STRESS f_y (KSI)	SHEAR FLOW q_s (K/IN)	SHEAR FLOW q_s (K/FT)
1	0 to 4.3	no. 2 def.	4.25	.10	38	0.89	10.7
2	4.3 to 24.4	1/4 in. pl.	6.38	.10	47	0.74	8.8
3	24.4 to 27.9	no. 2 def.	4.25	.10	38	0.89	10.7
4	27.9 to 31.4	no. 2 def.	3.50	.10	38	1.09	13.0
5	3.14 to 36.0	no. 2 def.	2.75	.10	38	1.38	16.6

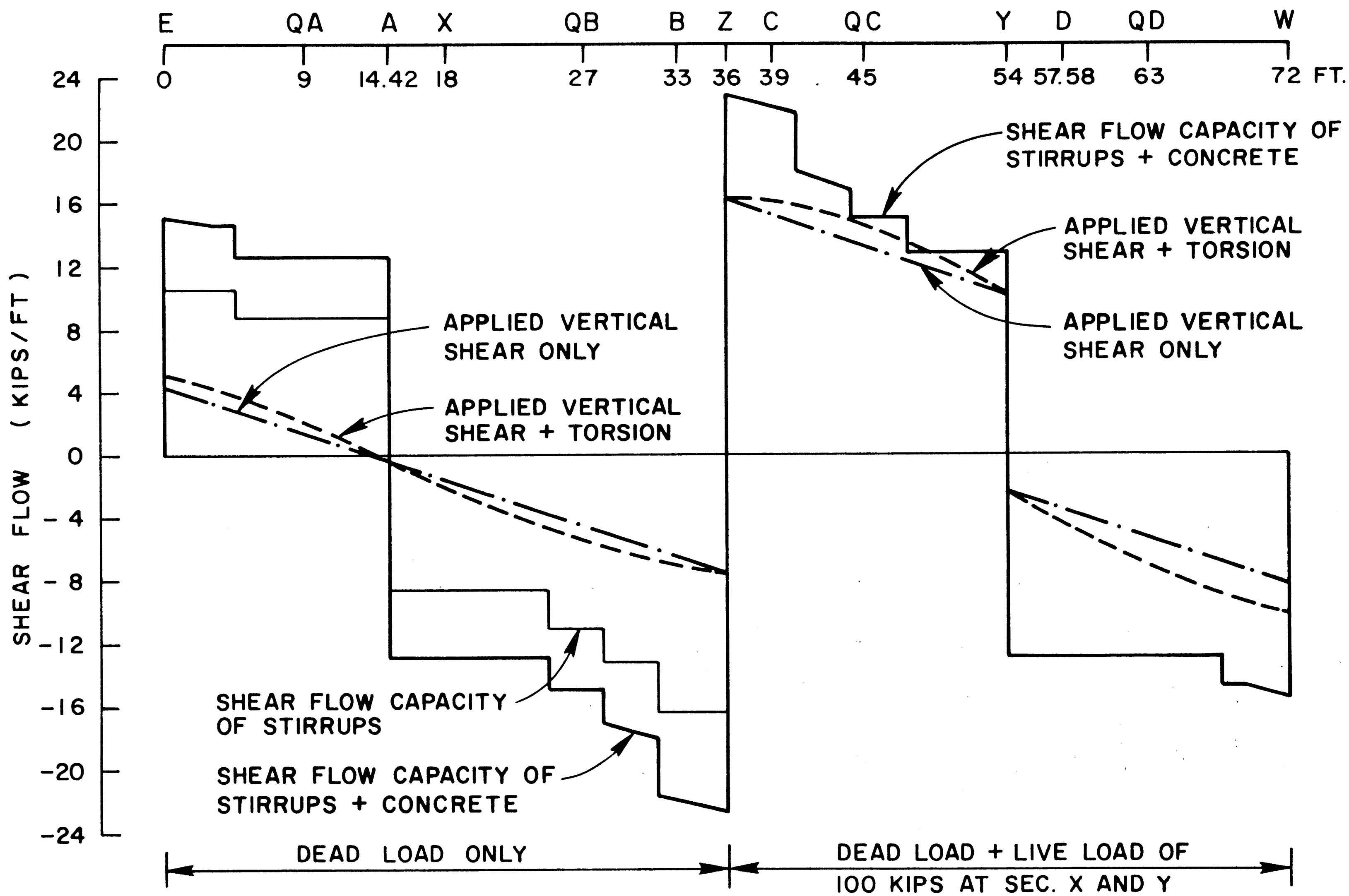

FIG. 8.21 SHEAR FLOW CAPACITY PER EXTERIOR GIRDER WEB FOR BRIDGE MODEL

only the total shear flow capacity is shown.

The estimated shear and torsion capacity is very conservative. The angle α of the compression forces in the girder webs has for simplicity been chosen to be 45°. However, when yielding starts in the vertical stirrups, a redistribution of forces takes place, which decreases the angle α of the compression struts. More forces are then carried by the longitudinal reinforcement and the shear-carrying capacity is increased. Leonhardt, Walther and Dilger [31, 32] have found that α varies between 30° and 40° for T-beams with reinforcement percentages similar to those in the bridge model. The angle has its lowest value for small amounts of vertical stirrups. For α = 30° and 40° the values of cot α are 1.75 and 1.20. This implies a possible increase of 20 to 75% in the shear capacity q_S of the vertical stirrups. In addition, the contributions of shear carried by the uncracked longitudinal concrete compression zone, interface shear transfer, and dowel action have also been estimated in a conservative way.

To determine the live load capacity, the shear flow due to dead load has to be considered. From the SAP frame analysis, Fig. 2.1, the shear forces V and the torsional moments T for a distributed dead load of 2.44 kips per ft can be calculated. The shear flows q_V (due to vertical shear) and q_T (due to torsion), which accompany the shear force V and the torsional moment T can be calculated from the following formulas

$$q_V = \frac{V}{5h}$$

$$q_T = \frac{T}{2A_0}$$

where h is the depth of the cross section and A_0 is the area enclosed by the cross-sectional box defined by the two exterior girder webs and the top and bottom slabs. For the bridge model h = 1.55 ft. and $A_0 = (1.55)(10.29) = 16.0\ ft^2$. The shear flow q_V due to vertical shear appears in all five girders of the bridge model, whereas the shear flow q_T due to torsion only appears in the inner girder 1 and the outer girder 5 as well as in the top and the bottom slabs. The two shear flows, q_V and q_T, will act in the same direction in one of these girder webs and in the opposite direction in the other girder web. For dead load the two flows will act in the same direction in the outer girder 5. The shear flow in this girder due to dead load shear and torsion is shown in the left span in Fig. 8.21. Due to symmetry the shear flow is identical in the right span, so that part of the figure is used to illustrate another load case.

From the SAP frame analysis influence values can also be obtained for different point loads, Figs 2.1 to 2.17. From these figures the shear flow per girder web due to dead load plus 100 kip loads at Sections X and Y have been calculated and plotted in the right span of Fig. 8.21. It can be seen that this loading produces a shear flow approximately equal to the calculated capacity between Sections QC and Y. The live load capacity with respect to local shear and torsion failure in the outer girder 5 would then be only about 100 kips. However, as has already been pointed out, this estimate is very conservative. To get a more realistic value the shear flow capacity q_s of the vertical stirrups may be increased from 20 to 75%. Then the live load capacity would rise from the estimated value of 100 kips to a higher value of about 120 to 175 kips. Furthermore, yielding of the stirrups in outer girder 5 does not necessarily lead to a collapse of the bridge. A redistribution of forces may take place and more of the load is then taken by the other girders.

For a discussion of failure mechanisms which can appear in combined shear, torsion, and bending, see the paper by Elfgren [33].

Another fact which must be considered is that there is always a risk that a local failure in some part of the structure abruptly reduces the load-carrying capacity. A local crushing or disintegrating of the concrete in a critical section may have this effect.

For the load case studied, the influence of the torsional moment on the shear flow is rather small, see Fig. 8.21. This is partly due to the excellent torsion-carrying capacity of box-girder sections. However, the load case studied consisted of loadings which were symmetrical about the longitudinal axis of the bridge and thus do not produce any high torsional moments. For eccentric loadings on the other hand, the torsional moments increase very sharply. Torsional shear flows of 10 times the magnitude here studied may then be ecountered. However, such load cases will probably not be the critical design cases, since maximum vertical shears in the girder webs generally occur with all lanes loaded.

8.3.3 Failure Behavior

The failure in the undiaphragmed Span II was governed by the spalling of the concrete in the bottom of outer girder 5 near Section Y, see Fig. 8.5. The spalling occurred for an applied load of 173 kips in the first loading cycle. It was caused by the high shear flow in combination with a transverse slab bending moment. The bending moment acted on the girder and the bottom slab and tried to open up the corner. The bending moment was increased by longitudinal cracks in the bottom slab under girders 2, 3, and 4. The cracks caused the cross-section to deform, Fig. 8.4, and this deformation augmented the stresses in the corner. When the shear flow and the transverse bending moment had reached a value for which the tensile stresses in the concrete exceeded the tensile strength, the corner was kicked out. The corner then lost its load-carrying capacity and the stiffness of the outer box of the box-girder section decreased. This caused large deformations to take place whereupon the applied external load dropped.

The maximum load of 173 kips is almost equal to the estimated load of 170 kips which was calculated to cause initial yielding of the longitudinal bottom reinforcement, Table 8.2. However, the transverse cracks in the bottom slab due to longitudinal bending were so small that no extensive yielding of the longitudinal bottom bars appeared to have taken place. Consequently it can be concluded that the yield moment capacity for the undiaphragmed Span II may have been slightly higher than 173 kips.

In Section 8.3.2 the shear and torsion live load capacity for the bridge model was estimated to be about 120 to 173 kips applied at Sections X and Y. The diagonal shear cracks in the girders did not indicate any extensive yielding before the failure load. However, the cracks did open up considerably at failure when the bottom corner of the outer girder 5 lost its load-carrying capacity. Undoubtedly the high shear and torsional stresses in the corner of girder 5 did contribute to the local failure there. However, if the corner detail had been stronger the shear and torsion capacity of the undiaphragmed span of the bridge model would probably have been somewhat higher than 173 kips.

After the local corner failure, the bridge model was reloaded. During this second loading cycle the maximum load that could be reached was 152 kips. The final collapse was governed by the shear and torsion capacity in girder 5. Extensive yielding took place in the vertical stirrups. The diagonal concrete compression struts in the girder could then not stand the high stresses any longer but crushed in a section about 6 ft. from Section Y towards the center bent support. This confirms the prediction shown in Fig. 8.21.

The failure in diaphragmed Span I during the third loading cycle had a character different from the local failure in the undiaphragmed Span II. In Span I wide transverse cracks in the bottom slab under the diaphragm due to longitudinal bending indicated yielding of the longitudinal bottom reinforcement even before the ultimate load 190 kips was reached. At the ultimate load wide diagonal shear cracks also indicated yielding in parts of the vertical stirrups. At the load of 190 kips, girder 4 punched through the bottom slab and spalling of the concrete started in the bottom of the outer girder 5. The load then dropped. A first flexural hinge had started to form at the ultimate load. However, no second flexural hinge had an opportunity to form before the punching failure in the bottom slab and the concrete spalling in the bottom of the outer girder 5 took place.

After the maximum load, the deflections in the diaphragmed Span X were increased gradually. A second hinge then formed in girder 5 about 5 ft. from Section X towards the center bent support, see Section 8.2.3. No such hinge developed in girder 1. Instead the flexural deformations were spread along the girder between Sections X and QB.

8.4 Comparison of Ultimate Strength Behavior for Straight and Curved Bridge Models

For the straight bridge model the calculated live load for longitudinal flexural yielding was 156 kips. This value is somewhat lower than the value of 170 kips for the curved bridge model. The difference is due to the slightly higher yield stress of the reinforcement used in the curved bridge model, 70 ksi vs. 62 ksi for the straight model. For shear and torsion it can be assumed that the cross sections of the two bridge models had fairly equal capacities.

For the undiaphragmed span the maximum test load was 170 kips for the straight bridge whereas it was 173 kips for the curved bridge. In the straight bridge yielding had started in the bottom longitudinal reinforcement bars for the maximum load. Besides the web of girder 2 pushed downward causing a major longitudinal crack in the bottom slab. Finally the movement of girder 2 caused local failures in the top and bottom slabs so that the ram bearing plate punched through the top slab. In the curved bridge no yielding of the longitudinal bottom reinforcement was observed. Instead the failure was caused by the local spalling of the concrete in the bottom of girder 5. However, even here longitudinal cracks in the bottom slab under the interior girders helped to initiate the failure, just as in the straight bridge.

In the curved bridge, outer girder 5 is the most highly stressed girder as it has the longest span. Furthermore the girder has to carry the highest shear flow as the vertical shear force and the torsional moment produce shear flows in the same direction in the girder web. For this reason the bottom corner of the outer girder is a rather weak point which can cause a premature failure. Special care ought therefore to be exercised in the designing of the outer girder in undiaphragmed curved bridges.

For the diaphragmed span the maximum test load was 170 kips for the straight bridge whereas it was 190 kips for the curved bridge. In both bridges yielding had started in the longitudinal bottom reinforcement prior to the maximum load. In the straight bridge the load decreased slowly after the maximum and a uniform yielding took place in Section X. In the curved bridge wide diagonal shear cracks were also observed at failure. Here the failure occurred when girder 4 punched through the bottom slab. No pronounced differences were observed for the failures of the diaphragmed spans of the two bridges. The higher maximum load for the curved bridge is reasonable because of the higher yield strength of its longitudinal bottom reinforcement.

From a comparison of the failures in the undiaphragmed and the diaphragmed spans it is obvious that the diaphragm has a very good load distributing function at ultimate loads. This is especially valuable in curved bridges.

Regarding conclusions for the failure behavior of full scale prototype bridges, it must be kept in mind that the two bridge models were tested with concentrated point loads at the mid-spans only. This is not a very likely load case for a real bridge, where instead a more distributed design live load is to be expected. Obviously, distributed loads are not as critical as point loads. The test loading procedure therefore measured the capability of the bridges to withstand the most severe load cases.

8.5 Summary

Failure of the curved box girder bridge model developed during three loading cycles. During the first two loading cycles, live loads were applied at both midspans I and II, Sections X and Y, on interior girders 2, 3, 4. After failure of the undiaphragmed Span II (Section Y) the displacements were frozen at Section Y by locking the three loading rams and during the third loading cycle only diaphragmed Span I (Section X) was loaded until failure occurred in Span I.

It can be concluded that failure in the undiaphragmed span occurred in the first loading cycle under a live load of 173 kips in both spans. The failure was initiated locally in the web of outer girder 5 near midspan Section Y due to a combination of shear, torsion and transverse slab bending. Yielding of the longitudinal reinforcement in the bottom slab at midspan due to longitudinal bending had not yet occurred.

Failure of the diaphragmed span occurred in the third loading cycle under a live load of 190 kips at midspan Section X only with the displacements frozen at midspan Section Y. The failure occurred after yielding of the longitudinal reinforcement in the bottom slab due to longitudinal bending and was due to the web of girder 4 punching through the bottom slab plus spalling of the concrete in the web of girder 5.

The local failures which appeared during the testing might partly be governed by the method of loading used in the test. The longitudinal cracks and the punching which occurred in the bottom slabs were likely caused by the concentrated loads on the top of girders 2, 3 and 4. Such phenomena are consequently not to be expected in actual bridges with distributed traffic loads. However, the bottom slab is a critical part of the bridge and the connections between the slab and the vertical girder webs ought to be carefully designed. This is especially true for the corners of exterior girder webs where high shear stresses from vertical shear forces and torsional moments may act together.

Finally it should be emphasized that the curved box girder bridge model exhibited excellent load carrying ability. Based on a live load of 38.5 kips at Sections X and Y, in addition to dead load, producing a design stress in the steel of 24 ksi, the bridge model had a live load overload capacity of 173/38.5 = 4.5, which is a substantial value.

9. CONCLUSIONS AND RECOMMENDATIONS FOR IMPLEMENTATION

A detailed presentation of the reduction, analysis and interpretation of the experimental and theoretical results obtained in testing a horizontally curved, continuous, two span, four cell, reinforced concrete box girder bridge model has been given. The horizontal curvature used in the model was selected to represent the sharpest curvature normally used for bridges in the California highway system. Results, in terms of reactions, deflections, strains and moments, for the response of the bridge to dead load, working stress loads and at or after overload stress levels have been presented. Single or several point loads, AASHO standard truck loads, construction vehicle loads and a moving fork lift truck load have all been considered. The behavior under sustained dead load during the load history of the model has been described. Finally, the structural behavior during the final loading phase to failure has been discussed in detail.

The most important conclusions from this study are summarized below.

1. The finite element program CELL provides an analytical solution of the bridge system as a three dimensional folded plate system, which can be used to accurately predict the longitudinal and transverse distribution of theoretical reactions, moments, deflections and internal membrane and plate bending forces assuming the bridge to be an elastic, homogeneous, isotropic and uncracked concrete structure. This has been verified in previously reported studies [14,16] on small scale aluminium

models of box girder bridges.

2. An analysis such as provided by the SAP program, in which the bridge system is assumed to be a simple three dimensional frame made up of one dimensional elements, can be used to accurately predict the longitudinal distribution of theoretical total reactions, moments and centerline deflections. This has been verified in Chapter 2 by comparing results from SAP with those from CELL.

3. Total reactions at the west, center and east supports are accurately predicted by theory for all load levels and types of loads studied during the experimental program. Cracking of the concrete does not significantly affect the magnitude and distirbution of the reactions. Either CELL or SAP can be used for the theoretical solutions.

4. The transverse distribution of the total reactions at each end to the five individual girder reaction supports is highly dependent on the type and the manner of installation of these supports and cannot be accurately predicted by theory, which assumes that the rigid end diaphragm rests on five unyielding supports.

5. As a result of 3, the total external moments at various sections of the bridge, under loadings to produce maximum effects, can be found by theory with confidence. These external moments are least sensitive to small errors in the values of the reactions for moments in midspan regions and most sensitive for moments over the center bent support.

6. From a study of 19 different midspan point load combinations it can be concluded that there is a general increase in the total moment at a section as the load moves transversely from inner girder 1 to outer girder 5. This increase is much more pronounced for negative moments near the center bent support than for positive moments in the midspan regions.

7. The transverse distribution of the total moment at a section in terms of percentage to each girder, can be accurately predicted by theory at working stress levels for both single point loads and uniform loads across the width of the bridge. At or after overload stress levels, agreement between theory and experiment decreases somewhat for single point loads, but remains good for uniform loads across the width of the bridge. Since actual critical girder design moments are created by truck live loads on all lanes, resulting in several wheel loads acting on the bridge width, the theory should be adequate for predicting design moments even at or after overstress levels.

8. Theory predicts the magnitude and distribution of live load deflections under point loads satisfactorily (within 10 to 20%) for the 24 to 30 ksi working stress levels provided theoretical values are multiplied by a factor of about 1.5 to account for cracking. After higher conditioning load stress levels of 40, 50, or 60 ksi the theory can no longer be used to accurately predict the distribution of deflections under working stress point loads. After the 60 ksi conditioning loads, deflections ranging from 1.1 to 2.2 times the theoretical value were found

for points some distance away and directly under the point load respectively.

9. For conditioning loads, consisting of point loads simultaneously applied on all five girders at midspan Sections X and Y, the ratio of the midspan deflection of outer girder 5 to that of inner girder 1 remained essentially the same for all stress levels. This ratio was 1.20 at diaphragmed Section X and 1.14 at undiaphragmed Section Y. The ratio of experimental to theoretical deflections at both sections was approximately 1.3 for the 24 ksi conditioning load and increased progressively for the subsequent higher conditioning loads to a maximum of 1.9 for the 60 ksi conditioning load.

10. Midspan dead load deflections immediately after removing the shoring were 0.40 in. for inner girder 1 and 0.48 in. for outer girder 5, at both Sections X and Y. Ratios of these experimental deflections to theoretical values based on uncracked section ranged from 1.5 to 1.6. During the following three weeks the deflections under sustained dead load increased about 55%. Subsequent applications of live loads causing increasingly higher steel stresses of 24, 30, 40, 50 and 60 ksi produced additional cracking and permanent deflections, so that at a time 4 months after removal of the shoring and just prior to loading to failure the sustained dead load midspan deflections had increased to maximum values of about 1.5 and 2.0 in. for girders 1 and 5 respectively. These are about 4 times the initial dead load deflections.

11. Comparing the effects of torsional support restraints at the center bent with the normal restraint case, the differences in results were small and could be ignored in practical design problems with similar center bent configurations. The differences were much larger however, where longitudinal restraints at the bottom of the end diaphragms were introduced and this effect should be considered in design if it exists.

12. Both theoretical and experimental results show that for the bridge tested the AASHO empirical formula $N_{WL} = S/7$ overestimates the actual value of the girder moment slightly for a two lane truck loading but underestimates it by as much as 30% for the three lane truck loading on the bridge.

13. The final loading to failure demonstrated that this type of bridge has an excellent overload capacity of 4.5 on the live load and has the ability, through its high torsional strength, to transfer loads laterally almost up to failure.

14. Differences between the behavior of Span I with a diaphragm and Span II without a diaphragm were not significant at working stress levels, but became more pronounced at very high overstress levels and during the final loading to failure.

15. Comparing the results found for the curved bridge model reported herein, which had the sharpest curvature normally used for bridges in California, with those of the similar straight bridge model reported on previously [10,11,12] it can be concluded that the general response of the two models was similar in almost all respects. While some differences in reactions,

deflections and moments do exist for the two bridge models for various loading conditions, they are not significant and these differences are adequately predicted by the analytical solutions described in this report. While the mode of failure was somewhat different for the two bridges, they had similar ultimate live load capacities, 170 kips for the straight bridge and 173 kips for the curved bridge. These ultimate loads represent an excellent overload capacity of greater than 4 on the live load.

On the basis of the above it can be concluded that the theoretical solutions and computer programs, previously developed at the University of California and described in detail in Refs. [1,2,5,6,7,13], which treat straight or curved box girder bridges as three dimensional folded plate systems, can be used as valuable tools to completely analyze these bridges. The programs can be used to considerable advantage in design to analyze unusual cases not covered in standard AASHO specifications and also they can be used to verify any proposed simplified design method which might replace the present AASHO method for usual bridge types.

The above programs, which assume the bridge model to be an elastic, homogeneous, isotropic and uncracked concrete structure, should be even more accurate in predicting the working stress response of uncracked prestressed concrete box girder bridges than the response of reinforced concrete bridges which experience cracking.

On the basis of the studies to date, it appears that for multicell box girder bridges of span to width ratios of 3 to 1 or greater, a simplified design method can be based on an analysis in which the bridge system is assumed to be a simple three dimensional frame made up of one dimensional elements. The section properties of the one dimensional elements representing the bridge can be obtained by treating the entire bridge cross section as an uncracked beam section. Numerous general purpose computer programs (e.g. SAP) are available to perform these analyses. The analytical model, made up of straight one dimensional elements, should have enough segments to adequately represent any curvature that exists and should include monolithic columns or other supporting elements as part of the three dimensional frame. Such an analysis can be used to predict the longitudinal distribution of total reactions, moments and deflections.

An important decision to be made with respect to a simplified design method is the number of wheel loads to be used as a design load. Present AASHO specifications for this should be reviewed and probably changed. Reports [3,30] containing detailed analytical studies in this regard and preliminary recommendations have been published previously.

It is now recommended that for implementation, a joint effort be made by representatives of the State of California Bridge Department and the faculty investigators to develop final recommendations for a simplified design method for straight and curved reinforced box girder bridges. Since both working stress design and load factor design (ultimate strength design) are now permissible in the 1973 AASHO specifications, both approaches should be considered. In this connection, the findings of the previous [10,11,12] and present research investigations with respect to overload stress levels and loading to ultimate failure for the straight and curved bridge models should be particularly helpful.

10. ACKNOWLEDGEMENTS

This investigation was sponsored by the Division of Highways, Department of Transportation, State of California, and the Federal Highway Administration, United States Department of Transportation.

The contents of this report reflect the views of the authors who are responsible for the facts and the accuracy of the data presented herein. The contents do not necessarily reflect the official views or policies of the State of California or the Federal Highway Administration. This report does not constitute a standard, specification, or regulation.

The planning, preparation, construction, supervision, testing, control, analysis and data reduction for a research project of the scope and size of the curved box girder bridge model of the present study necessitate the cooperative assistance and teamwork of all involved.

From the State of California Division of Highways, G. D. Mancarti, Assistant Bridge Engineer and R. E. Davis, Senior Bridge Engineer of the Research and Development Section, maintained a close and keen interest in the project in all its stages.

R. M. Stephen, S.E.M. Laboratory Manager, actively participated in the preliminary planning, design, instrumentation and contruction of the box girder bridge model, and deserves special thanks for his assistance and interest.

Of primary importance to the success of the project were the hard work and enthusiasm of the various Research Assistants, Students and Staff working for different periods on the research investigation.

Special acknowledgement should be given to A. Horeis, Graduate Research Assistant, who participated in all phases of the research program from its inception to the publication of the final reports.

J. Ho, A. F. Kabir, Y. J. Kang, C. S. Lin and S. Shankar, Graduate Research Assistants, worked on various phases of the investigation especially on analytical studies, computer programming and reduction of experimental data.

L. Elfgren, a postdoctoral student from Chalmers University of Technology, Sweden, who spent six months in Berkeley, was very helpful during the critical testing portion of the program. He also contributed greatly to the analysis and interpretation of the ultimate strength behavior of the bridge during its final loading to failure.

As always, the S.E.S.M. Laboratory staff provided excellent support. D. Wasley gave frequent and valuable help in the running of the S.E.S.M. Data Acquisition System. J. G. Foster, E. Cleave, A. D. Lawrence and A. Costa enabled full utilization of the skills and resources of the Mechanical and Electronics shops. R. Parsons as Mechanician and T. Brennan as Electronics Technician contributed toward the fabrication and preparation of the test set-up and instrumentation.

Finally acknowledgement is due to the drafting staff composed of A. Klash, G. Feazell and A. Pereda and the typing staff composed of I. Blowers. P. Ward, L. Larson and L. Tsai for their assistance in the production of the final reports.

11. REFERENCES

1. Scordelis, A. C., "Analysis of Simply Supported Box Girder Bridges," Structural Engineering and Structural Mechanics Report No. SESM 66-17, University of California, Berkeley, October 1966 (PB 175 646).

2. Scordelis, A. C., "Analysis of Continous Box Girder Bridges," Structural Engineering and Structural Mechanics Report No. SESM 67-25, University of California, Berkeley, November 1967 (PB 178 355).

3. Scordelis, A. C., and Meyer, C., "Wheel Load Distribution in Concrete Box Girder Bridges," Structural Engineering and Structural Mechanics Report No. SESM 69-1, University of California, Berkeley, January 1969 (PB 183 923).

4. Willam, K. J., and Scordelis, A. C., "Analysis of Orthotropic Folded Plates with Eccentric Stiffeners," Structural Engineering and Structural Mechanics Report No. SESM 70-2, University of California, Berkeley, February 1970 (PB 191 051).

5. Meyer, C., and Scordelis, A. C., "Computer Program for Prismatic Folded Plates with Plate and Beam Elements," Structural Engineering and Structural Mechanics Report No. SESM 70-3, February 1970 (PB 191 050).

6. Meyer, C., and Scordelis, A. C., "Analysis of Curved Folded Plate Structures," Structural Engineering and Structural Mechanics Report No. UC SESM 70-8, University of California, Berkeley, June 1970 (PB 193 535).

7. Willam, K. J., and Scordelis, A. C., "Computer Program for Cellular Structures of Arbitrary Plan Geometry," Structural Engineering and Structural Mechanics Report No. UC SESM 70-10, University of California, Berkeley, September 1970 (PB 196 143).

8. Meyer, C., "Analysis and Design of Curved Box Girder Bridges," Structural Engineering and Structural Mechanics Report No. UC SESM 70-22, University of California, Berkeley, December 1970 (PB 197 289).

9. Bouwkamp, J. G., Scordelis, A. C., and Wasti, S. T., "Structural Behavior of a Two Span Reinforced Concrete Box Girder Bridge Model, Volume I," Structural Engineering and Structural Mechanics Report No. UC SESM 71-5, University of California, Berkeley, April 1971 (PB 199 187).

10. Scordelis, A. C., Bouwkamp, J. G., and Wasti, S. T., "Structural Behavior of a Two Span Reinforced Concrete Box Girder Bridge Model, Volume II,"Structural Engineering and Structural Mechanics Report No. UC SESM 71-16, University of California, Berkeley, October 1971 (PB 210 431).

11. Scordelis, A. C., Bouwkamp, J. G., and Wasti, S. T., "Structural Behavior of a Two Span Reinforced Concrete Box Girder Bridge Model, Volume III,"Structural Engineering and Structural Mechanics Report No. UC SESM 71-17, University of California, Berkeley, October 1971.

12. Meyer, C., and Scordelis, A. C., "Computer Program for Non-Prismatic Folded Plates with Plate and Beam Elements," Structural Engineering and Structural Mechanics Report No. UC SESM 71-23, University of California, Berkeley, December 1971.

13. Lin, C. S., and Scordelis, A. C., "Computer Program for Bridges on Flexible Bents," Structural Engineering and Structural Mechanics Report No. UC SESM 71-24, University of California, Berkeley, December 1971 (PB 210 171).

14. Godden, W. G., and Aslam, M., "Model Studies of Skew Box Girder Bridges," Structural Engineering and Structural Mechanics Report No. UC SESM 71-26, University of California, Berkeley, December 1971.

15. Comartin, C. D., and Scordelis, A. C., "Analysis and Design of Skew Box Girder Bridges," Structural Engineering and Structural Mechanics Report No. UC SESM 72-14, University of California, Berkeley, December 1972.

16. Godden, W. G., and Aslam, M., "Model Studies of Curved Box Girder Bridges," Structural Engineering and Structural Mechanics Report No. UC SESM 73-5, University of California, Berkeley, March 1973.

17. Scordelis, A. C., Davis, R. E., and Lo, K. S., "Load Distribution in Concrete Box Girder Bridges," ACI Proceedings of First International Symposium on Concrete Bridge Design, Toronto, Canada, April 1967, ACI Publication SP-23, 1969.

18. Scordelis, A. C., and Davis, R. E., "Stresses in Continuous Concrete Box Girder Bridges," ACI Proceedings of Second International Symposium on Concrete Bridge Design, Chicago, April 1969, ACI Publication SP-26, 1971.

19. Scordelis, A. C., "Analytical Solutions for Box Girder Bridges," Proceedings, Conference on Modern Developments in Bridge Design and Construction, Cardiff, Great Britain, April 1971.

20. Bouwkamp, J. G., Scordelis, A. C., and Wasti, S. T., "Structural Behavior of a Reinforced Concrete Box Girder Bridge," Proceedings, Conference on Modern Developments in Bridge Design and Construction, Cardiff, Great Britain, April 1971.

21. Willam, K. J., and Scordelis, A. C., "Analysis of Eccentrically stiffened Folded Plates," Proceedings of IASS Symposium on Folded Plates and Prismatic Structures, Vienna, September 1970.

22. Meyer, C., and Scordelis, A. C., "Analysis of Curved Folded Plate Structures," Journal of the Structural Division, Proceedings of American Society of Civil Engineers, Volume 98, No. ST1, January 1972.

23. Willam, K. J., and Scordelis, A. C., "Cellular Structures of Arbitrary Plan Geometry," Journal of the Structural Division, Proceedings of American Society of Civil Engineers, Volume 98, No. ST 7, July 1972.

24. Godden, W. G., and Aslam, M., "Model Studies of Skew Multicell Girder Bridges," Journal of the Engineering Mechanics Division, Proceedings of the American Society of Civil Engineering, Volume 99, No. EM 1, February 1973.

25. Scordelis, A. C., Bouwkamp, J. G., and Wasti, S. T., "Study of AASHO Loadings on a Concrete Box Girder Bridge," Highway Research Record No. 428, Highway Research Board, Washington, D. C., 1973.

26. Scordelis, A. C., Bouwkamp, J. G., and Wasti, S. T., "Structural Response of a Concrete Box Girder Bridge," Journal of the Structural Division, Proceedings of the American Society of Civil Engineers, Volume 99, No. ST 10, October 1973.

27. Bouwkamp, J. G., Scordelis, A. C., and Wasti, S. T., "Ultimate Strength of a Concrete Box Girder Bridge," Journal of the Structural Division, Proceedings of the American Society of Civil Engineers, Vol. 100, No. ST 1, January 1974.

28. Davis, R. E., Kozak, J. J., and Scheffey, C. F., "Structural Behavior of a Concrete Box Girder Bridge," Highway Research Record No. 76, Highway Research Board, Washington, D. C., 1965.

29. "Standard Specifications for Highway Bridges," American Association of State Highway Officials, [AASHO], Eleventh Edition, Washington, D. C., 1973.

30. Sanders, W. W., and Elleby, H. A., "Distribution of Wheel Loads on Highway Bridges," National Cooperative Highway Research Program Report 83, Highway Research Board, Washington, D. C., 1970.

31. Leonhardt, F., and Walther, R., "Shear Tests on T-Beams with Varying Shear Reinforcement" (Schubversuche an Plattenbalken mit unterschiedlicher Schubbewehrung. In German). Deutscher Ausschuss für Stahlbeton, Heft 156, Berlin 1963, 84 pp.

32. Leonhardt, F., Walther, R., and Dilger, W., "Shear Tests on Continuous Beams" (Schubversuche an Durchlaufträgern. In German). Deutscher Ausschuss für Stahlbeton, Heft 163, Berlin 1964, 138 pp.

33. Elfgren, L., "Reinforced Concrete Beams Loaded in Combined Torsion, Bending and Shear. A Study of the Ultimate Load-Carrying Capacity." Division of Concrete Structures, Publication 71:3, Chalmers University of Technology, 2nd Ed, Göteborg 1972, 230 pp.

34. Wilson, E. L., "SOLID SAP - A Static Analysis Program for Three Dimensional Solid Structures," Structural Engineering and Structural Mechanics Report No. UC SESM 71-19, University of California, Berkeley, September 1971, Revised December 1972.

35. Kabir, A. F., and Scordelis, A. C., "Computer Program for Curved Bridges on Flexible Bents," Structural Engineering and Structural Mechanics Report No. UC SESM 74-10, University of California, Berkeley, September 1974.

Copies of most of the research reports in the above reference list have been placed on file with the U. S. Department of Commerce and may be obtained on request for cost of reproduction by writing to the following address:

National Technical Information Service
Operations Division
Springfield, Virginia 22151

The accession number (shown in parenthesis in the reference list) should be specified when ordering a particular report.